NASA CONTRACTOR REPORT

NASA CR-922

NASA CR-922

FACILITY FORM 602

(ACCESSION NUMBER) (THRU)

(PAGES) (CODE)

(NASA CR OR TMX OR AD NUMBER) (CATEGORY)

TWO-STAGE POTASSIUM TEST TURBINE

Volume I

Fluid Dynamic Design and Performance

by R. J. Rossbach and G. C. Wesling

Prepared by
GENERAL ELECTRIC
Cincinnati, Ohio
for Lewis Research Center

NATIONAL AERONAUTICS AND SPACE ADMINISTRATION • WASHINGTON, D. C. • FEBRUARY 1968

NASA CR-922

TWO-STAGE POTASSIUM TEST TURBINE

Volume I

Fluid Dynamic Design and Performance

By R. J. Rossbach and G. C. Wesling

Distribution of this report is provided in the interest of information exchange. Responsibility for the contents resides in the author or organization that prepared it.

Prepared under Contract No. NAS 5-1143 by
GENERAL ELECTRIC
Cincinnati, Ohio

for Lewis Research Center

NATIONAL AERONAUTICS AND SPACE ADMINISTRATION

For sale by the Clearinghouse for Federal Scientific and Technical Information
Springfield, Virginia 22151 – CFSTI price $3.00

PRECEDING PAGE BLANK NOT FILMED.

FOREWORD

The work described in this report is part of the Two-Stage Potassium Test Turbine Program conducted by the Space Power and Propulsion Section of the General Electric Company for the National Aeronautics and Space Administration under Contract NAS 5-1143 for the design, manufacture and testing of a two-stage turbine, using potassium vapor as the working fluid. This work was carried out under the Technical Management of Joseph P. Joyce, Space Power Systems Division, NASA-Lewis Research Center, with Thomas P. Moffitt, NASA-Lewis Research Center, Fluid System Components Division, as research consultant.

PRECEDING PAGE BLANK NOT FILMED.

ABSTRACT

The Space Power and Propulsion Section of the General Electric Company has been under contract to the National Aeronautics and Space Administration from May 8, 1961, to February 20, 1966, for the design, fabrication and test of a two-stage turbine suitable for operation in wet potassium vapor at temperatures of 1400 to 1600°F. The test turbine consisted of stages three and four of a five-stage 500 KW turbine and had a design flow capacity of 2.8 pounds per second at 1600°F turbine inlet temperature.

One principal objective of the program was to establish accurate fluid flow design methods for potassium turbines operating in the wet vapor region. The fluid flow design methods were verified when performance data measured during tests with potassium vapor agreed within five percent with values calculated prior to the tests.

PRECEDING PAGE BLANK NOT FILMED.

TABLE OF CONTENTS

TABLE OF CONTENTS

(Continued)

I. SUMMARY

A two-stage turbine for operation with potassium at inlet vapor temperatures up to 1600°F has been designed, fabricated and tested. These two stages represent stages 3 and 4 in a 5-stage, 500 KW conceptual turbine design for the generation of electrical power during long-time duration space missions. One major objective was the verification of fluid design and off-design calculation methods by comparing experimental performance data in potassium vapor with previously calculated performance. The fluid design was carried out and turbine blading was designed; the off-design performance of the turbine was calculated using the characteristics of this blading.

An argon efflux pressure measuring system suitable for the potassium vapor environment was developed especially for the performance test. In addition to providing inlet, exit and interstage pressures, the measuring system was utilized to measure turbine vapor flow rate in the vapor phase. The precision of the vapor flow rate measurement was demonstrated by the fact that the standard deviation of the experimental flow rate measurements from the calculated values was 0.044 pps. (The flow rate at design point rotational speed and pressure ratio was 2.2 pps at 1550°F inlet vapor temperature.)

Performance data were measured at two inlet vapor temperature levels, namely, 1550 and 1450°F and over total-to-static pressure-ratio and speed ranges of 1.4 to 4.4 and 15,400 to 20,000 rpm, respectively. The ability to design a turbine for operation with potassium vapor and to predict the off-design performance analytically was demonstrated by the close agreement

between the experimental performance and that obtained analytically. For example, the standard deviation of the experimental power output data from the analytical data was 5.8 KW. (The measured net blading power output at design speed and pressure ratio was 160 KW at 1550°F inlet temperature.) Individual data points were repeatable within 6 KW, indicating consistency in setting data points with reasonable tolerances and consistency in all pertinent instrumentation readings.

Another program objective was to evaluate performance degradation resulting from operation in a condensing potassium vapor. An endurance test of 2000 hours was completed with no change in turbine performance.

II. INTRODUCTION

In large space power systems, the radiator required for heat rejection is usually the largest and heaviest component. To minimize the radiator size, high cycle temperatures are desirable, because a surface will radiate heat in proportion to the fourth power of its temperature. For this reason, potassium and other alkali metals are attractive as Rankine cycle two-phase working fluids because they boil at moderate pressures and condense at high enough temperatures to permit the design of heat rejection radiators of reasonable size.

The turbine is a critical component of a space power system and presents the designer with a number of challenging problems. For a temperature-limited Rankine-cycle system and a given condenser temperature (or pressure), the cycle efficiency is known from elementary thermodynamics (1)* to be higher for a system in which the condition out of the boiler is nearly saturated rather than highly superheated. For a space power system these facts mean that for a given power output the radiator area will be larger for a cycle using superheated rather than nearly saturated vapor because the superheated cycle will have the higher flow rate and the latent heat per unit flow rate is the same for both cycles. As a result, high power Rankine-cycle space power systems utilize only moderate amounts of superheat, to limit the amount of moisture that will condense during the expansion process, making it necessary for at least part of the turbine expansion to occur in the wet region.

*Number in parentheses indicate references listed at the end of this report.

The operation of stages in the wet region causes losses in efficiency due to droplet drag and the occurrence of supersaturation. Turbine-blade corrosion and erosion may result when part of the expansion of the turbine is in the wet region. The damage, if any, depends upon such things as working fluid, wheel speed, blade material, temperature level, etc. (2). Blade damage limits the reliability of the turbine and eventually reduces performance.

In order to take into account supersaturation and droplet drag on turbine design, test data must be available on representative turbine stages run in the wet region. However, before such turbine stages can be designed, equilibrium thermodynamic property data and the effect of initial vapor quality on supersaturation and reversion must be known along with the polytropic expansion exponents of the working fluid. The potassium-vapor properties used are based upon experimental data obtained at the Naval Research Laboratory and are programmed on the digital computer (3). The effect of wetness on supersaturation and the polytropic expansion exponents was determined by measuring flow rates and wall pressure distributions in a converging-diverging nozzle tested in potassium vapor in the temperature range of 1450 to 1580°F and over the inlet vapor quality range of 85 to 99 percent (4).

A major contract objective was to verify a method for potassium vapor turbine design, including accurate calculation of off-design performance. In this report, the fluid dynamic design of a two-stage turbine is described and the results of the off-design performance analysis are presented. The test turbine and facility are briefly described along with some preliminary testing in steam and potassium vapor. Final performance data is presented and compared

with calculated data. The report is concluded by a discussion of the performance measured during the 2000-hour endurance test.

Another contract objective was to determine the integrity of the test turbine and determine the resistance of candidate blading materials to potassium vapor and liquid condensate. This was done in a 2000-hour endurance test. Only the fluid dynamic performance results of this test are presented in this report.

The potassium turbine design, fabrication and pretesting was carried out from 1961 through 1963. In December 1963 the facility was checked out with a convergent-divergent flow nozzle to determine polytropic exponents for the potassium vapor expansion process. Shown in Table I is a summary of turbine testing with potassium vapor.

PRECEDING PAGE BLANK NOT FILMED.

III. DESIGN

A. DESIGN REQUIREMENTS

The two-stage potassium test turbine comprises stages three and four of a five-stage 500 KW potassium turbine designed for space power applications. The five-stage turbine was designed to operate on wet potassium vapor at 1800°F inlet temperature, with a mass flow rate of 2.8 lbs. per second at a rotative speed of 19,200 rpm. The design utilizes vapor supersaturation theory with reversion to equilibrium state after each stage. The fluid dynamic characteristics of the preliminary design are briefly summarized as follows:

Stage	1	2	3	4	5
Tip Diameter, in.	7.59	8.14	8.83	9.65	10.95
Blade Height, in.	0.49	0.64	0.81	1.09	1.53
Tip Velocity, ft./sec.	636	681	739	808	916
Inlet Temperature, °F	1800	1700	1600	1495	1385
Inlet Pressure, psia	80	55.2	37.1	22.0	12.5
Inlet Quality, Percent	97.3	94.7	91.6	88.7	85.9
Nozzle Angle at Hub, °	75	75	74	73	70
Bucket Turning at Hub, °	127	127	124	121	108
Enthalpy Drop, Btu/lb.	29.1	31.2	35.5	38.5	38.2

Two stages were chosen for test so that one stage, the first, would supply vapor with natural condensate droplet distribution to the second or test stage. Stages three and four were chosen because the test facility was constructed with stainless steel which limited the maximum temperature to 1600°F.

B. DESIGN APPROACH

The design approach adopted followed steam turbine practice unless the peculiarities of the specific turbine and/or its working fluid required departures. Because of supersaturation in those steam turbine stages which operate below the saturated vapor line, supersaturation theory was used in the design of the test turbine. When supersaturated flow reverts to an equilibrium wet flow, a change in static pressure occurs due to momentum considerations. This phenomenon was accounted for in the design. The presence of moisture in a turbine stage causes a drag on the turbine blades which must be taken into account in the determination of the stage power output. Due to this effect, and the fact that the moisture tends to corrode and erode the blading, the incorporation of moisture removal devices were provided for in the design.

The velocity diagram studies were carried out on an axi-symmetric turbomachinery digital computer program. This program, which was developed for the design of gas turbines, but is similar to the one used for steam turbine design at General Electric permits the specification of arbitrary efficiency and energy extraction variations in the spanwise direction. In addition, the stream surface curvature and slope are correctly accounted for in the complete radial equilibrium equation. The vane blockage may also be varied in a spanwise direction. The program incorporates several options; among these are several design options and provisions for the determination of off-design performance.

A second digital computer program, which uses the inlet velocity vector, the blade profile coordinates, the solidity, the stagger and either the exit

flow direction or stagnation point location as input, was utilized in the design of the test turbine. This program, called the Cascade Analysis Program, solves for the velocity distribution around a blade profile in cascade. The only restrictive assumptions are incompressible and two-dimensional flow.

The following design procedure was utilized for the test turbine. Through the use of the design point values presented in Table II, an axi-symmetric solution was obtained for each stage taking into account supersaturation and reversion. In these solutions, free vortex tangential velocity distributions were assumed, as well as radially-constant total pressure and total enthalpy. Values of blading efficiencies were selected to be consistent with steam turbine practice. A total of five axial calculation stations was used for each stage resulting in two stations after each blade row. From the velocity diagrams thus generated, tentative blade profile shapes were selected from steam turbine catalogs for the hub, pitch, and tip sections of each blade row. The resulting blades were found to result in excessive dovetail fillet stresses and were modified to reduce the blade section cross-sectional area. The cascade analysis program was then used to verify the modified blade shape by generating the complete blade surface velocity distribution. Only modified blades which were shown to have a satisfactory velocity distribution were selected for the test turbine. The nozzle and bucket throat dimensions for the various blade sections were determined from empirical blading efficiency and flow coefficient data from similar blades.

C. VELOCITY DIAGRAMS

The final velocity diagrams were obtained using the flow path shown in Figure 1. Shown on the figure are the meridional stream lines for the potassium test turbine. Shown also are the coordinates of the flow path used for the final pass on the digital computer axi-symmetric turbomachinery design program. The stream line slope and curvature in the meridional plane were accounted for in the complete radial equilibrium calculation procedure. The flow curvatures along the hub are particularly gentle in order to preclude separation of the flow. Provisions for increases in the annular area through the nozzles are accommodated in the tip region where the centrifugal force on the fluid tends to make the fluid follow the flow path boundary selected.

The specifications on which the flow path depicted in Figure 1 is based are given in TableII. The turbine was designed assuming supersaturated flow in all the blade rows with reversion to the equilibrium state occurring at the inlet to each nozzle. The design was carried out between the inlet and exit pressure shown in Table II. Adjustments in the interstage pressure were made to balance the work split between the two stages.

Shown in Figure 2 are the final velocity diagrams at the tip, pitch, and hub of each stage of the potassium test turbine. The velocity diagrams indicate near impulse conditions at the hub.

Shown in Figure 3 is the radial distribution of several Mach numbers in the potassium test turbine. The hub value of the nozzle efflux Mach number was slightly under 0.9 for stage one and slightly over 0.9 for stage two.

Thus the nozzles are operating unchoked. The values of bucket relative and exit axial Mach numbers are low enough to minimize aerodynamic losses. The general level of Mach number rises somewhat from stage one to stage two.

Shown in Figure 4 is the radial distribution of reaction for the two stages of the potassium test turbine. In stage one the hub reaction is approximately 3 percent varying to approximately 32 percent at the tip. In stage two, the hub reaction is about 2.2 percent and the tip reaction is about 37.6 percent. A positive reaction was used at the hub to preclude flow separation. Another useful criterion at the hub is the acceleration of flow through the bucket as indicated by the bucket inlet and outlet angles. Shown in Figure 5 is the radial distribution of the vapor flow angles for the test turbine. Reference to the figures indicates that in stage one and two, the bucket exit vapor flow angle is 1 and 2 degrees, respectively, greater than the bucket inlet angle, indicating accelerating flow through the bucket hub.

Shown also in Figure 5 are the nozzle efflux angles for the two stages. The maximum nozzle efflux angles occur at the tip in both stages and are 77 and 75.5 degrees, respectively. High values of nozzle efflux angle were utilized in order to reduce the axial velocity level through the potassium turbine, thus increasing the blade heights to reasonable values.

The bucket turning angles for the two stages are 129.6 and 125.2 degrees, respectively. The pitch line outlet swirl angles are 28 and 25 degrees, respectively, for the two turbine stages. These moderately high values result because the stage fluid dynamic loadings are high and because of the desire to

maintain a positive hub reaction. Inasmuch as stages one and two are intermediate stages of a five-stage turbine, the level of pitch line outlet swirl angle appears reasonable.

Shown in Figure 6 are the radial distributions of axial velocity for the two stages of the test turbine. The distributions for the nozzle exit and bucket inlet have a negative slope due to the large concave inward curvatures of the streamlines at the tip compared to the hub. The distributions for the bucket and stage exit have a positive slope because of the large convex inward curvatures near the tip. The differences in axial velocity level between nozzle exit and bucket inlet and between bucket and stage exit are due to changes in radius and losses between blade rows.

D. VERIFICATION OF FROZEN EQUILIBRIUM SOLUTION

The digital computer design program which produces the velocity diagram data must be supplied with a value of the polytropic exponent which is used in the analysis of the entire stage using perfect gas aerodynamic relationships. Assuming that the values of velocity produced by the design program are correct, values of static temperature, static pressure and static specific volume were computed for the vapor assuming supersaturated flow and variable molecular weight. Shown in Figure 7 are the percent deviations of the properties obtained by use of the design program from the supersaturated property data. The maximum deviation for static temperature in either stage is 3.4 percent. Since the critical flow areas depend heavily on specific volume, the small deviations reported constituted a check upon the procedure used in the design digital computer program since the thermodynamic data of potassium was not known any closer than $\pm$ 1.2 percent when the design was laid down (1961).

E. NOZZLE PARTITIONS

It was decided that a twisted nozzle partition had several fluid-dynamic and mechanical design advantages over untwisted ones. Among these advantages are reduced unguided turning at the discharge and ease of manufacture. The final nozzle-partition profiles for stages one and two are shown in Figures 8 and 9, respectively. In both stages the nozzle-partition profiles at all radial locations are the same, but are stacked about the pressure (concave) surface trailing edge. The nozzle partition profiles have thick blunt leading edges, because they were considered less sensitive to performance changes over wide ranges of angle of attack and more resistant to moisture droplet erosion. The trailing edge thickness is 0.015 inch.

The first stage had 38 nozzle vanes with a solidity that varied from 1.7 at the hub to 1.45 at the tip. The second stage had 46 nozzle vanes with solidity varying from 1.76 at the hub to 1.47 at the tip. One half of each nozzle diaphragm was rotated through part of a space to avoid exciting the rotor blades at their natural frequency.

F. BUCKETS

Shown in Figures 10 and 11 are comparisons of the preliminary bucket blade drawings and the final configurations selected for stages one and two, respectively. Due to the fact that the blade trailing edges of the preliminary configurations for both stages overhung the bucket platform, the buckets could not be inserted into and removed from the turbine discs individually. It was necessary to insert the blades individually to permit test of rotor blades fabricated from different materials and to facilitate turbine assembly and disassembly. Therefore, a redesign of the bucket blading to remove the overhang

was required. The result was the final configurations shown in Figures 10 and 11. In the final configurations shown, a small positive clearance is provided which permits the individual insertion and removal of the buckets in each stage.

The obtaining of the final configurations of the buckets was complicated by the high hub turning angles (129.6 and 125.2 degrees, respectively, for stages one and two) required by the velocity-vector diagrams and marginal disc dovetail stresses caused by the planned test of TZM and TZC bucket blade sections.

The overhang is a direct result of the high turning angles and high solidity used. Intermediate designs indicated that reducing the bucket hub section thickness resulted in reduced bucket weight and dovetail stress but increased trailing edge overhang. Table III summarizes pertinent data concerning the preliminary and final configurations.

Shown in Figures 12 and 13 are the final hub, pitch, and tip bucket blade sections for stages one and two respectively. These blade sections were obtained indirectly through the use of the velocity-vector diagram data in the cascade analysis digital computer program. The latter program calculates the potential flow around an arbitrary cascade of airfoils specified as input. The result is the surface-velocity distribution around the airfoil. Profiles having unfavorable surface velocities distributions are modified until a satisfactory distribution results.

Shown in Figure 14 is a surface velocity distribution which is typical of those obtained for the final blade shapes. Specificially, Figure 14 is the surface velocity distribution for the hub section of the second-stage bucket.

Aside from slender cusps near the leading and trailing edges (which are merely due to discontinuities in the radii of curvature of the specified airfoil shape) the velocity distribution of Figure 14 is favorable. On the suction (convex) surface, a steady acceleration takes place until well downstream of the blade throat, where a deceleration is always expected. On the pressure (concave) surface, a steady acceleration from the 40 percent chord position to the trailing edge stagnation region assures good performance of this blade section.

Shown in Table IV are physical dimensions of the final test turbine buckets.

PRECEDING PAGE BLANK NOT FILMED.

IV. CALCULATED PERFORMANCE

A. DESIGN POINT

Shown in Figure 15 is the effect of tip clearance losses and other losses on the two-stage turbine total-to-total design-point efficiency as determined from an existing turbine efficiency computer program (TEP). The design inlet vapor temperature and vapor quality are 1600°F and 92 percent, respectively. The design total-to-total pressure ratio and speed are 2.95 and 19,200 rpm, respectively. At zero tip clearance, the calculated efficiency based upon supersaturated flow is 88 percent. Included in the losses at this condition are the velocity diagram losses, blade profile losses and the secondary flow loss. As the tip clearance increases, the calculated efficiency decreases due to the increased losses in the tip region. The methods for estimating the profile, secondary flow, and tip clearance losses are those of reference (5) At 25 mils radial clearance, the tip-clearance loss is about half of the total loss across the rotor. At 50 mils, which is the hot running clearance of the turbine rotor blades, this loss increases to about two-thirds of the total rotor loss. The tip clearance at assembly was a conservative choice, and the increased tip clearance at the elevated operating temperatures was due to differential expansion between 316 stainless steel and Udimet 700.

The design-point performance of the two-stage turbine in potassium vapor was estimated at a running or hot rotor blade clearance of 50 mils. At this point, under supersaturated conditions, the total-to-total efficiency was estimated to be 79.3 percent as shown by the upper most curve. When the ideal work is calculated from the potassium Mollier diagram at the same inlet conditions and

pressure ratio, the efficiency decreases to 74.7 percent, as shown by the middle curve. When the losses due to accelerating the liquid present to rotor speed, the efficiency becomes 70.5 percent as shown by the lower most curve. The corresponding total-to-static efficiency is 69.5 percent based on supersaturated vapor expansion, 67.2 percent based on equilibrium vapor expansion, and 63.3 percent when droplet drag losses are taken into account.

Profile losses can be reduced by making lighter loaded stages, i.e., lower ratio of specific work to the square of the blade speed. The supersaturation loss cannot be easily controlled. The loss due to the presence of moisture can be reduced by moisture extraction or the use of some superheat. In addition to reducing tip clearance, the tip clearance loss can be reduced by using rotating tip shrouds, at the cost of higher blade and disc stresses. The shrouds permit reducing the effective clearance between rotor and casing and reduce the deleterious effect of the interaction of clearance flow with the main stream.

B. OFF-DESIGN

In order to calculate predicted performance of the two-stage potassium turbine at various inlet temperatures, speeds and pressure ratios, a General Electric Co. gas turbine off-design computer program (TOD) was utilized, after modification for two-phase flow. It was assumed that supersaturated flow conditions existed throughout each stage with reversion to equilibrium occurring after each rotor. The reversion calculation is based on conservation of energy, momentum, and mass. The main results of the reversion calculation are the changes in vapor quality and temperature, with small pressure changes. The potassium properties used are those determined by the Naval Research Laboratory (NRL) (3). An example of a reversion calculation is presented in Appendix A.

For off-design calculations, incidence angle loss factors were determined assuming that only the component of the blade approach velocity parallel to the design approach direction was effective and the rest was lost. Bucket and nozzle exit flow deviation angle for each stage for all off-design cases did not vary but rather remained equal to the design values. It was further assumed that pitchline property and parameter values were representative of the average across the annulus area (6).

In order to use TOD, certain turbine fixed data input were required for all test points. Stage inlet polytropic exponent, n, was determined from each stage inlet condition of total temperature and vapor quality, x, using the relationship

$$n = n_{sat} - 1.13\ (1 - x)$$

where n_{sat} is the saturated polytropic exponent (3) computed from the NRL properties and 1.13 is the experimental constant derived from the convergent-divergent potassium nozzle tests performed under this contract (4). The gas constant which is also required as fixed input for each case is derived from the perfect gas law using turbine inlet conditions of total temperature and pressure and specific volume. Actual hardware dimensions such as hub and pitchline diameters were included. Inspection reports were used to obtain actual bucket angles and flow areas. From the nozzle flow test data, discussed under PRELIMINARY TESTS, effective flow area for each nozzle diaphragm was determined. The nozzle flow coefficients were set equal to 1.0 and the nozzle exit angles were adjusted so as to result in the effective flow area found during the flow tests of the diaphragms.

As indicated above, the TEP was used to estimate the level of predicted performance of the test turbine at approximately design conditions, namely, 19,200 rpm, 1600°F, 92 percent inlet vapor quality and a total-to-total pressure ratio of 2.95. The results of the TEP were used to determine the values of zero-incidence nozzle and bucket efficiencies for each stage to be used in TOD.

Shown in Table V is a comparison of the results of the TEP and TOD programs at approximately design conditions. The Turbine Efficiency Program (TEP) is a design program, based on Ainley and Mathieson (5), which calculates the turbine geometry and loss factors for given flow and work requirements. The Turbine Off Design program calculates the flow and work that would be obtained with a given geometry and loss factors. Therefore, an iterative procedure is required for exact matching of the results of the two programs.

It can be seen in Table V that the flow velocities and flow angles agree very well between the results of the two programs. The overall turbine total-to-total efficiency agrees within 1.5 percentage points between the two methods. The slight difference is attributed to differences in calculation procedures and in loss factors between the final runs of these programs.

The results of TOD were used as input for the Turbine Performance Parameter (TPP) digital computer program to obtain predicted values of turbine efficiency, turbine work and the corrected performance parameters. In the TPP program, turbine work is corrected for droplet drag losses which are determined by assuming that the moisture entering each stage must be accelerated to pitchline wheel speed upon entering the rotor. Turbine efficiency is then calculated using the values of flow and specific work output (after the droplet drag loss correction) for each stage. The ideal power is based on the total turbine flow and the isentropic enthalpy drop from the NRL wet properties (3).

The calculation procedure used to determine droplet drag losses, turbine actual specific work output and turbine efficiency are as follows:

$$\Delta h_d = \frac{(1-X_1)\ U_{P1}^2}{g\ J} + \frac{(1-X_2)\ U_{P2}^3}{g\ J}$$

$$\Delta h_a = X_1\ \Delta h_1 + X_2\ \Delta h_2 - \Delta h_d$$

$$\eta_t = \frac{\Delta h_a}{\Delta h'}$$

where

g	gravitational constant, 32.2 ft/sec^2
Δh	stage work, Btu/lb.
$\Delta h'$	ideal enthalpy change, Btu/lb.
Δh_d	enthalpy loss due to droplet drag, Btu/lb.
J	Joule's constant, 778 ft. lb/Btu
U_p	rotor pitch line speed, ft/sec
X	quality
η_t	turbine efficiency

subscripts

a	actual
1	first stage
2	second stage

C. OFF-DESIGN PERFORMANCE

Using the calculation methods described in the previous section, off-design performance was calculated for the turbine at the conditions of the planned performance test. These included a range of rotative speeds and turbine pressure ratios at inlet vapor temperatures of 1450 and 1550°F.

Shown in Figure 16 is the variation of calculated turbine power output with turbine total-to-static pressure ratio for a vapor inlet temperature of 1450°F. A similar plot for 1550°F inlet temperature is shown in Figure 17. These data are for 99 percent vapor quality at turbine inlet. The variation with rotative speed is seen to be quite small.

Shown in Figures 18 and 19 are the variation of calculated vapor flow rate as a function of turbine total-to-static pressure ratio for turbine inlet temperatures of 1450 and 1550°F, respectively. It can be seen that there is little flow variation with turbine speed and that the flow is constant for pressure ratios greater than about 3.3.

Shown in Figures 20 and 21 are the variation of calculated total-to-static turbine efficiency with total-to-static turbine pressure ratio and rotative speed for turbine inlet temperature of 1450 and 1550°F, respectively. The efficiency peaks at a pressure ratio of 2.25 at 20,000 rpm and at lower pressure ratios at lower rotative speeds. The off-design turbine performance data presented in reference (7) is from the same computer run as the data presented herein, however, the latter data is presented in a slightly different form. Turbine performance is presented as a function of total-to-static pressure ratio because it is felt that this is a more meaningful parameter than total-to-total pressure ratio for space powerplants.

V. TEST APPARATUS

A. TEST TURBINE AND REAR TRAIN

In the mechanical design of the test turbine, it was decided to isolate the problem of potassium turbine performance from other complicated space-power-turbine problems. As a result, the turbine was designed for operation on oil-lubricated bearings. Buckets were dovetailed to each disc to provide an easy method for removing and replacing blades, and for test of multiple rotor blade materials. The requirement for obtaining detailed turbine performance data required making provisions for interstage as well as inlet and outlet thermocouples and pressure taps.

Shown in Figure 22 is a cross-sectional drawing of the two-stage potassium turbine and starting system assembled for performance test. The potassium vapor enters from the left, flows around a bullet nose into an annulus, and then into the first-stage nozzle diaphragm. After leaving the second row of buckets, the potassium vapor flows through an outlet guide vane and into a scroll and discharges through the test floor. The present configuration, which is an overhung design, was chosen over a straddle mounted design becuase it eliminates a bearing and seal on the high-temperature, high-pressure end. Just aft of the last stage of the turbine is a pivoted-pad bearing lubricated with Mobil Socony DTE 797 oil. The thrust bearing consists of a preloaded duplex ball bearing shown at the right-hand side of the figure. Between the second stage and the pivoted-pad bearing there is a combination hydrodynamic seal, which consists of a rotating channel surrounding a stationary disc, is supplied with potassium liquid at 250°F. The buffer seal, consisting of two labyrinths with argon gas

injected between them, is between the hydrodynamic seal and the pivoted-pad bearing. Part of the argon gas flows out of the hydrodynamic seal with the potassium liquid and part of the argon flows across the second labyrinth into the bearing housing. The hydrodynamic and buffer seal permits a pressure differential up to about 25 psi to be maintained between the second-stage exit and the pivoted-pad bearing. The turbine rotor is made up of two discs and a stub shaft connected by means of curvic couplings and held together by a single centrally-located tie bolt. This tie bolt is prestressed to a tension of 10,000 lbs. during assembly of the turbine rotor.

A water brake for absorbing the energy output of the test turbine is mounted aft of the turbine. A steam turbine is connected to the test turbine shaft aft of the water brake to drive the test turbine to about 10,000 rpm at which speed the hydrodynamic seal can be established, maintaining the required pressure differential between the second-stage exit potassium vapor and the pivoted-pad bearing oil lubricant.

As indicated earlier, dovetail connections are used to attach the rotor blades to the discs, thus permitting the insertion of rotor blades fabricated from various types of material in the endurance test so that a relative evaluation of the impact erosion and chemical corrosion resistance can be obtained.

Because of the instrumentation internal to the turbine, which will be described below, it was decided to use a horizontally-split casing. Both the circumferential and horizontal flanges of the turbine are welded. The tip seals for each of the bucket rows and the interstage seal are made of unfilled abradable honeycomb 316 stainless steel material. Shown in Figure 23 is the

installation of the potassium test turbine in the turbine test facility. The turbine is surrounded by an environmental chamber which provides a cover of argon gas around the turbine casing, and instrumentation leads coming from the casing. The major purpose served by the environmental chamber is to prevent air from entering the turbine at subatmospheric pressures in the event of a potassium leak.

B. INSTRUMENTATION

1. Performance Test Instrumentation

Shown in Figure 24 is a schematic diagram showing the test turbine performance instrumentation stations. For overall performance, the primary stations are 1, 3, 7 and 8. Stations 4, 5 and 6 in the figure are internal to the turbine and are useful in finding load distribution and stage reaction. Shown in Figures 25 and 26 are schematic diagrams showing the location and number of sensors in each of the instrumentation station. Station 2, which is associated with the liquid injector, has been retained because the injector itself is still fitted. However, this injector was not used after the initial performance testing. The details of the instrumentation at each of these instrumentation stations are delineated in Figure 27.

Delineated in Table VI is the instrumentation used for the determination of performance of the potassium turbine. Shown in the table are the parameters measured, the location, range, type of sensor and readout. Shown in Table VII is a list of the instruments continuously recorded during performance testing. The instruments listed in this table were used to establish test points, study transients if they occurred, and monitor measurements essential to the safety

of the test turbine during performance testing. The turbine inlet pressure, which ranges from 10 to 35 psia on the Sanborn, was set for each test point by reference to Channel B-5. The pressure ratio across the turbine was established from Channel B-6, which records the total pressure differential between stations 3 and 7. This channel measures differential pressure in the range 0 to 25 psig. The pressure ratio depends upon the setting of a condenser pressure. This pressure was read on Channel C-4, which was connected to the Taylor gage at station 8.

Turbine efficiency was calculated as the ratio of actual turbine work to ideal work. Actual turbine work was calculated from measured values of torque, flow rate and rotative speed. Ideal turbine work was calculated using measured values of inlet and exit pressure and inlet quality.

The inlet and exit pressures of the test turbine were obtained from the static and total head tubes which are part of the efflux measuring system and are located at stations 3 and 7. The efflux pressure measuring system is described in Appendix B.

Turbine vapor flow rate was measured with an instrumented and calibrated inlet bullet nose annulus (cross section A in Figure 27). A differential pressure transducer connects a total head tube and a static tap (items 20-24 in Table VI), permitting the measurement of total to static pressure differential in the bullet nose annulus. The effective area of the bullet nose annulus was determined from testing with air.

The torque measuring system consists of two temperature-compensated, strain-gaged torque meters. One of these connects the casing of the water

brake to the turbine casing through an extension of the environmental chamber and measures the reaction torque of the water brake. The other torque meter connects the casing of the steam turbine to the casing of the potassium turbine and measures the reaction torque of the steam turbine. The parasitic torques of the bearings and seals are determined by driving the water brake and potassium turbine with the steam turbine with no potassium vapor flowing in the test turbine.

Although the inlet and exit conditions of the turbine are obtained from pressure measurements, temperature measurements are also necessary in order to calculate efficiency. Shown in Figure 28 is a throttling calorimeter which takes a sample of potassium vapor at station 1. The temperature and pressure of the vapor sample must be measured after throttling so that the inlet enthalpy can be determined. The pressure is measured by means of the efflux system and the temperature is measured with a chromel-alumel thermocouple. The reference temperature for all of the thermocouples including the calorimeter is measured by means of a thermister in the copper alloy thermal sink (CATS). In addition, thermocouples at stations 1, 3, 7 and 8 are utilized to validate static pressures measured with the efflux system at these same stations. This is done by calculating the vapor pressure which corresponds to the measured temperature.

The speed of the turbine is measured by means of a DC generator actuated by a six tooth gear on the turbine shaft. The generator output is a voltage proportional to the speed of the turbine. This device is calibrated against a Berkeley counter.

An error analysis was made using the data reduction program to determine the percentage change in calculated turbine efficiency for a one percent variation in the input parameters. Shown in Table VIII are the estimated accuracies of the measurements which enter into the calculation of turbine efficiency and their influence coefficients. These influence coefficients are ratios of the percentage change in turbine efficiency for a one percent change in the parameter. Negative values mean that calculated turbine efficiency is low when the parameter is in error on the high side. These ratios of turbine efficiency change to the change in parameter were calculated at design pressure ratio and speed for turbine vapor inlet temperatures of 1450 and 1550°F.

The estimated measurement accuracies and influence coefficients were applied to typical data points and a probable error was calculated as the square root of the sum of the squares of the errors due to each measurement. This probable error in turbine efficiency was calculated to be 2.85 percent for the 1550°F case and 3.8 percent for the 1450°F case.

In this test, much of the instrumentation involved is intended to monitor operation of the mechanical system to insure safe operation, and identify its dynamic characteristics. The rotor dynamic and critical speeds are sensed by accelerometers and velocity pickups located within the potassium turbine and on the rear of the run-up turbine as shown in Figure 29.

Figure 29 also shows the several temperatures on the test rig which are both monitored and recorded during running. These comprise bearing temperatures for each of the test rig components.

Temperatures are measured in the two bearings of the test turbine as shown below.

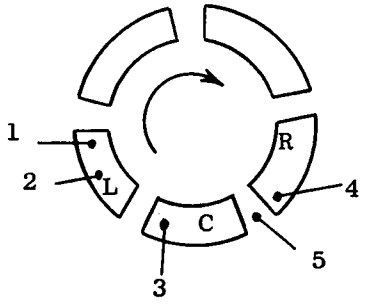

Pivoted-pad Bearing

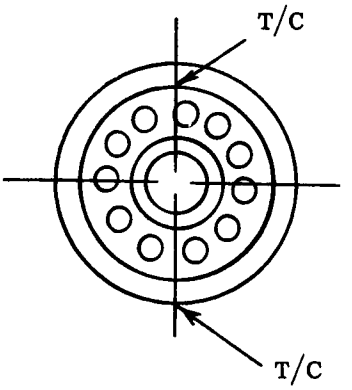

Ball Thrust Bearing

A large number of additional measurements, as delineated in Table VI, are made on the various pieces of readout during performance testing.

2. Endurance Test Instrumentation

In order to eliminate a source of argon, in which minute quantities of oxygen and water vapor may be present, to the turbine during endurance testing, no efflux pressure measuring devices were used. Limp-diaphragm pressure transducers were used at station 1, 7 and 8 (See Figure 30) and in the throttling calorimeter. The bullet-nose annulus instrumentation could not be used for flow rate measurement, therefore, the EM flow meter was used.

Shown in Table IX is the instrumentation which was used on the test turbir for endurance testing. The parameters read on the continuous recorders are shown in Table X. The instrumentation on the turbine is shown in Figure 30. Shown also in this figure are the borescope apertures which permit visual inspection of the turbine blading without disassembly when it is shut down.

C. TEST FACILITY

Shown in Figure 31 is an isometric sketch of the turbine test facility. The natural circulation boiler is on the left. It has a natural gas-heated fire box containing twenty-four flat-flame burners. Heat is transferred to the 174 element tube bundle by radiation. The tubes are welded between a 20-inch outside diameter upper drum and an 8 5/8-inch outside diameter lower drum, each in excess of 25 feet in length. Four 4 1/2-inch outside diameter downcomers also connect the upper and lower drums. Not shown is an 8-inch diameter pipe between the upper and lower drums which contains 200 lbs of zirconium sheet for hot trapping. Also not shown is a centrifugal separator which was installed at the boiler outlet to minimize liquid carryover.

The air-cooled condenser hangs from the test turbine dolly as can be seen in Figure 31. It consists of 84 finned-tubes arranged in two banks. The air enters the condenser fore and aft, so as to cancel tube-bundle air-drag forces, and discharges on the far side. The lower drum which contains 150 lbs of titanium foil hot trapping material is approximately 8-feet long and has an inside diameter of 20 inches. For the removal of argon gas from the potassium vapor, the condenser has a vertical packed column through which potassium liquid at 250°F circulates at the rate of 10 gpm. The argon gas is removed by means of a vacuum system.

The helical induction electromagnetic pump, shown on the floor in Figure 31, between the boiler and condenser, takes the condensate from the condenser and pumps it into the boiler. At 1400°F the rated head of the pump is 150 psi and the rated flow is 42 gpm. The pump is followed in the flow circuit by an electromagnetic flow meter which measures the amount of liquid leaving the condenser.

The normal EMFM inlet tube temperature was from 500 to 1000°F and the flow rate from 10 to 25 gpm.

In addition to the main loop the turbine test facility has eight sub-loops. The argon extraction system removes argon which enters the facility from the seal or pressure instrumentation. The argon reclamation system removes oil and potassium that is carried with the argon from the potassium-to-oil seal. The low-pressure lubricating oil system supplies oil to the turbine water brake and steam turbine. The high-pressure lubricating system supplies oil to the test turbine bearings. There is a water system for the water brake and a steam system for the steam turbine. A vacuum system is needed to evacuate the argon gas from the loop before startup. Finally there is a sub-loop to supply the hydrodynamic seal with liquid potassium.

Shown in Figure 32 is a exterior view of the turbine test facility. The equipment in the foreground is the vapor scrubber system which maintains a flow of cooling air through the test cell and is used to wash the potassium oxide from the cooling air in the event of potassium leaks in the test cell o boiler. The 3000-KW (thermal) gas-fired boiler is shown at the right-hand side of the figure. The condenser cooling air discharge is also shown.

The turbine test facility is constructed of Type 316 stainless steel whi has a practical maximum material temperature of 1600°F, and limits the potass vapor temperature to about 1550°F. Vapor at a quality in excess of 98 percen as measured by a throttling calorimeter, can be expected out of the boiler. The air-cooled condenser has the capacity to provide an exit pressure of abou 1.5 psia, corresponding to a vapor temperature of 1040°F.

PRECEDING PAGE BLANK NOT FILMED.

VI. PRELIMINARY TESTS

A. STEAM PRE-TESTING

The turbine was run with steam to check out the operation of the performance instrumentation, particularly the efflux pressure measurement system, and the liquid spray equipment, which was used to provide various values of inlet vapor quality.

Test points were set from control room readout instruments, which included a Sanborn recorder for inlet pressure and steam flow orifice pressure difference, a Berkeley counter for rotative speed and spray liquid flow rate. Additional measurements, which were needed to control the tests and to insure safety, were monitored on Sanborn recorders.

Performance data recording was accomplished by the use of a digital data handling system, and later Sanborn recorders. The digital system has in use 76 channels which measured inlet, exit, and interstage pressures and temperatures, calorimeter temperature and pressure, injector spray mass flow rate, injector spray temperature and pressure, torque, flow and speed. Pressures were obtained from a modified efflux system. This system had a solenoid-operated, ganged fluid switch for stopping the argon flow prior to scanning the pressure readings by means of the digital data handling system.

The liquid spray system, the efflux pressure measurement system and the digital data handling system all functioned satisfactorily. The major objectives of steam pre-testing, operational checkout of the turbine and instrumentation, were achieved. The results of steam testing were presented in reference (8).

B. NOZZLE DIAPHRAGM FLOW CHECK

Knowledge of the exit effective flow areas of the two-stage potassium test turbine nozzle diaphragms was required for the estimation of turbine off-design performance, as indicated above. Therefore, each nozzle diaphragm was tested in dry air making use of the Flow Analysis Calibration Test Stand (FACT) to determine the effective area.

A complete list of the instrumentation, including type of sensor and range, is presented in Table XI. The flow rate was determined with a 2.25-inch diameter calibrated ASME flow nozzle. During testing, the experimental data were obtained through the use of a digital data handling system.

All tests were carried out with the respective nozzle diaphragms choked. The air dew point for all test points was as shown on Table XII. In order that the Reynolds Number effect, if any, be determined, each diaphragm was tested at inlet pressures of 40, 50 and 60 psia. Five scans by the digital data handling system were made for each test point to establish the degree of repeatability and to reduce random errors through averaging.

The data resulting from the test are summarized in Table XII. The results are plotted against the Reynolds Number in Figure 33. The characteristic dimension is the mean distance between nozzle diaphragm partitions in a plane perpendicular to the flow direction at the exit. The calculated discharge areas for the three test pressures were within 0.17 percent of the mean. Thus, no Reynolds Number effect is discernible. The first-stage nozzle diaphragm discharge area obtained from averaging all fifteen data points is 6.217 square inches compared to the design value of 5.558. This 10.6 percent increase in discharge area over the design value can be accounted for by a

proportionally larger nozzle partition spacing, than the design value. The second-stage nozzle diaphragm discharge area obtained from averaging all 15 data points is 8.213 square inches, which is 2.2 percent less than the design value of 8.4 square inches. The larger first stage nozzle area causes the second stage to do more of the work with a reduction in turbine efficiency of about one point.

C. PRELIMINARY TESTING

On July 13, 1964, six turbine test points were obtained. The experimental data were presented in reference (9). Reliable pressure readings were obtained at each instrumentation station. Unstable facility boiler operation made it impossible to control turbine rotational speed within reasonable limits, e.g., $\pm$ 250 rpm.

Potassium performance test data were obtained on the two-stage turbine on September 28, 29 and 30 and October 2, 4 and 8, 1964. In the six days of testing, all of the test points for 1450 and 1550°F were run. The data were taken despite the fact that the facility boiler was unstable under some operating conditions, causing severe speed excursions (e.g., 15,000 to 3,000 rpm and acceleration to 15,000 rpm in 4 to 7 seconds.). The measured turbine performance was not good because steady state conditions were not achieved and because instrumentation leaks and subsequent potassium fires damaged portions of the turbine. Despite the quality of the data the turbine demonstrated mechanical integrity by its ability to endure numerous violent speed excursions.

At 1450°F turbine inlet temperature, the speed was found to be the most stable when the main throttle valve was nearly closed causing a decrease in vapor temperature across the valve from 1550°F to 1450°F. At 1550°F, no

throttling was possible across the main vapor valve. As a result, testing was carried out by first achieving a turbine inlet vapor temperature of 1550°F and then cutting boiler firing rate to 20-25 percent of maximum just long enough to make four data scans with the digital data handling system. After about 10 to 12 hours of boiler operation, however, stability was improved enough to permit taking data without reducing the firing rate of the boiler periodically.

1. Transient Measurements

Instrumentation was installed in the facility to determine causal relationships during unstable operating conditions. All transient measurements were recorded on four continuous recorders. The quantities recorded on the respective recorders are shown in Table XIII.

Shown in Figure 34 are a series of traces which show typical speed excursions. Turbine operation is self sustaining and water has been admitted to the water brake. Immediately the speed began to oscillate. Part a shows that as the speed decreased, torque rose. There is an indication of steam turbine vibrations as the speed dropped.

During the 33rd minute, the turbine experienced the first abrupt deceleration. The speed dropped from 17,000 to 5,000 in two seconds. The torque trace also had a minimum value coincident with the minimum speed. Delayed responses are to be noted for the pad bearing and aft bearing temperatures, pad bearing lube flow and the ball bearing lube flow. Also, the potassium side of the turbine seal, turbine inlet pressure and condenser pressure decreased. Bullet nose velocity showed a reversal in flow.

During the 39th minute, a series of three abrupt decelerations of the turbine occurred, which followed the same pattern as the previous surge. Note particularly that boiler feed pressure dropped immediately prior to the speed surge but began to rise before the sharp decrease in speed occurred. The flow reversal indication in the bullet nose occurred slightly before or simultaneously with the speed surge. Condenser pressure was approximately 7 psi, just prior to the three speed surges. The condenser pressure rose after each of the first two speed surges, but showed a dip during the third. For the three speed dips, there were corresponding turbine inlet temperature rises and in turn, these corresponded to three rises in turbine inlet pressure of about 2 psi. The boiler feed pressure rise was also approximately 2 psi. Turbine inlet temperature before the three speed dips was approximately 1427°F.

Various operational techniques were used in attempts to achieve stable operation. These included manual control of the boiler feed, partial closing of the main vapor throttle valve, reduced firing rate of the boiler, and control of the boiler liquid level. Although most of these techniques had some effect on the stability of the system, the most effective was control of the boiler liquid level. The relationship between liquid level and speed instability was noted during testing in March, 1965 and steady speed control was achieved by holding the liquid level to about 3 or 4 inches above the bottom of the boiler vapor drum.

2. Preliminary Performance Measurements

During September and October, 1964, about 45 hours of performance testing were carried out and the performance data are tabulated in reference (7). The

values of parasitic torque of the bearings and seals as a function of speed, which were added to the measured torque to calculate the output of the turbine blading, are shown in Figure 35.

Shown in Figures 36 and 37 are the variations of total-to-total turbine efficiency with rotative speed, for total pressure ratios of 2.1 and 3.2, respectively. The curves represent calculated performance and the symbols represent measured data. These plots show that the measured data is about 20-30 points lower in efficiency than the calculated performance. This is consistent with the test data for 1550°F inlet vapor temperature.

Shown in Figure 38 is a similar plot of total efficiency versus speed for a total pressure ratio of 3.6 ± 0.1. There is a very significant difference in this plot, namely, that some of the test data points agree with predicted performance. The shaded symbols represent data points taken on October 8, 1964, the date on which most of the test data were taken. They show the same discrepancy of 15-20 points in efficiency between predicted and test performance as shown in Figures 36 and 37. The unshaded symbols represent data points taken on October 4, 1964 and prior to that date. These data fall around the calculated curve.

On four occasions, there were potassium leaks due to failures of instrumentation lines at the turbine casing. The fires resulting from the contact of hot potassium with air were minor, although the fire on October 4, 1964 was somewhat greater than the previous ones. After each incident, the faulty instrumentation lines were repaired and testing was resumed. Subsequent disassembly of the turbine revealed that significant damage had been done to the turbine flow passage.

The fire on October 4, 1964 occurred at the condensate drain and caused considerable damage to the second stage nozzle diaphragm. Air was drawn into the turbine at the bottom of the casing causing the potassium to burn through the second-stage nozzle-diaphragm outer band. The potassium also burned 0.25 inch pieces off the trailing edge (length 0.985 in.) of each of the five nozzle diaphragm partitions near the hub. More serious was the loss of about five inches around the periphery of the second stage tip seal, resulting in an average increase in tip clearance of 32 mils. Inspection at the end of the test also revealed extensive erosion and/or corrosion damage to the first stage buckets, resulting in sharp leading edges. The turbine performance apparently was adversely affected by the loss of parts of the nozzle diaphragm, the tip seal and the sharp leading edges of the first stage buckets. Other damage consisted of mechanical erosion and/or chemical corrosion of nozzle diaphragm partitions and the second stage buckets. The considerable damage sustained by the turbine, presumably on October 4, accounts for a large part of the performance degradation measured during this test.

PRECEDING PAGE BLANK NOT FILMED.

VII. PERFORMANCE TEST

Prior to the final performance test all damage sustained by the turbine was repaired and it was reassembled. In addition, a number of changes were made in the test facility to reduce the possibility of unstable operation. These are described in the turbine test facility topical report, number 23 in the Bibliography. Procedures were devised to insure better control of the test. The most important of these was the identification of tolerance limits for each test variable including rotational speed which permitted determining quickly whether a given data point was good. If the data point was not within established tolerances, it was repeated immediately.

A. PARASITIC TORQUE TEST

Prior to the performance testing the water brake was driven by the steam turbine with the potassium turbine disconnected to check that the two torque meters indicated the same torque, and that they came to zero at static conditions. This was done to insure that no torque is transmitted through the flexible hoses to the water brake and steam turbine. Shown in Figure 39 are the results of this test on May 5, 1965. The plot indicates that the two torque meters are reading the same torque, including the zero reading, within 5 in. lb.

Because of the requirement to perfect fluid dynamic design and performance calculation methods, the power output of the turbine blading is sought during performance testing. Therefore, the parasitic torque contributed by the turbine bearings and the hydrodynamic seal must be obtained. The sum of measured shaft output torque and parasitic torque equals the torque output of the turbine

blading. The parasitic torque is determined by carrying out a parasitic torque test prior to a performance test. The parasitic torque is the difference between the steam turbine and water brake torque meter values when driving the test-turbine shaft, including the water brake, with the steam turbine. During parasitic torque testing water-brake seal flow, lube oil flow and inlet temperature, and turbine hydrodynamic seal flow and inlet potassium temperature were carefully controlled to the values expected during performance testing. The test turbine was run with argon in the facility. By running constant speed tests at three or more levels of argon pressure, data like that shown in Figure 40 is obtained where the parasitic torque at different rotational speeds is plotted against argon density. The argon causes windage losses during parasitic testing which are a function of argon density. If the test data is extrapolated to zero density, the windage torque on the test turbine blades is zero and the remaining torque is the sought for bearing and seal parasitic torque at the rotative speeds used. These bearing and seal torque values are plotted in Figure 41.

These data define a parasitic torque curve which may be represented by the equation

$$Q_{pt} = 0.00583N$$

where

Q_{pt} = Parasitic torque, in. lb.

N = Rotative speed, rpm.

Shown for comparison are similar data obtained March 17 to 23, 1965. The test data for the two series of tests compare favorably. The data given by the line were used in the reduction of the turbine performance data obtained May 19 to 21, 1965 and presented herein.

B. INSTRUMENTATION VALIDATION

Before considering the performance data the validity of some of the important measurements will be established. The instrumentation stations are shown in Figure 24.

Shown in Figure 42 are comparisons of measured pressure and temperature at station 1, upstream of the turbine. On the ordinate is the pressure measured by the efflux system and on the abscissa is the vapor pressure of potassium at the measured temperature. The good correlation lends credence to the measurements. Shown in Figure 43 are comparisons of measured pressure and temperature at station 3, the turbine inlet. The ordinate and abscissa are similar to those of Figure 42. The 1.0 psi deviation of the measured pressure from the vapor pressure corresponds to 7.5 to 11°F temperature error, for 1550 and 1450°F, respectively. Although the error could be in either the pressure or temperature measurement or both, since the calibration data for the transducers and readout system have at most an error in repeatability of 0.08 psi and zero shift of 0.15 psi, it is more likely that it is a thermocouple error. There was only one thermocouple at station 3 and it indicated virtually the same temperature as at station 1. However, since the flow area is smaller at station 3 than at station 1, a higher velocity, corresponding to a lower static pressure, and possibly lower temperature than station 1 would be expected at station 3.

Shown in Figure 44 is the variation of station 7 static pressure with the vapor pressure. At the highest pressures shown the measured and vapor pressures correspond. At the lowest pressures shown the measured pressure is substantially above the vapor pressure. It is difficult to identify what temperature is measured by a thermocouple in high velocity two phase flow. At station 3,

where the temperature appears to be high, it could be argued that a stagnation temperature was measured. At station 7, where the temperature appears to be low, a different explanation is needed. The discrepancy appears to be a function of turbine pressure ratio or Mach number. One hypothesis was based on the fact that the pressure distribution around a cylinder in crossflow can result in an average static pressure lower than the free stream static pressure, and therefore, a lower temperature might be measured. However, at the greater turbine pressure ratios there was a discrepancy of up to 50°F between the measured temperature at station 7 and the equilibrium vapor temperature based on an integrated surface pressure distribution around the thermocouple.

Another hypothesis is that there may be some supersaturation at station 7 for the larger turbine pressure ratios. Shown in Figure 45 is the ratio of a measured to vapor pressure (degree of supersaturation) plotted against the turbine total-to-static pressure ratio. For the two values of turbine inlet temperature the degrees of supersaturation agree at the same turbine pressure ratios, indicating that some supersaturation may occur at station 7.

Shown in Figure 46 is the variation of the static pressure at station 8 with the vapor pressure at the same station. The correlation is good and indicates no measurable supersaturation. The amount of argon from the efflux pressure measuring devices carried along with the vapor gas stream is at least as large at station 8 as it is at station 7, precluding the possibility that the measured pressure at station 7 is the sum of the partial pressures of argon and potassium while the temperature indicates the vapor pressure only.

C. PERFORMANCE DATA

The performance testing program was carried out from May 19 through May 21, 1965. Performance data were taken at vapor inlet temperatures of 1450 and 1550°F, six total-to-static pressure ratios from 1.4 to 4.4, and six rotative speeds from 15,400 to 20,000 rpm. At each test point the data were checked immediately to confirm that the desired condition had been obtained within the specified tolerances on speed, inlet and exit pressures. This concurrent data checking, together with stable operation of the facility and improved operational techniques, resulted in a well controlled performance test. One third of the data points, namely, at total-to-static pressure ratios of 1.4 and 3.3, were taken a second time to determine whether the performance data were repeatable.

Using the parasitic torque data of Figure 41, the performance data were processed on the digital computer. The results from the data reduction program are presented in reference (10). Shown in Figures 47 through 52 is the variation of turbine power output with pressure ratio and rotative speed at a turbine inlet temperature of 1450°F. The symbols indicate the test points taken on three different days. The solid lines indicate the performance which had been calculated prior to the test and which was presented previously in this report. The measured data are in good agreement with the calculated performance. The 1450°F data have a standard deviation from calculated of 3.8 KW. Similar data is presented in Figures 53 through 58 for an inlet temperature of 1550°F. For this temperature the standard deviation from calculated performance is 7.7 KW. The repeatability of the data is usually within 3 KW for both temperatures. At 1450°F and a pressure ratio of 3.3 the

measured power increased from about 93 KW at 15,400 rpm to about 98 KW at 20,000 rpm. At 1550°F the power increased from 150 to 160 KW for the same pressure ratio and speed range.

Shown in Figures 59 through 64 is the variation of flow rate with pressure ratio and rotative speed for an inlet temperature of 1450°F. Similar data for an inlet temperature of 1550°F is shown in Figures 65 through 70. These mass flow rates were calculated from the measurement of the difference between the total and the static pressures in the turbine inlet annulus and previously calibrated in air (11). The measured flow rate is seen to agree well with the calculated data. The standard deviation of the experimental data from the calculated data for an inlet temperature of 1450°F is 0.042 pps. The same value for 1550°F is 0.045 pps. The data is usually repeatable to within 0.07 pps but always within 0.10 pps. Turbine speed had practically no effect on flow rate in the speed range of these tests.

Shown in Figures 71 through 76 is the variation of turbine total-to-static efficiency with total-to-static pressure ratio and rotative speed for an inlet temperature of 1450°F. Similar data for an inlet temperature of 1550°F is presented in Figures 77 through 82. The turbine efficiency can be seen to agree well with the calculated values in the low-pressure ratio ranges in spite of the steep slope. At the higher pressure ratios, however, the measured efficiency is above the calculated value. The standard deviation of the experimental points from the calculated values at the same test conditions is 4.0 percentage points for 1450°F and 4.6 percentage points for 1550°F. The repeatability averages 4 percentage points. At a pressure ratio of 3.3, the efficiency increased from 0.65 at 15,400 to 0.70 at 20,000 rpm

for both 1450 and 1550°F inlet temperatures. This change in efficiency with speed is reflected in the variation in turbine power discussed previously; the flow rate is practically constant in this speed range at a given temperature and pressure ratio.

The highest measured total-to-static efficiency was 0.75 and occurred at 17,300 rpm, at a total-to-static pressure ratio of 2.0 at both 1450 and 1550°F inlet temperature. The turbine efficiency could be improved by designing for less work in each stage and by controlling the tip clearance loss by reducing tip clearances and providing bucket covers.

PRECEDING PAGE BLANK NOT FILMED.

VIII. ENDURANCE TESTING

A. ENDURANCE TEST POINT

It was necessary to determine the probable wheel operating temperatures for prospective endurance test conditions so that it could be established at which conditions the design life of the turbine was not exceeded. Shown in Figure 83 is the variation in wheel temperature with rotative speed assuming the wheels were at the saturation temperature of the vapor corresponding to the measured static pressure immediately upstream of the wheels during performance testing. The temperatures are shown for both stages, a range of values of total-to-total pressure ratio and three turbine inlet temperatures, namely, 1450, 1500, and 1500°F. Based upon the measured data for 1450 and 1550°F inlet vapor temperatures, the wheel temperatures for an inlet temperature of 1500°F were calculated. Shown in Figure 84 is the variation of the allowable turbine inlet temperature for a range of rotative speeds and for both the first and second stage. The curves are based upon wheel dovetail stresses, which are limiting, assuming TZM and TZC refractory blades in the second stage and U-700 blades in the first stage. The allowable stress used was 90 percent of the rupture stress for the temperature shown. The data from Figure 83 were used to indicate operating conditions at inlet temperatures of 1450, 1500, and 1550°F and at several turbine pressure ratios. Figure 84 was prepared assuming a 2000-hour endurance test. Indications from the figure are that at the selected turbine inlet temperature, 1500°F, rotative speeds up to 19,250 are permissible at an inlet total-to-exit total pressure ratio of 2.95 and above and that at those conditions the first stage is limiting. Because of more favorable vibratory characteristics of the turbine and load train established during performance testing at speeds around 18,250 rpm, that speed was selected instead of 19,250 rpm.

Shown in Figure 85 is the variation of second-stage inlet vapor quality calculated for an inlet vapor temperature, inlet vapor quality, and rotative speed of 1500°F, 99 percent, and 18,250 rpm, respectively, as a function of total-to-total pressure ratio. At the design pressure ratio the vapor quality into the second stage was calculated to be 0.959 or about 96 percent and was close to the minimum. Thus for an endurance test where the maximum amount of liquid in the vapor is desired, the design pressure ratio is quite satisfactory.

Shown in Figure 86 is the experimentally determined turbine inlet vapor quality plotted against measured turbine flow rate obtained during the recent performance test at 1550°F. All of these data were obtained without throttling the vapor upstream of the turbine. Based upon the experimental flow rates at a total-to-total pressure ratio and rotative speed of 2.95 and 18,300 rpm, respectively, for temperatures of 1450 and 1550°F (1.44 and 2.22 pps, respectively) the calculated flow rate during endurance testing is 1.80 pps. Reference to Figure 86 indicates that the inlet vapor quality at a flow of 1.80 pps should be about 0.998. Shown in Figure 87 is a calculated velocity diagram for the endurance test condition. The second stage inlet quality is estimated to be 0.967 rather than 0.959 because the inlet quality is higher than 99 percent.

Since no total pressures are measured during endurance testing, the selected endurance test condition must be converted to static pressures, especially at the exit. Shown in Figure 88 is the calculated variation of total-to-static pressure ratio across the turbine with total-to-total pressure ratio for an inlet temperature and rotative speed of 1500°F and 18,250 rpm, respectively. The design total-to-total pressure ratio, 2.95, corresponds to a total-to-static pressure ratio of 3.47.

The endurance test condition selected was as follows:

Inlet Temperature, °F	1500 ± 10
Total-To-Static Pressure Ratio	3.47 ± 0.25
Rotative Speed, rpm	18,250 ± 200

The vapor pressure corresponding to a temperature of 1500°F is 24.6 psia. The correct exit pressure should then be 7.1 psia. Shown in Figure 89 is the variation of hub static pressure at turbine exit with exit temperature, based on the performance test results. A pressure of 7.1 psia corresponds to an exit temperature of 1240°F, which was held for the endurance test.

Shown in Figure 90 is the calculated variation in the ratio of turbine torque to inlet total pressure with rotative speed and total-to-static pressure ratio. Disregarding the effect of variations in the polytropic exponent the turbine torque is corrected for varying inlet conditions be dividing it by the inlet total pressure. The data of Figure 90 permits the determination of variations in torque to be expected when the inlet pressure, pressure ratio or speed is different from the specified test conditions. For example, the tolerances on inlet temperature, exit pressure and speed of ± 10°F, ± 0.5 psi and ± 200 rpm result in the following respective variations in torque: ± 16.8, ± 18.4 and ± 5.5 in. lb.

Shown in Figure 91 are the measured values of torque obtained during performance testing. Based on these data the expected torque at the endurance test condition was (24.1)(24.6) or 593 in. lb.

B. ENDURANCE TEST PREPARATIONS

In preparation for the endurance test, a number of instrumentation calibration curves were prepared from test data obtained during performance testing.

Shown in Figures 45a and 45b are the variations in the ratio of turbine exit static pressure to the vapor pressure corresponding to the measured temperature at the same station with turbine total-to-static pressure ratio. Since the curves for the 1450 and 1550°F data are nearly identical, it was assumed that the supersaturation ratio (ratio of measured to vapor pressure) is constant for a given turbine total-to-static pressure ratio. The variation of hub static pressure at turbine exit with exit temperature was calculated for 1500°F inlet temperature, using this assumption, and is shown in Figure 89.

In order to eliminate a source of contamination to the turbine during endurance testing, no efflux pressure measuring devices were used. Limp-diaphragm pressure transducers were used at stations 1, 7 and 8, and in the throttling calorimeter. Because of the elimination of the efflux pressure measuring system the bullet nose annulus instrumentation could not be used for flow rate measurement and the electromagnetic flow meter was used. Shown in Figure 92 is the comparison between the EM flow meter and bullet nose annulus data obtained during the performance test. The wide scatter band is caused by the inability to hold a constant liquid level in the condenser during performance testing, and the sensitivity of flow rate to changes in condenser level. The free liquid surface in the condenser is 1620 $in.^2$. Therefore, a change in liquid level of one inch per minute would result in an apparent error in flow rate measurement of 0.74 lb. per second.

Shown in Figure 93 is the variation of water brake torque (obtained from a heat balance on the water brake) versus the torque meter reading. This curve

is presented in case the torque meter malfunctions during the test. A similar curve for the steam turbine torque meter is shown in Figure 94 . The data for both curves were obtained during the final performance test.

C. ENDURANCE TEST PERFORMANCE

A parasitic torque test, conducted as described previously, was run to determine the mechanical losses of the turbine bearings and seals. The results of the parasitic torque test of September 13, 1964 are shown in Figure 95 as a function of rotative speed and argon density in the turbine. Shown in Figure 96 are the results of a similar test run on October 8, 1965 before resumption of the endurance test.

Shown in Figure 97 are the parasitic torque values taken from Figures 95 and 96 at zero density, corresponding to zero blade windage loss. These data can be represented by the equation

$$Q_{pt} = 0.0053N$$

where

Q_{pt} = parasitic torque in inch pounds

N = rotative speed in rpm.

After completion of the parasitic torque test, the endurance test was begun. The conditions set were 1500°F inlet temperature, 18,250 rpm, and 1240°F exit temperature. The exit temperature was selected to set a total-to-static pressure ratio of 3.47 across the turbine. A digital scan of the performance instrumentation was made at two hour intervals. These data were examined to determine that the test point was being held and that the data

were consistent. It was quickly noticed that the torque signal was decreasing at an alarming rate (7 percent in 10 hours). A check on the enthalpy change of the water through the water brake indicated no corresponding decrease. It was concluded that the torque meter was in error. Subsequently, it was discovered that the cooling air to the torque meter was not on. It was then reasoned that the erroneous torque signals were caused by the creep of the torque meter strain gauges due to the high temperature of the environment. Therefore, the temperature rise of the water through the water brake was used as the torque indicator for the first 254 hours. A calibration curve (Figure 93) constructed from test data obtained during the performance test was used to correct the heat balance torque of the water brake to the level of measurements experienced during performance testing. During the shutdown, after 254 hours of testing, the torque meter was readjusted and was used as the torque signal in subsequent testing.

A data reduction program was written to permit evaluation of the data obtained during the endurance testing. The output of this program is presented in reference (12). Included are measurements of rotative speed, torque, temperatures, pressures, flow, and calculations of torque from the water brake temperature rise, inlet quality and a corrected torque. The corrected torque for the first 254 hours was based on the water brake temperature rise, and corrected for variations of inlet pressure, rotative speed and turbine pressure ratio using predicted performance data, shown in Figure 90. Subsequently, the corrected torque was based on the torque measured by the torque meter, and corrected for variations in test conditions.

Shown in Figure 98 are plots of the more significant parameters for the 2000-hour endurance test, the points plotted were taken at the same time every day. The top strip shows the variation of rotative speed, and is the average of five readings taken during each scan of the digital recorder. In general, the speed was held within ± 100 rpm, which is only half of the tolerance of ± 200 rpm specified in the test plan. The next two strips show the variation of temperature at turbine inlet and at turbine exit. The plotted inlet temperature was measured upstream of the turbine and is the average of the readings of two thermocouples. The reading of a third thermocouple was about twenty degrees higher than the other two and was not used in the average. The thermocouples at station 3, in the bullet nose, indicated about two degrees higher than those at station 1. The exit temperature is the average of two measurements out of four. Two thermocouples which indicated about fifteen degrees lower than the average and twenty degrees higher than the average, respectively, were not used in the calculated average.

The next two strips show the variation of turbine inlet and outlet static pressures measured with limp diaphragm gauges. Although the test point was set by inlet and outlet temperatures based on correlations of temperature and pressure from the performance test data, the measured pressures are presented to indicate the variations with time. The measured exit pressure is about one psi lower than the correlation of efflux exit pressure versus exit temperature, shown in Figure 89.

The next strip shows the variation of net blading torque. This parameter is an indication of turbine aerodynamic performance and is calculated by sub-

tracting the steam turbine torque from that absorbed by the water brake and adding the parasitic torque, which is due to the losses of the test turbine bearings and seals. For the first 254 hours the water brake torque was calculated from the enthalpy rise of the water and corrected through the use of Figure 93. During the shutdown, the torque meter was readjusted and used for subsequent testing for the water brake torque measurement.

The last strip shows the variation of turbine flow rate as measured with the electromagnetic flow meter. The flow rate is about 10 percent higher than predicted but this is not inconsistent with previous electromagnetic flow meter measurements as shown in Figure 92.

Initially the turbine inlet condition was set by a thermocouple located at the turbine inlet station. After about 100 hours of endurance testing it was apparent that the thermocouple had drifted. After switching to a thermocouple upstream of the turbine for two days, it was decided to control the inlet condition to the upstream Taylor gauge reading. This resulted in better control of the test conditions, and is reflected in the reduced scatter of the parameters shown in Figure 98 for the remainder of the test. Although the accuracy of the Taylor gauge and the thermocouple are about the same, i.e., about 1 psi or 10 °F, the Taylor gauge is considered to be more stable because it is in a cooler environment.

Except for one accidental shutdown after 254 hours, caused by inadvertently energizing the over-speed trip during a routine speed calibration, the 2000-hour endurance test was completed without incident. It was noticed that the torque meters were subject to zero shift as the test progressed. This caused an apparent

decrease of about 25 in. lb. in the corrected torque from the resumption of the endurance test until completion. However, after the completion of the test, it was determined that both torque meters were reading low and that the net blading torque at the end of the test shown on Figure 98, should be corrected upward 30 in. lb. This correction brought the blading torque at the completion of the endurance tests back to the value measured at the beginning of the test within 5 in. lb., indicating no loss in turbine performance after 2000 hours of operation.

PRECEDING PAGE BLANK NOT FILMED.

IX. CONCLUSIONS

In order to verify fluid dynamic design methods for potassium turbines running in condensing potassium vapor, to determine the relative erosion and corrosion resistance of candidate refractory bucket alloys, and to assess performance degradation resulting from operation in a condensing potassium vapor, a two-stage, potassium test turbine was designed, built and tested. The following was concluded from the fluid dynamic testing and performance during endurance testing:

1. The ability to design a turbine for operation with potassium vapor and to predict the off-design performance analytically was demonstrated by the close agreement between the experimental performance and that obtained analytically prior to testing. For example, the standard deviation of all the experimental power output data from the predicted values was 5.8 KW. The repeatability was within 6 KW.

   The turbine total-to-static efficiency determined from performance measurements also agreed well with the values calculated before testing. The standard deviation of all the efficiency data from the calculated values was 4.4 percentage points. The repeatability was within about 4 percentage points.

2. With the single exception of turbine exit vapor quality, all performance measurements were made with adequate accuracy. Notable among the many measurements made were pressure and

vapor flow rate. The efflux pressure measuring system, developed for measuring pressures in two phase potassium flow and discussed in Appendix B, gave pressure measurements consistent with temperature measurements at the same locations and with analytical performance data calculated prior to testing.

The consistency of flow rate measurements made with air-calibrated efflux pressure measuring system instrumentation was demonstrated by the fact that the standard deviation of the experimental flow measurements from the predicted values was 0.044 pps. (The flow rate at design point pressure ratio and 1550°F inlet vapor temperature was 2.2 pps.) The repeatability was within 0.1 pps.

3. The feasibility of operating a potassium turbine with refractory buckets over long time periods was demonstrated by a 2000-hour endurance test at 1500°F. There was essentially no degradation in torque of the turbine from the beginning to the end of this endurance test.

APPENDIX A

REVERSION CALCULATION

The reversion from supersaturated to equilibrium conditions is calculated by maintaining conservation of energy, mass and momentum.

Energy

$$H_{T2} = H_{T1} = H_{S2} + \frac{V_2^2}{2gJ} \tag{1}$$

Continuity

$$w_{g1} = \frac{A_1 V_{x1}}{v_{s1}} \; ; \; v_{s1} \text{ based on gas flow from NUTOD} \tag{2}$$

$$w_2 = \frac{A_2 V_{x2}}{v_{s2}} \; ; \; v_{s2} \text{ based on total flow} \tag{3}$$

$$\frac{w_{g1}}{x_1} = w_2 = w_1, \text{ based on total flow} \tag{4}$$

$$\frac{A_1 V_{x1}}{x_1 v_{s1}} = \frac{A_2 V_{x2}}{v_{s2}} \quad \text{or} \quad V_{x2} = \frac{V_{x1} v_{s2}}{x_1 v_{s1}} \text{ for constant A.} \tag{5}$$

Momentum

$$(P_{s1} - P_{s2}) = \frac{w_{g1}}{g A} (V_{x2} - V_{x1}) \tag{6}$$

$$(P_{s1} - P_{s2}) = \frac{V_{x1}}{g v_{s1}} (V_{x2} - V_{x1}) \tag{7}$$

$$V_{x2} = \frac{v_{s1} g (P_{s1} - P_{s2})}{V_{x1}} + V_{x1} \tag{8}$$

Sample calculation from off-design program.

Gas constant:

$$P_{so} = 10.88 \text{ psia}$$

$$T_{so} = 1338°F \ (1798°R)$$

$$v = 42.07 \text{ ft}^3/\text{lb}$$

$$R = \frac{144 \ P_{so} \ v}{T_{so}} = \frac{144 \ (10.88)(42.07)}{1798}$$

$$R = 36.67 \text{ ft lb/lb } °R$$

Conditions before reversion:

Temperature, $T_{s1} = 1068°F \ (1528°R)$

Axial Velocity, $V_{x1} = 526$ ft/sec

Tangential Velocity, $V_{u1} = 414.2$ ft/sec

Static Pressure, $P_{s1} = 5.78$ psia

Absolute Velocity, $V_1 = 669.5$ ft/sec

Vapor Quality, $X_1 = 0.9524$

Static Specific Volume, $v_{s1} = \frac{R \ T_{s1}}{144 \ (P_{s1})} = \frac{(36.67)(1528)}{(144)(5.78)}$

$$v_{s1} = 67.40 \text{ ft}^3/\text{lb}$$

Total Enthalpy, H_{T0} (at entrance to stage) = 1155 Btu/lb

Enthalpy Change $\Delta h_1 = 37.24$ Btu/lb

Total Enthalpy, H_{T1} (before reversion) = $H_{T0} - X_1 \ \Delta h_1 = 1155 - (37.24)(.9524)$

$$H_{T1} = 1120 \text{ Btu/lb}$$

Assume P_{s2} = 5.695 psia and iterate until equations (9) and (15) agree.

Using the momentum equation (8)

$$V_{x2} = \frac{(67.40)(32.2)\left[5.78 - 5.695\right]}{526}(144) + 526 = 576.5 \text{ ft/sec}$$

Assume $V_{u2} = V_{u1} = 414.2$ ft/sec (constant moment of momentum)

Then $V_2 = \sqrt{(414.2)^2 + (576.5)^2} = 709.8$ ft/sec (Pythagoras)

Using the energy equation (equation (1) recast),

$$H_{s2} = H_{T1} - \frac{V_2^2}{2gJ} = 1120 - \frac{(709.8)^2}{2(32.2)(778)} = 1110 \text{ Btu/lb}$$

Using NRL potassium properties, at P_{s2} = 5.695 psia

$$X_{s2} = \frac{H_{s2} - H_L}{H_V - H_L} = \frac{1110-327}{1181-327} = .9172$$

$$v_{s2} = (.9172)\left[76.72 - .02333\right] + .02333 = 70.37 \text{ ft}^3/\text{lb}$$

Using the continuity equation (5)

$$V_{x2} = \frac{V_{x1}\, v_{s2}}{X_1\, v_{s1}} = \frac{(526)(70.37)}{(.9524)(67.40)} = 576.6 \text{ ft/sec}$$

The exit axial velocity from equations (9) and (15) agree, therefore, the assumed value of P_{s2} = 5.695 lb/in^2 was correct.

Comparison of conditions before and after reversion:

	Before	After
Tangential Velocity, ft/sec	414.2	414.2
Axial Velocity, ft/sec	526.0	576.6
Specific Volume, ft^3/lb	67.40	70.37
Static Pressure, lb/in^2	5.78	5.695
Absolute Velocity, ft/sec	669.5	709.8
Enthalpy, Btu/lb	1120	1110
Vapor Quality	0.9524	0.9172
Temperature, °R	1528	1687

Nomenclature

A	cross sectional flow area
g	gravitational constant
H, h	enthalpy
J	mechanical equivalent of heat
P	pressure
R	gas constant
T	temperature
V	velocity
v	specific volume
w	flow rate
x	quality

Subscripts

o	stage entrance
1	before reversion
2	after reversion
g	gas
L	liquid
s	static
T	total
u	tangential
V	vapor
x	axial

PRECEDING PAGE BLANK NOT FILMED.

APPENDIX B

DEVELOPMENT OF EFFLUX PRESSURE MEASURING SYSTEM FOR PERFORMANCE EVALUATION OF POTASSIUM VAPOR TURBINE

I. SUMMARY

In the preparation for the performance testing of the potassium vapor turbine, it was recognized that a device was required to measure total and static pressures before and after blade rows in a turbine having flow passages no higher than one inch.

Existing limp diaphragm pressure transducers which had previously been developed for alkali metal service were known to have an accuracy of about $\pm$ 1 percent and were known to require an access hole to the fluid which was at least 1/2 inch in diameter, which is impossible in a small turbine. The direct connection of the sensor line to either a pressure transducer or a manometer was ruled out because potassium vapor would condense and freeze in the sensor line, rendering the pressure measuring device inoperative.

The pressure measuring device (efflux) that was developed is based upon flowing a metered amount of an inert gas through the sensor lines into the test facility. The flow of inert gas into the test facility prevents the diffusion of potassium vapor into the sensor line. By this technique the potassium vapors can be contained within the facility and pressure transducers which operate in an inert gas, moderate temperature environment can be used for the measurements. The device was developed

by making tests with air, steam and potassium vapor. When fully developed, the efflux measuring device was used to measure total and static pressures in the two-stage potassium turbine at inlet and outlet, and the static pressures between all blade rows. In addition, an important application of this device was the measurement of potassium vapor flow rate by means of the measurement of total and static pressures in the calibrated annulus ahead of the potassium vapor turbine. The efflux pressure measuring device may work equally well in the measurement of the pressure of alkali metal vapors other than potassium.

II. INTRODUCTION

In the early phases on planning for design and evaluation of space power turbomachinery development, it was decided that about 40 pressure measurements would be required to evaluate potassium turbine performance. At that time, commercial high-temperature pressure transducers were being used for pressure measurements on alkali-metal heat transfer loops. These pressure transducers had demonstrated reliability and an accuracy of 1 to 2 percent of full scale; however, their cost was approximately ten times that of precision, moderate-temperature pressure transducers for gas service. In addition, the high-temperature transducers were connected to the test piece by means of a 0.5-inch pipe. There was no space available for nipples of this size to make detailed fluid dynamic measurements on small sized turbomachinery. In view of these considerations, it was decided to develop a pressure measuring system specifically for alkali-metal vapor turbine testing.

The pressure measuring device that was developed is based upon the continuous efflux of inert gas into the test facility through the pressure measurement lines. By this technique the potassium vapors can be contained within the facility and pressure transducers, used for the measurements, operate in an inert gas, moderate-temperature environment. The technique lends itself to the standard methods for pressure switching and the application of high-accuracy commercial transducers.

III. DESIGN

Shown in Figure A-1 is a schematic diagram of the efflux system used to measure the pressure of potassium vapor in the 3000 KW test facility. In the efflux system, argon flows through a filter, an efflux system assembly, a solenoid valve, a potassium vapor trap, and into the test vehicle. The flow of argon prevents potassium vapor from entering the pressure transducer measuring system. A lead connects the scani-valve to a tee which is between the efflux system assembly and the test vehicle. This scani-valve is a fluid switch permitting 12 separate pressures to be read on the same precision transducer. The transducer is connected to the central terminal of the scani-valve. Prior to the taking of a reading, an emergency-purge valve located in the efflux system assembly is opened permitting the argon to flow through a much larger orifice so as to flush the sensor line of any potassium vapor attempting to proceed from the test vehicle to the tee.

In designing the actual hardware for the potassium turbine measurements, one of the primary concerns was ease of maintenance. Figure A-2 is a photograph of a typical efflux system assembly. The basic module will accommodate five individual pressure measurements with common continuous efflux and emergency

purge manifold and individual orifices and plenum chambers. Connections on each plenum are available for hooking up transducer and pressure sensing lines. The flow of argon is metered by means of a small (0.005 in. diameter) orifice in the efflux system assembly. Hypodermic needles were found to be the most economical orifice.

In order to avoid cross coupling between channels in the emergency purge manifold, it was necessary to include a check valve in each purge line. Standard tire valves were found to work reliably and are brazed to each of the emergency purge needles.

The module is designed such that it can be easily disassembled for replacement or clean out of components by removing the six assembly bolts. A single plenum section disassembled is shown in Figure A-2. The continuous efflux hypodermic needle and the emergency purge needle with tire valve are also shown in proper position. The springs indicated at both ends of the photograph are required to couple the section together and position the needles tightly against their seat.

IV. DEVELOPMENT

In the original concept of the efflux pressure measuring device (PMD), it was planned to operate the efflux system with the argon flowing continuously (and, therefore, the solenoid switches were not required). It was realized that for this method of operation there were certain sources of error such as line pressure drop and fluid dynamic effects at the pressure tap, but after some analysis, it was felt that these errors could be determined by calibration.

Tests were conducted to determine the reliability and accuracy of the efflux PMD. One of the developmental tests was the operation of the efflux device in the 50 KW potassium heat transfer facility. The objectives of this test were:

1. To determine whether the efflux device is acceptable from an operational standpoint in a potassium vapor facility.
2. To compare the response and actual values of pressure with those of the limp diaphragm pressure transducer.

Shown in Figure A-3 is a schematic diagram of the 50 KW two-phase potassium loop with the efflux system installed. The flow through the loop is by natural convection. The loop consists of a boiler, condenser, dump tank and an argon removal subsystem. The vertical boiler has limp diaphragm gauges at the upper and lower ends. These gauges give the boiling pressure in addition to the liquid level in the boiler.

Shown in Figure A-4 is a plot of the efflux pressure readings against those of the adjacent limp diaphragm gauge taken in the 50 KW potassium loop. These data extend over a range of pressures from about 5 to 16 psia. In this pressure range, the deviations of the efflux readings from the limp diaphragm gauge are in the range of 0.1 to 0.4 psi. The agreement is considered good in consideration of two facts:

1. The accuracy of the limp diaphragm gauge is about $\pm$ 0.5 psi, or $\pm$ 1 percent of a 50 psi gauge.
2. Calibrations in steam on the efflux device indicated that over the pressure range of 5 to 16 psia, the deviation of the efflux measurements from the true value are 0.1 to 0.4 psi.

Reference to Figure A-4 indicated that the maximum pressure attained in the 50 KW facility was about 16 psia. This pressure corresponded to a vapor temperature of 1400°F, which is the limit of the 50 KW loop. During potassium testing the efflux device would be subjected to a pressure of 37.5 psia, which corresponds to a vapor temperature of 1600°F (Reference 13). During the testing of the flow nozzle in steam, the efflux device was used up to a pressure of 39 psia. Subsequent inspection revealed no moisture had diffused back to the hypodermic needle chambers.

Shown in Figure A-5 is a typical time-dependent trace of efflux-system measured pressure during which time the efflux gas flow was periodically shut off 28 times for nine-second intervals. The corresponding limp diaphragm gauge trace is also shown in Figure A-5. A random system surge is marked along with the paper position corresponding to numbered readings. The pressure scale is also shown. Unfortunately, the two charts were run at different speeds, making detailed comparisons awkward.

Reference to Figure A-5 indicates that the pressure read by the efflux system dropped to the facility pressure when the argon gas was turned off and returned to the original level when turned on. The significant point, however, is that in spite of turning the efflux gas off 28 times, no malfunction of the efflux system occurred.

The test demonstrated that the efflux system is acceptable from an operational standpoint for use with potassium vapor. This is substantiated by the facts that neither artificial surges nor periodically turning off the gas in the efflux system caused plugging of the system. In addition, the test demonstrated that the response of the efflux system is better than that of the limp diaphragm gauge (Reference 14).

A converging-diverging flow nozzle was tested prior to the turbine testing to check out the operation of the 3000 KW facility and to obtain some basic data on the expansion of potassium vapor (Reference 4). This converging-diverging nozzle was first calibrated in the Flow Analysis Calibration Test (FACT) stand, to determine the effective flow areas through the nozzle.

During air tests of the converging-diverging nozzle an attempt was made to obtain calibration data for the error in pressure reading, which changes with stream Mach number by taking readings with and without the argon flowing. On the average, this difference resulted in an error of about 2 percent at a Mach number of unity and decreases to zero at vanishing values of Mach number. However, the Mach number effect contained a considerable amount of scatter, indicating that no precise correlation could be made. Therefore, in the interest of removing potentially unknown errors during nozzle testing in potassium, where pressure readings were required to an accuracy of 0.25 psi, it was decided to shut off the argon efflux flow by means of solenoid valves while the readings were taken, thereby eliminating the source of error. The efflux pressure measuring device had been utilized in this manner during tests conducted in the 50 KW loop and no system plugging was experienced. The solenoid valves as well as the scani-valve for each pressure measuring line are controlled by the digital data handling system circuitry so that the transducer is vented to the test vehicle for approximately 4 seconds before the digital data handling system secures a reading.

An efflux solenoid valve control permits the selection of the efflux channels for which the solenoid valves are to be closed. Normally all solenoid valves are open, permitting argon to flow through the instrument lines into the facility.

(The flow rate is about 1.3×10^{-5} lb/sec for each sensor line.) This condition is signaled by a "ready" light. On pushing the "start" button, the selected (or all of the) solenoid valves close, and after a predetermined time interval for pressure stabilization, scanning of the pressure lines commences. Lights signal which of four scanners is being read. After scanning, the solenoids are all opened and an emergency argon purge of about 3.5×10^{-5} lb/sec for each line is actuated for a few seconds to clear the pressure lines of any potassium vapor. Then the device returns to the ready position or normal argon efflux.

Shown in Figure A-6 is an interior view of the cabinet which houses the equipment for the efflux system, showing the following equipment:

- 4 pressure scanning modules - upper left and right
- 8 (2 not shown) efflux blocks - back and side walls
- 40 solenoid valves - floor
- reference pressure transducer - center
- argon pressure controller - center

The empty compartment at upper center is for the pressure module control.

The efflux system equipment cabinet is connected to the turbine or nozzle test piece by pressure leads. Cables connect this cabinet to the terminal box at the digital data handling system location. The required sequencing of the various channels is accomplished by making the required connections on programming panels.

The terminal box just described is connected to the digital data handling system. This system is capable of scanning between any two channels from 1 to 600 and recording the results in decimal format with 4 digits on paper tape beside a data channel number and/or recording on punched tape using a 6-character

word compatible with IBM and other standard reading devices. When the printer is used the maximum recording rate is 5 bits of data per second. The punched tape includes a 20-character word which can be used for fixed data. The analog-to-digital converter has an accuracy of 0.01 percent and the gain accuracy is 0.02 percent of full scale. The gain can be changed three times per scan and 10-volts, 100-millivolt and 10-millivolt ranges are available.

Four scanner modules are controlled by a matrix from 48 control inputs originating in the digital system. While one scanner is being moved to the next point, the remaining three are in various phases of stabilization which takes two seconds. The scanners are read sequentially at the rate of 1 per second. Each scanner module has its own precision transducer (accurate to 0.1 percent of full scale of 0.1 psi).

During the checkout of the 3000 KW two-phase potassium turbine test facility, some difficulty was encountered with the efflux pressure measuring system. The 1/8-inch O.D. tubes which sense the loop pressure became plugged several times. Potassium vapor had apparently diffused to the cooler regions of the sensing tubes where it froze. The efflux system was modified to include the installation of vapor traps in eight of the efflux lines. The efflux pressure measuring device with the vapor trap installed is shown schematically in Figure A-1.

Figure A-7 shows the general construction of the demister trap used in this facility. A thermocouple was attached to the side of the 1.0-inch pipe section and the entire demister capsule and part of the 3/8-inch tube was traced with heating wire. In operation, the demister capsule was heated to 200-300°F, and held at that temperature. The theory of operation is that as the potassium

vapor tends to back diffuse or migrate into the cold efflux line, it will condense on the extensive surface of the wire demister. At 200°F, the potassium remains liquid, and as the liquid accumulates, it will eventually drain back into the potassium loop. Drainage is aided by the constant inflow of argon into the top of the demister capsules and gravity.

During the facility checkout, nearly all efflux pressure lines without demisters in the line plugged repeatedly. The eight efflux pressure taps that contained demisters remained open during this test. Consequently, demister traps were installed in all efflux lines. All efflux lines were changed to 3/8-inch O.D. x 0.125 wall tubing in the hot region instead of 1/8-inch O.D. x 0.030 wall tubing. All efflux tube connections were made by welding instead of brazing. Figure A-8 shows the installation of the demister capsules on the potassium turbine. In subsequent test runs (boiling between 1450°F - 1580°F for a period of 75 hours), only one sensor line out of 36 plugged.

In conjunction with the use of these traps, the efflux control system was modified to shut off the argon flow to each of the sensing lines sequentially, as the pressures are scanned. Since the settling time of the pressure measuring device has been established as approximately 1.5 seconds, the argon flow is shut off for four seconds prior to reading the pressure. Thus, each sensing line is open directly to the potassium environment for a shorter period of time, although enough time is allowed for adequate pressure stabilization during scanning.

V. EVALUATION

Before each period of performance testing, the efflux pressure measuring system was calibrated over a range of 0 to 50 psia, by pressurizing the loop with argon, with repeatability and accuracy of better than 1/2 percent being obtained. Pressure measurements taken during performance testing of the potassium vapor turbine were plotted against the vapor pressures corresponding to the measured temperatures to determine how well the efflux system worked. Some of these plots were presented as Figures 42 through 46 of this report, and discussed in connection with performance testing of the potassium turbine.

Shown in Figure A-9 is a comparison of measured total pressure with the vapor pressure corresponding to the measured temperature at the turbine inlet station. The correlation is much better than it was for static pressure at this station (Figure 43), indicating that the thermocouple may be reading closer to a total temperature. It also seems possible that what appears to be scatter in the pressure measurements is at least partially attributable to other factors such as velocity. For instance, the difference between measured total and static pressure was used to calculate the vapor flow rate through the turbine with good results, as discussed later. The velocity head is about 0.75 psi for a velocity of 400 ft/sec.

For comparison with Figure 42, the static pressures at station 1, measured with a limp diaphragm gauge, are shown in Figure A-10. The limp diaphragm pressure measurements seem to have a little less scatter than the efflux measurements, although the correlation with vapor pressure is not as good at 1450°F inlet temperature.

Shown in Figure A-11 is a typical plot of interstage static pressures. The symbols denote test measurements and the lines show the predicted pressure levels. Although there are some deviations, the overall conclusion is that the efflux system gave very satisfactory pressure measurements.

Originally, the turbine flow rate was determined by measuring the liquid flow rate out of the condenser with an electromagnetic flow meter. The liquid flow rate and vapor flow rate through the turbine are equal only when the condenser liquid level is constant and there is no change in loop inventory. It was very difficult to maintain a constant liquid level in the condenser because the liquid surface was large (1600 sq.in.) compared to the flow area through the (1 in. diameter) flowmeter. A small change in condenser liquid level results in a large change in EMFM reading. The result was sizeable flow measurement errors. Consequently, the instrumentation in the annulus immediately upstream of the turbine inlet, which was used successfully to sense velocity transients during early performance testing, was utilized to measure steady state flow rate during performance testing. A calibration test in air was made of the inlet annulus instrumentation in the Flow Analysis Calibration Test (FACT) stand. The inlet annulus and the first stage nozzle diaphragm were used for this calibration test.

The good agreement between measured flow rate and calculated flow rate, shown in Figures 59 through 70, indicates that the inlet annulus differential pressure measurements obtained with the efflux system yield flow rates which have less scatter than those from the electromagnetic flow meter and are at levels which are in good agreement with the predicted flow rates.

VI. CONCLUDING REMARKS

The efflux pressure measuring system has been developed and successfully used in over 125 hours of potassium vapor testing. The performance of the efflux system compared favorably with that of the limp diaphragm pressure transducer. The figures presented in this report showing the good results obtained in measuring turbine pressures, flow rates and efficiency are evidence that the efflux pressure measuring system was instrumental in obtaining good performance data. It is expected that this type of system will find application in the development testing of alkali metal vapor systems and components.

PRECEDING PAGE BLANK NOT FILMED.

REFERENCES

1. D.B. Mackay: "Design of Space Powerplants". Prentice-Hall, Inc., Englewood Cliffs, 1963, pp 83-98.

2. B. Wood: "Wetness in Steam Cycles", Proceedings of the Institute of Mechanical Engineers, V. 174, No. 14, pp 491-534, 1960.

3. G.C. Wesling and M.E. McCarthy: "Thermodynamic Properties of Potassium Vapor From 1300 - 2700°R Using Naval Research Laboratory Experimental Data". Appendix A of Quarterly Progress Report No. 14 of Two-Stage Potassium Test Turbine, General Electric Company, November 8, 1964, NASA - CR - 54285.

4. R.J. Rossbach: "Critical Flow of Potassium Vapor Through Instrumented Converging-Diverging Nozzle ". A.S.M.E. Preprint No. 65-GTP-22, January 15, 1965.

5. D.G. Ainley and G.C.R. Mathieson: "A Method of Performance Estimation For Axial-Flow Turbines". A.R.C. (British) R. and M. No. 2974, December, 1951.

6. R.H. Cavicchi and R.E. English: "A Rapid Method For Use in Design of Turbines Within Specified Aerodynamic Limits." NACA TN 2905, April, 1953.

7. E. Schnetzer: Two-Stage Potassium Test Turbine. Quarterly Progress Report No. 15. Contract NAS 5-1143, NASA-CR-54392, February, 1965.

8. E. Schnetzer: Two-Stage Potassium Test Turbine. Quarterly Progress Report No. 11. Contract NAS 5-1143, February, 1964.

REFERENCES (Continued)

9. E. Schnetzer: Two-Stage Potassium Test Turbine. Quarterly Progress Report No. 13. Contract NAS 5-1143, NASA-CR-54211, August, 1964.

10. E. Schnetzer: Two-Stage Potassium Test Turbine. Quarterly Progress Report No. 17. Contract NAS 5-1143, NASA-CR-54897, August, 1965.

11. E. Schnetzer: Two-Stage Potassium Test Turbine. Quarterly Progress Report No. 16. Contract NAS 5-1143, NASA-CR-54643, May, 1965.

12. E. Schnetzer: Two-Stage Potassium Test Turbine. Quarterly Progress Report No. 18. Contract NAS 5-1143, NASA-CR-54917, November, 1965.

13. J.P. Stone, C.T. Ewing, J.R. Spann, E.W. Steinkuller, D.D. Williams, and R.R. Miller: "High Temperature Properties of Sodium, Potassium, and Cesium", NRL Report 6128, August, 1964.

14. E. Schnetzer: Two-Stage Potassium Test Turbine, Quarterly Progress Report No. 6. Contract NAS 5-1143, November, 1962.

TABLE I

POTASSIUM TURBINE TESTS

DATE	OPERATING TIME ON POTASSIUM, HRS.	ACC. TIME	INLET TEMPERATURE, °F	ROTATIONAL SPEED, RPM	POWER RANGE, KW	REMARKS
July, 1964	4	4	1200 - 1500	12,000 - 16,000	30-80	Potassium to Oil Seal Failure
October, 1964	45	49	1450 - 1580	15,000 - 21,000	40-180	Facility Instabilities and Boiler Failure
March, 1965	14	63	1450	15,000 - 20,000	90-135	Leak in Bearing Housing
May, 1965	53	116	1450 - 1550	15,000 - 20,000	10-200	Performance Test Completed
September, 1965			1500	18,250	140	2000-Hour Endurance Test Initiated
September, 1965	254	370	1500	18,250	140	Inadvertent Actuation of Speed Trip
October, 1965 – December, 1965	1746	2116	1500	18,250	140	2000-Hour Endurance Test Completed

TABLE II

TWO-STAGE POTASSIUM VAPOR TURBINE DESIGN POINT CONDITIONS

Rotative Speed, rpm	19,200
Vapor Flow Rate, pps	2.8
Inlet Vapor Temperature, °F	1600
Inlet Total Pressure, psia	37.5
Exit Total Pressure, psia	12.71
Stage One Inlet Quality, Percent Vapor	91.4
Stage Two Inlet Quality, Percent Vapor	89.4

TABLE III

COMPARISON OF DESIGN DATA FROM PRELIMINARY AND FINAL BUCKET DESIGNS

Stage	1		2	
Configuration	Prelim.	Final	Prelim.	Final
Trailing Edge Overhang	Yes	No	Yes	No
Dovetail Angle, Deg.	5.25	7.75	2.75	7.50
Bent Platform	No	No	Yes	No
Hub Area, sq. in.	.1020	.1043	.1113	.1215
Pitch Area, sq. in.	.0847	.0835	.0947	.0998
Tip Area, sq. in.	.0630	.0630	.0771	.0771
Centrifugal Load on Bucket, lb.	1408	1386	1908	2068
Clearance for Replacement, in.	None	.029	None	.046

TABLE IV

PHYSICAL DIMENSIONS OF FINAL TEST TURBINE BUCKETS

Stage	1			2		
Radial Location	Tip	Pitch	Hub	Tip	Pitch	Hub
Radius	4.40	4.08	3.76	4.80	4.40	4.00
Blade Inlet Angle, Deg.	59.0	62.4	65.3	52.3	57.3	62.0
Blade Exit Angle, Deg.	64.6	66.2	63.0	62.6	64.8	64.0
Maximum Thickness, In.	.137	.165	.190	.1475	.1735	.194
Aerodynamic Chord, In.	.618	.646	.682	.724	.752	.789
Axial Width, In.	.584	.6345	.684	.6815	.736	.789
Stagger Angle, Deg. (Measured from line tangential to blade)	22.0	15.2	8.9	22.5	15.5	9.5
Solidity	1.41	1.61	1.85	1.46	1.68	1.98
Leading Edge Radius, In.	.015	.0125	.010	.015	.0135	.012
Trailing Edge Radius, In.	.0075	.0075	.0075	.0075	.0075	.0075

TABLE V

COMPARISON OF RESULTS OF DESIGN AND OFF DESIGN PROGRAMS AT APPROXIMATELY DESIGN FLOW CONDITIONS

QUANTITY	First Stage		Second Stage	
	TEP	TOD	TEP	TOD
Inlet Total Temperature, °F	1600	1600	1499	1499
Inlet Total Pressure, psia	38.24	38.24	24.6	24.6
Inlet Vapor Quality	.92	.92	.89	.89
Dry Vapor Flow, pps	2.67	2.67	2.59	2.59
Rotative Speed, rpm	19200	19200	19200	19200
Specific Work, Btu/lb.$_m$	30.65	30.65	43.0	43.0
Nozzle Exit Angle, deg.	70.85	70.85	72.0	72.0
Bucket Inlet Flow Angle, deg.	37.3	37.2	39.6	39.7
Bucket Exit Angle, deg.	64.5	64.6	63.7	62.2
Stage Exit Flow Angle, deg.	26.3	29.8	39.0	37.1
Total to Total Efficiency (no droplet drag loss)	.805	.782	.796	.752
Total to Static Efficiency (no droplet drag loss)	.722	.715	.657	.606
Bucket Inlet Pitch Diameter, in.	8.09	8.09	8.68	8.68
Bucket Inlet Blade Length, in.	.744	.743	1.03	.98
Reaction at Hub	.44	.445	.55	.56
Reaction at Pitch	.52	.53	.63	.65
Bucket Inlet Axial Velocity, fps	320.	320.	323.	323.
Bucket Exit Pitch Diameter, in.	8.13	8.12	8.72	8.71
Bucket Exit Blade Length, in.	.715	.71	.98	.94
Bucket Exit Axial Velocity, fps	424.	423.	600.	638.
Nozzle Total to Static Pressure Ratio	1.248	1.247	1.322	1.321
Stage Total to Static Pressure Ratio	1.615	1.625	2.24	2.42
Stage Total to Total Pressure Ratio	1.535	1.555	1.922	2.005
Pitch Velocity Ratio, $\bar{u}/vo$	.466	.463	.402	.386
Overall Total to Total Efficiency (Supersaturated Flow, no moisture)			.807	.792
Bucket Tip Clearance (Running), in.	.05	.05	.05	.05

NOTE: All angles referenced from axial

TABLE VI

POTASSIUM VAPOR TURBINE TEST INSTRUMENTATION

Item No.	Parameter	Location	Station	Range	Sensor	Control Room Readout
1	Vapor Total Temp., °F	045-1	1	1400-1650°F	CA T/C	Digital
2	Vapor Total Temp., °F	135-1	1	1400-1650°F	CA T/C	Digital
3	Vapor Total Temp., °F	235-1	1	1432-1682°F	CA T/C	Sanborn
4	Vapor Total Temp., °F	315-1	1	1400-1650°F	CA T/C	Digital
5	Vapor Total Temp., °F	315-2	1	1400-1650°F	CA T/C	Digital
6	(Reference) Vapor Total Pressure	360-1	1	0-50 psia	Efflux	Digital
7	Vapor Total Pressure	360-2	1	0-50 psia	Efflux	Digital
8	(Alternate Reference) Vapor Total Pressure	360-3	1	0-50 psia	Efflux	Digital
9	Vapor Total Pressure	065-1	1	0-50 psia	Efflux	Digital
10	Vapor Total Pressure	300-1	1	0-50 psia	Efflux	Digital
11	Vapor Static Pressure	080-1	1	0-50 psia	Efflux	Digital
12	Vapor Static Pressure	280-1	1	0-50 psia	Efflux	Digital
13	Calorimeter Temp., °F	Calorimeter 010-1	1	1400-1650°F	CA T/C	Digital
14	Calorimeter Pressure	Calorimeter 010-1	1	0-50 psia	Efflux	Digital
15	Spray Liquid Temp., °F	Liquid Injector	2	1432-1682°F	CA T/C	Digital
16	Spray Liquid Pressure	Liquid Injector	2	0-150 psig	Statham & Taylor Gage	Digital
17	Spray Liquid Flow	Liquid Injector	2	0-10 MV See Curve	EMFM	Digital
18	Vapor Total Pressure	Inlet Duct 292-1	3	0-50 psia	Efflux	Digital
19	Vapor Total Pressure	Inlet Duct 286-2	3	0-50 psia	Efflux	Digital
20	Vapor Total Pressure	Inlet Duct 280-3	3	0-50 psia	Statham on Efflux	Digital
21	Vapor Total Pressure	Inlet Duct 074-1	3	0-50 psia	Efflux	Sanborn & Digital

TABLE VI (CONTINUED)

POTASSIUM VAPOR TURBINE TEST INSTRUMENTATION

Item No.	Parameter	Location	Station	Range	Sensor	Control Room Readout
22	Vapor Static Pressure	Inlet Inner 090-1	3	0-50 psia	Efflux	Digital
23	Vapor Static Pressure	Inlet Outer 270-1	3	0-50 psia	Efflux	Digital
24	Vapor Static Pressure	Inlet Inner 270-1	3	0-50 psia	Efflux	Digital
25	Vapor Static Pressure	Inlet Outer 090-1	3	0-50 psia	Efflux	Digital
26	Vapor Static Pressure	Upstr. Rotor 1-Tip 082-1	4	0-50 psia	Efflux	Digital
27	Vapor Static Pressure	Upstr. Rotor 1-Hub 082-1	4	0-50 psia	Efflux	Digital
28	Vapor Temperature	Wheel Space 120-1	4	650-1650°F	CA T/C	Digital
29	Vapor Temperature	Wheel Space 330	4	650-1650°F	CA T/C	Digital
30	Vapor Static Pressure	Upstr. Nozzle 2-Tip 270-1	5	0-50 psia	Efflux	Digital
31	Vapor Static Pressure	Upstr. Nozzle 2-Hub 270-1	5	0-50 psia	Efflux	Digital
32	Vapor Temperature		5	650-1650°F	CA T/C	Deleted
33	Vapor Temperature		5	650-1650°F	CA T/C	Deleted
34	Vapor Static Pressure	Upstr. Rotor 2-Tip 282-1	6	0-50 psia	Efflux	Digital
35	Vapor Static Pressure	Upstr. Rotor 2-Hub 278-1	6	0-50 psia	Efflux	Digital
36	Vapor Temperature		6	650-1650°F	CA T/C	Deleted
37	Vapor Temperature		6	650-1650°F	CA T/C	Deleted
38	Vapor Total Pressure	Upstr. OGV 300-1	7	0-50 psia	Efflux	Digital
39	Vapor Total Pressure	Upstr. OGV 300-2	7	0-50 psia	Efflux	Digital
40	Vapor Total Pressure	Upstr. OGV 300-3	7	0-50 psia	Efflux	Digital
41	Vapor Total Pressure	Upstr. OGV 79-1	7	0-50 psia	Efflux	Digital
42	Vapor Static Pressure	Upstr. OGV Tip 063-1	7	0-50 psia	Efflux	Digital

TABLE VI (Cont'd)

POTASSIUM VAPOR TURBINE TEST INSTRUMENTATION

Item No.	Parameter	Location	Station	Range	Sensor	Control Room Readout
43	Vapor Static Pressure	Upstr. OGV Hub 063-1	7	0-50 psia	Efflux	Digital
44	Vapor Static Pressure	Upstr. OGV Tip 284-1	7	0-50 psia	Efflux	Digital
45	Vapor Static Pressure	Upstr. OGV Hub 284-1	7	0-50 psia	Statham Efflux	Digital
46	Vapor Temperature	OGV 128	7	650-1650°F	CA T/C	Digital
47	Vapor Temperature	OGV 142	7	650-1650°F	CA T/C	Sanborn Digital
48	Vapor Temperature	OGV 156	7	650-1650°F	CA T/C	Digital
49	Vapor Temperature	OGV 230	7	650-1650°F	CA T/C	Digital
50	Vapor Temperature	OGV 45	7	650-1650°F	CA T/C	Digital
51	Vapor Temperature	OGV 308	7	650-1650°F	CA T/C	Digital
52	Vapor Temperature	SW-1	8	650-1650°F	CA T/C	Digital
53	Vapor Temperature	SW-2	8	650-1650°F	CA T/C	Digital
54	Vapor Temperature	SE-1	8	650-1650°F	CA T/C	Digital
55	Vapor Temperature	NE-1	8	650-1650°F	CA T/C	Digital
56	Vapor Temperature	NW-1	8	650-1650°F	CA T/C	Digital
57	Vapor Total Pressure	S-1	8	0-50 psia	Efflux	Digital
58	Vapor Total Pressure	S-2	8	0-50 psia	Efflux	Digital
59	Vapor Total Pressure	S-3	8	0-50 psia	Efflux	Digital
60	Vapor Total Pressure	W-1	8	0-50 psia	Efflux	Digital
61	Vapor Total Pressure	E-1	8	0-50 psia	Efflux	Digital
62	Deleted to No. 160 Vapor Static Pressure	N-1 Main Cond.	8	0-50 psia	Taylor Statham	Digital &Sanborn
63	Vapor Static Pressure	SE	8	0-50 psia	Efflux	Digital

TABLE VI (Cont'd)

POTASSIUM VAPOR TURBINE TEST INSTRUMENTATION

Item No.	Parameter	Location	Station	Range	Sensor	Control Room Readout
64	Vapor Static Pressure	NE	8	0-50 psia	Efflux	Digital
65	Calorimeter Insulation Temperature	T/C 122 Exit Superheater	8	1150-1650°F	CA T/C	Digital
66	Calorimeter Insulation Temperature	T/C 123 Exit Superheater	8	1150-1650°F	CA T/C	Digital
67	Calorimeter Insulation Temperature	T/C 124 Exit Superheater	8	1150-1650°F	CA T/C	Digital
68	Calorimeter Insulation Temperature	T/C 125 Exit Superheater	8	1150-1650°F	CA T/C	Digital
69	Calorimeter Insulation Temperature	T/C 126 Exit Superheater	8	1150-1650°F	CA T/C	Digital
70	Calorimeter Insulation Temperature	T/C 127 Exit Superheater	8	1150-1650°F	CA T/C	Digital
71	Calorimeter Insulation Temperature	T/C 128 Exit Superheater	8	1150-1650°F	CA T/C	Digital
72	Calorimeter Insulation Temperature	T/C 129 Exit Superheater	8	1150-1650°F	CA T/C	Digital
73	Calorimeter Pressure	Aft Htr. "A"	8	0-50 psia	Efflux	Digital
74	Calorimeter Pressure	Aft Htr. "B"	8	0-50 psia	Efflux	Digital
75	Calorimeter Temp.	Aft Htr. "A"	8	1150-1650°F	CA T/C	Digital
76	Calorimeter Temp.	Aft Htr. "B"	8	1150-1650°F	CA T/C	Digital
77	Insulation Temperature	Compensating Heater	1	1150-1650°F	CA T/C	Digital
78	Insulation Temperature	Compensating Heater	1	1150-1650°F	CA T/C	Digital
79	Insulation Temperature	Compensating Heater	1	1150-1650°F	CA T/C	Digital
80	Insulation Temperature	Compensating Heater	1	1150-1650°F	CA T/C	Digital
81	Condenser Liquid Level	Condenser	11	0-6 inches	Ohmart & Brown	Sanborn
82	Main Condenser Flow	Main EMFM	11	0-10 MV	EMFM	Sanborn &Digital
83	Flow Temp. of Main Condenser	Main EMFM	11	432-932°F	CA T/C	Sanborn &Digital
84	Spray EMFM Temp. At Flowmeter	Spray EMFM		432-932°F	CA T/C	Digital

TABLE VI (Cont'd)

POTASSIUM VAPOR TURBINE TEST INSTRUMENTATION

Item No.	Parameter	Location	Station	Range	Sensor	Control Room Readout
85	Speed (Berkeley)	Steam Turbine	11	0-25,000 rpm	Magnetic Pickup	Berkeley
86	Speed (Sanborn & Digital)	Steam Turbine	11	0-25,000 rpm	Magnetic Pickup	Sanborn &Digital
87	Steam Turbine Torque	Steam Turbine	11	0-200 in/lbs	Bytrex	Digital
88	Potassium Turbine Torque	Glove Box	11	0-100 lbs	Loadcell	Dial & Sanborn Digital
89	Condenser Liquid Temperature	Condenser	11	300-1300°F	CA T/C	Digital
90	R.T.D. C.A.T.S. Block Temperature	CATS Block		5.6 MV	R.T.D.	Digital
91	Vapor Static Pressure Compliment of No. 26	Upstr. Rotor-1 Tip 280-1	4	0-50 psia	Efflux	Deleted
92	Vapor Static Pressure Compliment of No. 27	Upstr. Rotor-1 Hub 280-1	4	0-50 psia	Efflux	Deleted
93	Transducer Power Supply 5.0 Volts	Control Room		5.0 Volts		Digital
94	Standard Resistor R/D Network			5.6 MV		Digital
	TURBINE PAD BEARING					
95	Pad Bearing Temp. Pad #2	Pad Bearing		250°F	CA T/C	TR #3-1
96	Pad Bearing Temp. Pad #2	Pad Bearing		250°F	CA T/C	TR #3-2
97	Pad Bearing Temp. Pad #1	Pad Bearing		250°F	CA T/C	TR #3-3
98	Pad Bearing Temp. Pad #5	4-R Pad			CA T/C	Sanborn
99	Pad Bearing Cavity Temperature				CA T/C	TR #3-4
100	Pad Bearing Lube Inlet Pressure	Pad Bearing			Gauge	Visual & Wrng.Sig.
101	Pad Bearing Lube Flow	Pad Bearing		0-200 H_2O (3 gpm)	Foxboro D.P. Cell	Sanborn
102	"K" Turbine Bearing Lube Temperature Out	Outlet Oil Line		250°F	CA T/C	Digital TR #3-5
103	"K" Turbine Bearing Lube Temperature In	Inlet Oil Line		250°F	CA T/C	Digital TR #3-6
104	Stabilizer Bearing Temperature			250°F	CA T/C	TR #3-7

TABLE VI (Cont'd)

POTASSIUM VAPOR TURBINE TEST INSTRUMENTATION

Item No.	Parameter	Location	Station	Range	Sensor	Control Room Readout
	TURBINE BALL	BEARING				
105	Rear Ball Thrust Bearing Temperature			32-282°F	CA T/C	Sanborn
106	Forward Ball Thrust Bearing Temperature			250°F	CA T/C	Sanborn & TR #3-8
107	Ball Bearing Lube Oil Pressure In			200 psig	Bourdon Gauge	Visual & Wrng.Sig.
108	Ball Bearing Lube Oil Flow			0-200"H_2O (3 gpm)	Foxboro D.P. Cell	Sanborn
	STEAM TURBINE	BEARING				
109	Temp. Steam Turbine Bearing Forward			250°F	CA T/C	TR #3-9
110	Temp. Steam Turbine Bearing Middle			250°F	CA T/C	TR #3-10
111	Temperature Steam Turbine Bearing Aft			250°F	CA T/C	TR #3-11
112	Temperature Steam Turbine Lube In			250°F	CA T/C	TR #3-12
113	Temperature Steam Turbine Lube Out			250°F	CA T/C	TR #3-13
114	Steam Turbine Lube Oil Pressure			80 psig	Bourdon Gauge	Warning Light
115	Steam Turbine & H_2O Brake Lube Oil Flow			1 gpm	Flow-rator	Warning Light
	WATER BRAKE					
116	H_2O Brake, Water Inlet Temperature			60°F	CA T/C	TR #3-14 Digital
117	H_2O Brake, Water Outlet Temperature			150°F	CA T/C	Digital TR #3-15
118	Temperature H_2O Brake Bearing Forward			180°F	CA T/C	TR #3-16
119	Temperature H_2O Brake Bearing Aft			180°F	CA T/C	TR #3-17
120	H_2O Brake; Water Flow			0-50 gpm	D.C. Generator	Gauge
121	H_2O Brake; Lube Oil Flow			1 gpm	Flow-rator	Warning Light

TABLE VI (Cont'd)

POTASSIUM VAPOR TURBINE TEST INSTRUMENTATION

Item No.	Parameter	Location	Station	Range	Sensor	Control Room Readout
	V I B R A T I O N					
122	Displacement Steam Turbine Aft Bearing Vert.			0-5 mils	Vib.P/U	Sanborn
123	Displacement Steam Turbine Aft Bearing Hor.			0-5 mils	Vib.P/U	Sanborn
124	Displacement Aft "K" Turbine Vertical			0-5 mils	Vib.P/U	Sanborn
125	Displacement Aft "K" Turbine Horizontal			0-5 mils	Vib.P/U	Sanborn
126	Accel. Pad Bearing Vertical			0-10 g's	Accel.	Visual
127	Accel. Pad Bearing Horizontal			0-10 g's	Accel.	Visual
	H Y D R O D Y N A M I C	S E A L				
128	Temp. Seal "K" In			500°F	CA T/C	Digital& TR#3-18
129	Temp. Seal "K" Out			1000°F	CA T/C	Digital& TR#3-43
130	Slinger Seal Turbine Inlet Pressure P-11			0-150 psig	Taylor Gauge	Visual
131	P-6 Oil Side Seal Pressure			0-30 psig	Taylor Gauge	Visual
132	"K" Seal Flow			0-5 MV See Curve	Pace + EMFM	Flow Rec. &Digital
133	Temp. Argon Seal In			500°F	CA T/C	TR#3
134	Turbine Argon Inlet Pressure P-7	Lab.Seal Inlet at Man.		100 psig	Pressure Gauge	Visual
135	Bearing Sump Wall Temperature			500°F	CA T/C	Multipt. Rec.
136	Lube Cart Pressure Out			200 psig	Gauge	Visual
137	Stabilizer Bearing Lube Pressure			200 psig	Gauge	Visual
138	Stabilizer Bearing Piston Actuating Pressure			200 psig	Gauge	Visual
139	P-8 Potassium Side Seal Pressure			-30" Hg to 100 psig	Taylor & Statham	Sanborn &Visual
140	Argon Header Press.P-1			0-60 psig	Taylor Gauge	Visual

TABLE VI (Cont'd)

POTASSIUM VAPOR TURBINE TEST INSTRUMENTATION

Item No.	Parameter	Location	Station	Range	Sensor	Control Room Readout
141	Argon Extraction Flow	Downstream of VPL-8	11	0-10 MV See Curve	EMFM	Sanborn
142	Boiler Feed Pressure	Boiler Inlet			Wiancko & Tylr.Gage	Sanborn
143	Turbine Shaft 270° Movement Radial	Stabilizer Bearing			Bently Gage	Oscillo-Scope
144	Turbine Bearing Housing Temp.(Fwd)	Bearing Housing	Section E		CA T/C	TR #1-4
145	Turbine Bearing Housing Temp.(Aft)	Bearing Housing	Section F		CA T/C	TR #1-13
146	Turbine Casing Fwd.Temperature	Turbine Casing	3	1400°F	CA T/C	Multipt. Rec.
147	Turbine Casing Aft. Temperature	Turbine Casing	5	1400°F	CA T/C	Multipt. Rec.
148	8" Vapor Line Temp.	6"Aft of Spray Line	2	1400°F	CA T/C	Multipt. Rec.
149	8" Vapor Line Temp.	14"Aft of Spray Line	2	1400°F	CA T/C	Multipt. Rec.
150	Pad Bearing Ring Temp. #1 T/C 24°	Pad Bearing Ring			CA T/C	TR #3-19
151	Pad Bearing Ring Temp. #2 T/C 50°	Pad Bearing Ring			CA T/C	TR #3-20
152	Bullet Nose Delta-P	Between Items #21 & 25	3	0-1.5 psid	Efflux & Pace P3	Digital &Sanborn
153	Turbine Delta-P	Between Items #18 & 41	3 & 7	0-50 psid	Efflux & Pace P3	Digital &Sanborn
154	Boiler Feed Temperature	At Boiler Feed EMFM			CA T/C	Sanborn
155	Boiler Feed Flow	Boiler Input		----	EMFM	Sanborn
156	Exit Calorimeter Htr. "B" Power Input	Exit Calorimeter	8	0-5 KW	Hall X-Ducer	Dial & Digital
157	Exit Calorimeter Htr. "A" Power Input	Exit Calorimeter	8	0-5 KW	Hall X-Ducer	Dial & Digital
158	Compensating Heater Power Input	Compensating Heater	2	0-5 KW	Hall X-Ducer	Dial & Digital
159	Vapor Static Pressure		1		Taylor & Pace	Digital
160	Vapor Static Pressure		7		Taylor & Statham	&Digital
161	Turbine Shaft Movement Radial (180°)	Stabilizer Bearing			Bently Gage	Oscillo-Scope

TABLE VI (Cont'd)

POTASSIUM VAPOR TURBINE TEST INSTRUMENTATION

Item No.	Parameter	Location	Station	Range	Sensor	Control Room Readout
162	Boiler Liquid Level	Boiler			"J" Tube	Sanborn
163	Boiler Liquid Level	Boiler			Ohmart Gage	Recorder + Dial
164	VPL-11 Valve Stem Position	VPL-11			Linear Motion Pot.	Sanborn
165	Water Brake Valve Stem Position	Water Brake Valve			Linear Motion Pot.	Sanborn
166	Boiler Discharge Temperature (Skin)	Upstream of VPL-11		1650°F	Skin CA T/C	Sanborn &Digital
167	Vapor Temperature	Midstream 022°	3	1650°F	CA T/C	Digital
168	Water Brake Forward Vibration Vertical	Water Brake			Vib. P/U	G.E. Vib. Meter
169	Water Brake Forward Vibration Horizontal	Water Brake			Vib. P/U	G.E. Vib. Meter
170	Water Brake Water Flow	Water Brake Inlet			Potter	Digital
171	Vapor Drum Separator Heat. Exch. T/C 47	Vapor Drum			CA T/C	Sanborn
172	Vapor Drum Separator Heat Exch. T/C 48	Vapor Drum			CA T/C	Sanborn
173	Delta -P at Bullet Nose	Item 20 Item 24	3	.0-1.5 psid	X-Ducer	Sanborn + Digital
174	200 "lb Bytrex Temperature	Body of 200" lb Bytrex		150°F	Skin CA T/C	TR #3-14

TABLE VII

SANBORN LIST

SANBORN NUMBER	CHANNEL NUMBER	ITEM NUMBER	QUANTITY
A	1	86	Speed
"	2	88	Water Brake Torque
"	3	106	Forward Bearing Temperature
"	4	98/105*	Pad Bearing Temperature or Rear Ball Bearing Temperature
"	5	108	Ball Bearing Lube Flow
"	6	101	Pad Bearing Lube Flow
"	7	122/123*	Steam Turbine Vibrations Vertical or Horizontal
"	8	124/125*	Potassium Turbine Vibrations Vertical or Horizontal
B	1	139	Potassium Side Seal Pressure (P_8)
"	2	159	Station No. 1 Taylor gage
"	3	3	Turbine Inlet Temperature (Station #1)
"	4	171/ 172	Boiler Separator Heat Exchanger Differential Temp.
"	5	21	Turbine Inlet Pressure (Station #3)
"	6	153	Turbine Differential Pressure (Between Station #s 3 and 7)
"	7	166	Boiler Discharge Vapor Temperature
"	8	160	Station No. 7 Taylor Gage
C	1	82	Main Condenser Flow
"	2	141	Argon Extraction Flow
"	3	81	Condenser Level
"	4	62	Station Number 8 Pressure (Taylor Gauge)
D	1	86	Speed
"	2	142	Boiler Pressure (Taylor Gage)
"	3	152/173*	Bullet Nose Annulus Differential Pressure
"	4	162	Boiler Liquid Level "J" Tube
"	5	164/165*	VPL-11 Position or Water Brake Inlet Valve Position
"	6	155	Boiler Feed Flow
"	7	154	Boiler Feed Temperature
"	8	47	Turbine Exit Temperature (Station #7)

* Switch must be provided to read either value on Sanborn Recorder.

TABLE VIII

ACCURACY OF TURBINE EFFICIENCY INSTRUMENTATION

Quantity	Estimated Accuracy	Influence Coefficient*	
		1450°F	1550°F
Inlet Pressure	± 0.25 psia	-0.79	-0.91
Exit Pressure	± 0.25 psia	.76	.85
Differential Pressure	± 0.015 psi	-0.5	-0.5
Water Brake Torque	± 10 in. lb.	0.91	1.04
Calorimeter Pressure	± 0.25 psia	0.015	0.02
Calorimeter Temperature	± 5°F	-0.24	-0.27
Reference Temperature	± 2°F	-0.029	-0.033
Speed	± 44 rpm	1.28	1.28

$$\text{*Influence Coefficient} = \frac{\text{Percentage error in calculated turbine efficiency}}{\text{Percentage error in measured parameter}}$$

TABLE IX

POTASSIUM TURBINE TESTING - 3000 KW FACILITY

ITEM NO.	PARAMETER	LOCATION	STATION RANGE		SENSOR	CONTROL ROOM READOUT	CATS or REFLEX NO. DIGITAL NO.	CHANNEL OR POSITION
1	Vapor Total Temp., °F	045-1	1	1400-1650°F	CA T/C	Digital		
2	Vapor Total Temp., °F	135-1	1	1400-1650°F	CA T/C	Digital		
3	Vapor Total Temp., °F	235-1	1	1432-1682°F	CA T/C	Sanborn		1-B
4	Vapor Total Temp., °F	315-1	1	1400-1650°F	CA T/C	Digital		
5	Vapor Total Temp., °F	315-2	1	1400-1650°F	CA T/C	Digital		
13	Calorimeter Temp., °F	Calorimeter 010-1	1	1400-1650°F	CA T/C	Digital		
28	Vapor Temperature	Wheel Space 120		1450-1650°F	CA T/C	Digital		
29	Vapor Temperature	Wheel Space 330	4	650-1650°F	CA T/C	Digital		
32	Vapor Temperature	Deleted	5	650-1650°F	CA T/C			
33	Vapor Temperature	Deleted	5	650-1650°F	CA T/C			
46	Vapor Temperature	OGV 128	7	650-1650°F	CA T/C	Digital		
47	Vapor Temperature	OGV 142	7	650-1650°F	CA T/C	Digital		
48	Vapor Temperature	OGV 156	7	650-1650°F	CA T/C	Digital		
49	Vapor Temperature	OGV 230	7	650-1650°F	CA T/C	Digital		
50	Vapor Temperature	OGV 45	7	650-1650°F	CA T/C	Digital		
51	Vapor Temperature	OGV 308	7	650-1650°F	CA T/C	Sanborn		2-B
52	Vapor Temperature	SW-1	8	650-1650°F	CA T/C	Digital		
53	Vapor Temperature	SW-2	8	650-1650°F	CA T/C	Digital		
54	Vapor Temperature	SE=1	8	650-1650°F	CA T/C	Digital		
55	Vapor Temperature	NE-1	8	650-1650°F	CA T/C	Digital		
56	Vapor Temperature	NW-1	8	650-1650°F	CA T/C	Digital		
62	Vapor Static Pressure	N-1 Main Cond.	8	0-50 Psia	Taylor Statham	Digital & Sanborn		
81	Condenser Liquid Lev.	Condenser	11	0-6 inches	Ohmart & Brown	Sanborn		3-C
82	Main Condenser Flow	Main EmFm	11	0-10 MV	EmFm	Sanborn & Digital		
83	Flow Temp. of Main Condenser	Main EmFm	11	432-932°F	CA T/C	Sanborn & Digital		

TABLE IX

POTASSIUM TURBINE TESTING - 3000 KW FACILITY

(CONTINUED)

ITEM NO.	PARAMETER	LOCATION	STATION	RANGE	SENSOR	CONTROL ROOM READOUT		CHANNEL OR POSITION
85	Speed (Berkeley)	Steam Turb.	11	0-25,000 rpm	Magnetic Pickup	Berkeley		
86	Speed Sanborn & Digital	Steam Turb.	11	0-25,000 rpm	Magnetic Pickup	Sanborn & Digital		7-B
87	Steam Turbine Torque	Steam Turb.	11	0-200 in/lb	Bytrex	Dial & Digital		
88	Potassium Turbine Torque	"K" Turbine	11	0-100 lb	Sanborn & Loadcell	Dial & Digital		2-A
89	Condenser Liquid Temperature	Condenser	11	300-1300°F	CA T/C	Digital		
90	R.T.D. C.A.T.S. Block Temperature	CATS Block			R.T.D.	Digital		
93	Transducer P-s 5.0 volts			5.0 volts		Digital		
94	Standard Resistor R.T.D. Network			5.6 MV		Digital		
	TURBINE PAD BEARING							
95	Pad Bearing Temp. Pad #2	Pad Bearing		250°F	CA T/C	TR #3-1		
96	Pad Bearing Temp. Pad #2	Pad Bearing		250°F	CA T/C	TR #3-2		
97	Pad Bearing Temp. Pad #1	Pad Bearing		250°F	CA T/C	TR #3-3		
98	Pad Bearing Temp. Pad #5	4-R Pad		250°F	CA T/C	Sanborn		4-A
99	Pad Bearing Cavity Temp.					TR #3-4		
100	Pad Bearing Lube Inlet Pressure	Pad Bearing		200 psig	Bourdon Gauge	Visual & Wrng.Sig		
101	Pad Bearing Lube Flow	Pad Bearing		0-200 H_2O (3 gpm)	Foxboro D.P.Cell	Sanborn		6-A
102	"K" Turbine Bearing Lube Temperature Out			250°F	CA T/C	Digital & TR #3-5		
103	"K" Turbine Bearing Lube Temperature In			250°F	CA T/C	Digital & TR #3-6		
104	Stabilizer Bearing Temperature			250°F	CA T/C	TR #3-7		
	TURBINE BALL BEARING							
105	Rear Ball Thrust Bearing Temperature			32-282°F	CA T/C	Sanborn TR#3-20		4-A
106	Forward Ball Thrust Bearing Temperature			250°F	CA T/C	Sanborn & TR#3-8		3-A
107	Ball Bearing Lube Oil Pressure In			200 Psig	Bourdon Gauge	Visual & Wrng.Sig		
108	Ball Bearing Lube Oil Flow			0-200 H_2O (3 gpm)	Foxboro D.P.Cell	Sanborn		5-A

TABLE IX

POTASSIUM TURBINE TESTING - 3000 KW FACILITY

(CONTINUED)

ITEM NO.	PARAMETER	LOCATION	STATION	RANGE	SENSOR	CONTROL ROOM READOUT		CHANNEL OR POSITION
	STEAM TURBINE BEARING							
109	Temp. Steam Turbine Bearing Forward			250°F	CA T/C	TR #3-9		
110	Temp. Steam Turbine Bearing Middle			250°F	CA T/C	TR#3-10		
111	Temperature Steam Turbine Bearing Aft.			250°F	CA T/C	TR#3-11		
112	Temperature Steam Turbine Lube In			250°F	CA T/C	TR#3-12		
113	Temperature Steam Turbine Lube Out			250°F	CA T/C	TR#3-13		
114	Steam Turbine Lube Oil Pressure			80 psig	Bourdon Gauge	Warning Light		
115	Steam Turbine & H_2O Brake Lube Oil Flow			1 gpm	Flow-Rator	Warning Light		
	WATER BRAKE							
116	H_2O Brake, Water Inlet Temperature			60°F	CA T/C	Digital		
117	H_2O Brake, Water Outlet Temperature			150°F	CA T/C	Digital & TR#3-18		
118	Temperature H_2O Brake Bearing Forward			180°F	CA T/C	TR#3-16		
119	Temperature H_2O Brake Bearing Aft.			180°F	CA T/C	TR#3-17		
120	H_2O Brake; Water Flow			0-50 gpm	D.C. Generator	Gauge		
121	H_2O Brake; Lube Oil Flow			1 gpm	Flow-Rator	Warning Light		
	VIBRATION							
122	Displacement Steam TurbineAftBearing Vert.			0-5 Mils.	Vib.P/U	Sanborn		7-A
123	Displacement Steam Turbine Aft. Bearing Hor.			0-5 mils.	Vib.P/U	Sanborn		7-A
124	Displacement Aft "K" Turbine Vert.			0-5 mils.	Vib.P/U	Sanborn		8-A
125	Displacement Aft "K" Turbine Hor.			0-5 mils.	Vib.P/U	Sanborn		8-A
126	Accel. Pad Bearing Vert.			0-10 g's	Accel.	Visual		
127	Accel. Pad BearingHor			0-10 g's	Accel.	Visual		
	HYDRODYNAMIC SEAL							
128	Temp. Seal "K" In			500°F	CA T/C	Digital & TR #2-9		
129	Temp. Seal "K" Out			1000°F	CA T/C	Digital & TR #2-10		

TABLE IX

POTASSIUM TURBINE TESTING - 3000 KW FACILITY

(CONTINUED)

ITEM NO.	PARAMETER	LOCATION	STATION	RANGE	SENSOR	CONTROL ROOM READOUT		CHANNEL OR POSITION
130	Slinger Seal Turbine Inlet Pressure P-11			0-150 psig	Taylor Gage	Visual		
131	P-6 Oil Side Seal Pressure			0-30 psig	Foxboro & Wiancko	Sanborn & Visual		6-B
132	"K" Seal Flow			See Curve 0-25 MV	Pace & EmFm	Flow Rec. & Digital		
133	Temp. Argon Seal In			500°F	CA T/C	TI#3-46		
134	Turbine Argon Inlet Pressure P-7	Lab Seal Inlet at Man.		100 psig	Pressure Gauge	Visual		
136	Lube Cart Pressure Out			200 psig	Gauge	Visual		
137	Stabilizer Bearing Lube Pressure			200 psig	Gauge	Visual		
138	Stabilizer Bearing Piston Actuating Pres.			200 psig	Gauge	Visual		
139	P-8 Potassium Side Seal Pressure			-30"Hg to 100 psig	Taylor & Statham	Sanborn& Visual		5-B
140	Argon Header Press. P-1			0-60 psig	Taylor Gauge	Visual		
141	Argon Extraction Flow	Downstream of VPL-8	11	0-10 MV See Curve	EmFm	Sanborn		2-C
142	Boiler Drum Pressure	Boiler Inlet			Wiancko & Tylr.Gag	Sanborn		3-B
143	Turbine Shaft 270° Movement Radial	Stabilizer Bearing			Bently Gage	Oscillo-scope		
144	Turbine Bearing Housing Temp. (Fwd)	Bearing Housing	Sec. E		CA T/C	TR #2-11		
145	Turbine Bearing Housing Temp. (Aft)	Bearing Housing	Sec. F		CA T/C	TR #2-12		
146	Turbine Casing Fwd. Temperature	Turbine Casing	3	1400°F	CA T/C	TR #2-14		
147	Turbine Casing Aft. Temperature	Turbine Casing	5	1400°F	CA T/C	TR #2-15		
148	8" Vapor Line Temp.	6" Aft. of Spray Line	2	1400°F	CA T/C			
149	8" Vapor Line Temp.	14" Aft of Spray Line	2	1400°F	CA T/C	TR #1-2		
150	Pad Bearing Ring Temp. #1 T/C24°	Pad Bearing Ring			CA T/C	TR#3-19		
151	Pad Bearing Ring Temp. #2T/C50°	Pad Bearing Ring			CA T/C	TR#3-20		
155	Boiler Feed Flow	Boiler Input			EmFm	Sanborn		1-C
159	Vapor Static Pressure		1		Taylor & Pace	Digital		8-B
160	Vapor Static Pressure		7		Taylor & Statham	Digital		
161	Turbine Shaft Movement Radial(180°)	Stabilizer Bearing			Bently Gage	Oscillo-scope		

TABLE IX

POTASSIUM TURBINE TESTING - 3000 KW FACILITY

(CONTINUED)

ITEM NO.	PARAMETER	LOCATION	STATION	RANGE	SENSOR	CONTROL ROOM READOUT		CHANNEL OR POSITION
163	Boiler Liquid Level	Boiler			Ohmart Gage	Recorder & Dial		
166	Boiler Discharge Temperature (Skin)	Upstream VPL-11		1650°F	Skin CA T/C	Sanborn &Digital		
167	Vapor Temperature	Midstream .022	3	1550°F	CA T/C	Digital		
168	Water Brake Forward Vibration Vertical	Water Brake			Vib.P/U	GE Vib. Meter		
169	Water Brake Forward Vibration Horizontal	Water Brake			Vib.P/U	GE Vib. Meter		
170	Water Brake Water Flow	Water Brake Inlet			Potter	Digital		
171	Vapor Drum Separator Heat Exch. T/C 47	Vapor Drum			CA T/C	Sanborn		4-B
172	Vapor Drum Separator Heat Exch. T/C 48	Vapor Drum			CA T/C	Sanborn		4-B
174	200"lb Bytrex Rear Temperature Flange	Top of 200 lb Byt.		150°F	Skin CA T/C	Digital		
176	1250"lb Bytrex Fwd. Flange Temp.	Top of Fwd. Flange		150°F	Skin CA T/C	Digital		
177	1250"lb Bytrex Rear Flange Temp.	Top of Rear Flange		150°F	Skin CA T/C	Digital		
178	Bearing Housing Fwd.	Bottom Centerline	Sec F		Skin CA T/C	TR 3-7		
179	Bearing Housing Mid	Bottom Centerline	Sec F		Skin CA T/C	TR 3-14		
180	Bearing Housing Aft.	Bottom Centerline	Sec F		Skin CA T/C	TR 3-15		
181	Vapor Total Temp.	Inlet Duet	3	1550°F	CA T/C	Digital		
182	Vapor Total Temp.	Inlet Duet	3	1550°F	CA T/C	Digital		
183	Vapor Total Temp.	Inlet Duet	3	1550°F	CA T/C	Digital		
184	Throttling Calorimeter Taylor Gage	Inlet Calorimeter	1		Taylor Gage	Digital		

TABLE X

POTASSIUM TURBINE TEST - 3000 KW FACILITY

SANBORN INSTRUMENTATION

ITEM NO-	PARAMETER	SANBORN NO.	STATION LOCATION #	LOCATION	SENSOR	RANGE IN UNITS	DIGITAL CHANNEL	CALIBRATION	TURBINE SYSTEM NO.	CELL WIRING	ATTENUATION
86	RPM	1A	11	Steam Turbine	6 Tooth Gear & Magnetic P/U	0-25,000 rpm		0-2500 cps			
88	Water Brake Torque	2A	11	Aft of "K" Turbine	Strain Gage Bytrex	0-1250 in/lbs		0-1250 in/lbs			
106	Fwd. Ball Bearing Temp.	3A		"K" Turbine	CA T/C	32° - 282°F	No	32° - 282°F			
98	Pad Bearing Temp.	4A		"K" Turbine	CA T/C	32° - 282°F	No	32° - 282°F			
105	Rear Ball Bearing Temp.	4A		"K" Turbine	CA T/C	32° - 282°F	No	32° -282°F			
108	Ball Bearing Lube Flow	5A		Lube Inlet	Foxboro D/P Cell	0-200" H_2O See Curve	No	3 - 15 psig			
101	Pad Bearing Lube Flow	6A		Lube Inlet	Foxboro, D/P Cell	0-200 " H_2O See Curve	No	3 - 15 psig			
122	Steam Turbine Vib.Vert.	7A		Aft. Face of Steam Turbine	Velocity P/U	0-5 mils	No				
123	Steam Turbine Vib.Horiz.	7A		Aft. Face of Steam Turbine	Velocity P/U	0-5 mils	No				
124	"K" Turbine Vib. Vert.	8A		Flange of "K" Turbine Bearing Housing	Velocity P/U	0-5 mils	No				
125	"K" Turbine Vib. Horiz.	8A		Flange of "K" Turbine Bearing Housing	Velocity P/U	0-5 mils	No				
3	Turbine Inlet Temp. 1	1B	1	Inst. Section 235-1	CA T/C	1332°F - 1532°F	No	4°F/Line			
51	Turbine Exit Temp. 7	2B	7	O.G.V. Inlet	CA T/C	1032°F - 1432°F	No	8°F/Line			
142	Boiler Vapor Drum Pressure	3B		Boiler Drum	Taylor Gage & Statham 10538	0-60 psig	No	3 - 15 psig			
171 172	Boiler Heat Exchanger ΔT	4B		Vapor Separator Heat Exchanger							
139	"K" Side Seal Pres. P-8	5B		"K" Side Seal Manifold	Taylor Gage & Statham 10537	0-50 psia	No	0-50 psia			
131	Oil Side Seal Pres. P-6	6B		Oil Sump at Bearing	Foxboro & Wiancko 70756	0-30 psig	No	3 - 15 psig			
86	RPM	7B	11	Steam Turbine	6 Tooth Gear & Magnetic P/U	0-25,000 rpm		0-2500 cps			
159	Station 1 Taylor Gage Vapor Static	8B	1	Downstream of VPL 11	Taylor Gage & Pace	0-30 psia	No	0-30 psia			
155	Boiler Feed Flow	1C		Boiler Input	EmFm	No Calibration	No	0-10 MV			
141	Argon Extraction Flow	2C		Downstream VPL-8	EmFm	See Curve	No	0-10MV			
81	Condenser Liquid Level	3C		Condenser	Ohmart Gage (Brown Indicator)	0-6 Inches	No	0-100%			
62	Vapor Static Pressure Station 8 Taylor Gage	4C	8	M-1	Taylor Gage & Statham 10538	0-20 psia		0-5 MV			

TABLE XI

LIST OF INSTRUMENTATION

NOZZLE FLOW TEST

Item No.	Parameter	Sensor	Range	Accuracy
1	ASME Nozzle Throat Static Pressure	50 psig Transducer	40-70 psia	± 0.1 %
2				
3	ASME Nozzle Total Pressure	150 psig Transducer	50-132 psia	± 0.1 %
4				
5	Nozzle Diaphragm Static Pressure	20 psig Transducer	15-15 psia	± 0.1 %
6				
7				
8				
9				
10				
11				
12				
13				
14				
15	Nozzle Diaphragm Total Pressure	50 psig Transducer	40-60 psia	± 0.1 %
16				
17				
18				
19	ASME Nozzle Total Temperature	Copper-Constantan Thermocouple	Ambient	± 4°F
20				
21	Nozzle Diaphragm Total Temperature	Copper-Constantan Thermocouple	Ambient	± 4°F
22				

TABLE XII

SUMMARY OF NOZZLE DIAPHRAGM FLOW TEST DATA

Configuration	Test Point	Inlet Total Pressure Psia	Inlet Total Temperature °R	Air Dew Point Temp ° F	Air Flow #/Sec	Effective Area In^2	Average Effective Area In^2	Reynolds Number	Average Reynolds Number
3rd Stage Diaphragm	1	40.038	518.76	-47.0	5.808	6.207	6.208	197,329	197,044
	2	39.939	518.74	-49.0	5.797	6.210		196,980	
	3	39.914	518.69	-49.0	5.793	6.209		196,849	
	4	39.859	518.83	-49.0	5.780	6.205		196,430	
	5	40.079	518.83	-47.0	5.816	6.210		197,632	
	6	49.861	519.44	-46.0	7.253	6.225	6.227	246,528	246,583
	7	49.894	519.58	-45.0	7.257	6.225		246,660	
	8	49.995	519.67	-47.0	7.271	6.225		247,142	
	9	49.862	519.73	-47.0	7.258	6.231		246,609	
	10	49.772	519.73	-48.0	7.239	6.227		245,976	
	11	59.874	520.64	-47.0	8.688	6.216	6.215	295,281	295,197
	12	59.863	520.62	-47.0	8.689	6.217		295,241	
	13	59.880	520.69	-47.0	8.684	6.213		295,109	
	14	59.843	520.62	-47.0	8.687	6.218		295,274	
	15	59.860	520.69	-47.0	8.683	6.213		295,081	
4th Stage Diaphragm	1	39.979	529.16	-23.8	7.588	8.200	8.201	161,914	161,814
	2	39.923	529.35	-23.8	7.576	8.201		161,625	
	3	40.011	529.44	-21.0	7.592	8.200		161,997	
	4	39.970	529.48	-25.0	7.586	8.201		161,844	
	5	39.934	529.44	-24.0	7.579	8.201		161,690	
	6	50.013	530.57	-27.0	9.508	8.222	8.224	202,895	202,806
	7	49.906	530.37	-29.0	9.495	8.227		202,610	
	8	49.965	530.43	-29.0	9.503	8.224		202,853	
	9	50.019	530.34	-27.0	9.509	8.220		202,948	
	10	49.938	530.41	-29.0	9.502	8.228		202,723	
	11	59.871	531.16	-32.0	11.364	8.211	8.212	242,469	242,755
	12	60.064	531.46	-32.0	11.401	8.213		243,384	
	13	59.855	531.27	-32.0	11.361	8.212		242,408	
	14	59.968	531.39	-27.0	11.382	8.212		242,854	
	15	59.918	531.32	-29.5	11.373	8.212		242,659	

TABLE XIII

QUANTITIES MEASURED ON THE CONTINUOUS RECORDERS

Recorder No. A

1. Speed
2. Water Brake Torque
3. Forward Ball Bearing Temperature
4. Pad Aft Ball Bearing Temperature
5. Pad Bearing Lube Flow
6. Ball Bearing Lube Flow
7. Steam Turbine Vibrations
8. Potassium Turbine Vibrations

Recorder No. B

1. Potassium Side Seal Pressure (P-8)
2. Spray EMFM Temperature
3. Turbine Inlet Temperature
4. Liquid Injection Temperature
5. Turbine Inlet Pressure
6. Exit Static Pressure (Inoperative)
7. Main Condenser EMFM Temperature (Figures 37 and 38)
   Boiler Discharge Temperature (Figures 39, 40 and 41)
8. Spray Flow

Recorder No. C

1. Main Condenser Flow
2. Argon Extraction Flow
3. Condenser Liquid Level
4. Condenser Static Pressure (Taylor Gage)

Recorder No. D

1. Speed
2. Boiler Feed Pressure
3. Bullet Nose Velocity
4. Acceleration of Main Throttle Valve Stem
5. Position of Boiler Feed Control Valve
6. Boiler Feed Flow (Figures 39, 40 and 41)

NOTE: The traces made by Recorders A, B, C and D are to be found on parts a, b, c, and d of each figure.

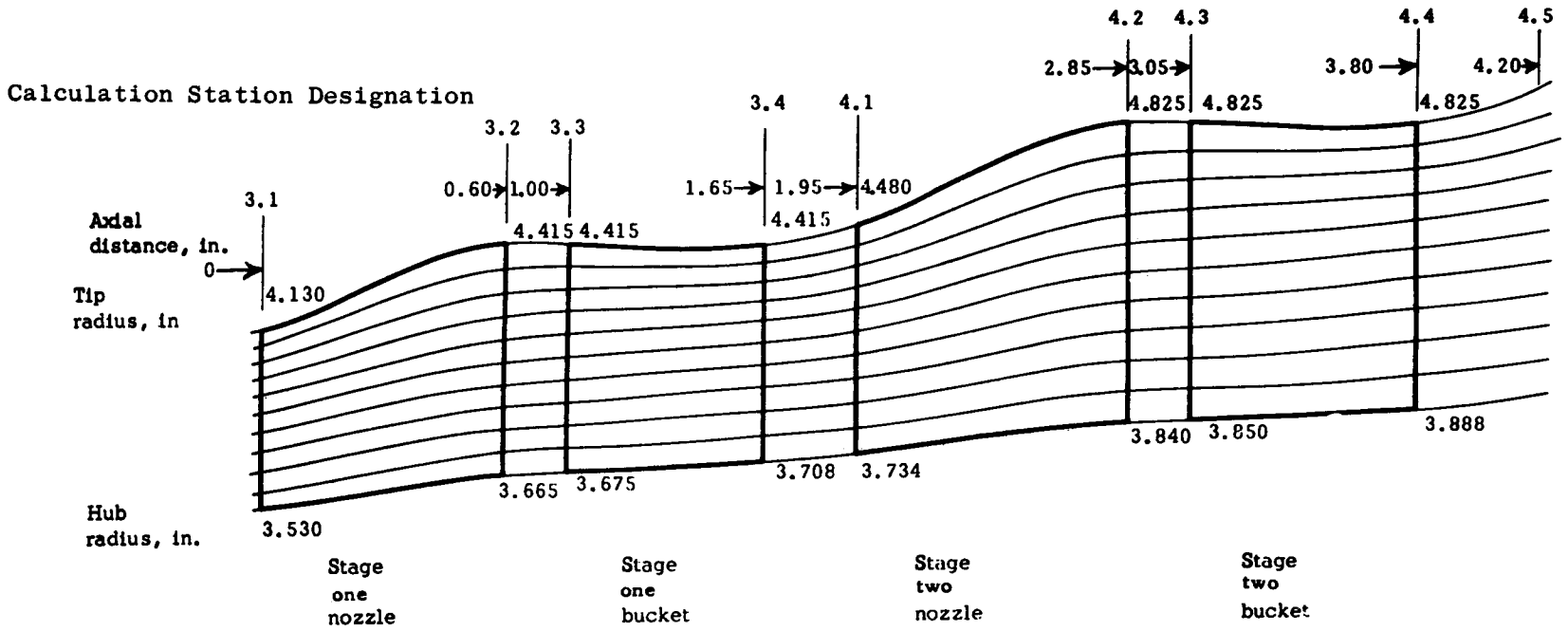

Figure 1. Test Turbine Flow Path Showing Meridional Streamlines.

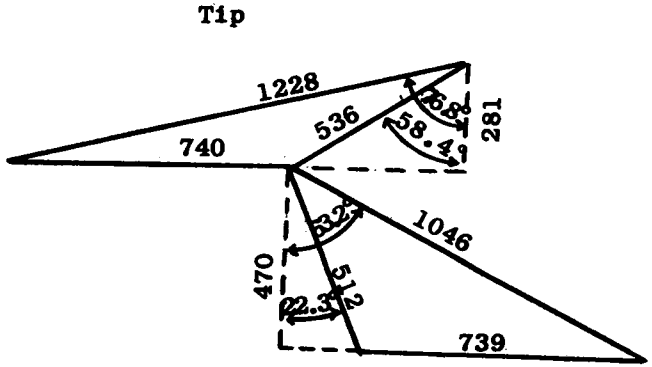

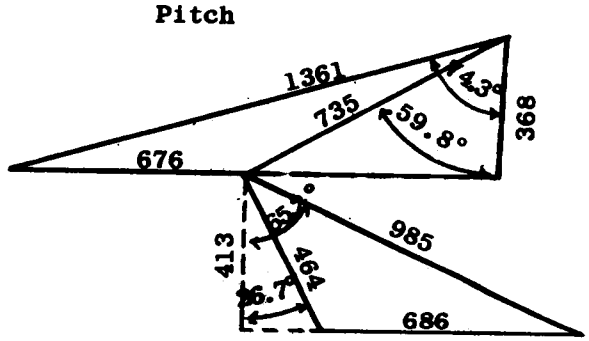

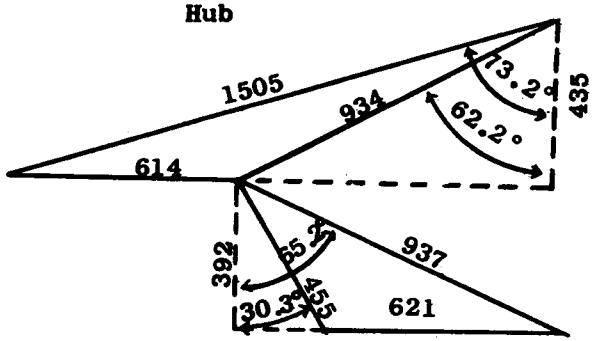

(a) Stage 1

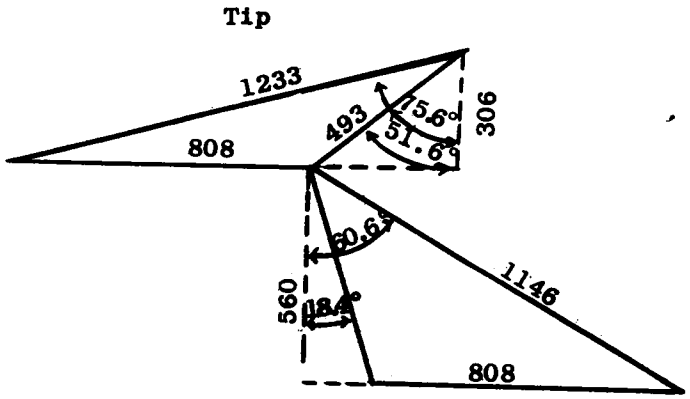

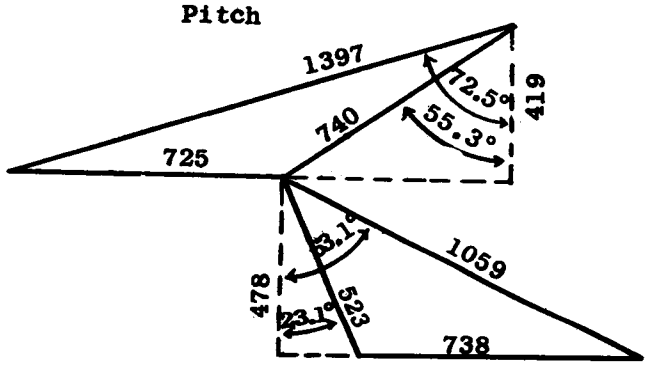

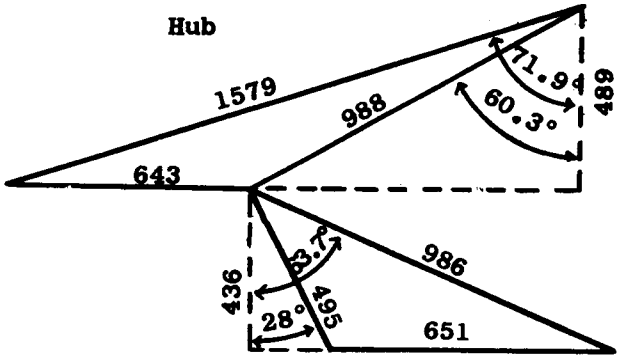

(b) Stage 2

Figure 2. Velocity Diagrams For Test Turbine.

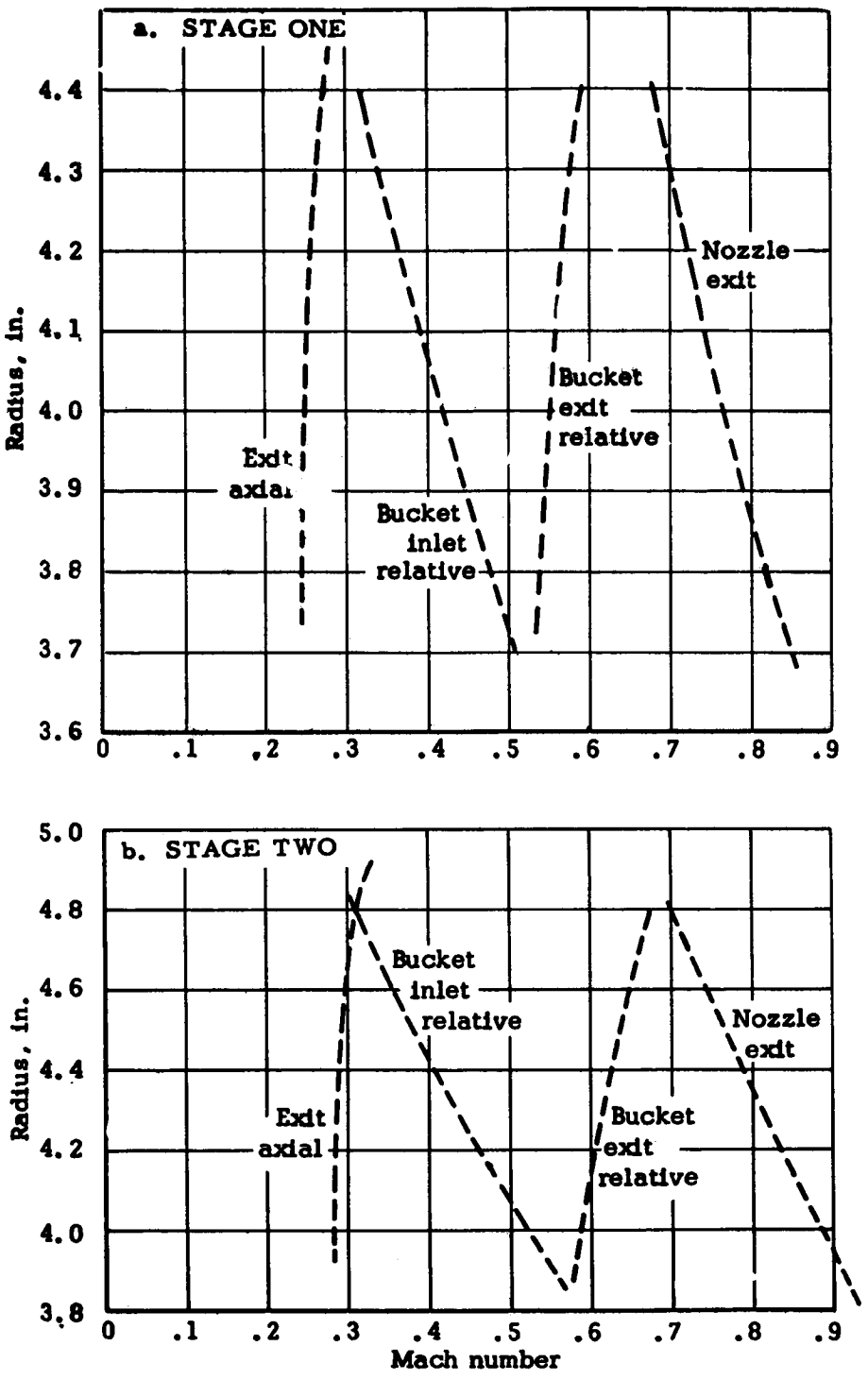

Figure 3. Radial Mach Number Distributions For Test Turbine.

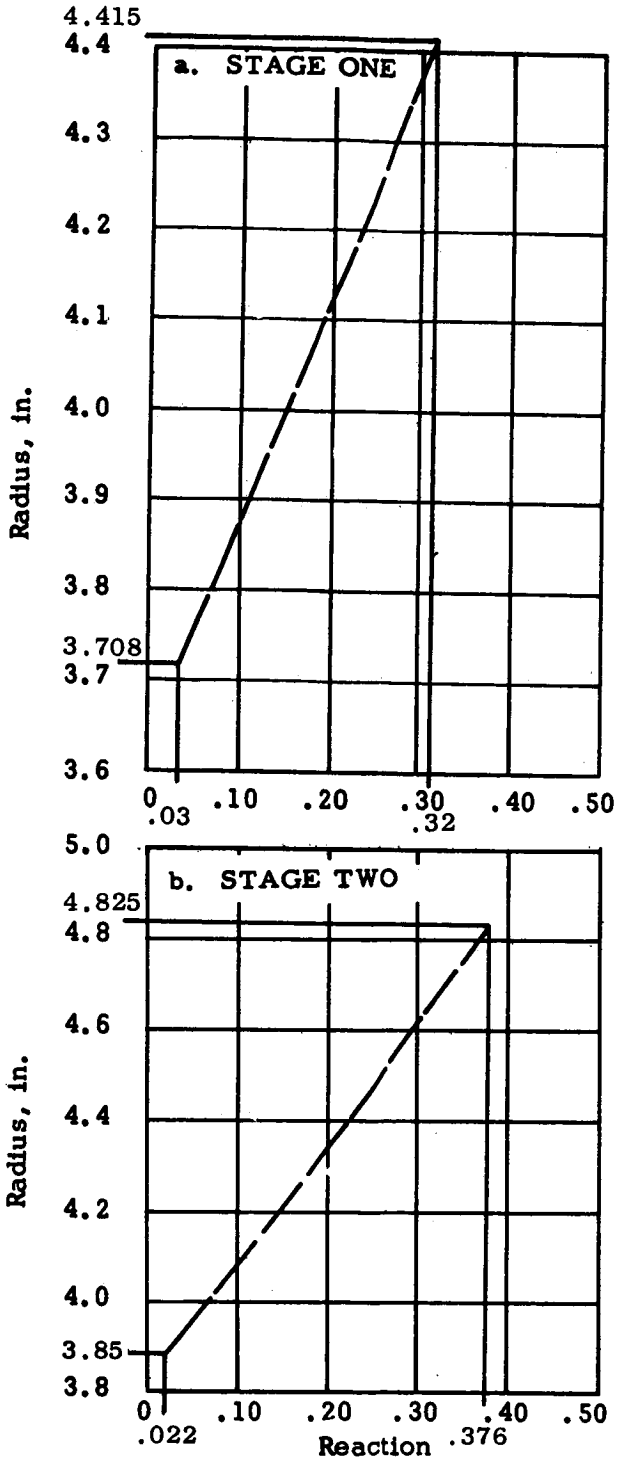

Figure 4. Radial Distribution of Reaction For Test Turbine.

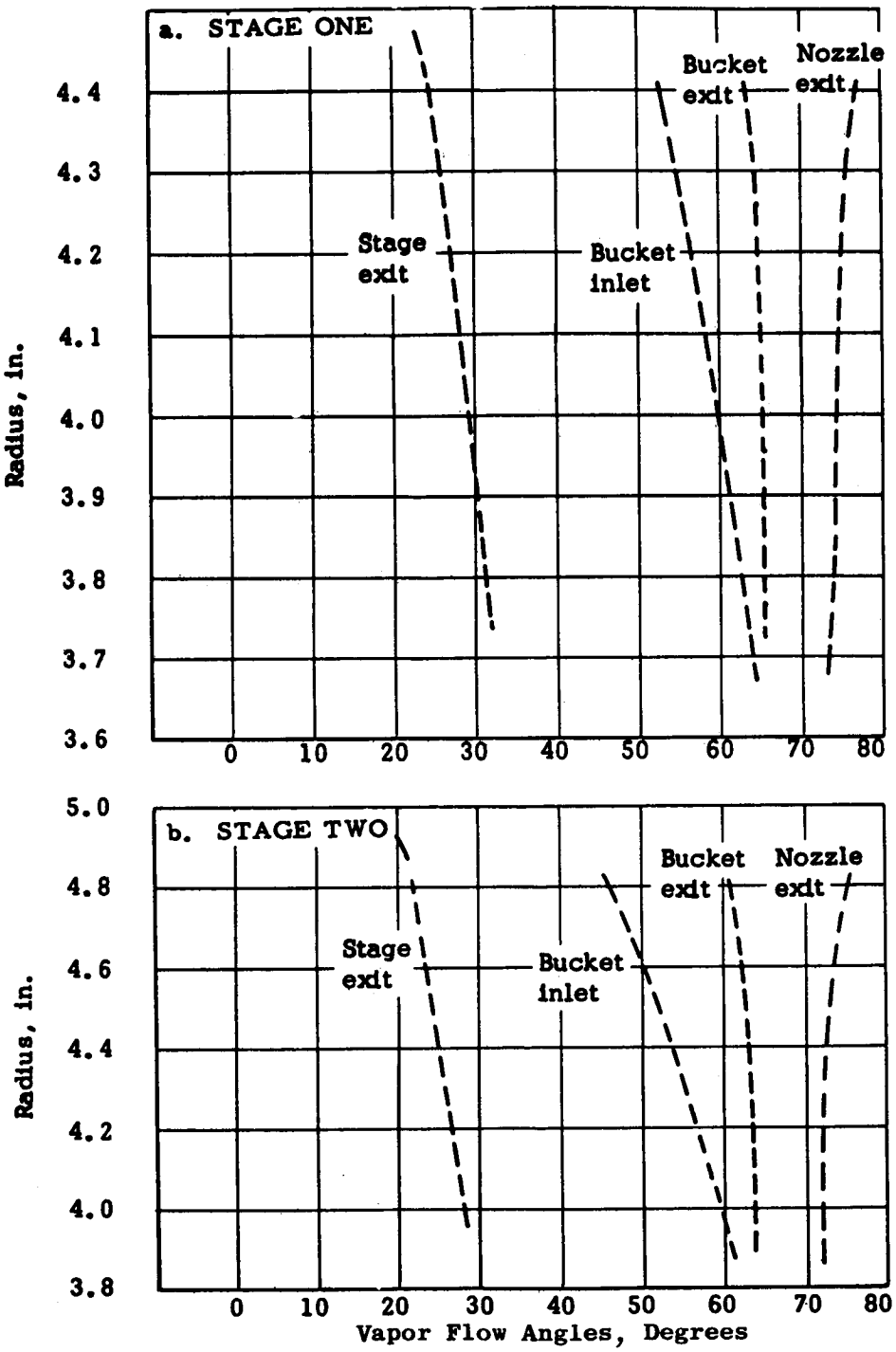

Figure 5. Radial Distribution of Vapor Flow Angles For Test Turbine.

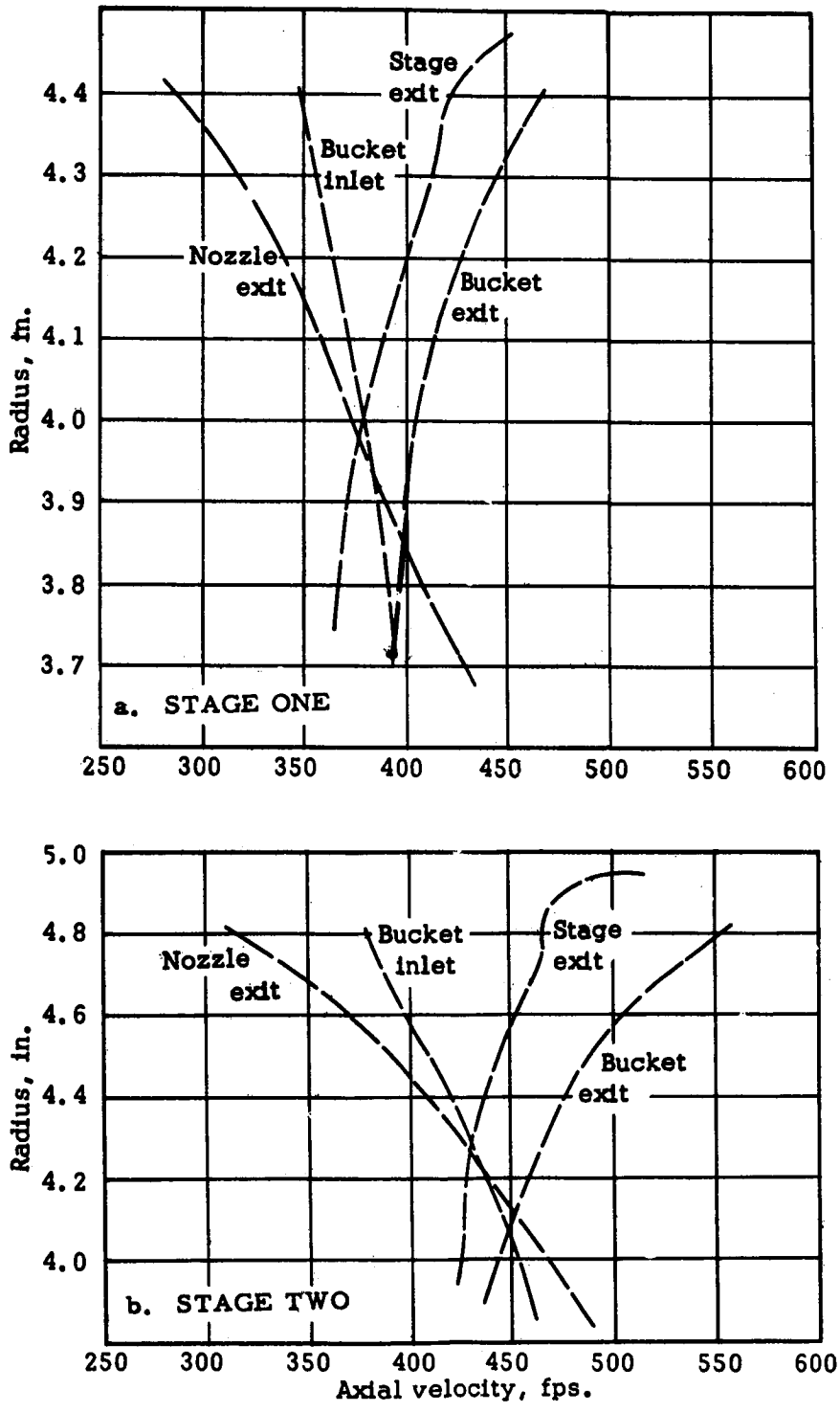

Figure 6. Radial Distributions of Axial Velocity for Test Turbine.

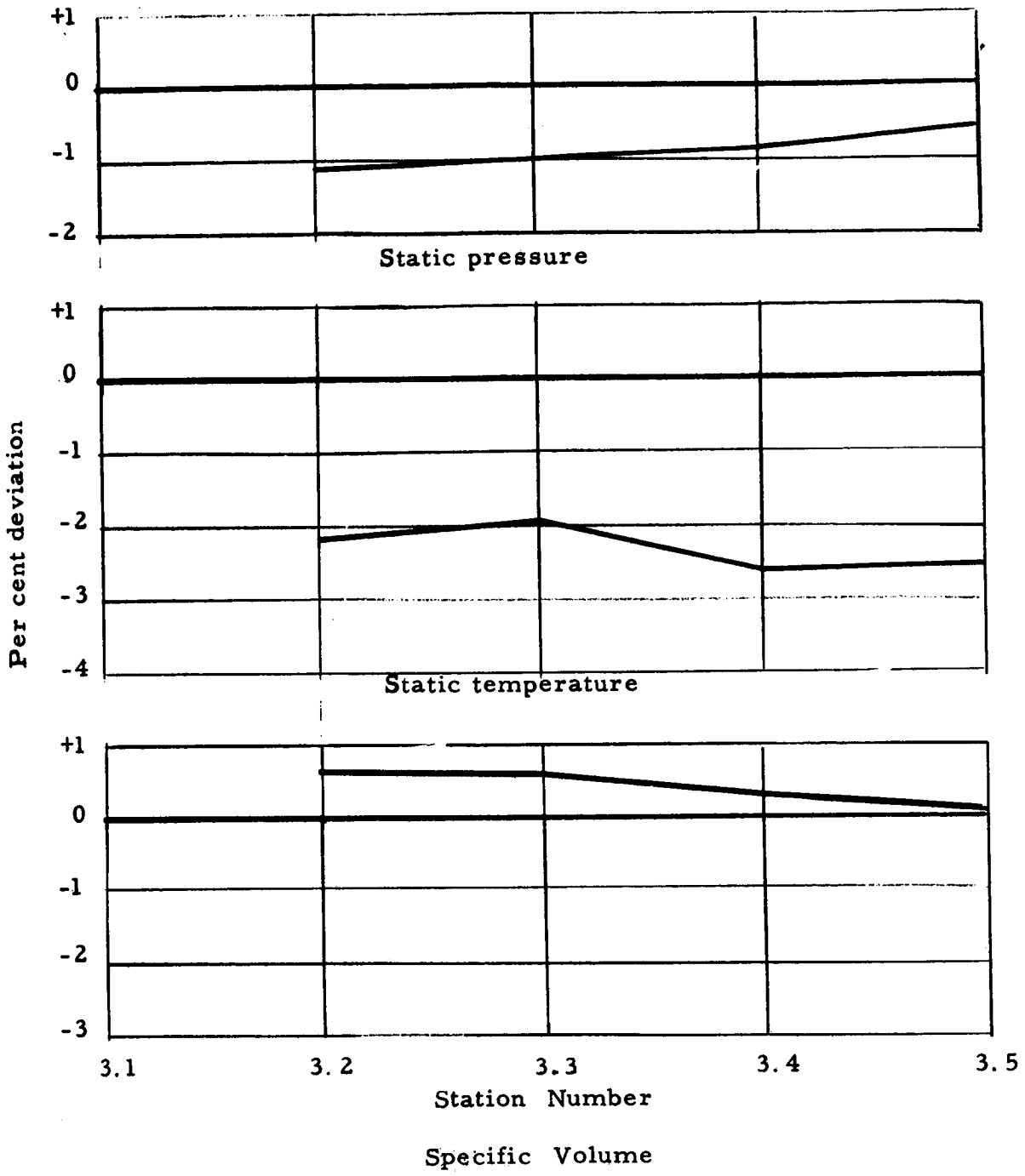

(a) Stage 1

Figure 7. Per Cent Deviation of Design Calculations From Supersaturated Properties of Potassium.

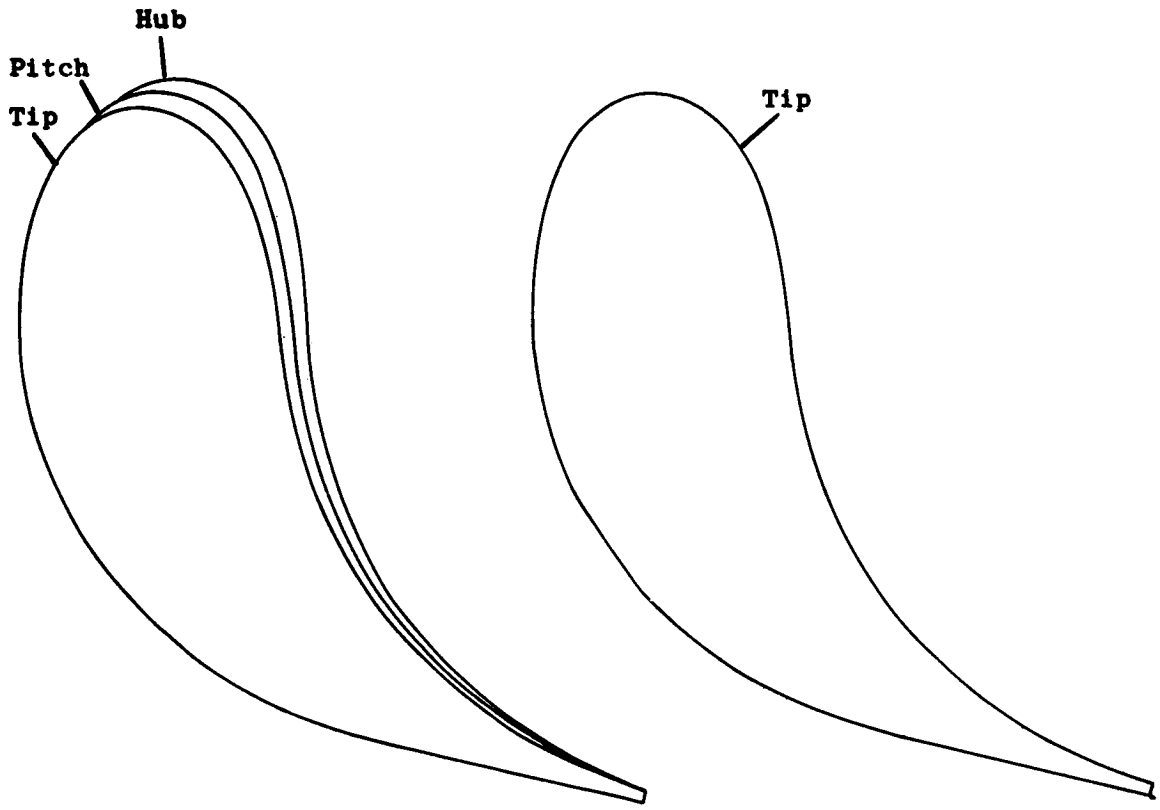

Figure 8. Final First Stage Nozzle Partition Section Profiles.

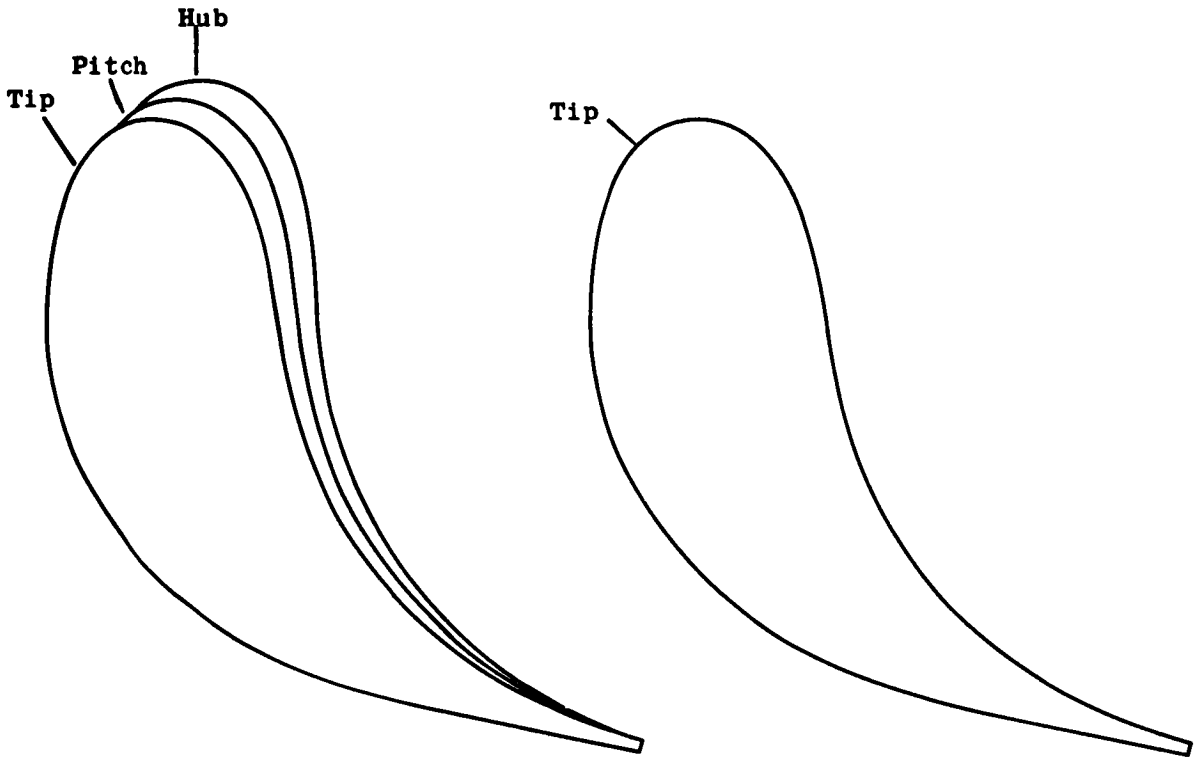

Figure 9. Final Second Stage Nozzle Partition Section Profiles.

(a) Preliminary

(b) Final

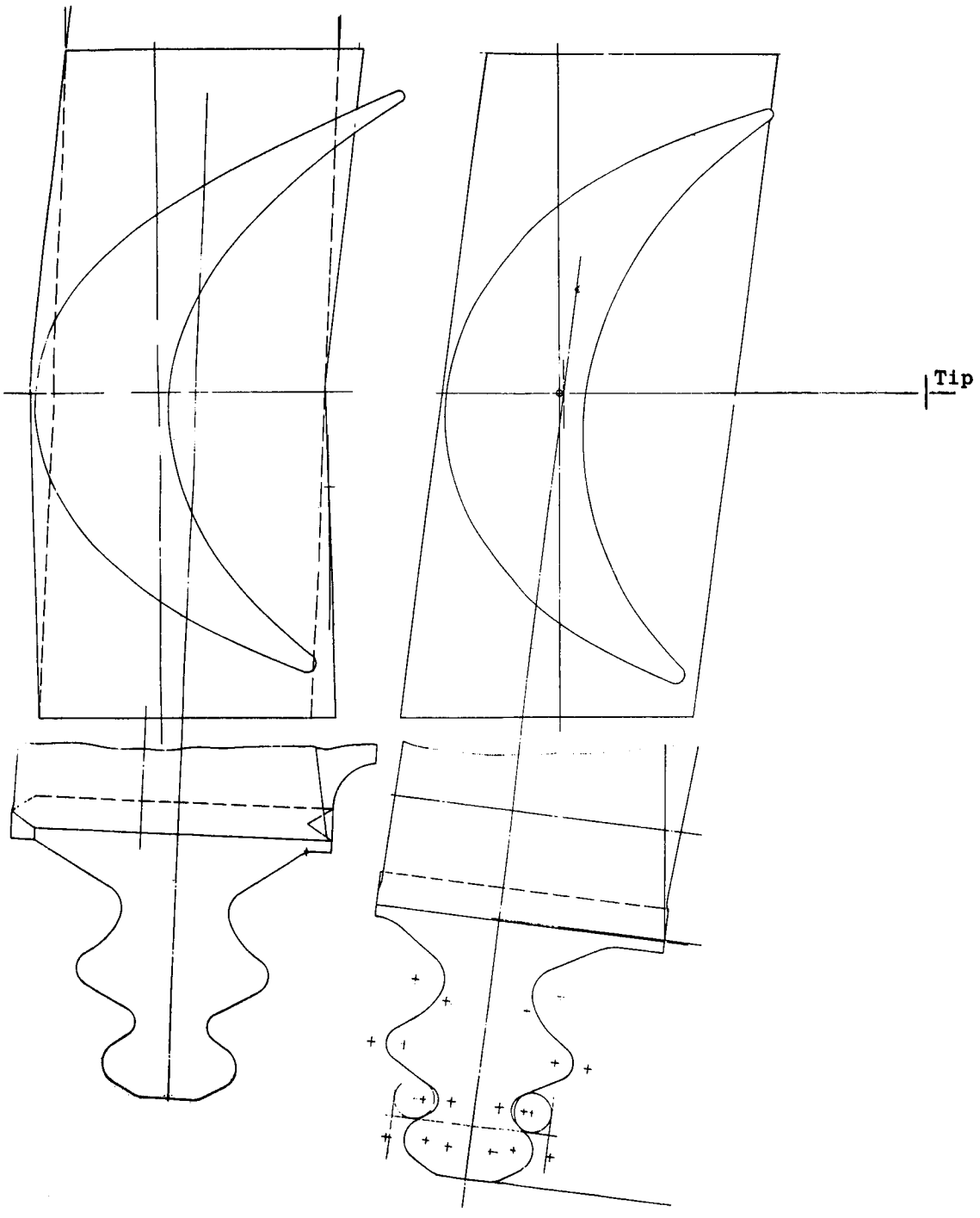

Figure 10. Comparison of Preliminary and Final First Stage Bucket Configurations. (See Table III for Dimensions)

(a) Preliminary

(b) Final

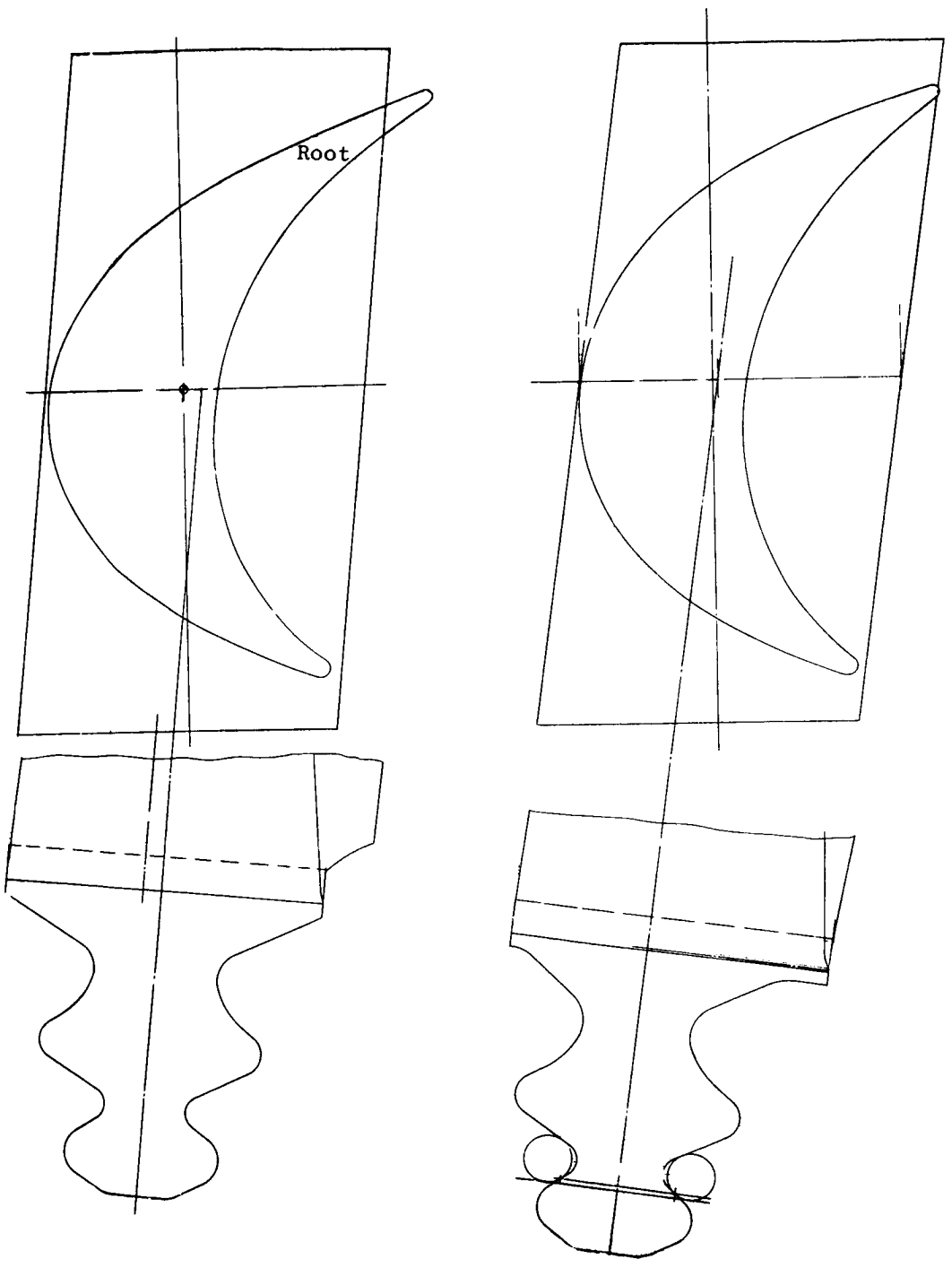

Figure 11. Comparison of Preliminary and Final Second Stage Bucket Configurations. (See Table III for Dimensions)

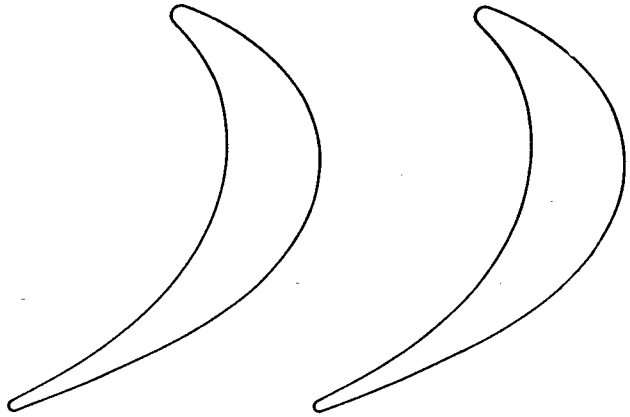

a. Tip

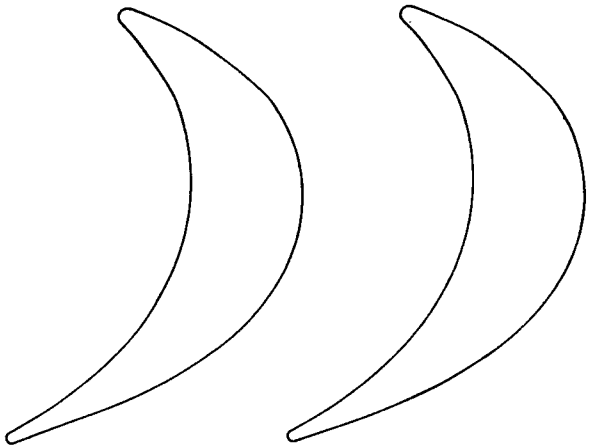

b. Pitch

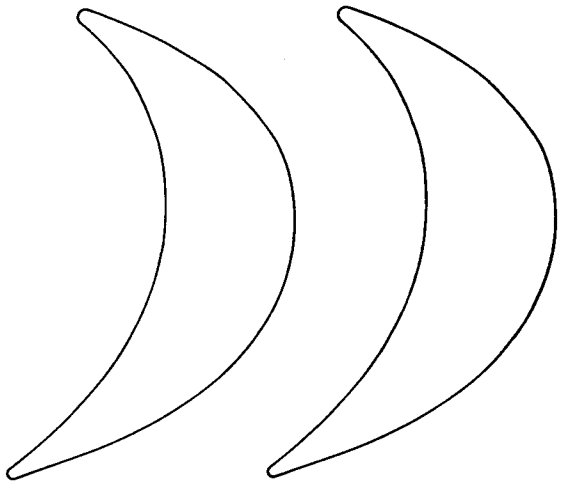

c. Hub

Figure 12. Final First Stage Bucket Blade Sections.
(See Table III for Dimensions)

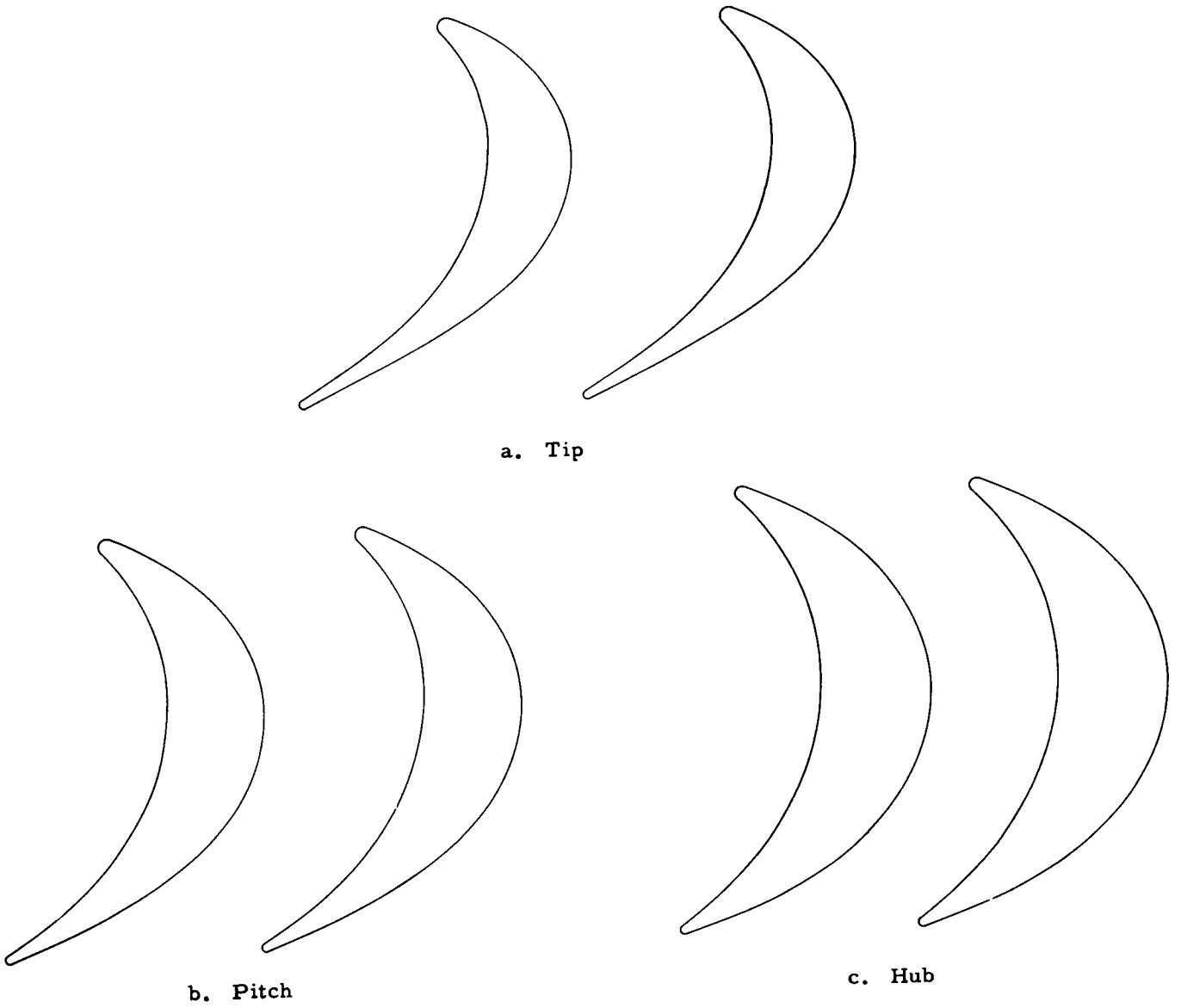

a. Tip

b. Pitch

c. Hub

Figure 13. Final Second Stage Bucket Blade Sections.
(See Table III for Dimensions)

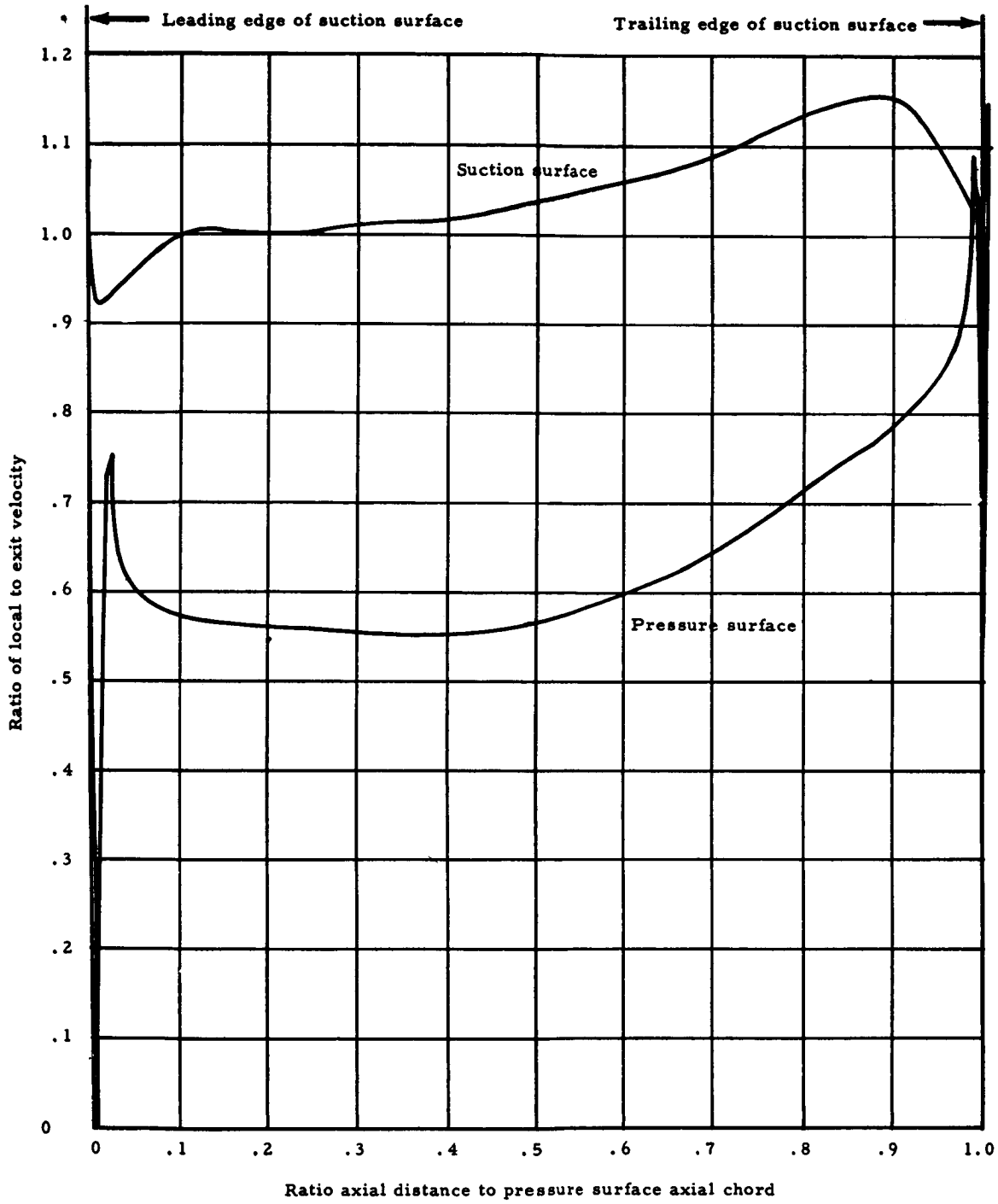

Figure 14. Velocity Distribution Around the Final Second Stage Bucket Hub Section.

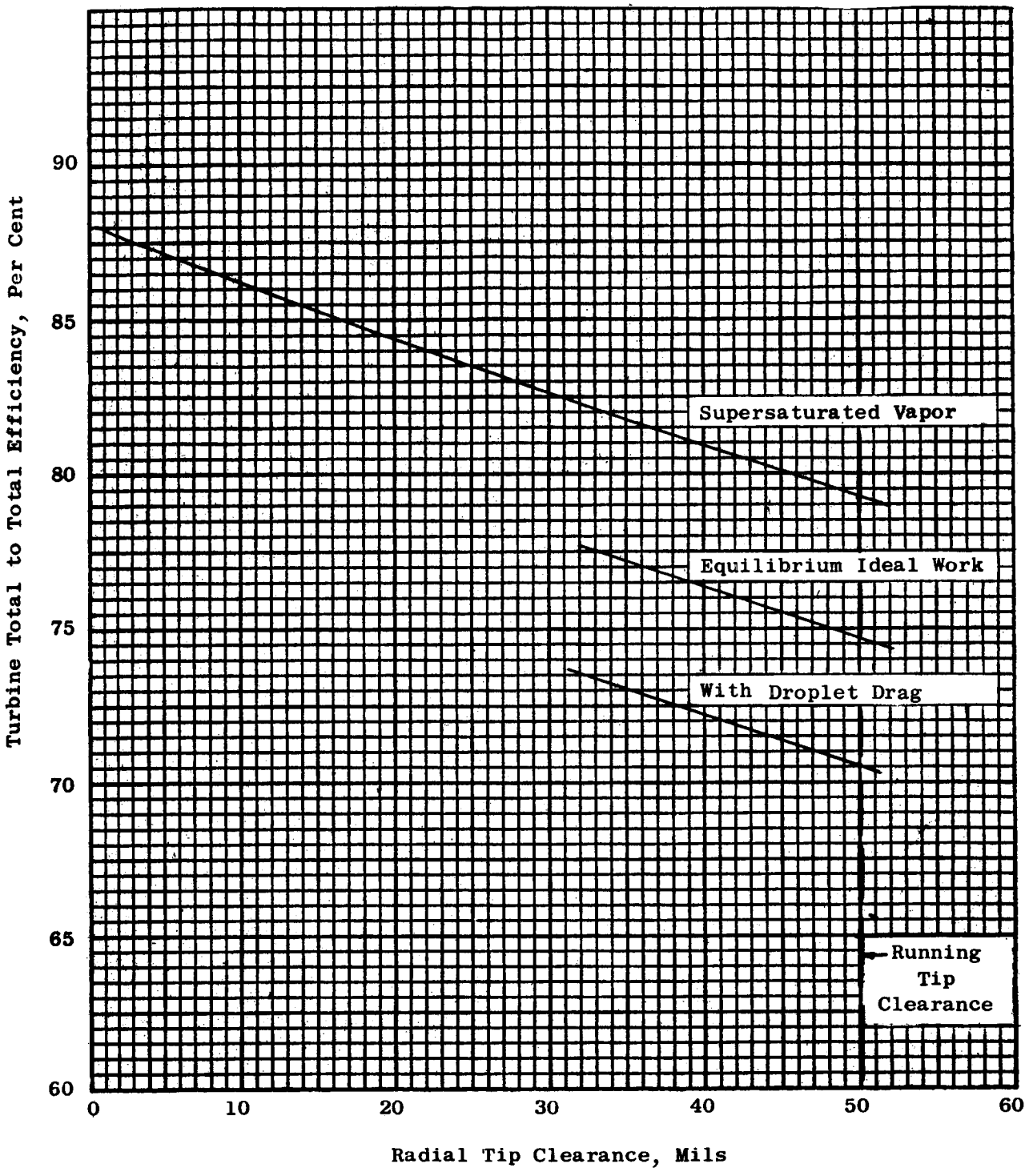

Figure 15. Effect of Tip Clearance and Other Losses on Design Point Turbine Total to Total Efficiency.

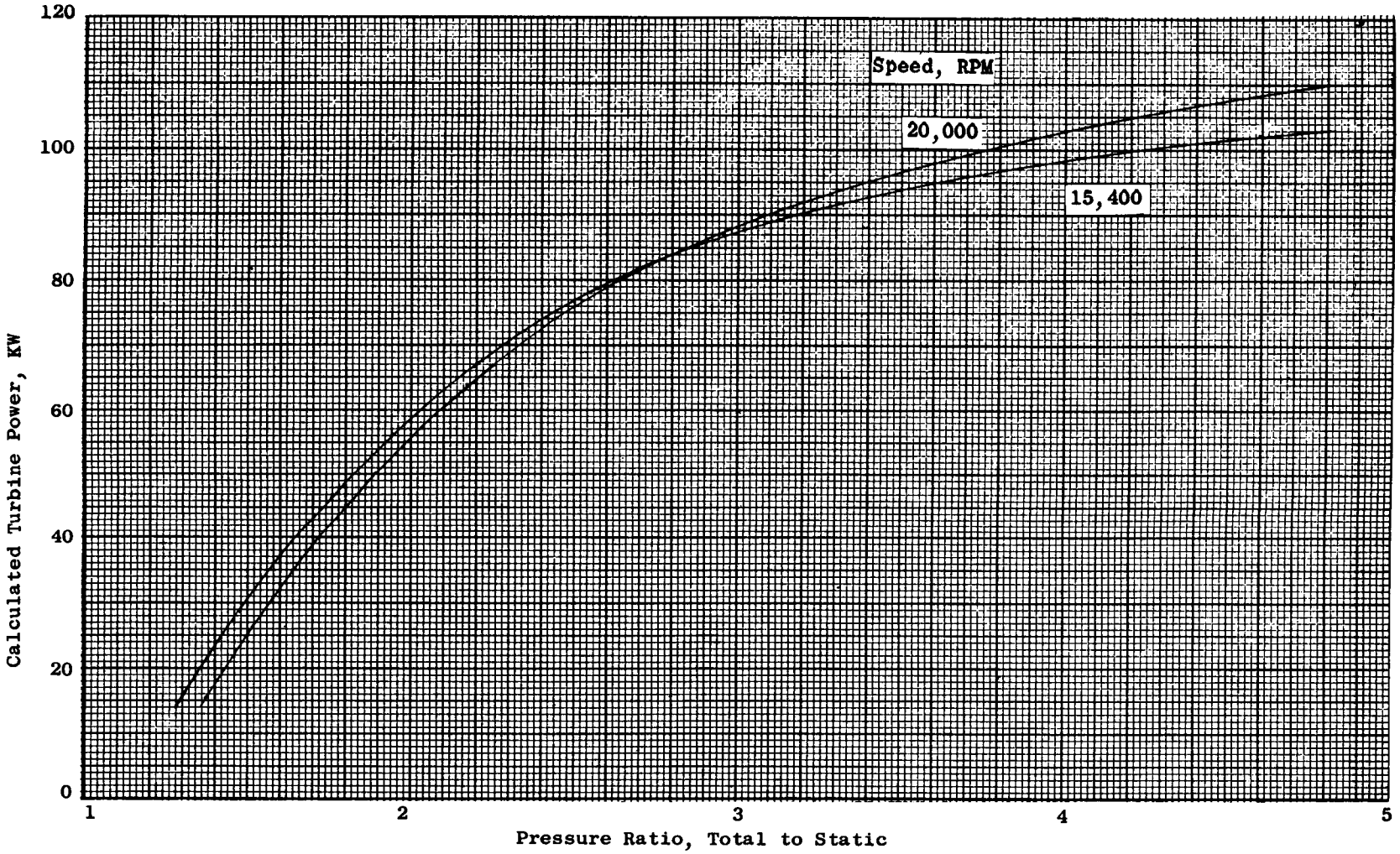

Figure 16. The Variation of Calculated Turbine Power, kw, With Pressure Ratio, Total to Static. Turbine Inlet Temperature, 1450°F, Inlet Vapor Quality, 99 Percent.

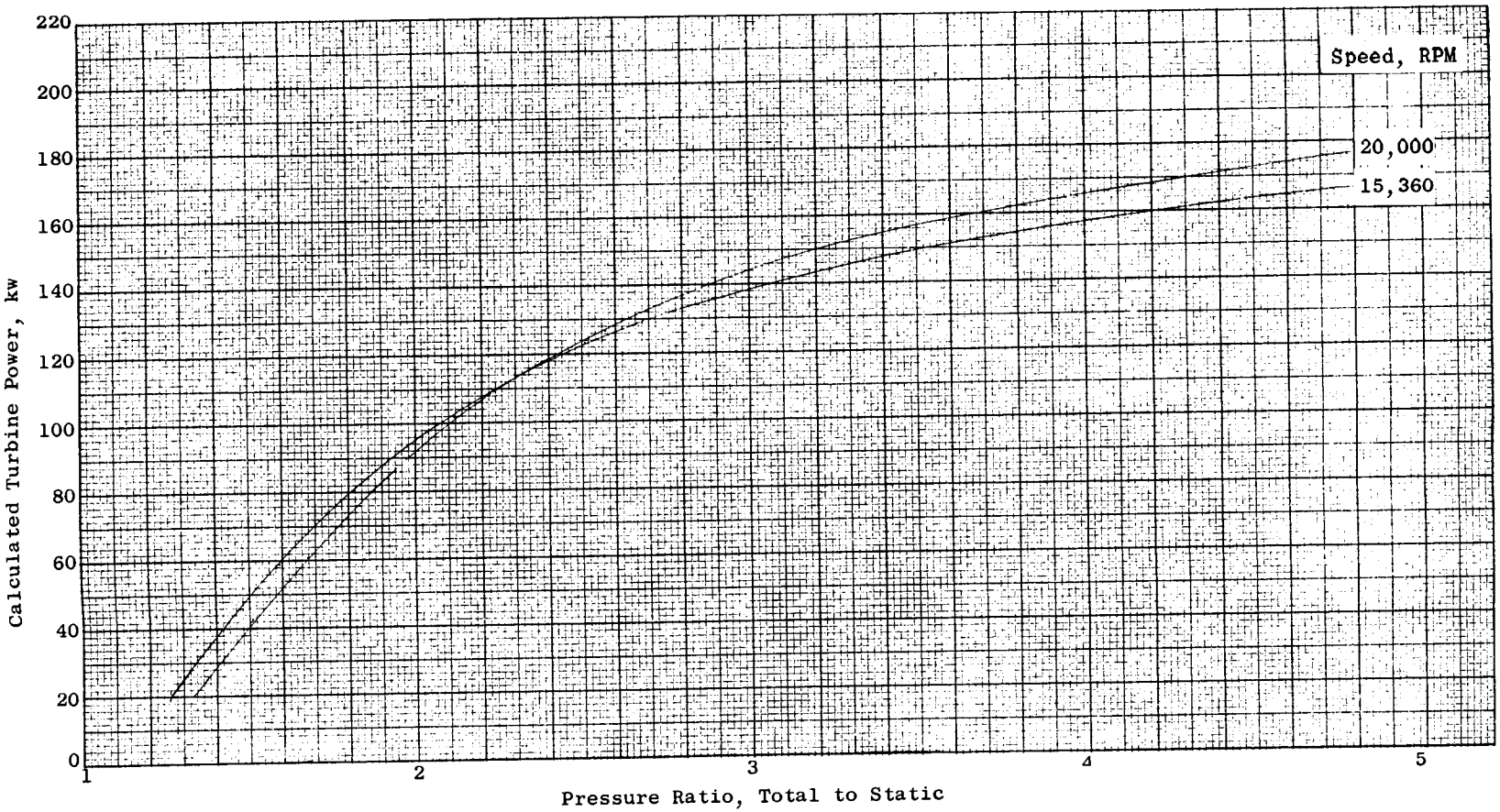

Figure 17. The Variation of Calculated Turbine Power, kw, With Pressure Ratio, Total to Static. Turbine Inlet Temperature, 1550°F, Inlet Vapor Quality, 99 Percent.

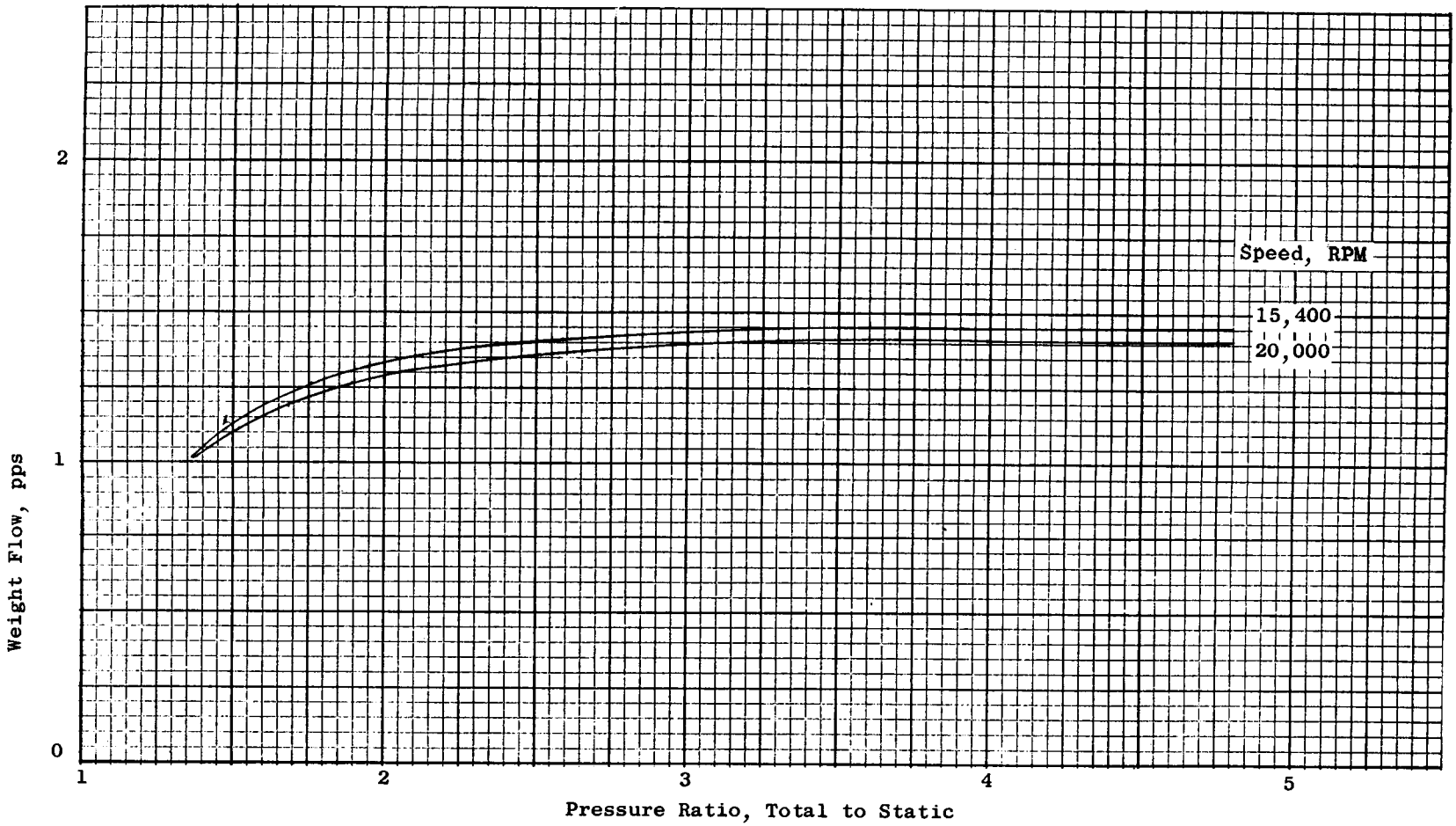

Figure 18. The Variation in the Calculated Weight Flow With Pressure Ratio, Total to Static. Turbine Inlet Temperature, 1450°F, Inlet Vapor Quality, 99 Percent.

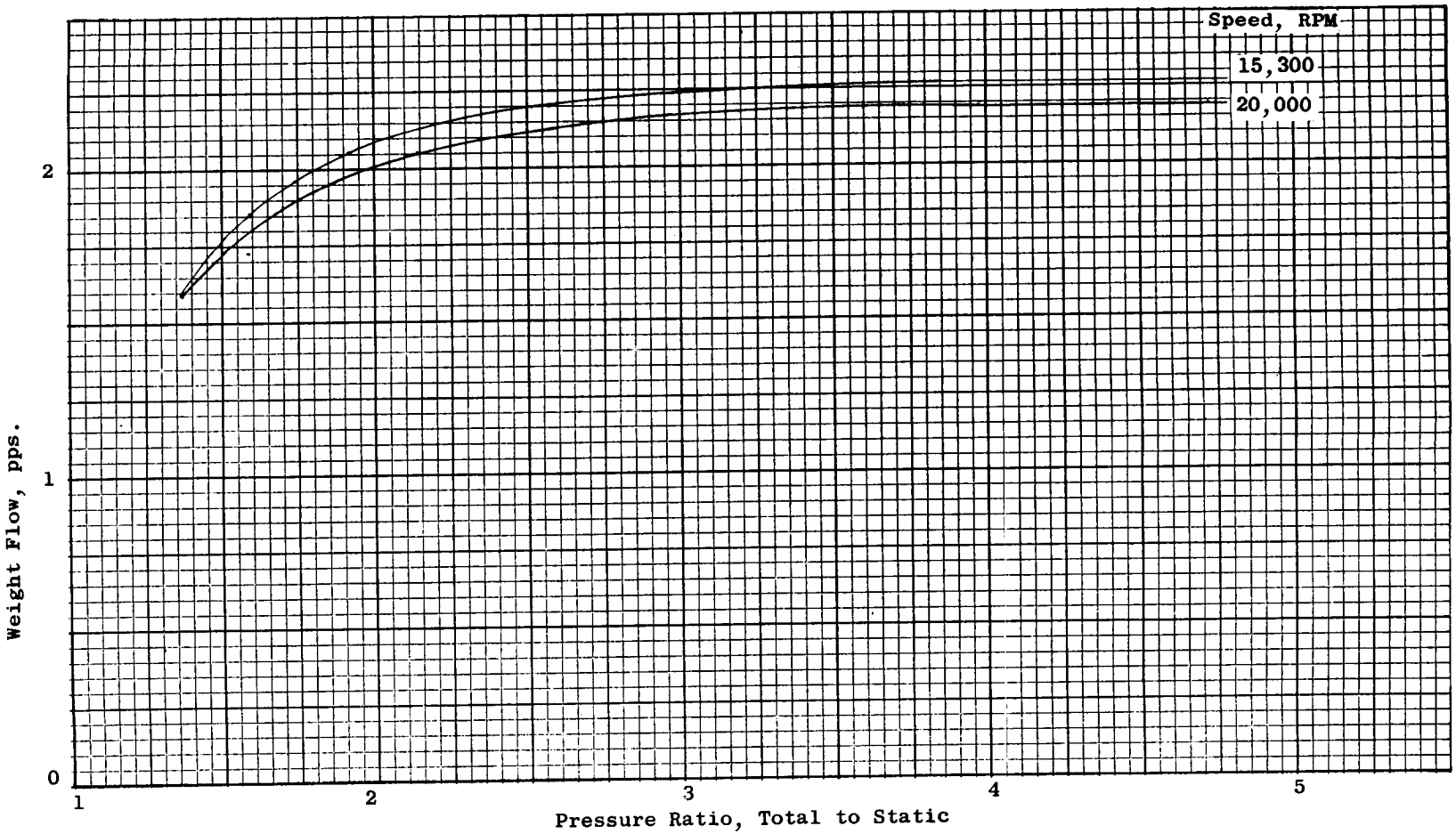

Figure 19. The Variation in the Calculated Weight Flow With Pressure Ratio, Total to Static, Turbine Inlet Temperature, 1550°F, Inlet Vapor Quality, 99 Percent.

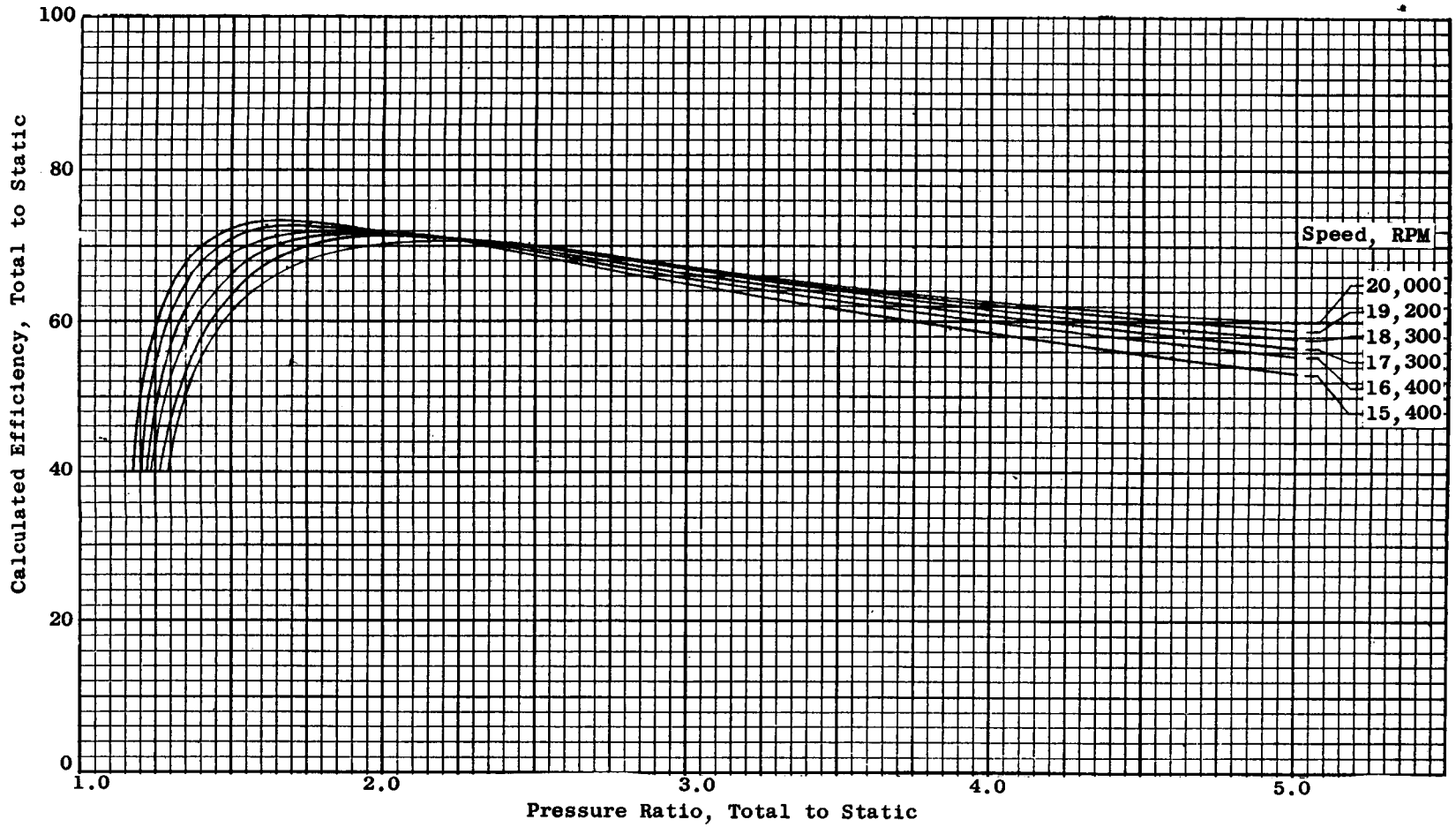

Figure 20. The Variation in the Calculated Efficiency, Total to Static With Pressure Ratio, Total to Static. Turbine Inlet Temperature, 1450°F, Inlet Vapor Quality, 99 Percent.

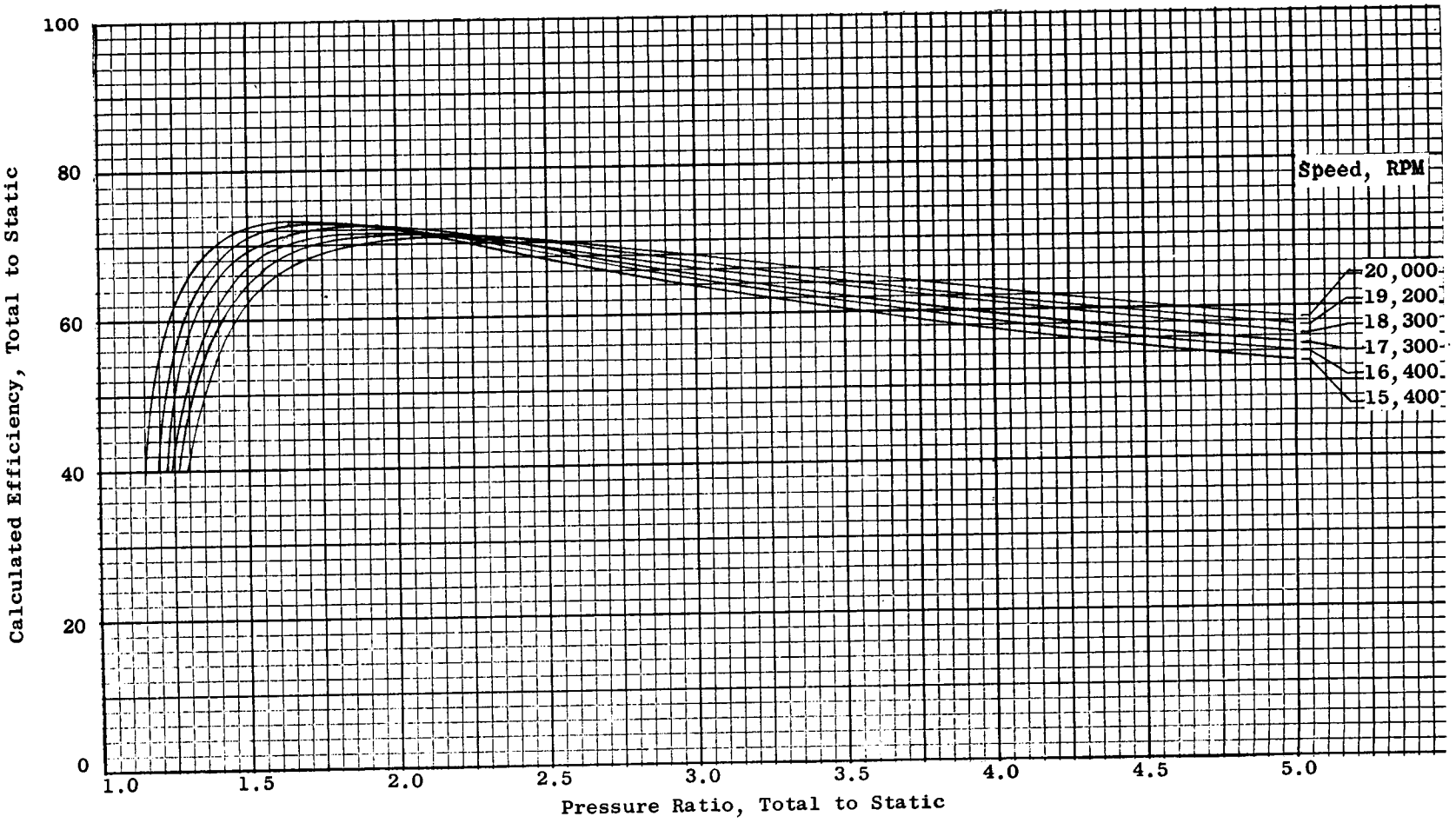

Figure 21. The Variation in the Calculated Efficiency, Total to Static With Pressure Ratio, Total to Static. Turbine Inlet Temperature, 1550°F, Inlet Vapor Quality, 99 Percent.

PRECEDING PAGE BLANK NOT FILMED.

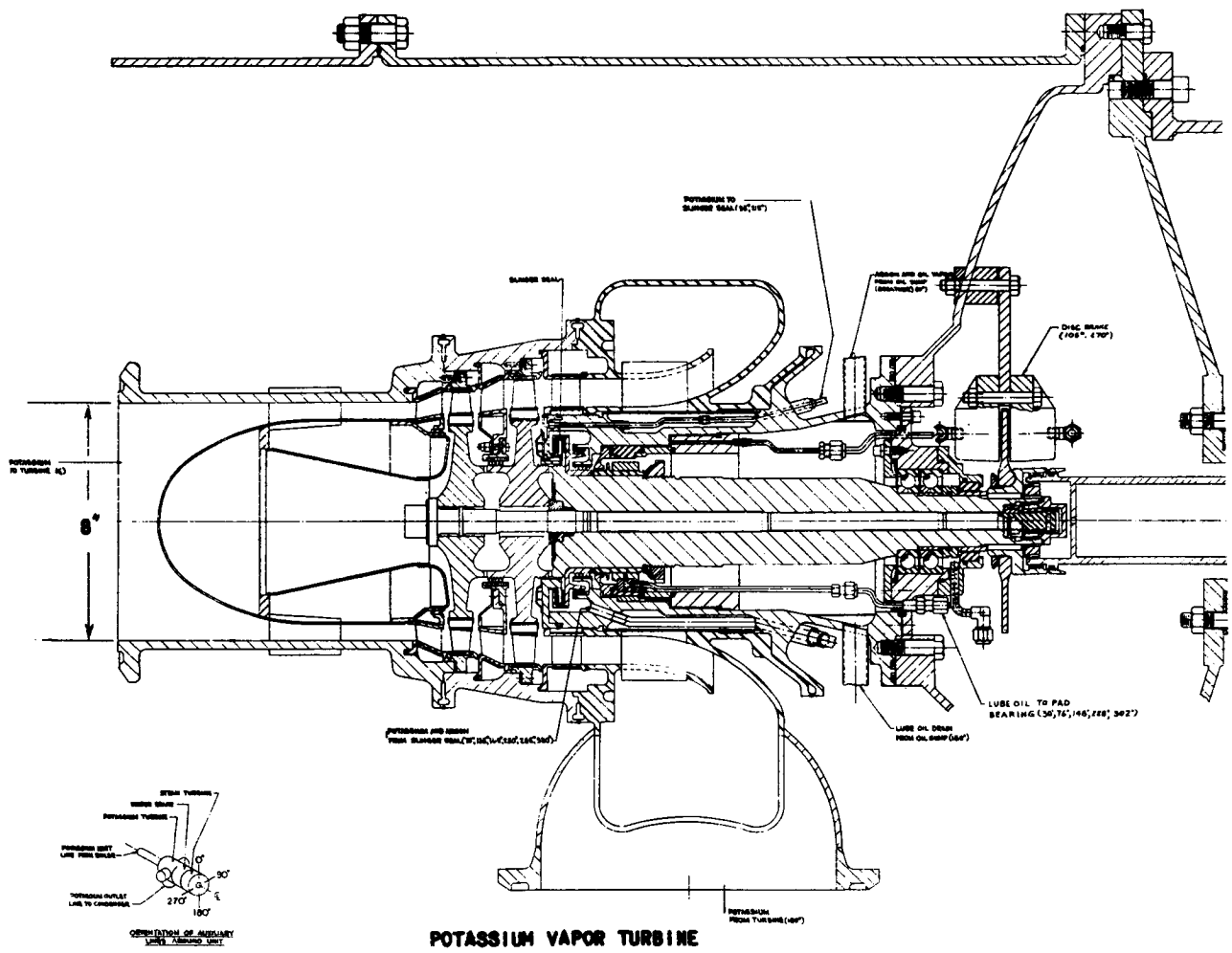

Figure 22.

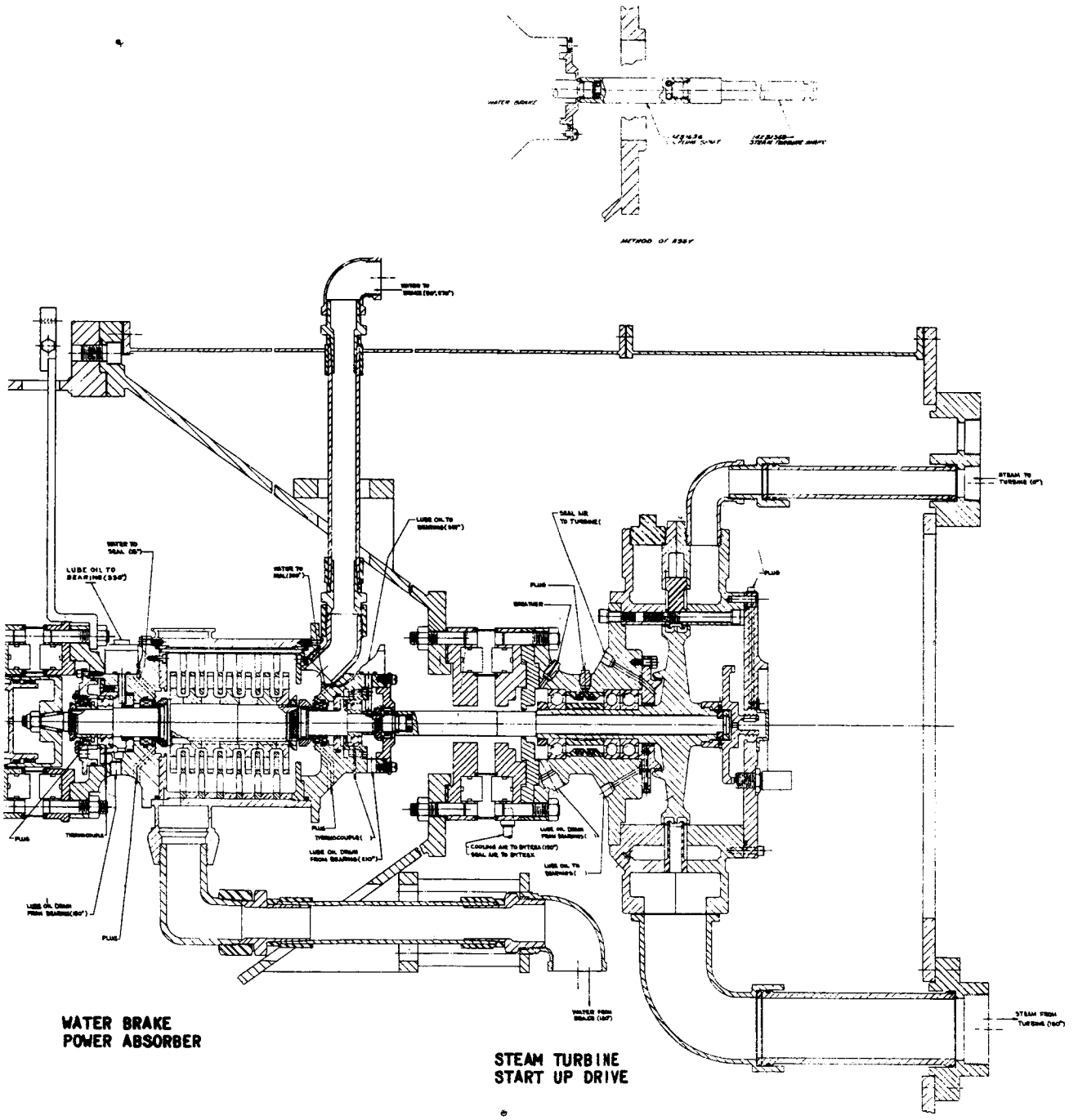

Potassium Turbine Loading and Starting System.

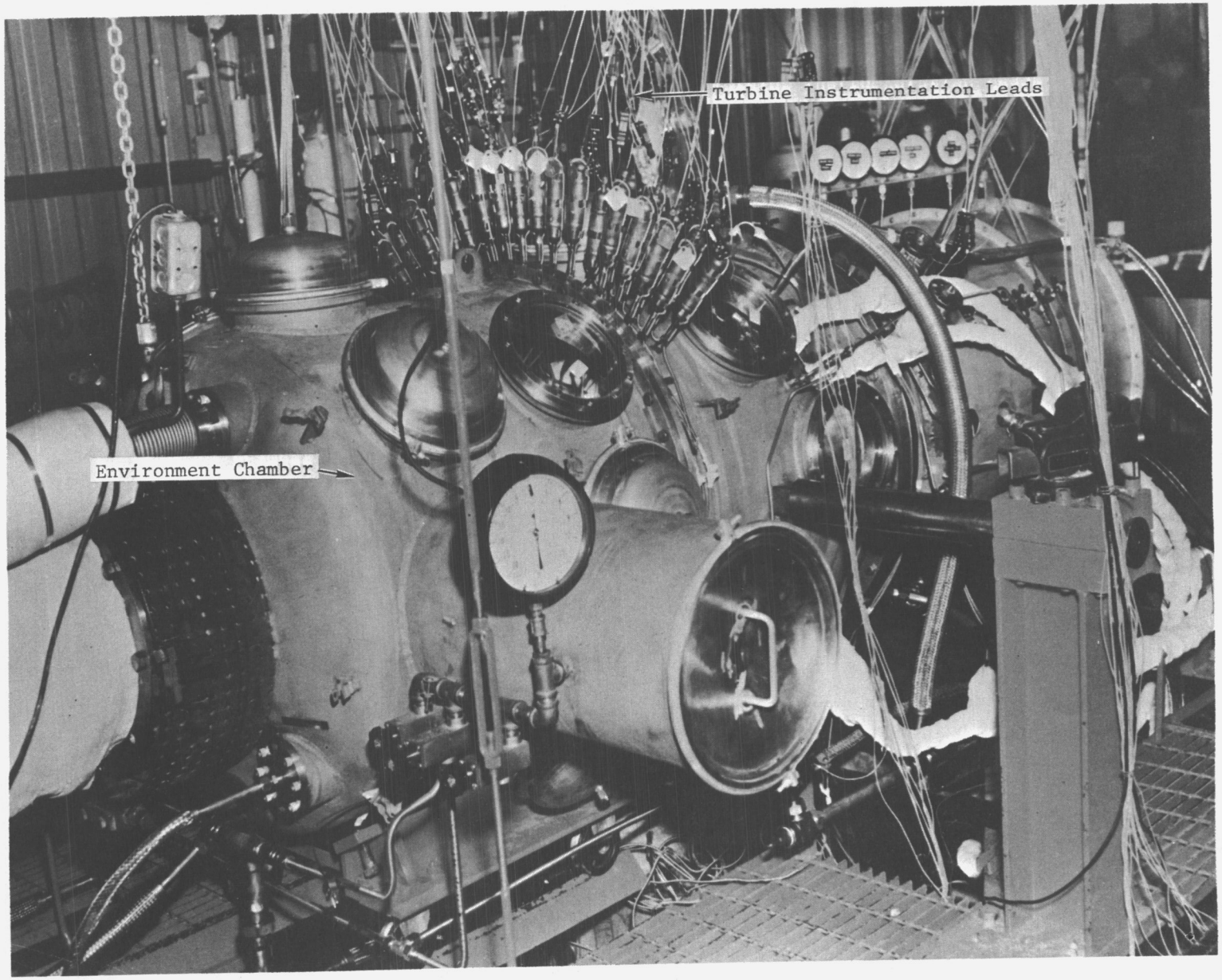

Figure 23. Potassium Turbine Test Installation.

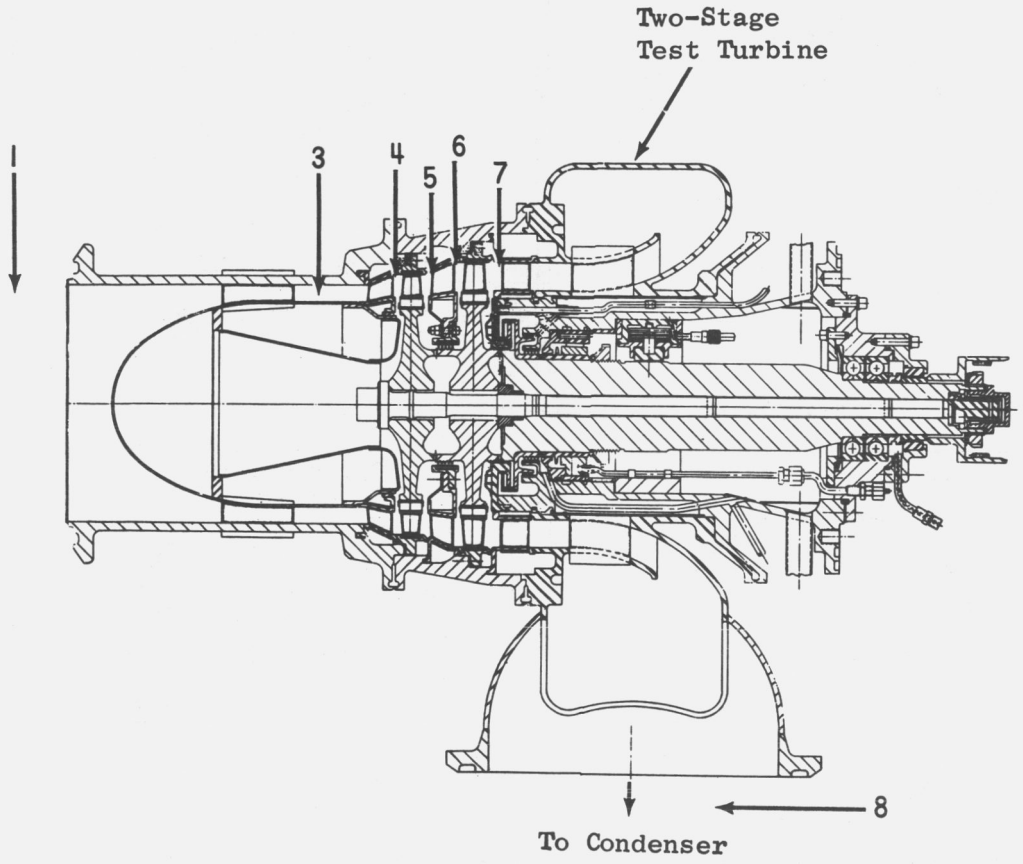

Figure 24 Turbine Performance Instrumentation Stations.

Note: All total pressure and total temperature sensors arranged in equal area annuli.

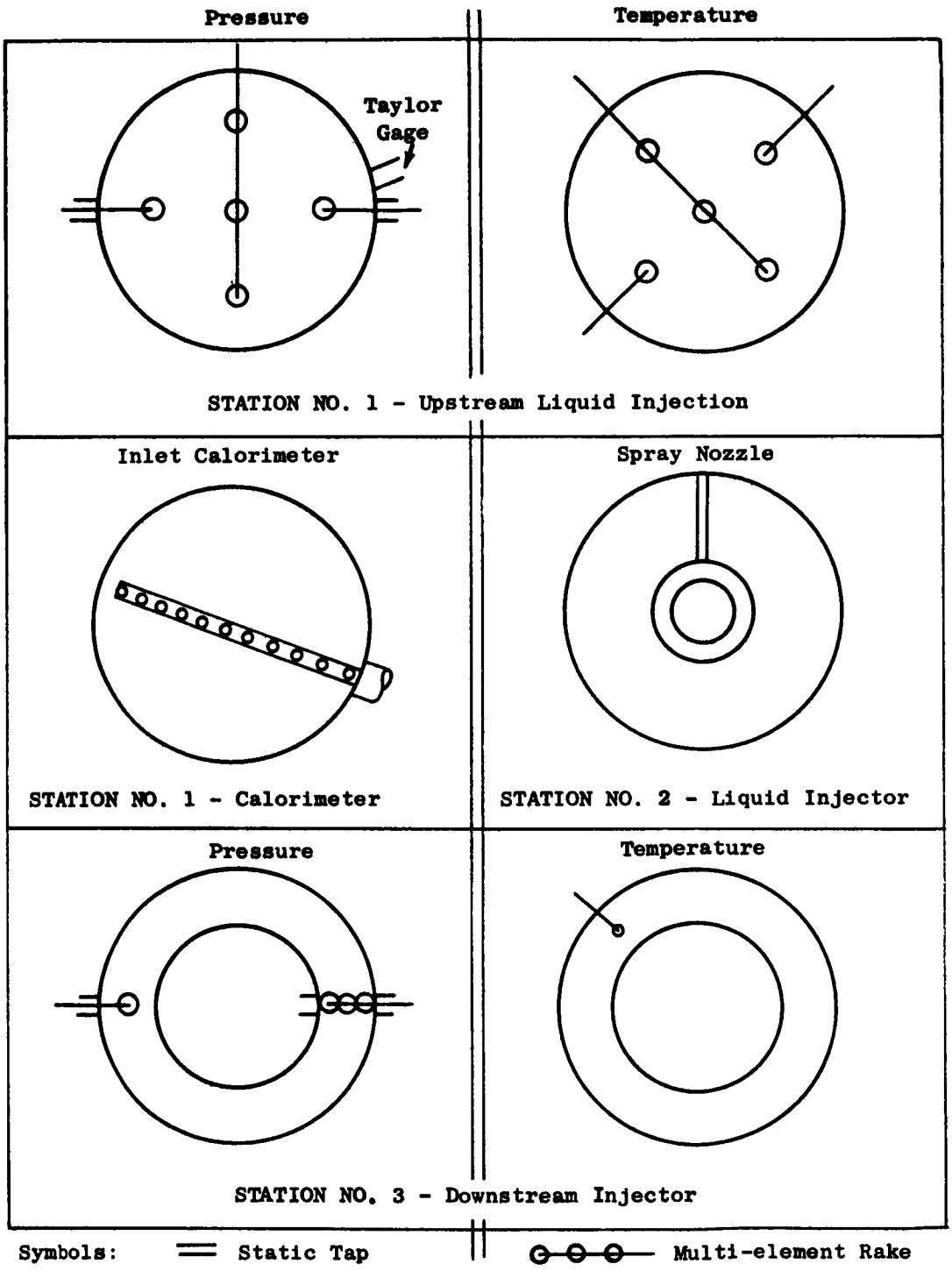

Figure 25. Potassium Test Turbine Instrumentation Location

Note: All total pressure and total temperature sensors arranged in equal area annuli.

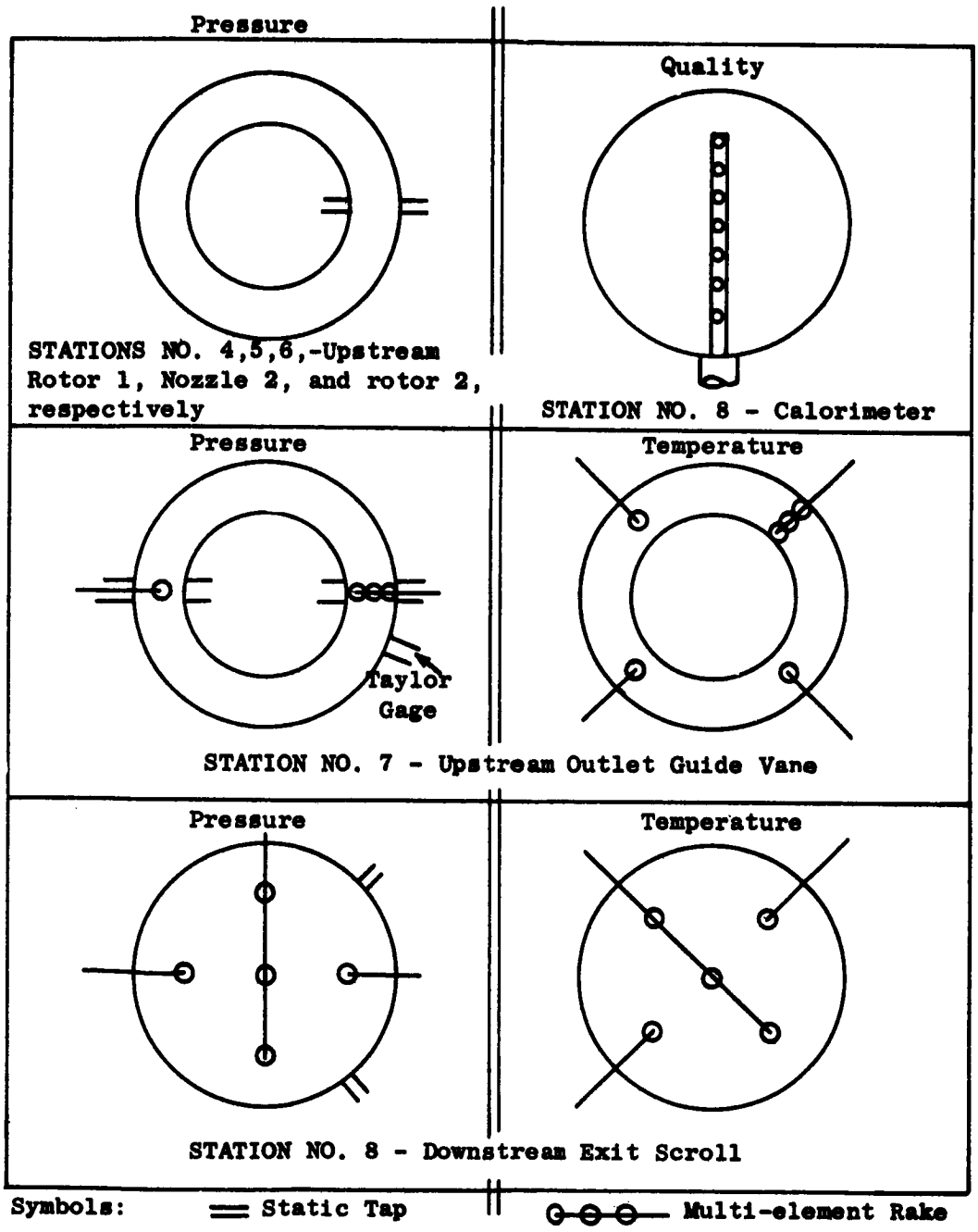

Figure 26. Potassium Test Turbine Instrumentation Location

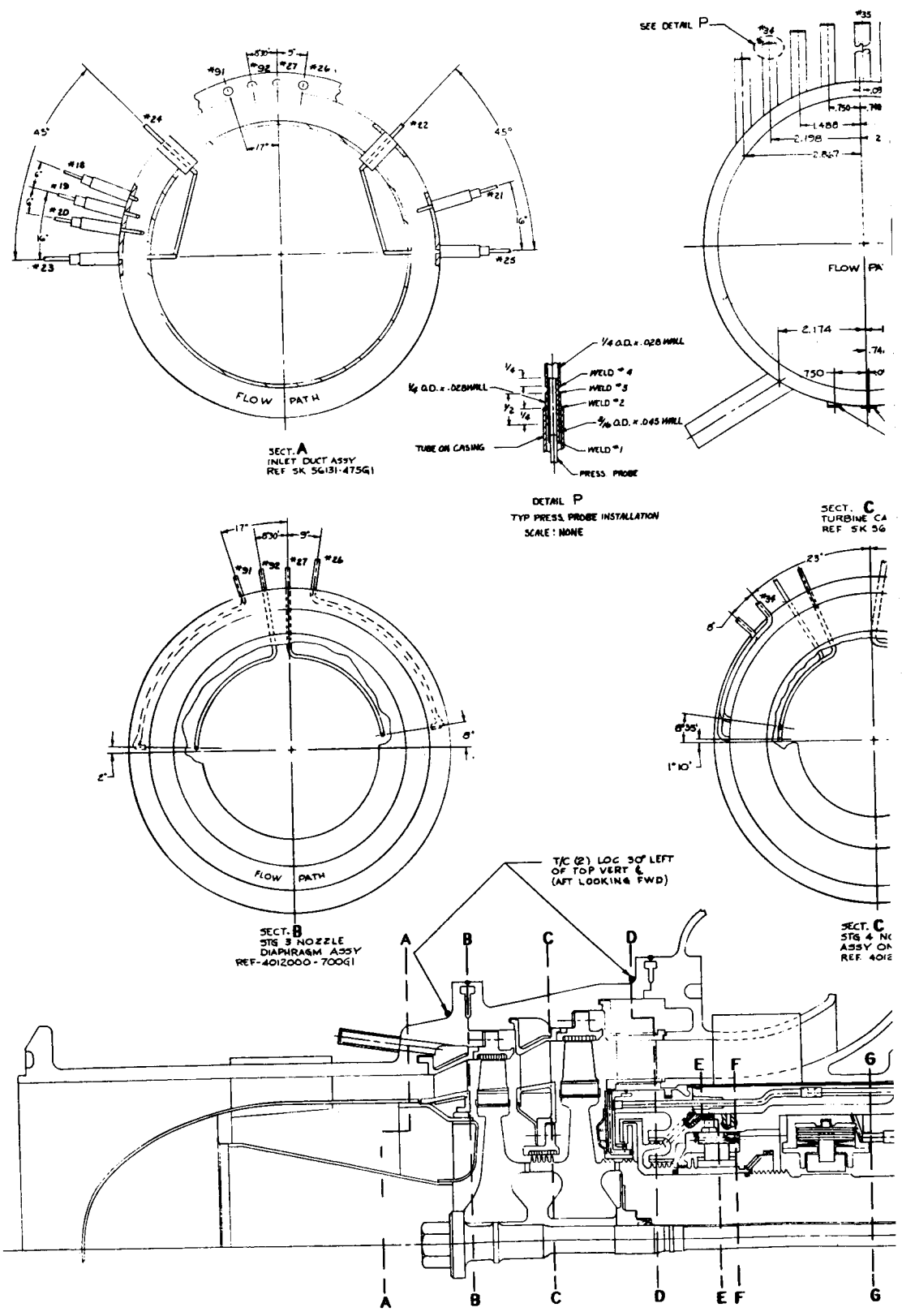

Figure 27. Instrumentation

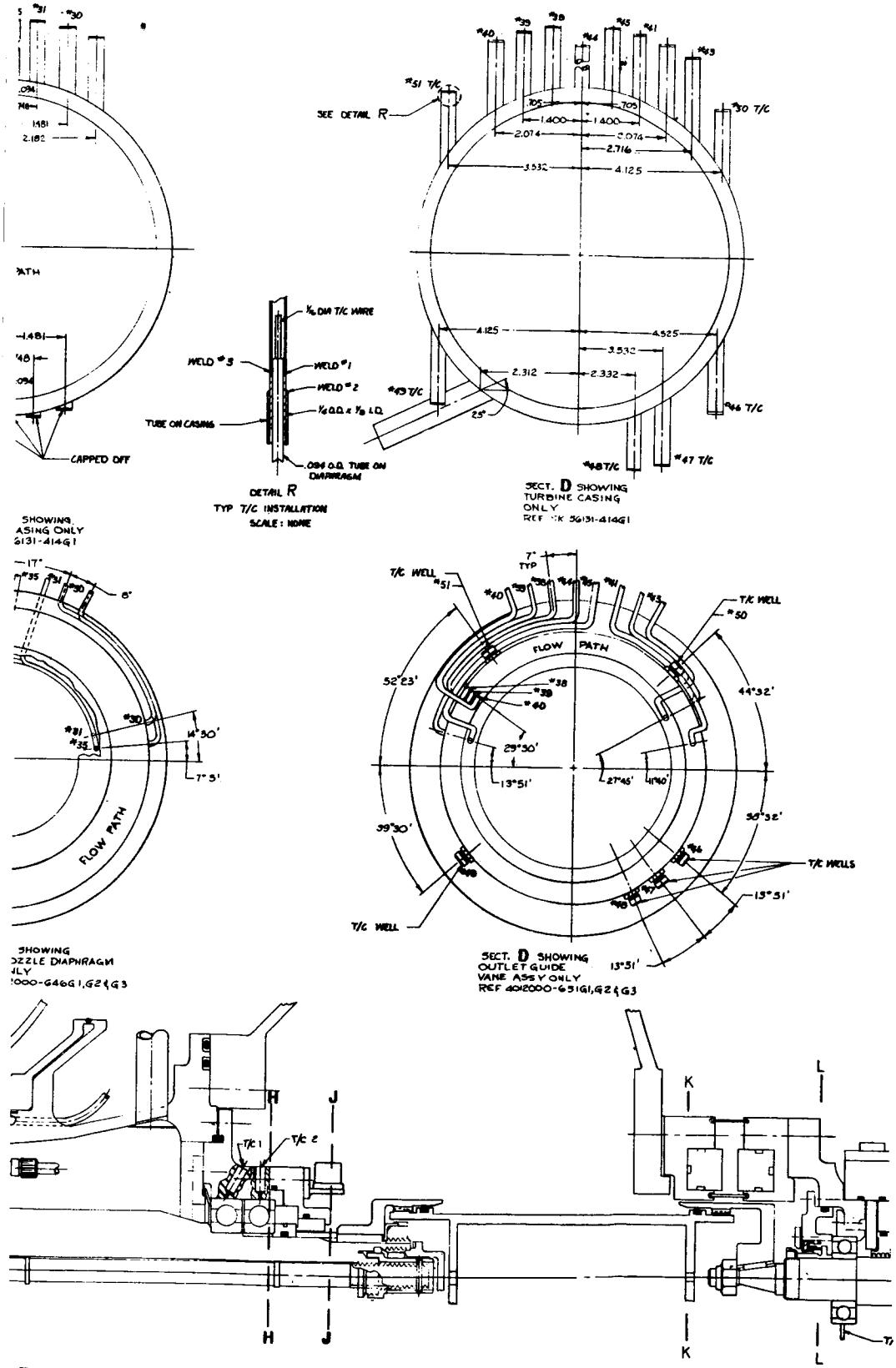

Drawing Potassium Turbine.

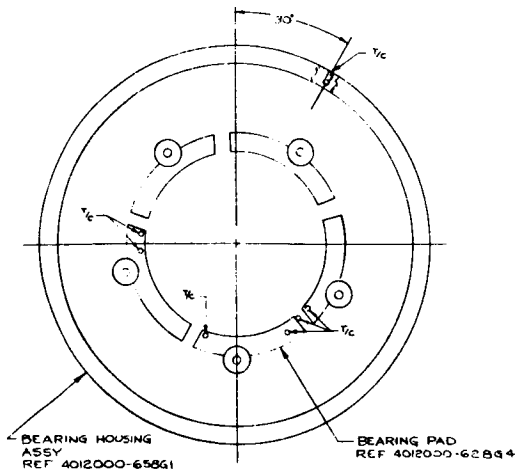

SECT. E

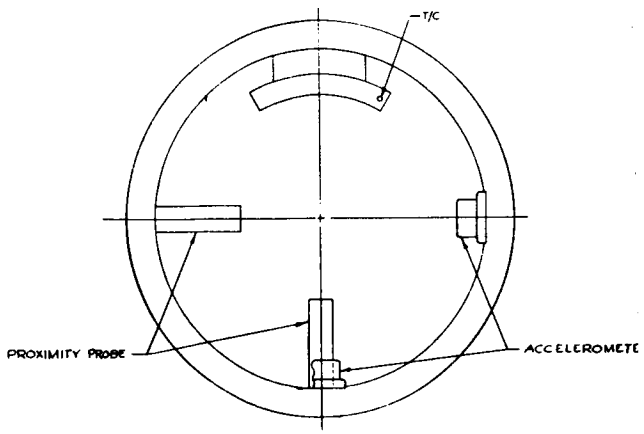

SECT. G
STABILIZER BRG
MTG RING
REF 1190275291

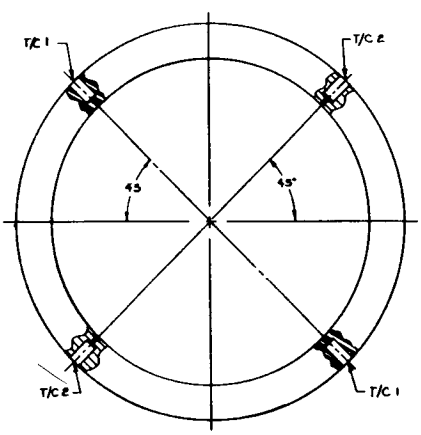

SECT. H
THRUST BRG
HOUSING
1190277391

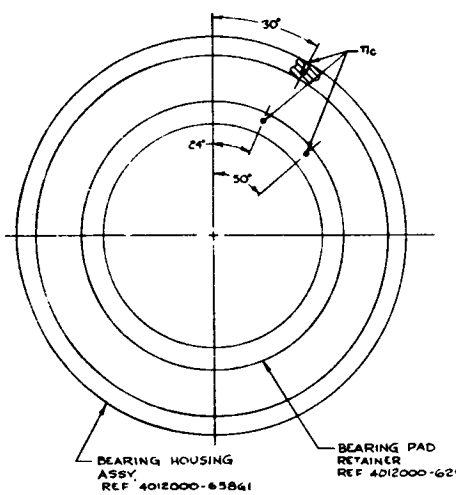

SECT. F

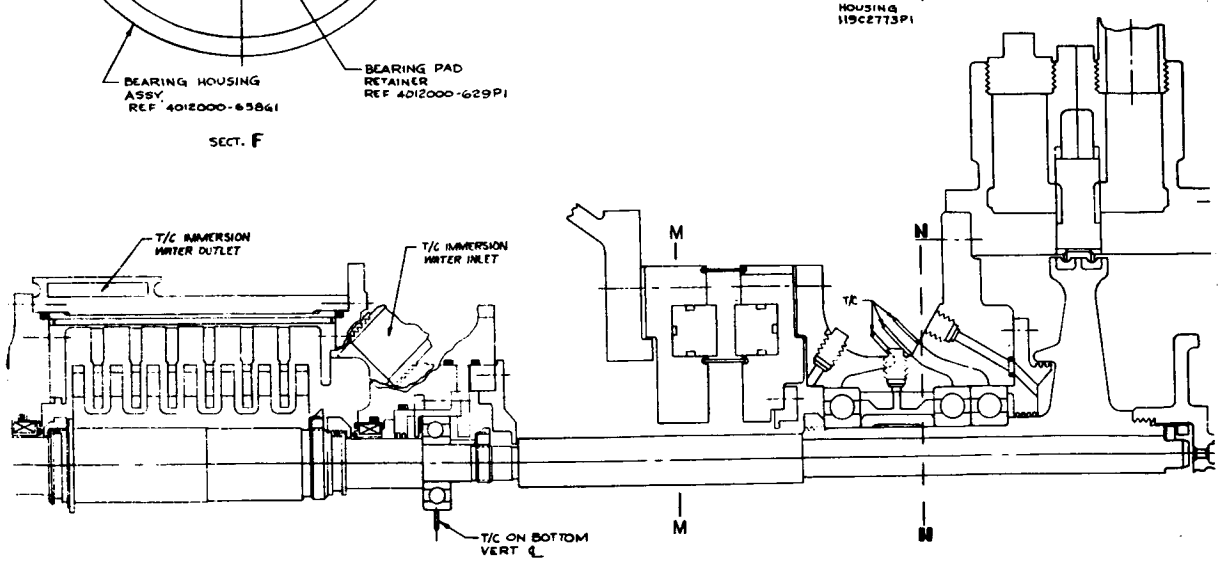

Figure 27. Concluded. Instr

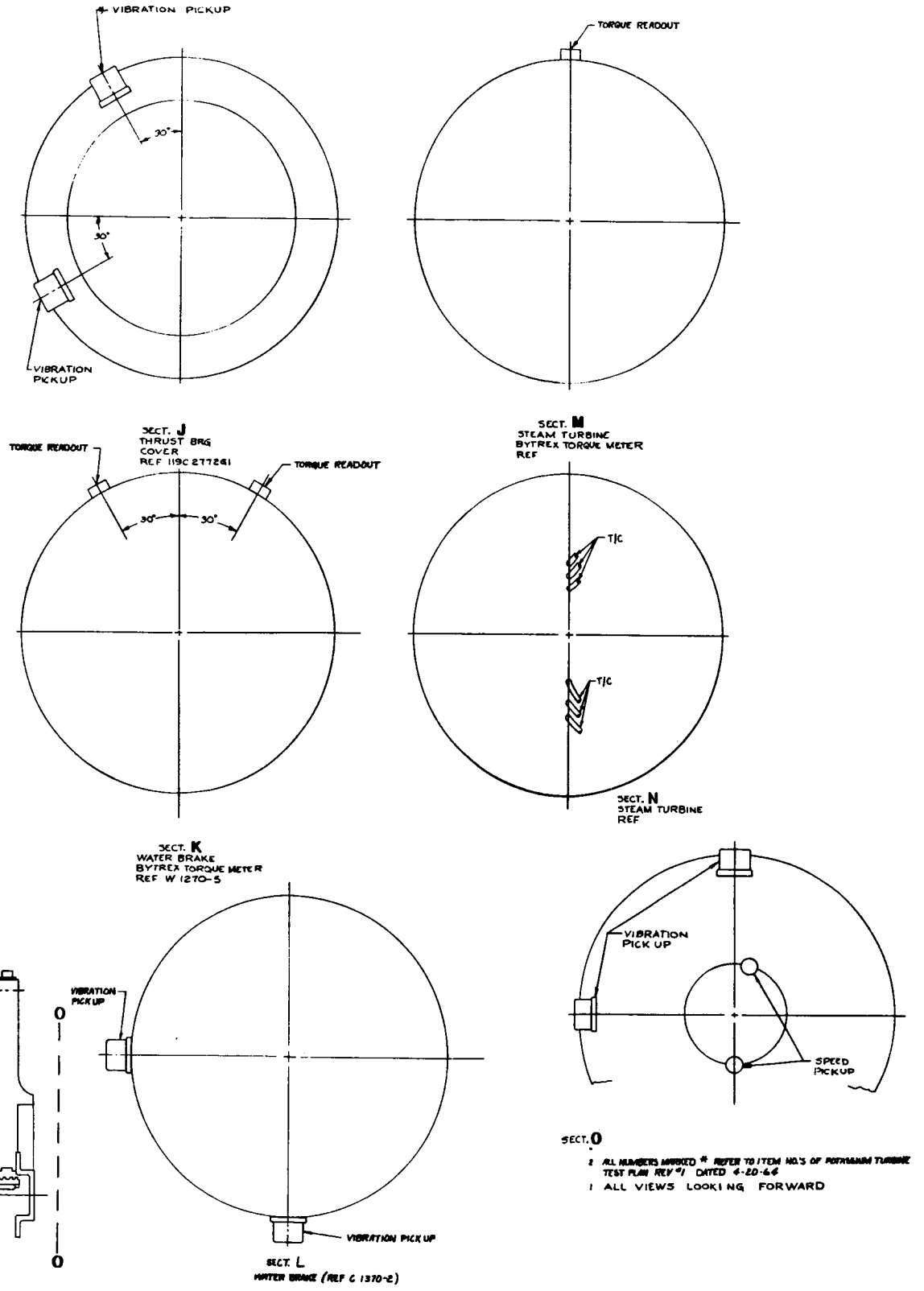

umentation Drawing Potassium Turbine.

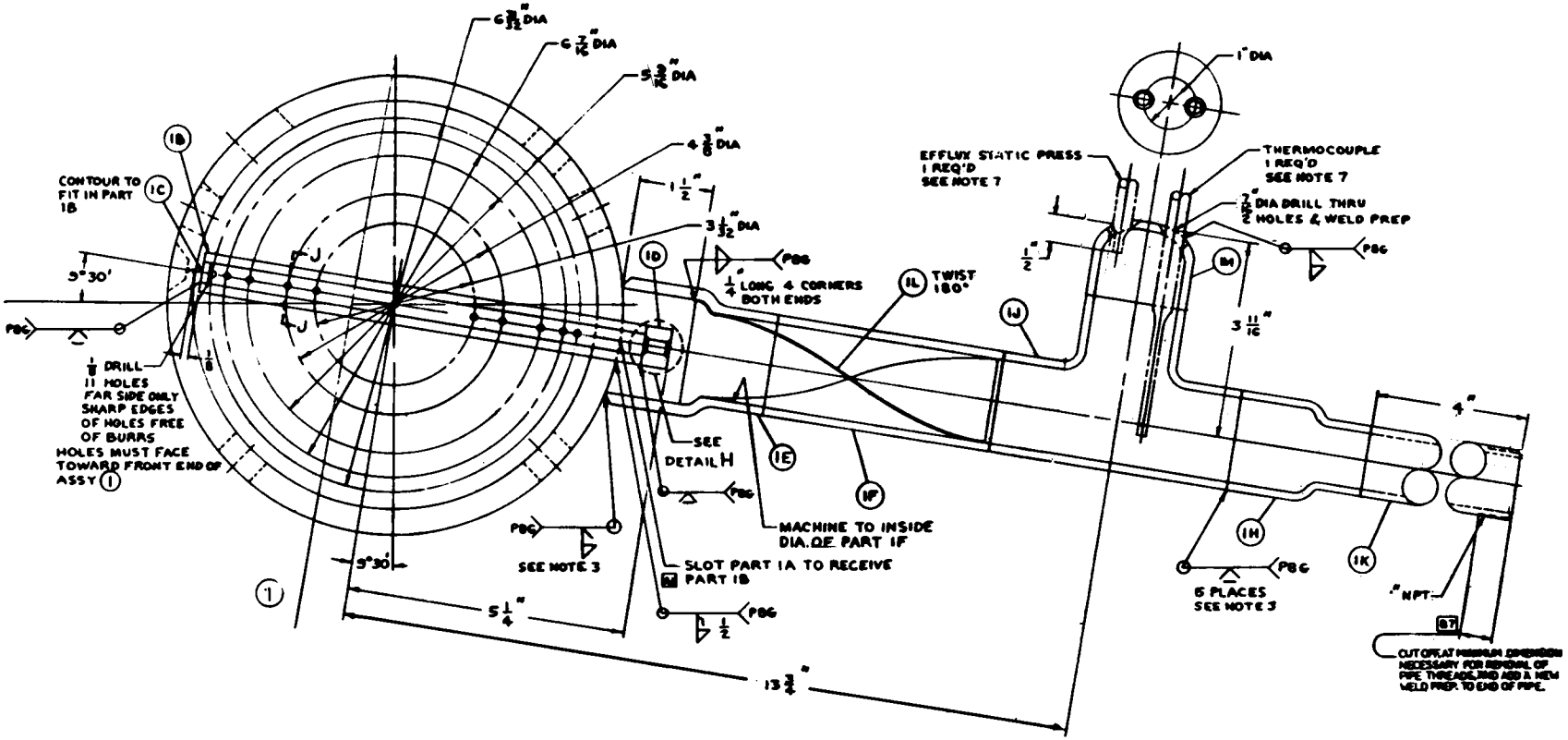

Figure 28. Throttling Calorimeter.

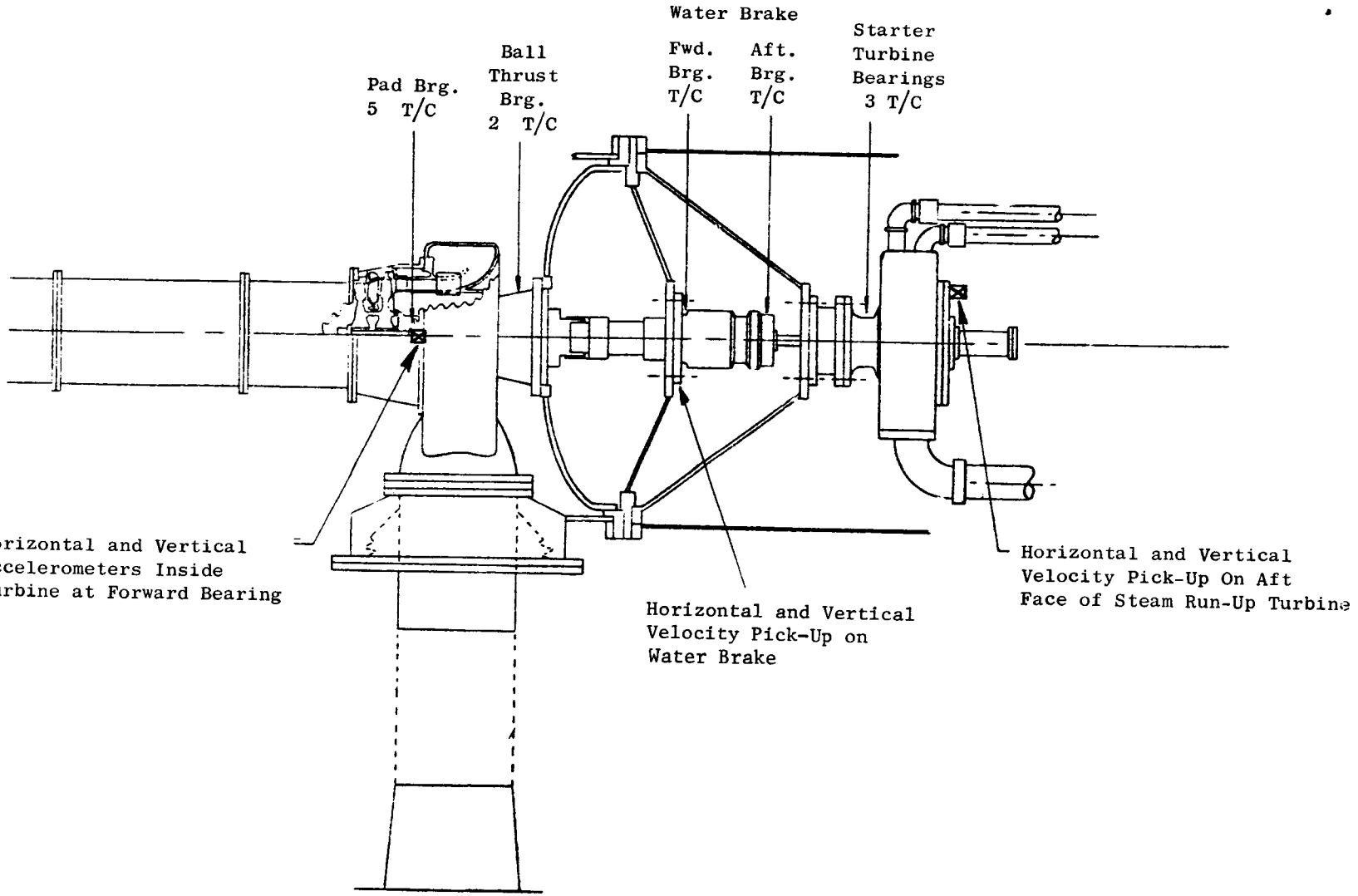

Figure 29. Instrumentation in the Test Rig System.

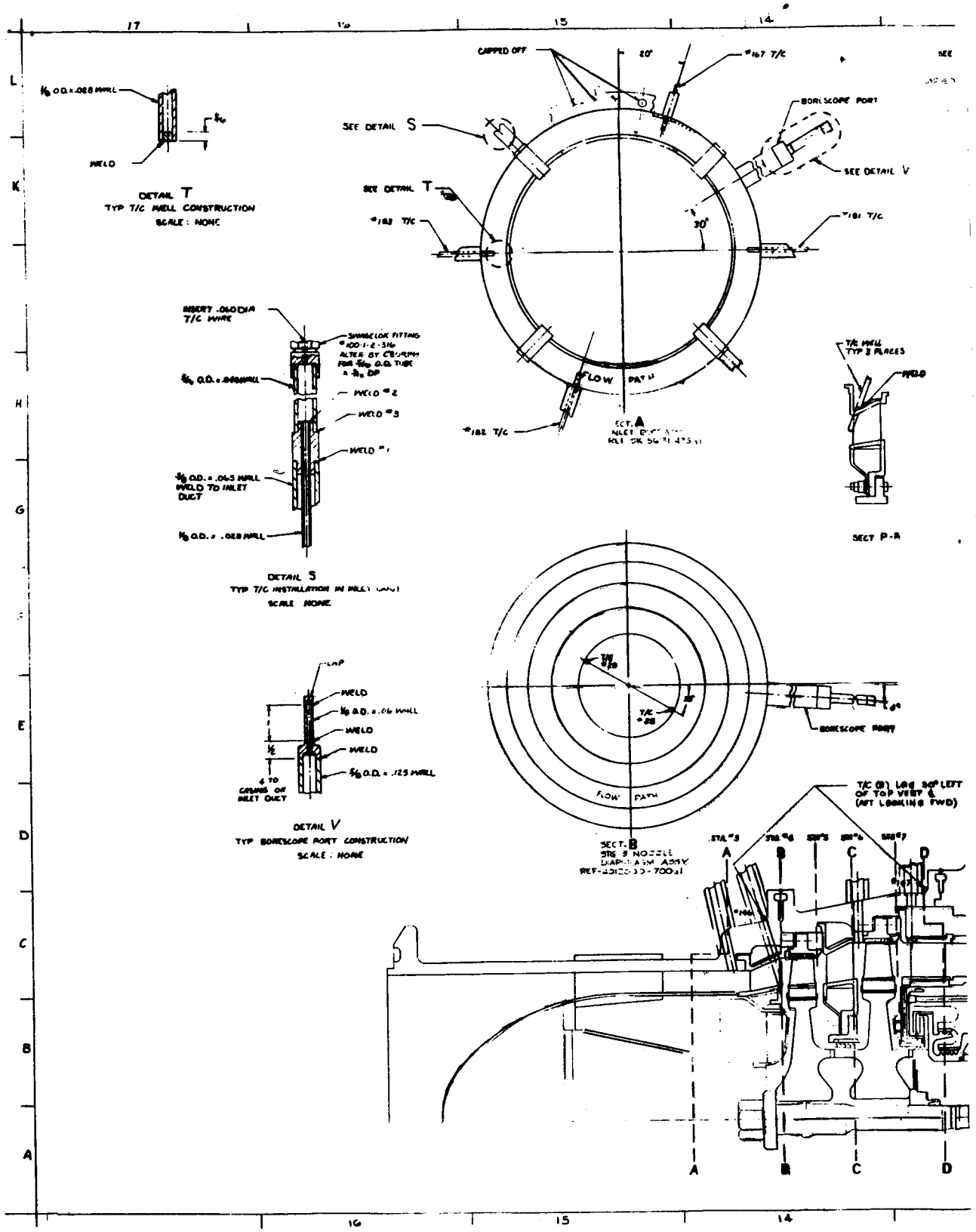

Figure 30. Instrumentation for

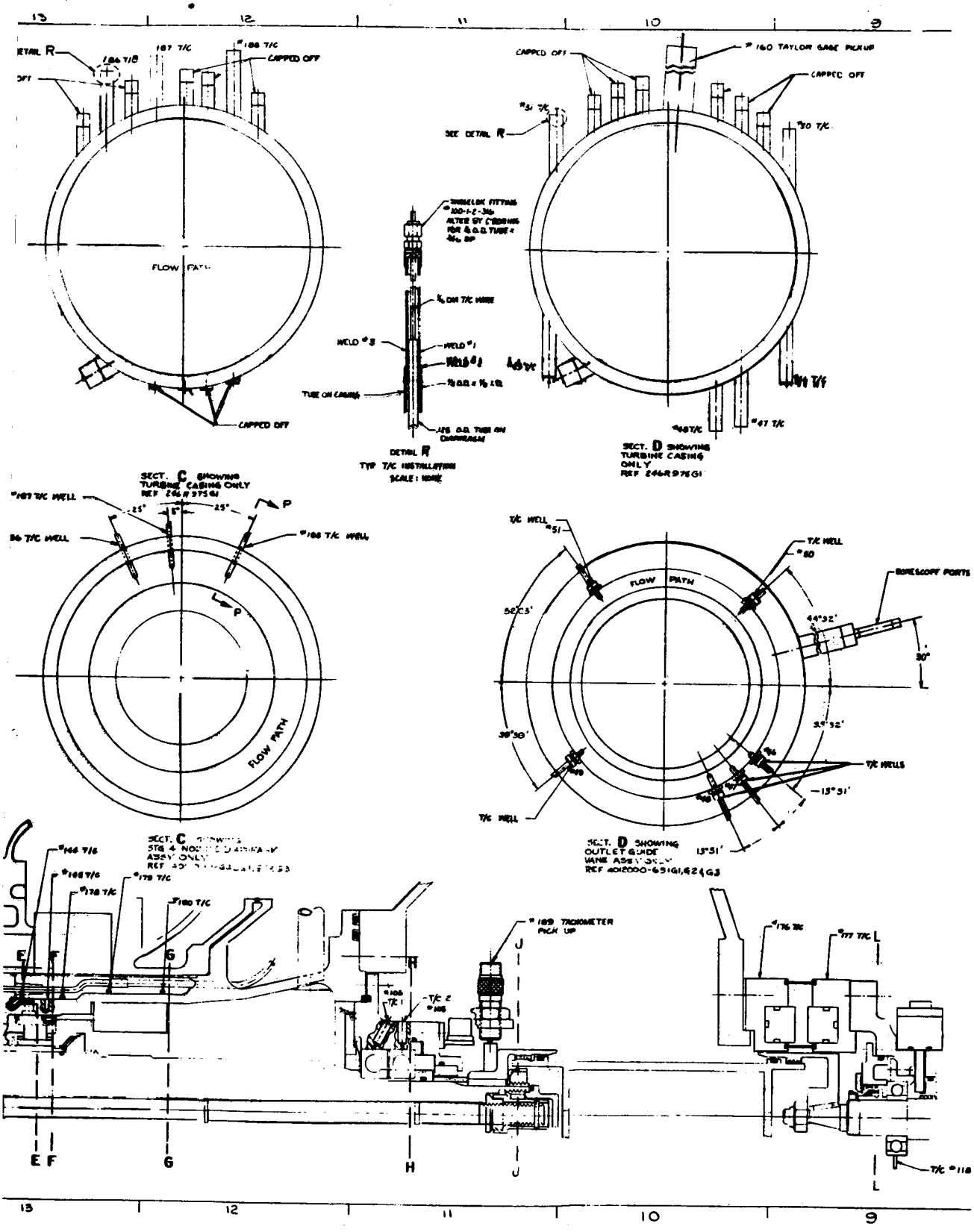

the Turbine Endurance Test.

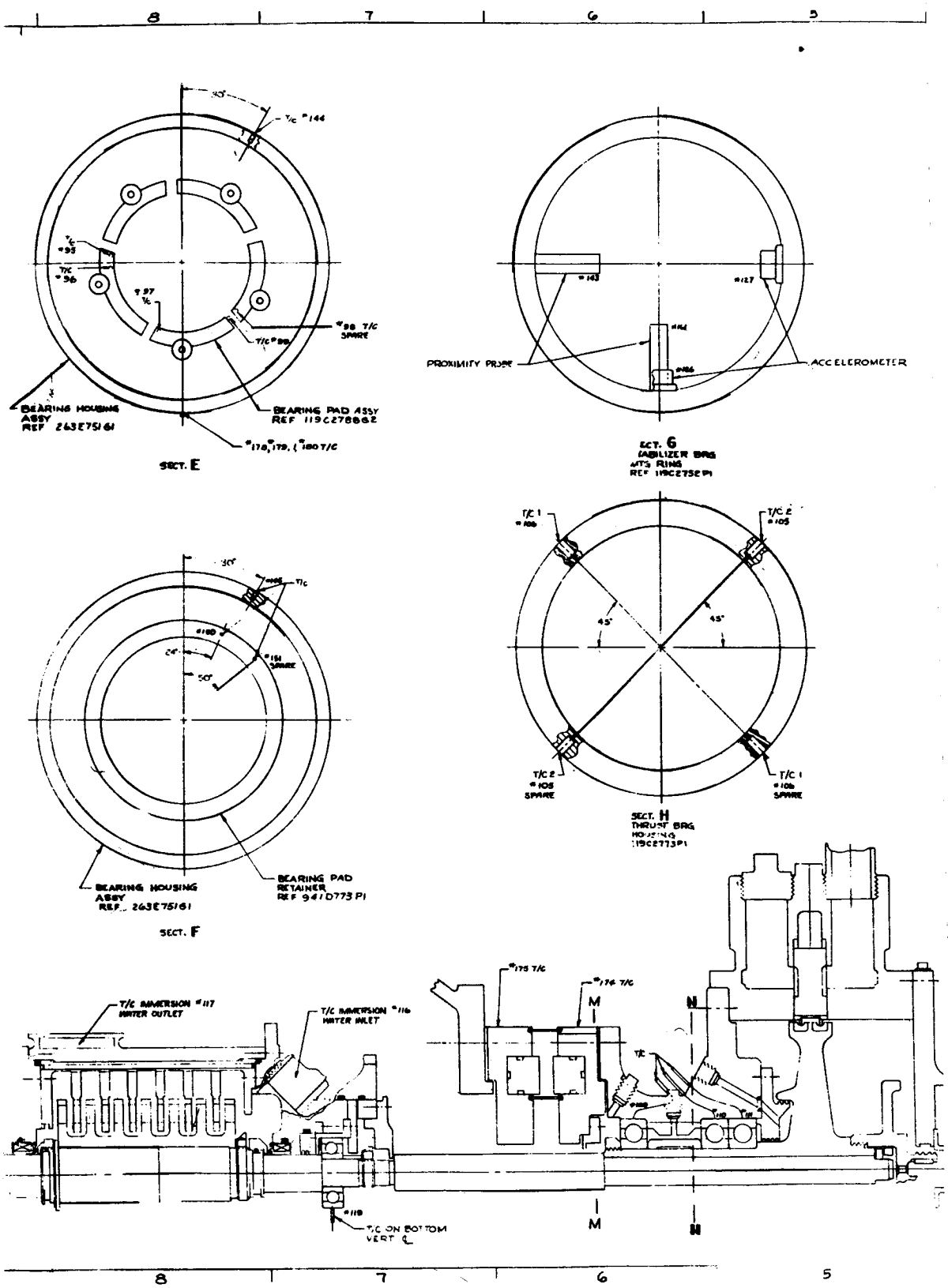

Figure 30. Concluded. Instr

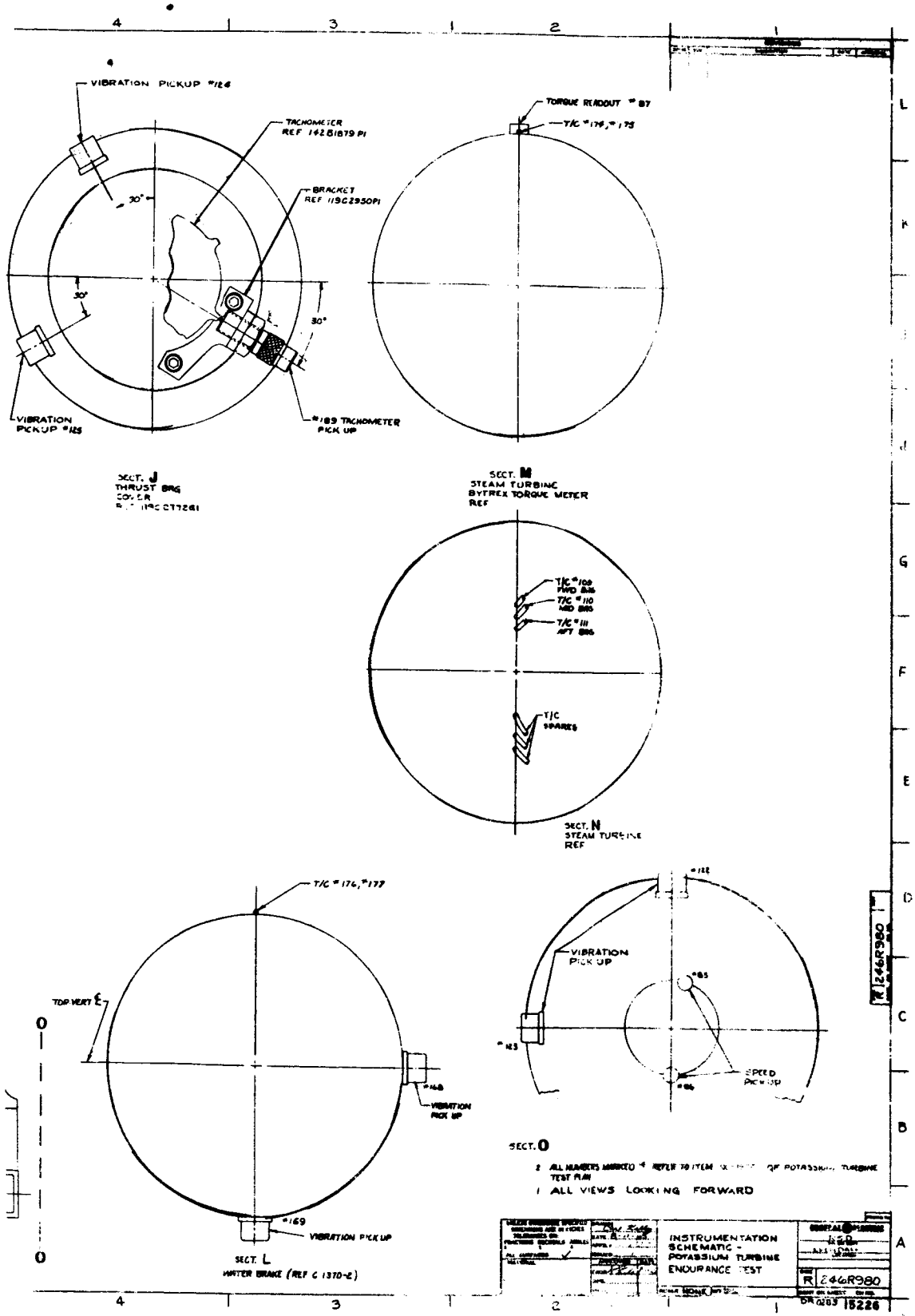

umentation for the Turbine Endurance Test.

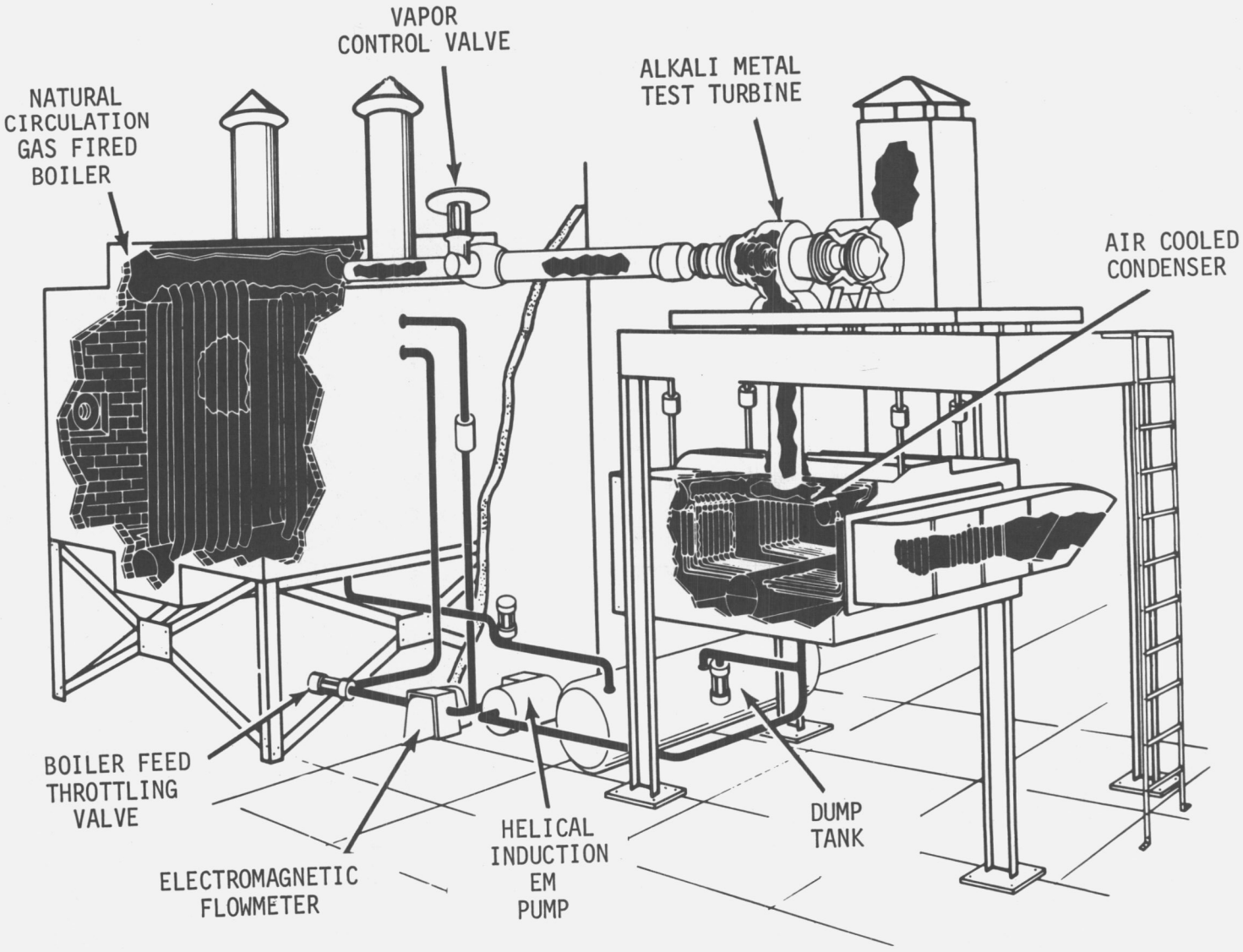

Figure 31. 3000 KW Turbine Test Facility.

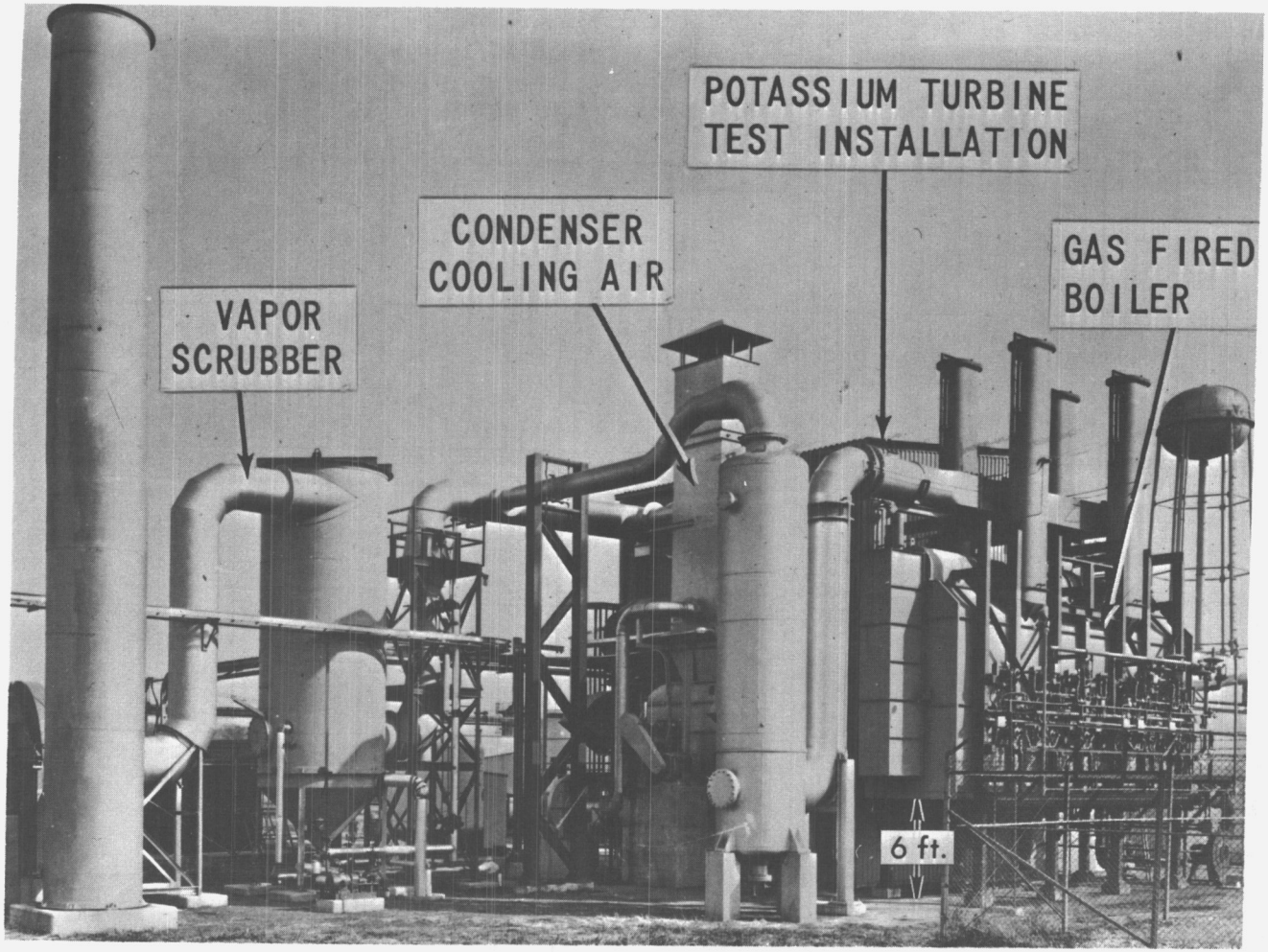

Figure 32. Turbine Test Facility.

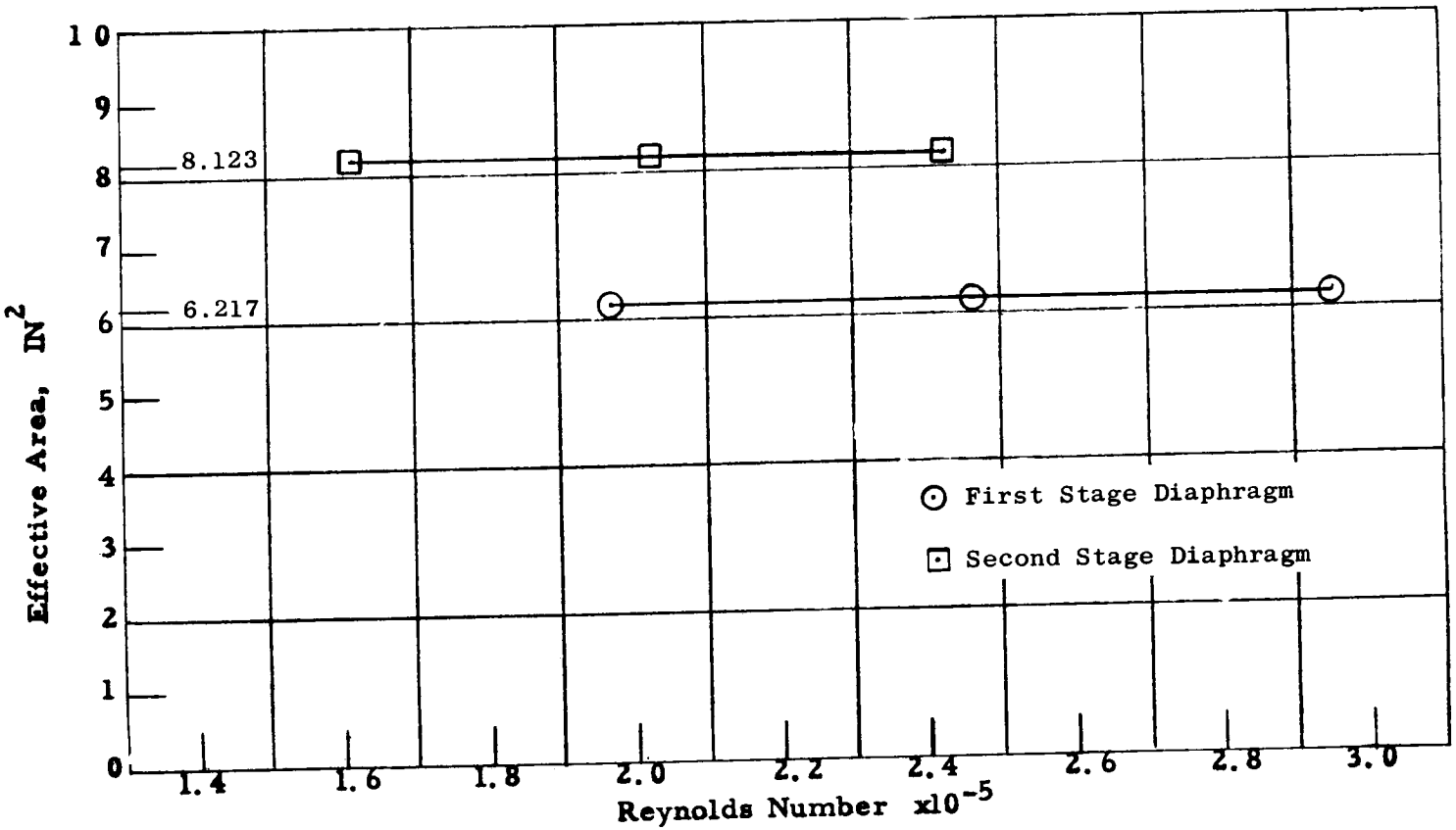

Figure 33. Nozzle Diaphragm Effective Area Versus Reynolds Number.

PRECEDING PAGE BLANK NOT FILMED.

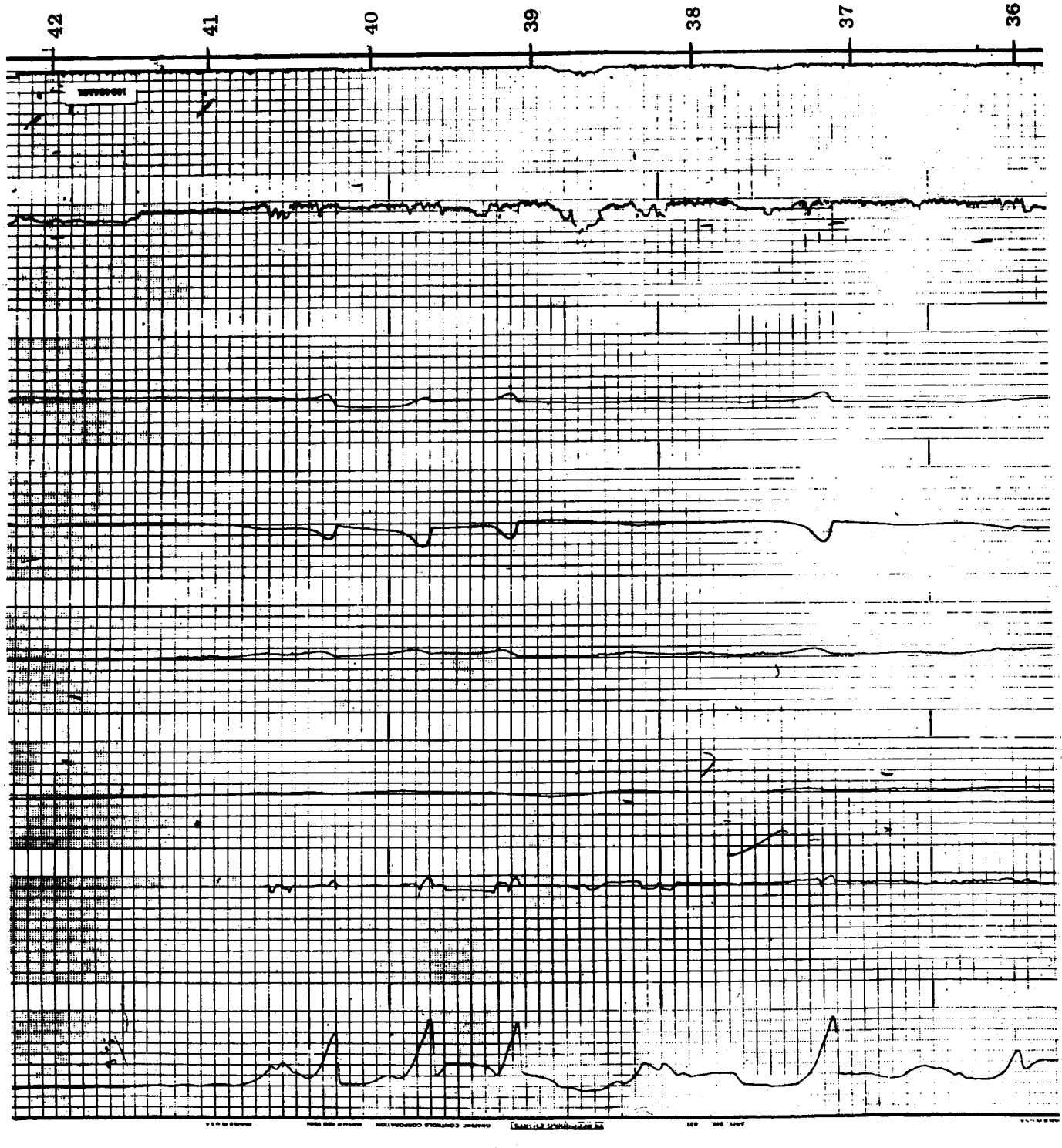

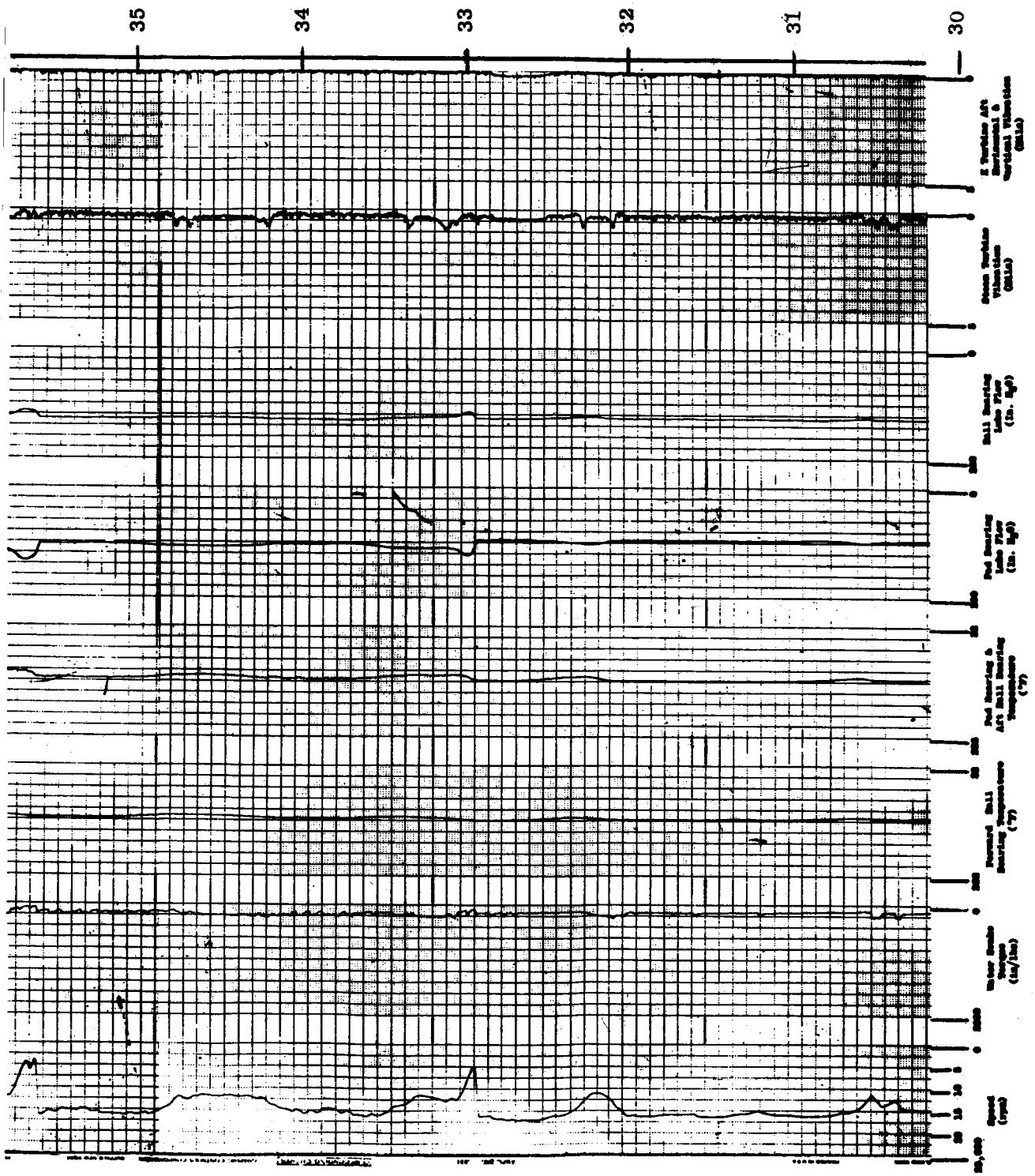

Figure 34a. Typical Speed Surge without Spray Flow (100464A01)

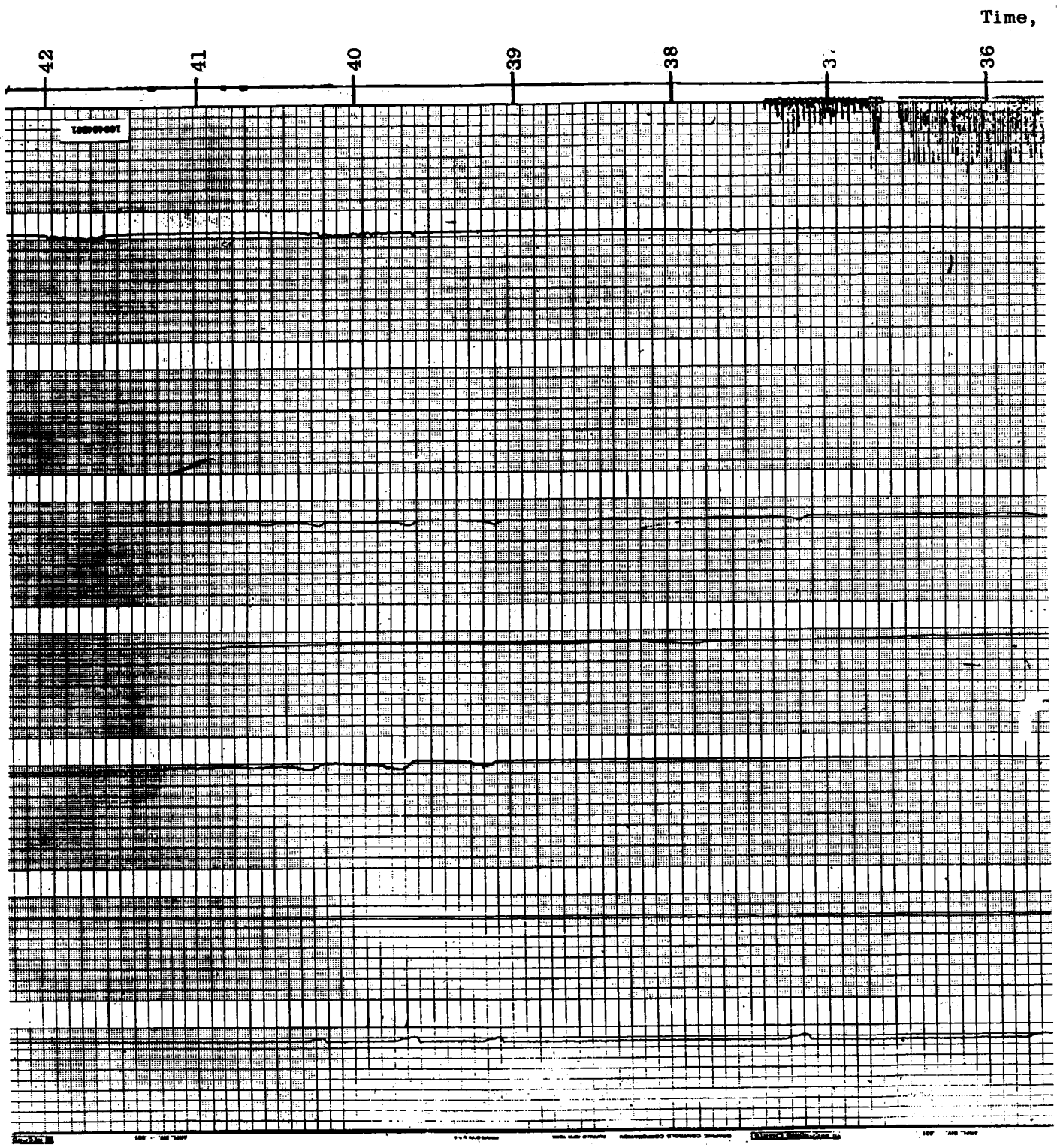
Time,
42
41
40
39
38
36

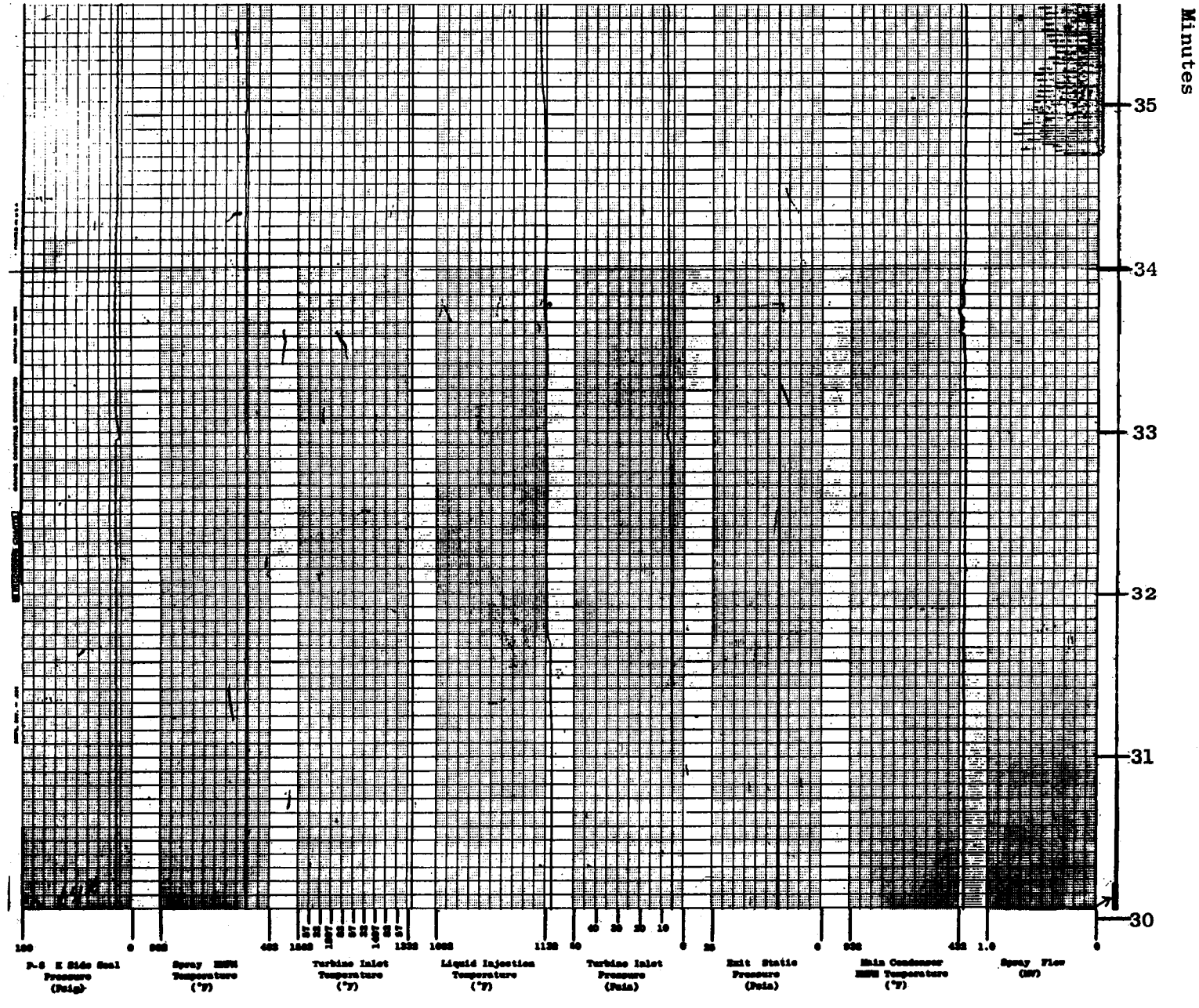

Figure 34b. Typical Speed Surge without Spray Flow (100464B01)

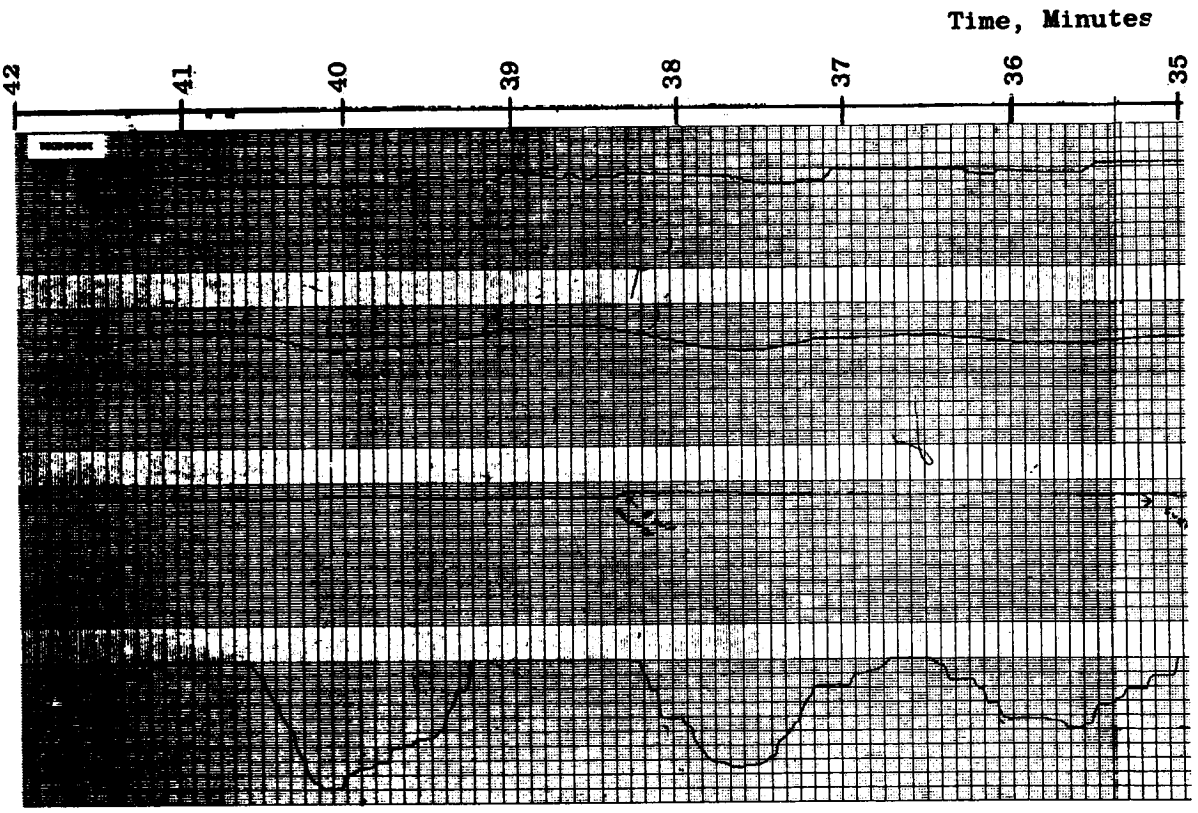
Time, Minutes
42
41
40
39
38
37
36
35

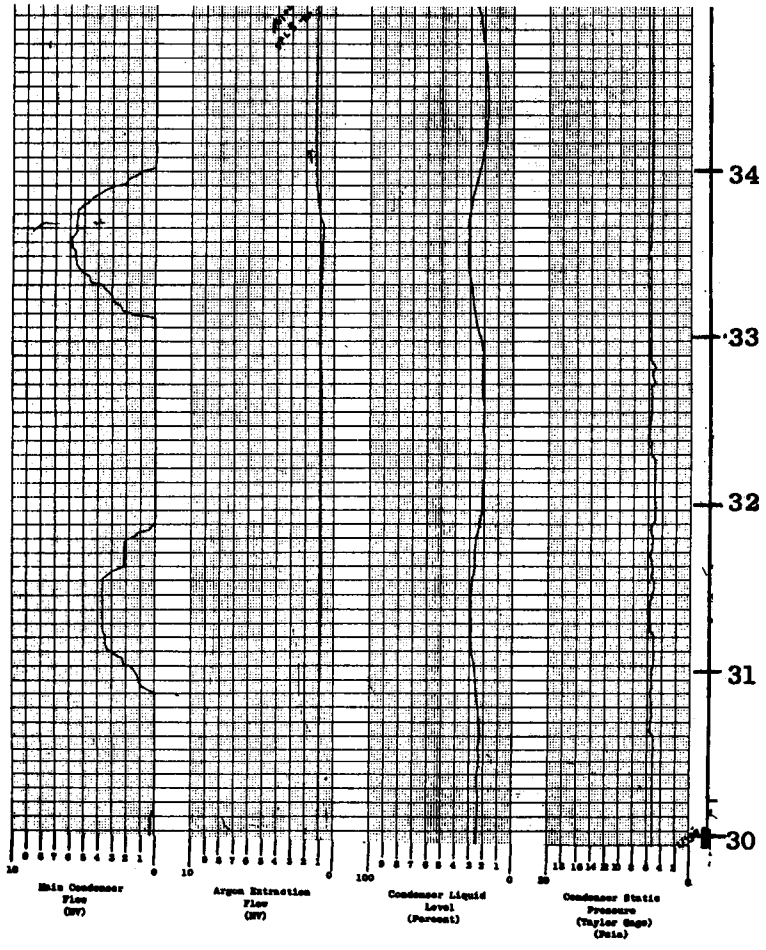

Figure 34c. Typical Speed Surge without Spray Flow (100464C01)

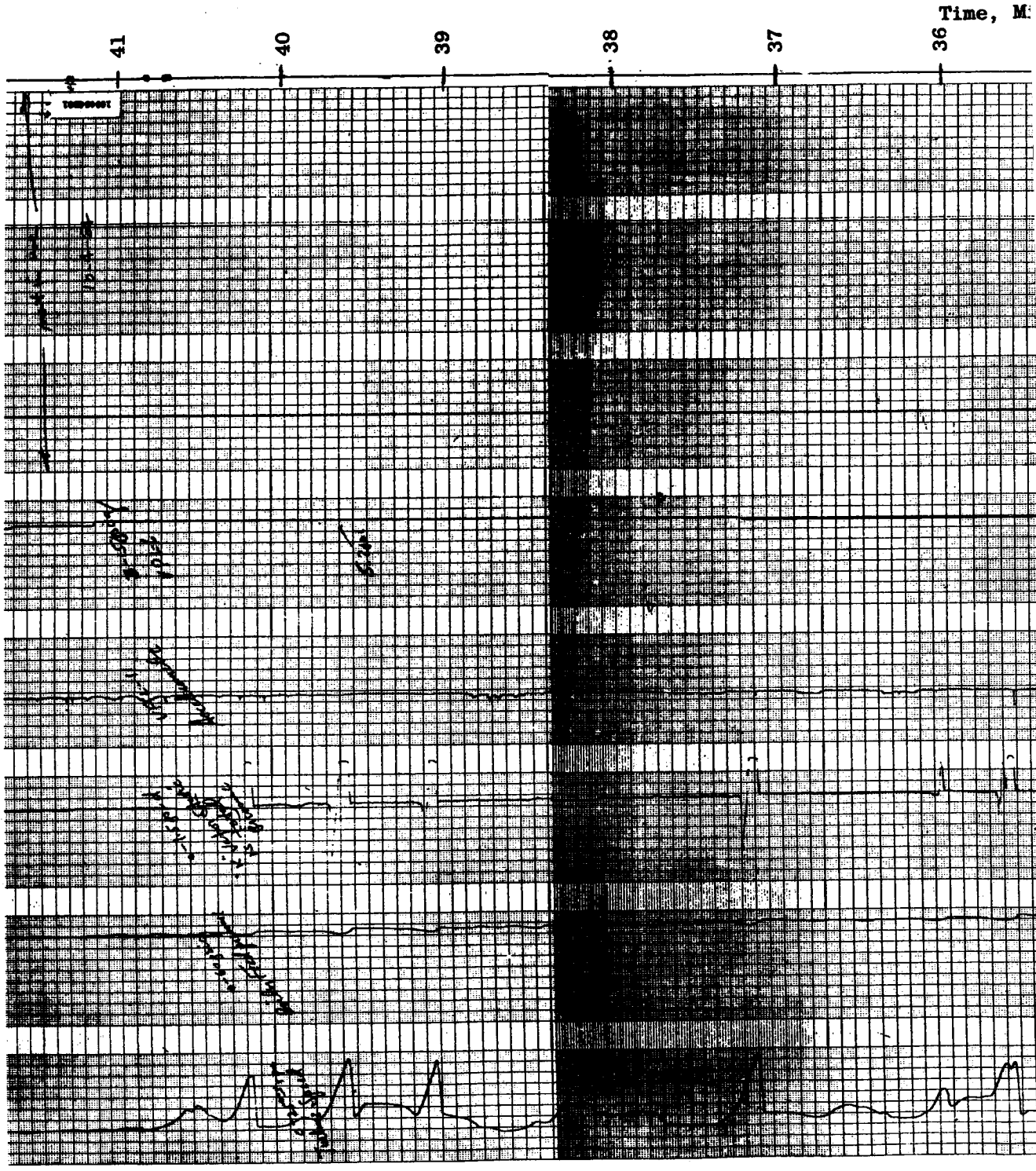
Time, M
41
40
39
38
37
36

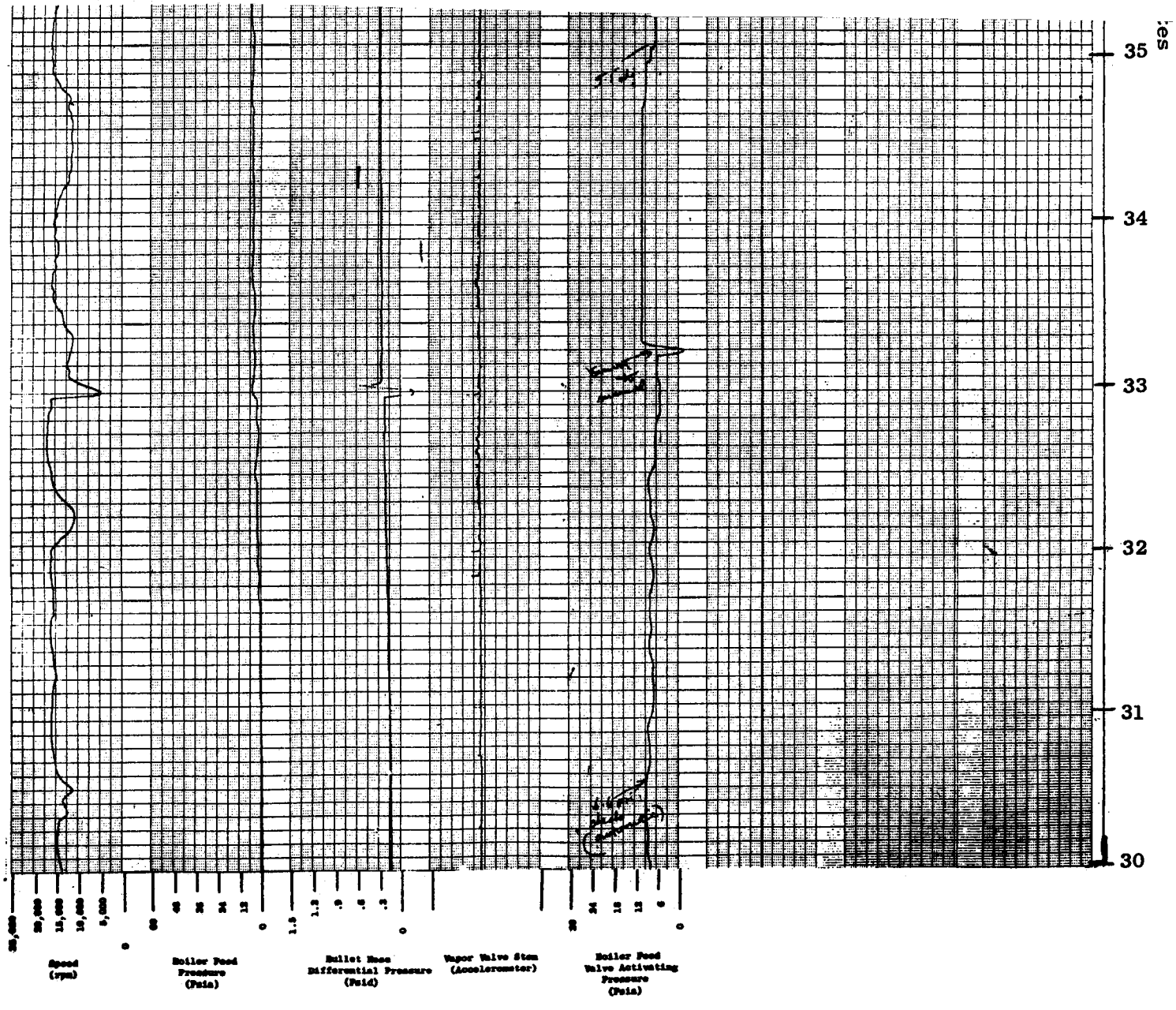

Figure 34d. Typical Speed Surge without Spray Flow (101464D01)

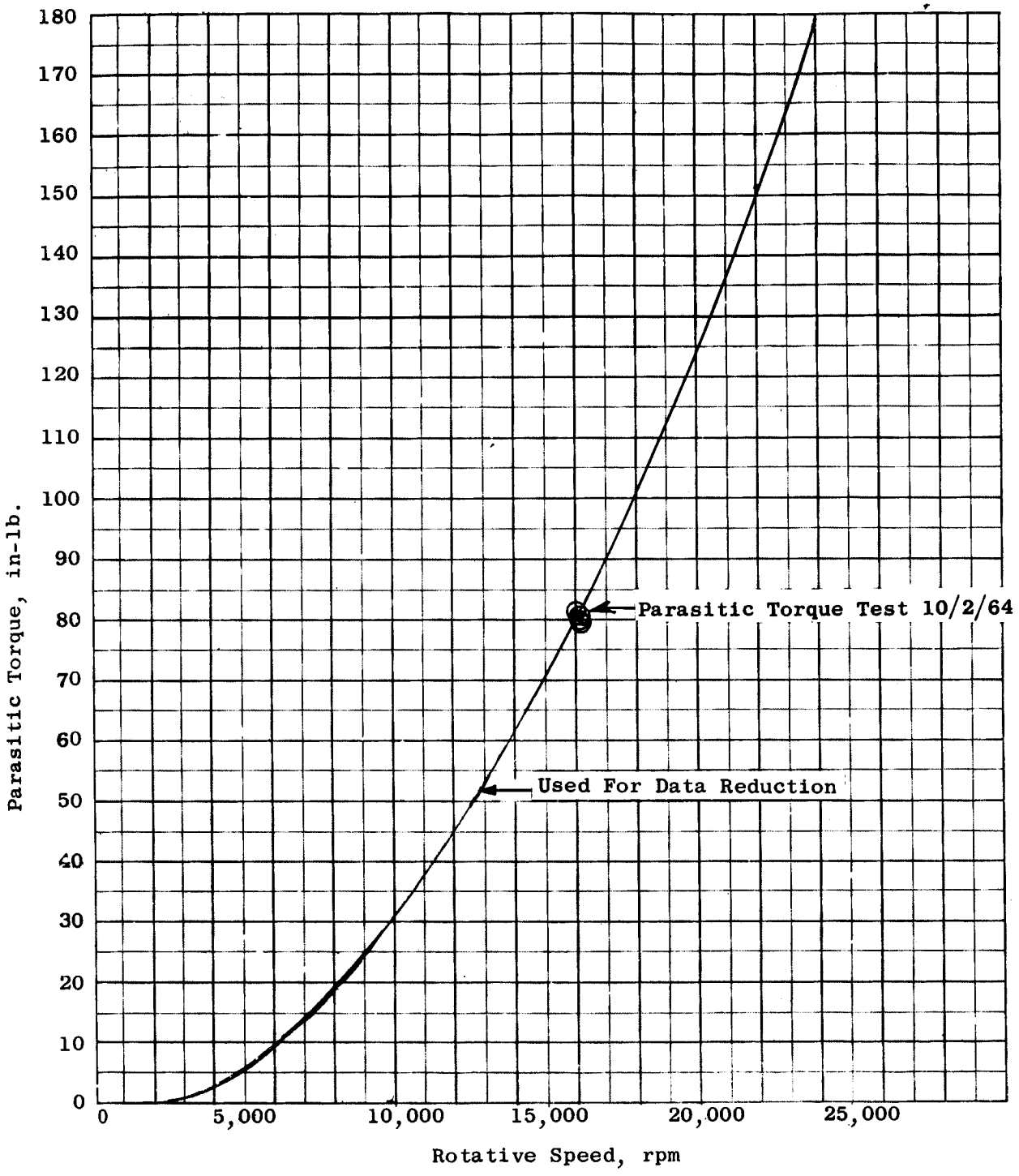

Figure 35. Comparison of Parasitic Torque Values for Data Reduction With Parasitic Torque Test Values.

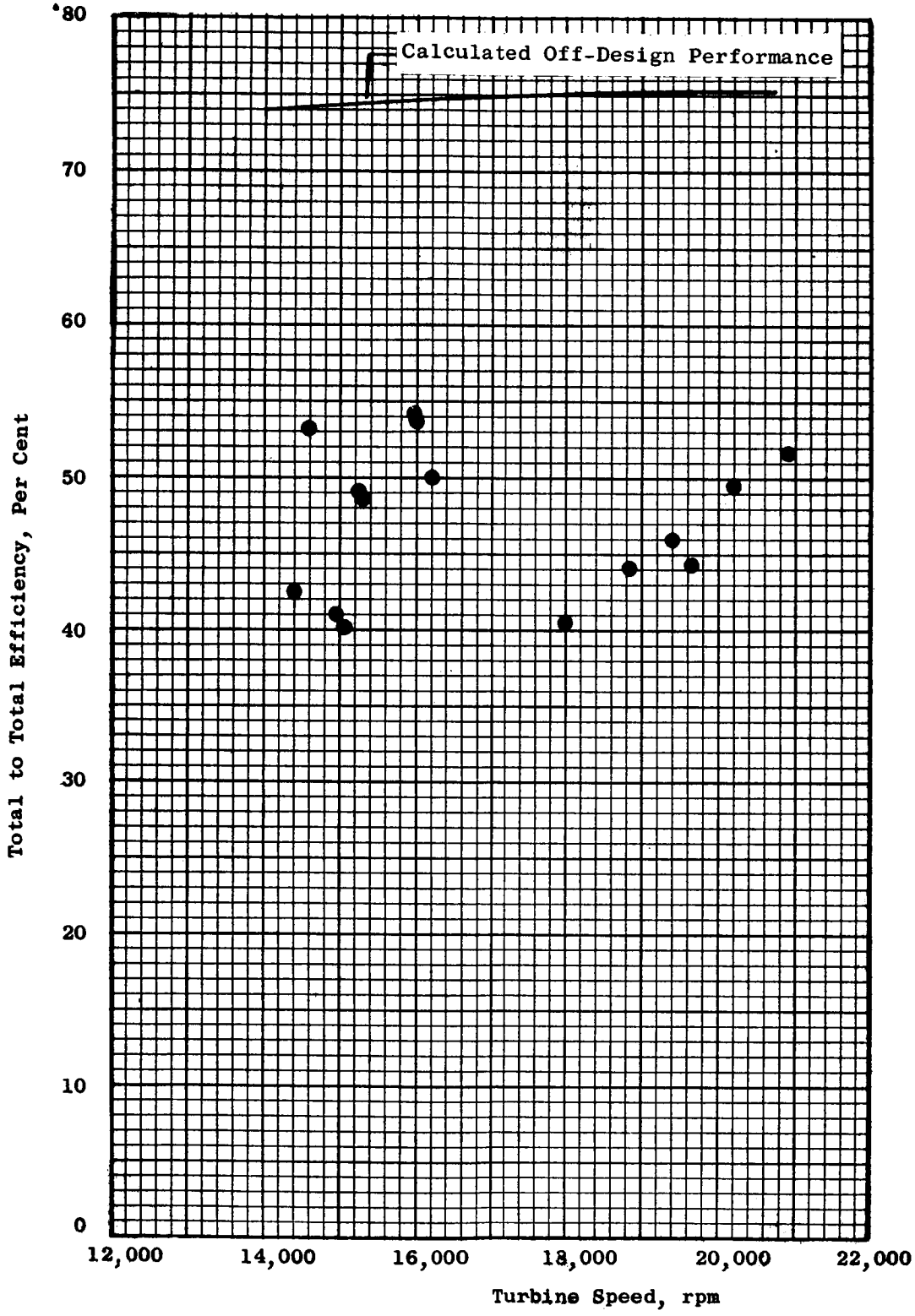

Figure 36. Comparison of Preliminary Turbine Performance and Calculated Data. Inlet Temperature, 1450°F; Zero Spray Flow; Total to Total Pressure Ratio, 2.1 $\pm$ .1.

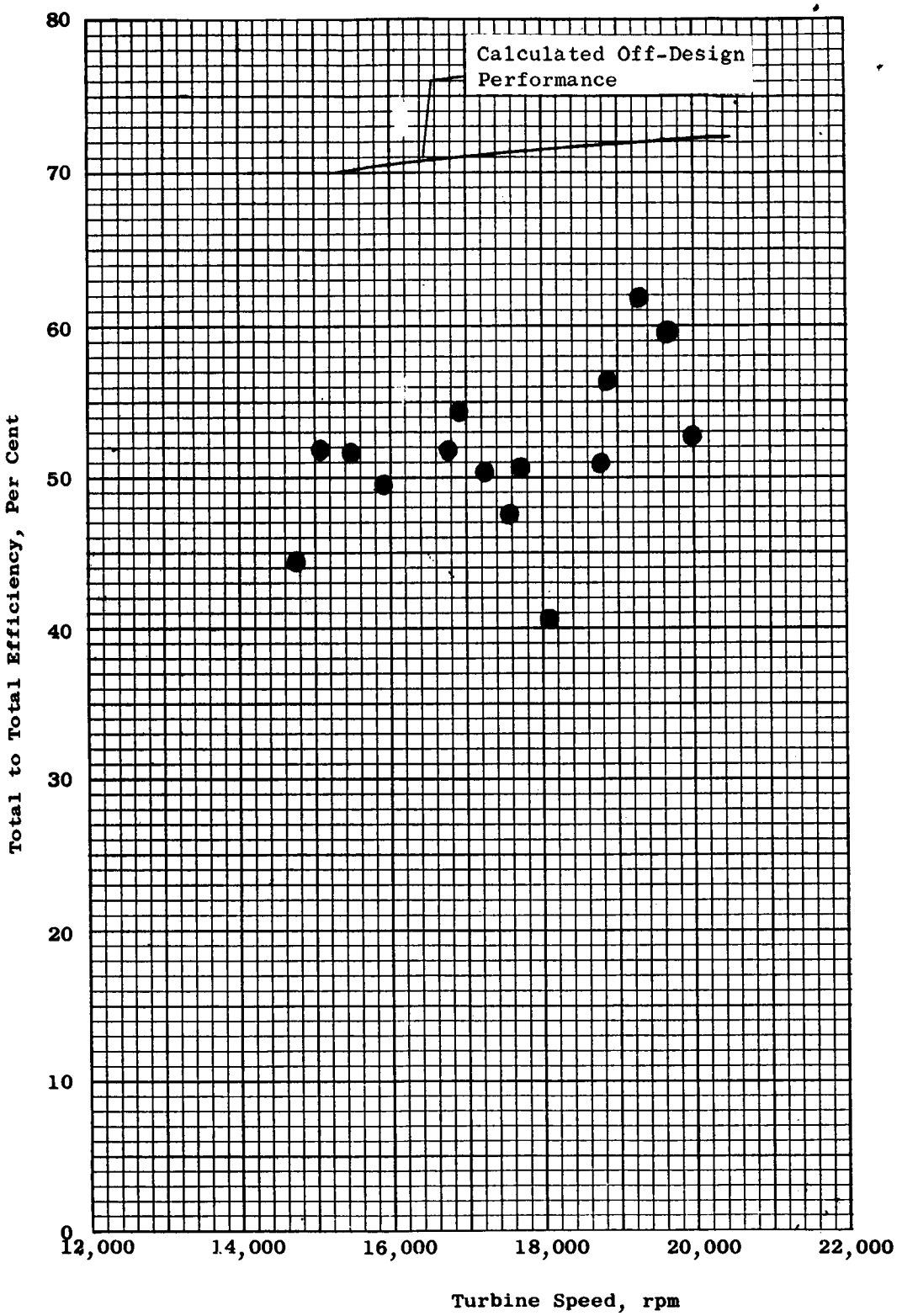

Figure 37. Comparison of Preliminary Turbine Performance and Calculated Data. Inlet Temperature, 1450°F; Zero Spray Flow; Total to Total Pressure Ratio, 3.2 $\pm$ .1.

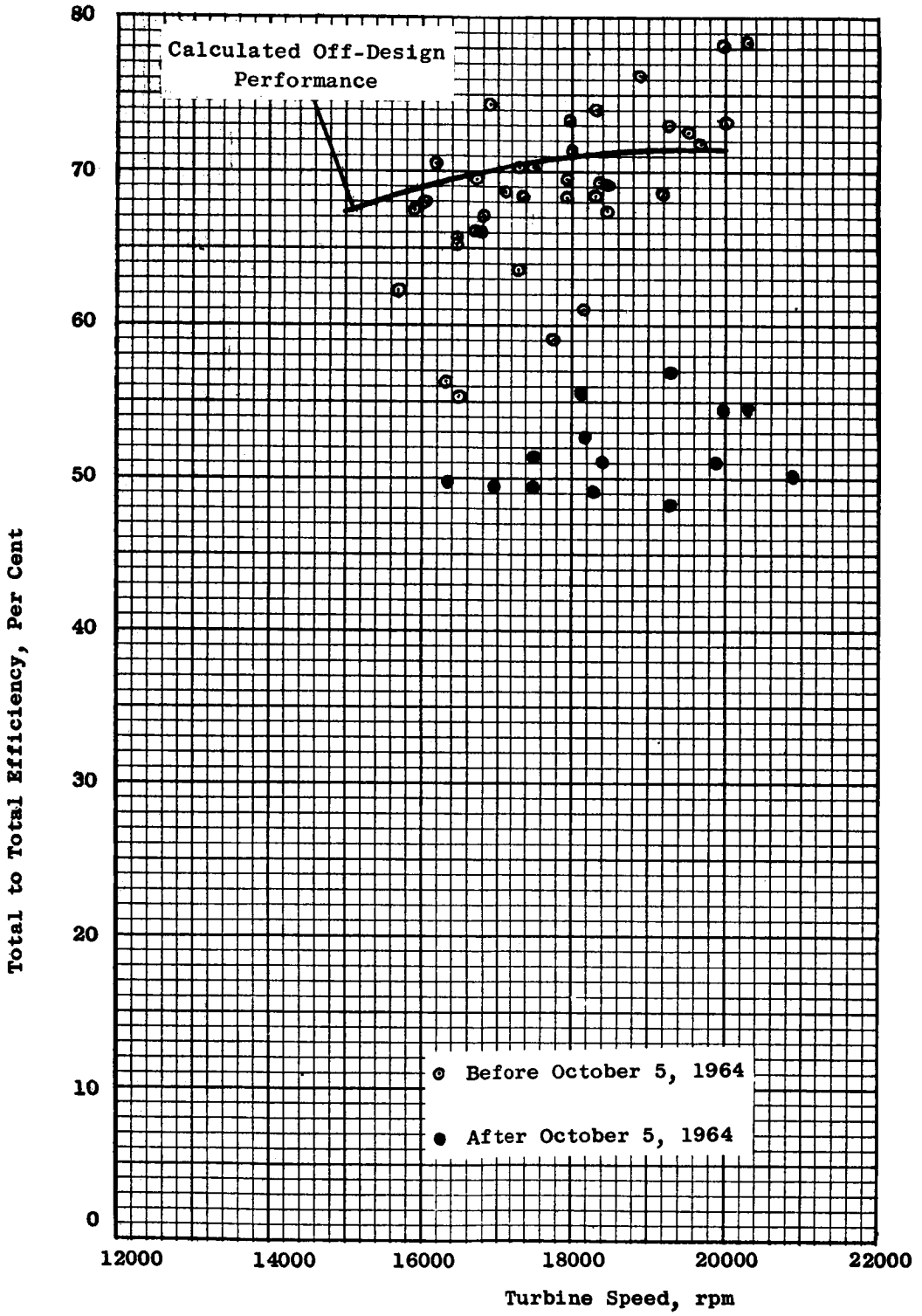

Figure 38. Comparison of Preliminary Turbine Performance and Calculated Data. Inlet Temperature, 1450°F; Zero Spray Flow; Total to Total Pressure Ratio, 3.6 ± .1.

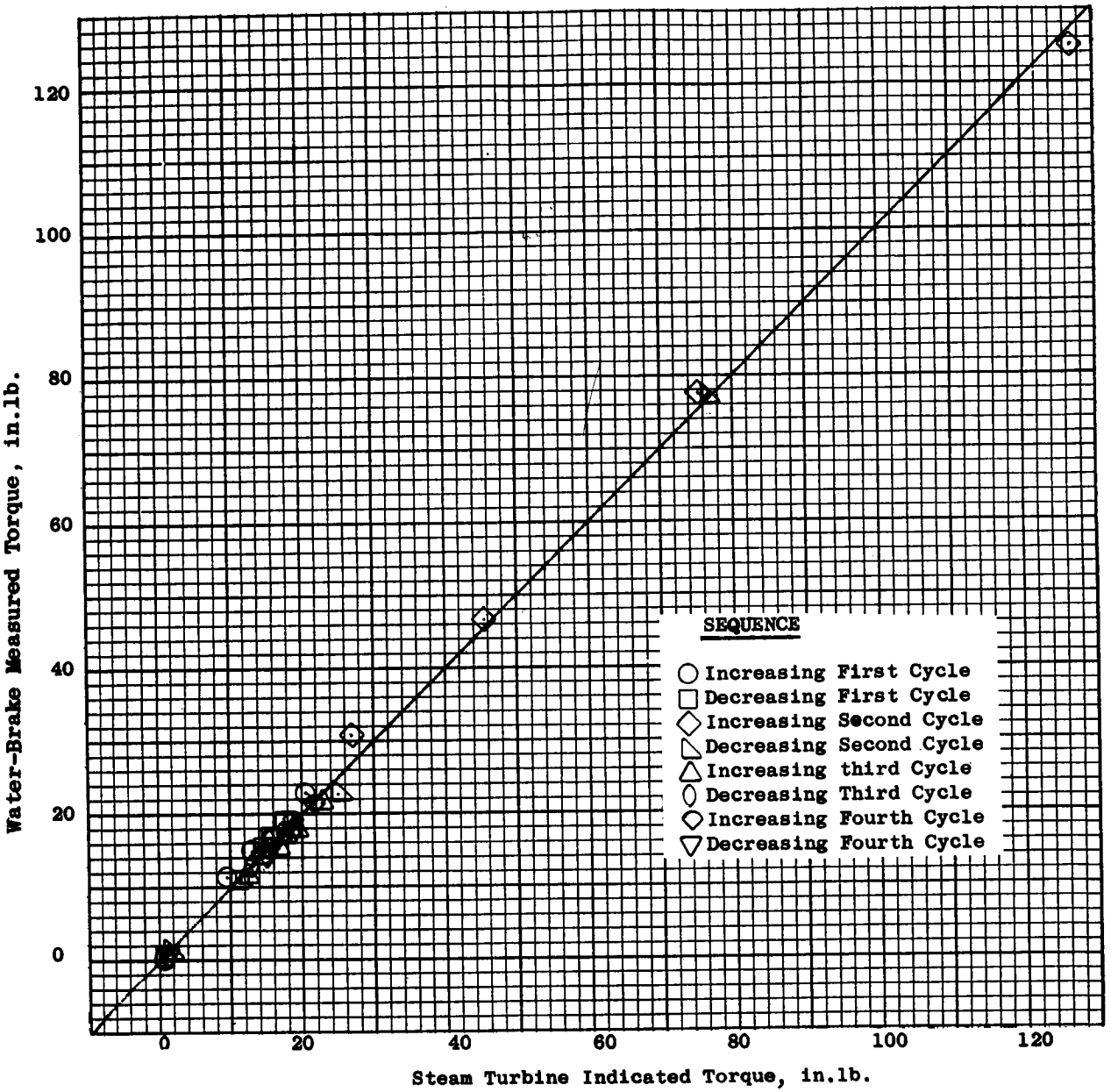

Figure 39. Rotational Calibration of Bytrex Torque Measurement System, Test Date 5/5/65.

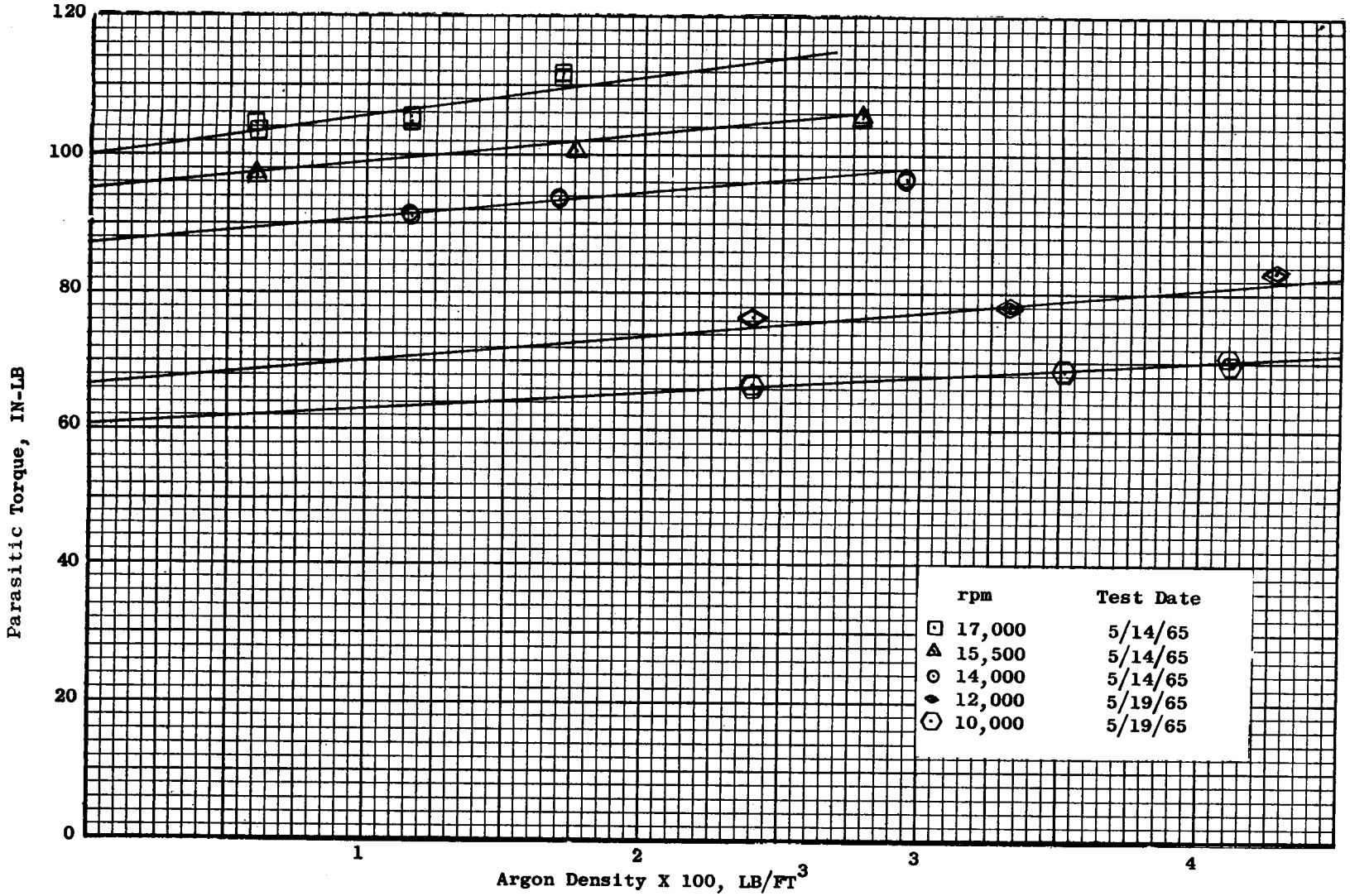

Figure 40. Parasitic Torque Variation With Rotative Speed and Density.

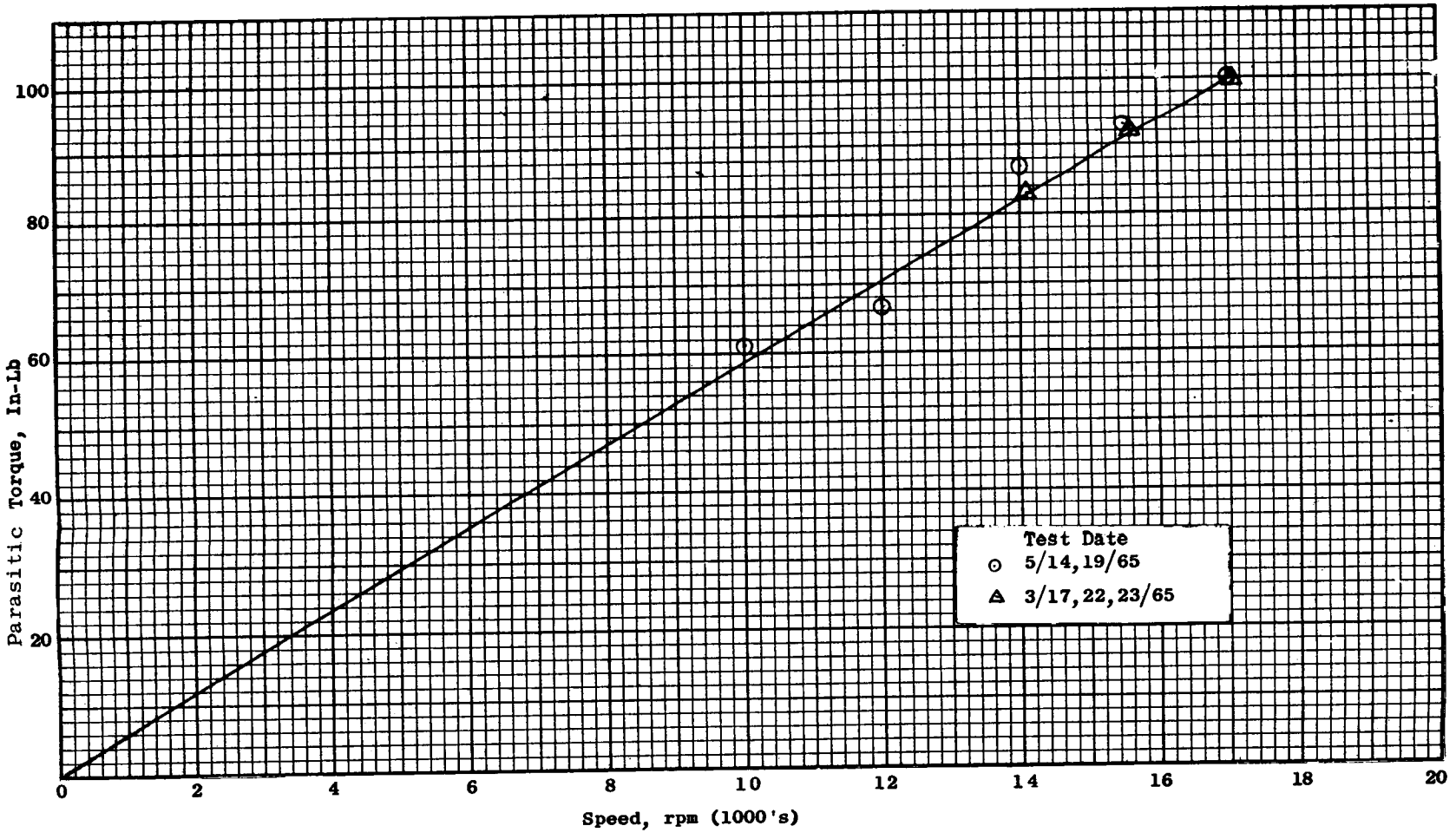

Figure 41. Parasitic Torque Variation With Rotative Speed From Several Tests.

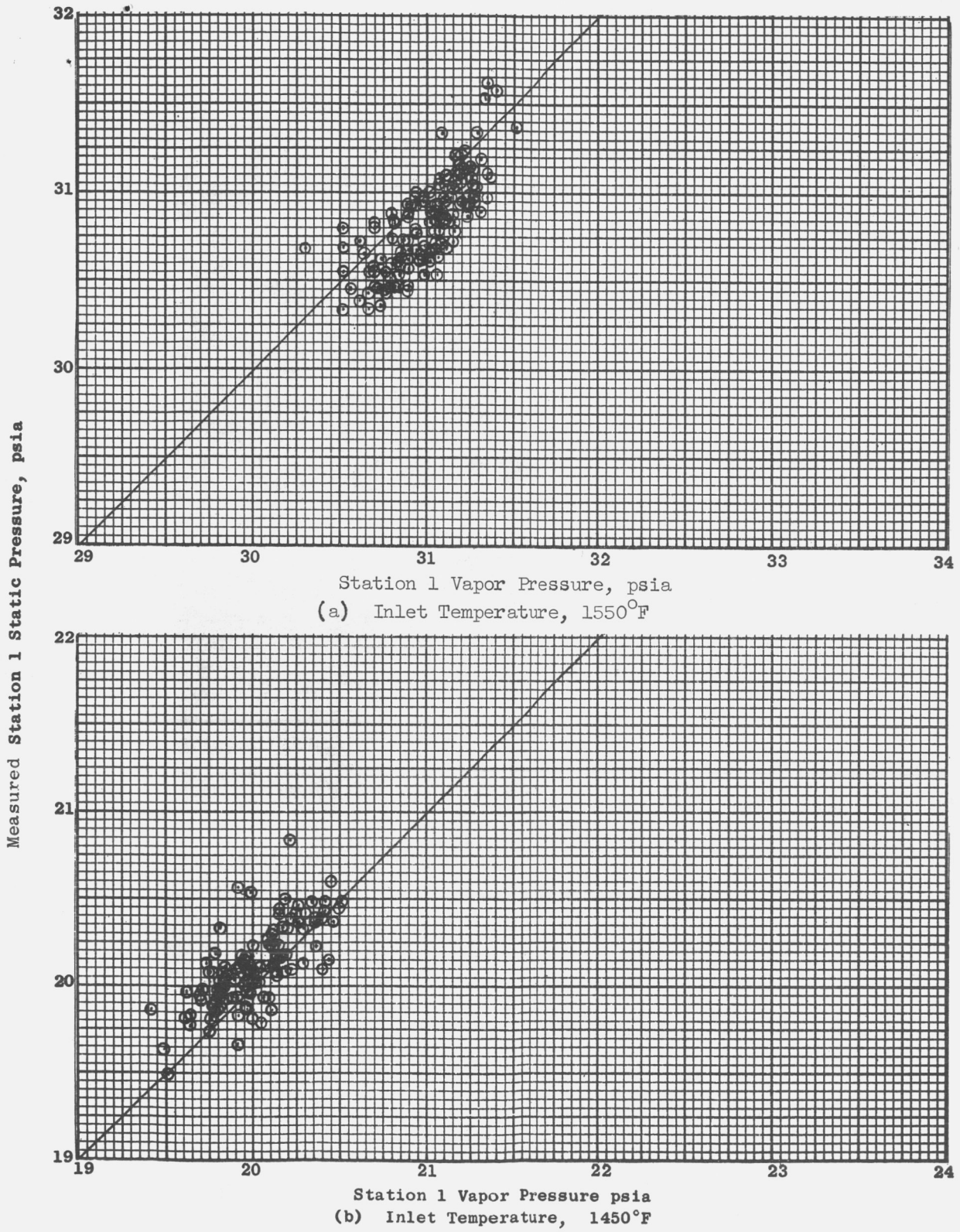

Figure 42. Comparison of Pressure Measured by Efflux System With Vapor Pressure at Station 1.

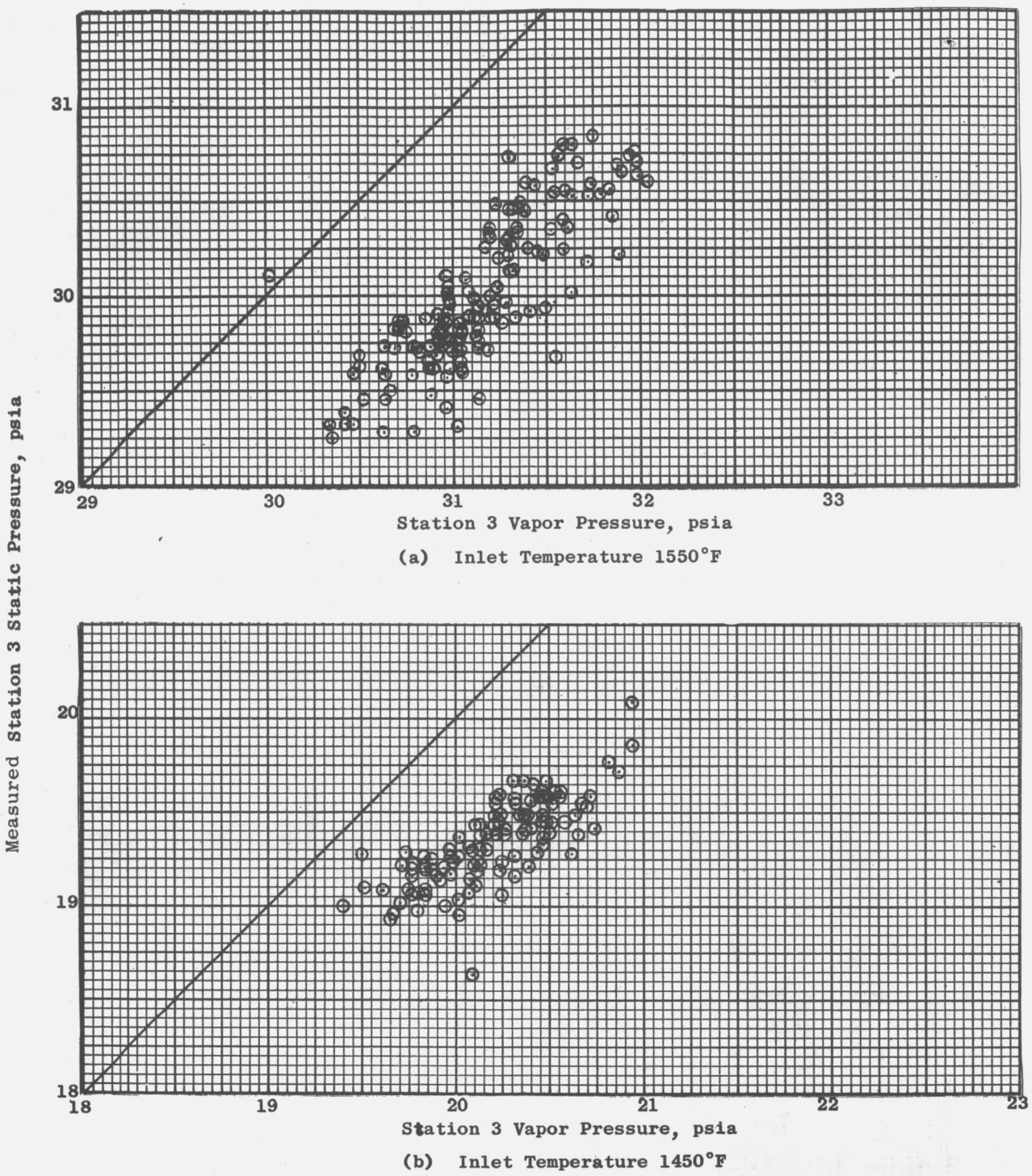

Figure 43. Comparison of Pressure Measured by Efflux System With Vapor Pressure at Turbine Inlet.

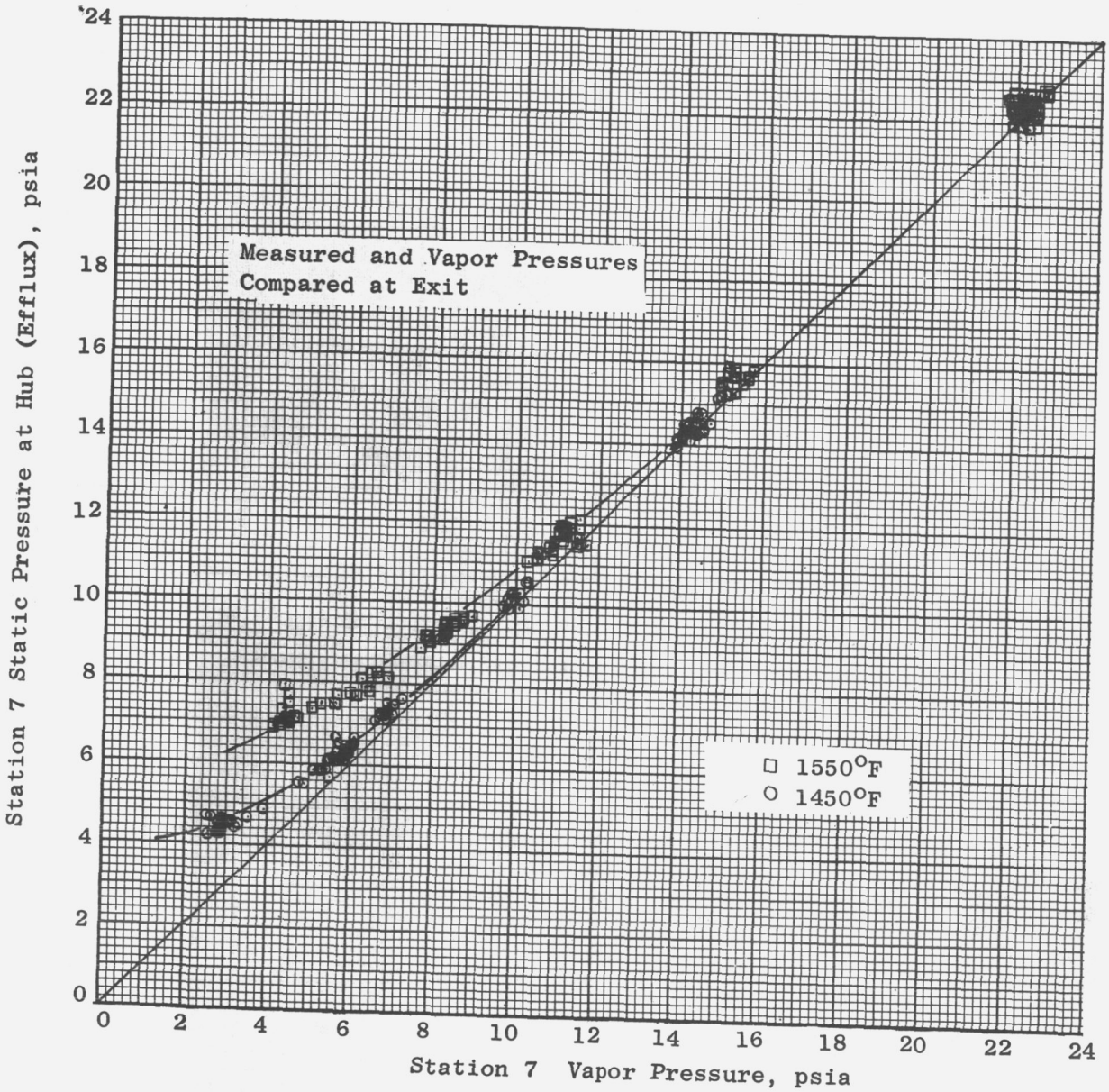

Figure 44. Comparison of Measured Pressure with Vapor Pressure at Turbine Exit.

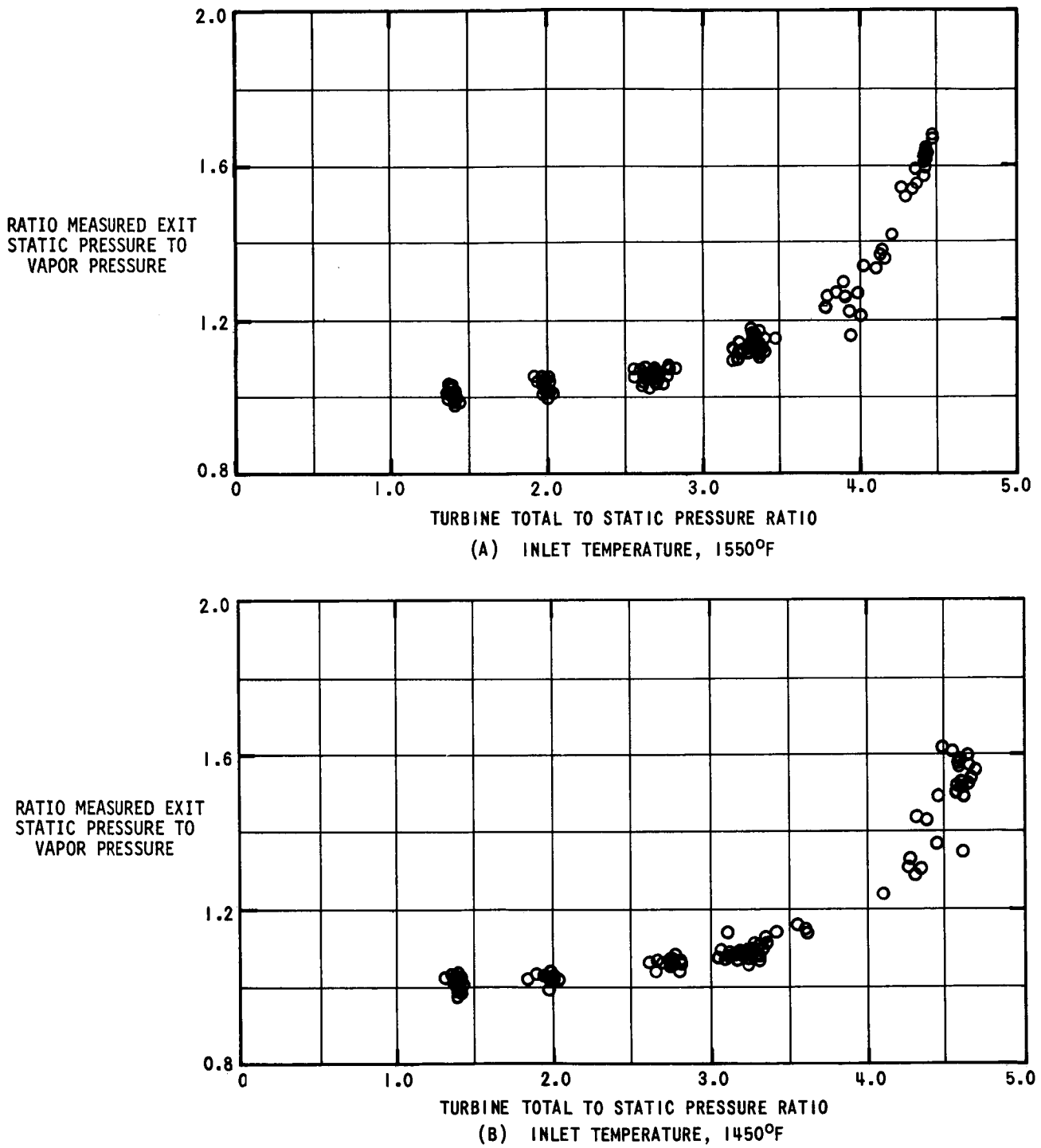

Figure 45. Ratio of Measured Pressure to Vapor Pressure at Station 7.

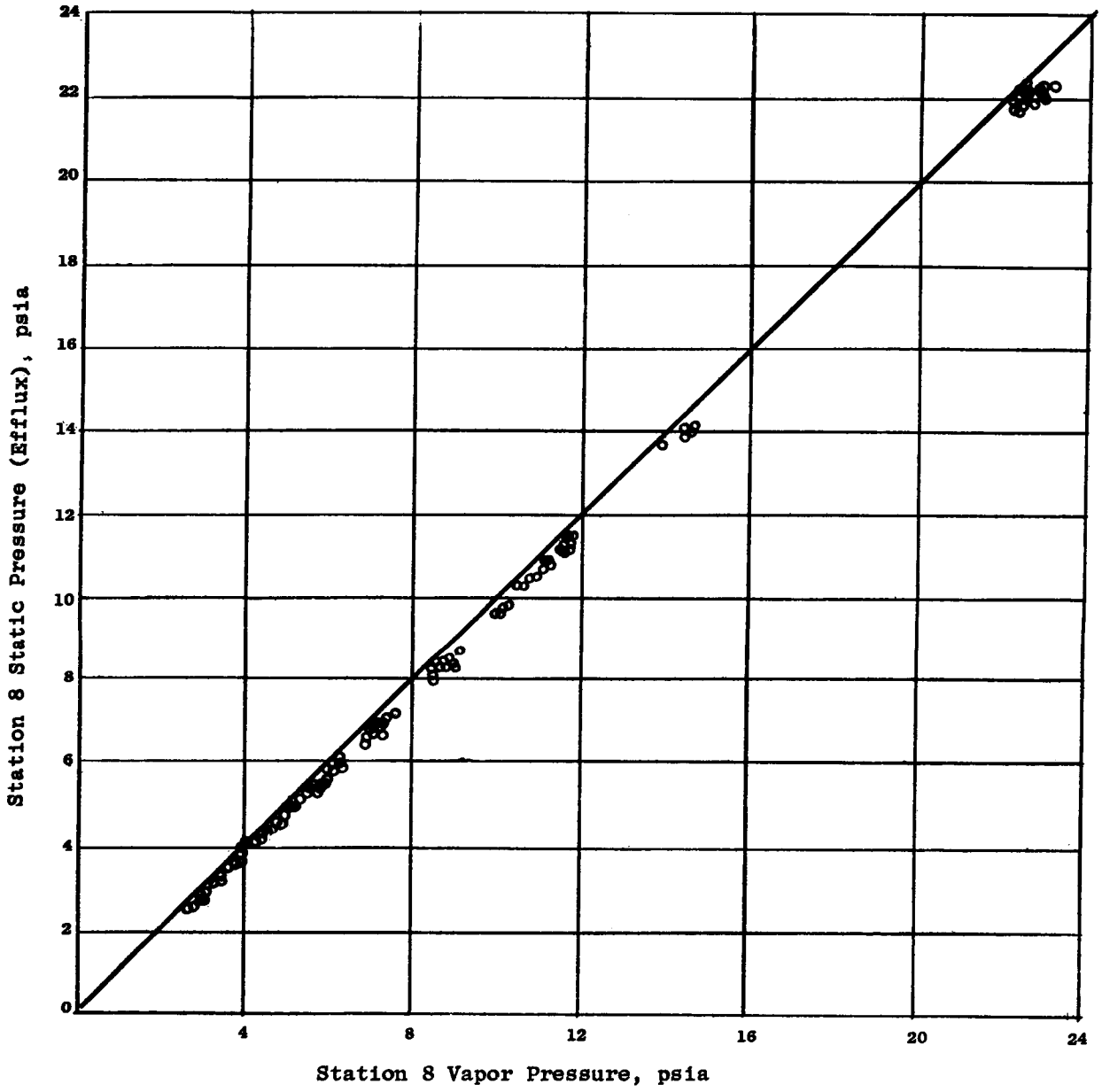

Figure 46. **Comparison of Measured Pressure With Vapor Pressure Downstream of the Turbine.**

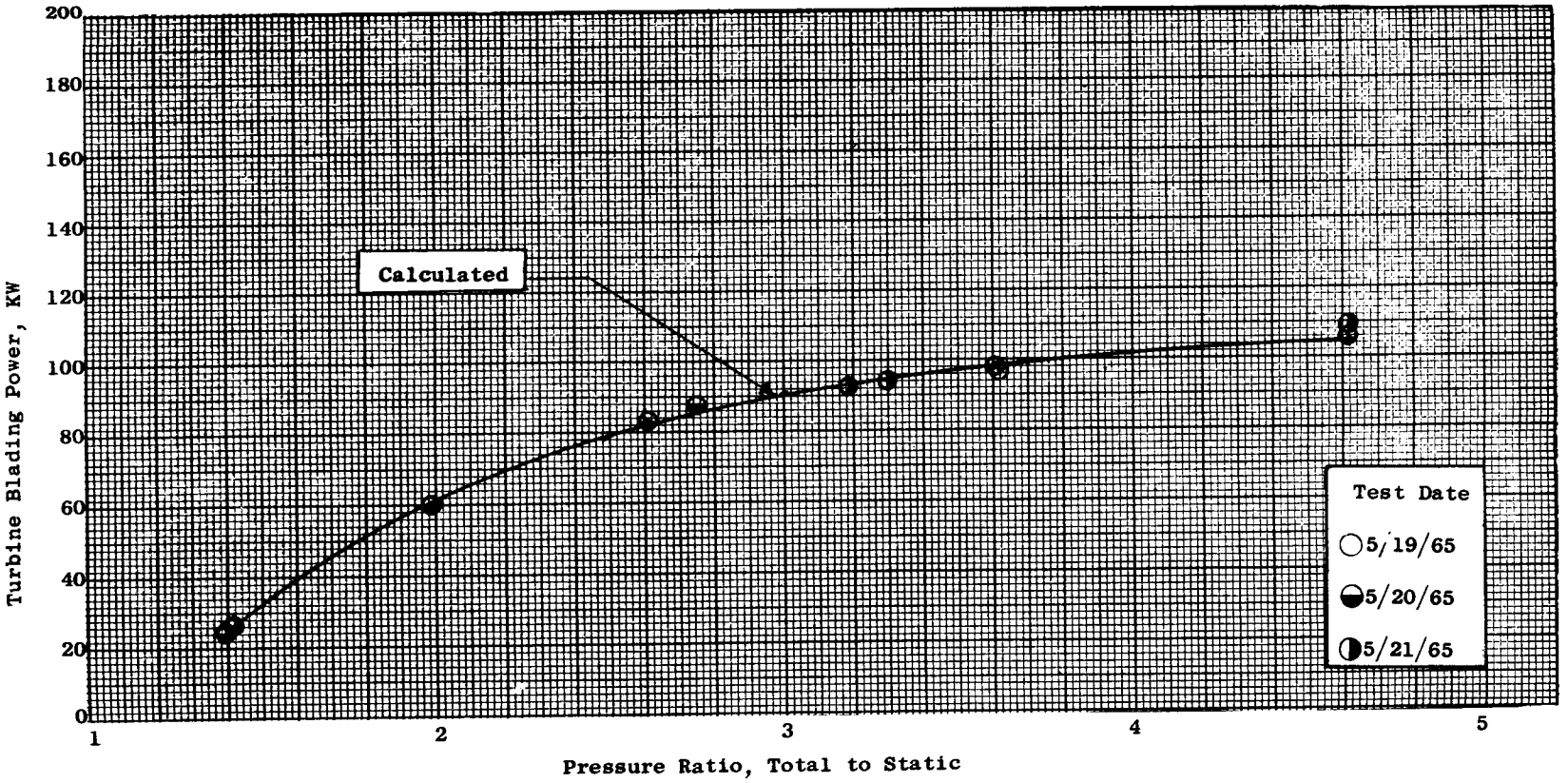

Figure 47. Comparison of Measured and Calculated Turbine Blading Power Versus Total to Static Pressure Ratio. Inlet Temperature, 1450°F, Rotative Speed, 15,4000 rpm.

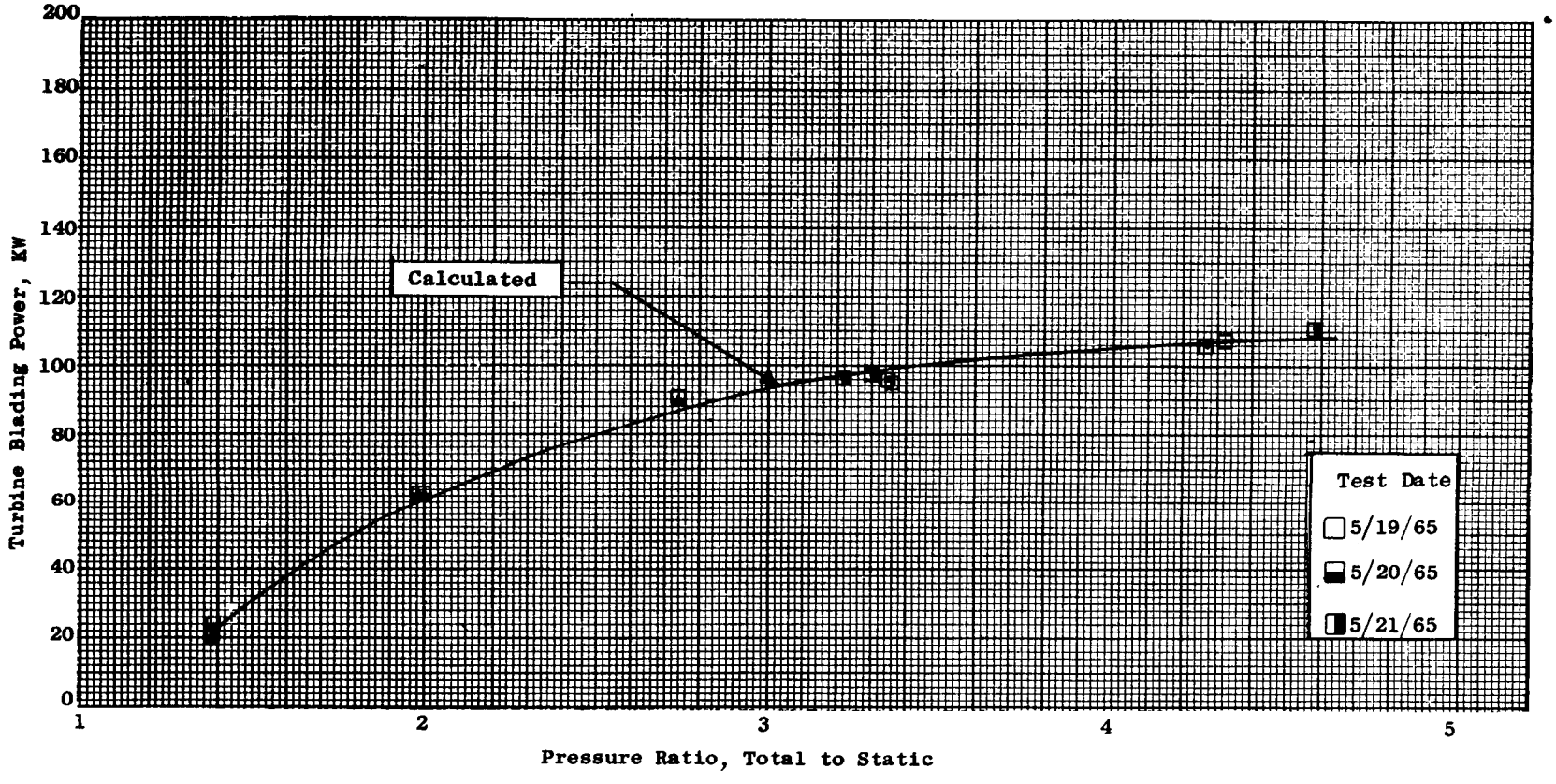

Figure 48. Comparison of Measured and Calculated Turbine Blading Power Versus Total to Static Pressure Ratio. Inlet Temperature, 1450°F, Rotative Speed, 16,400 rpm.

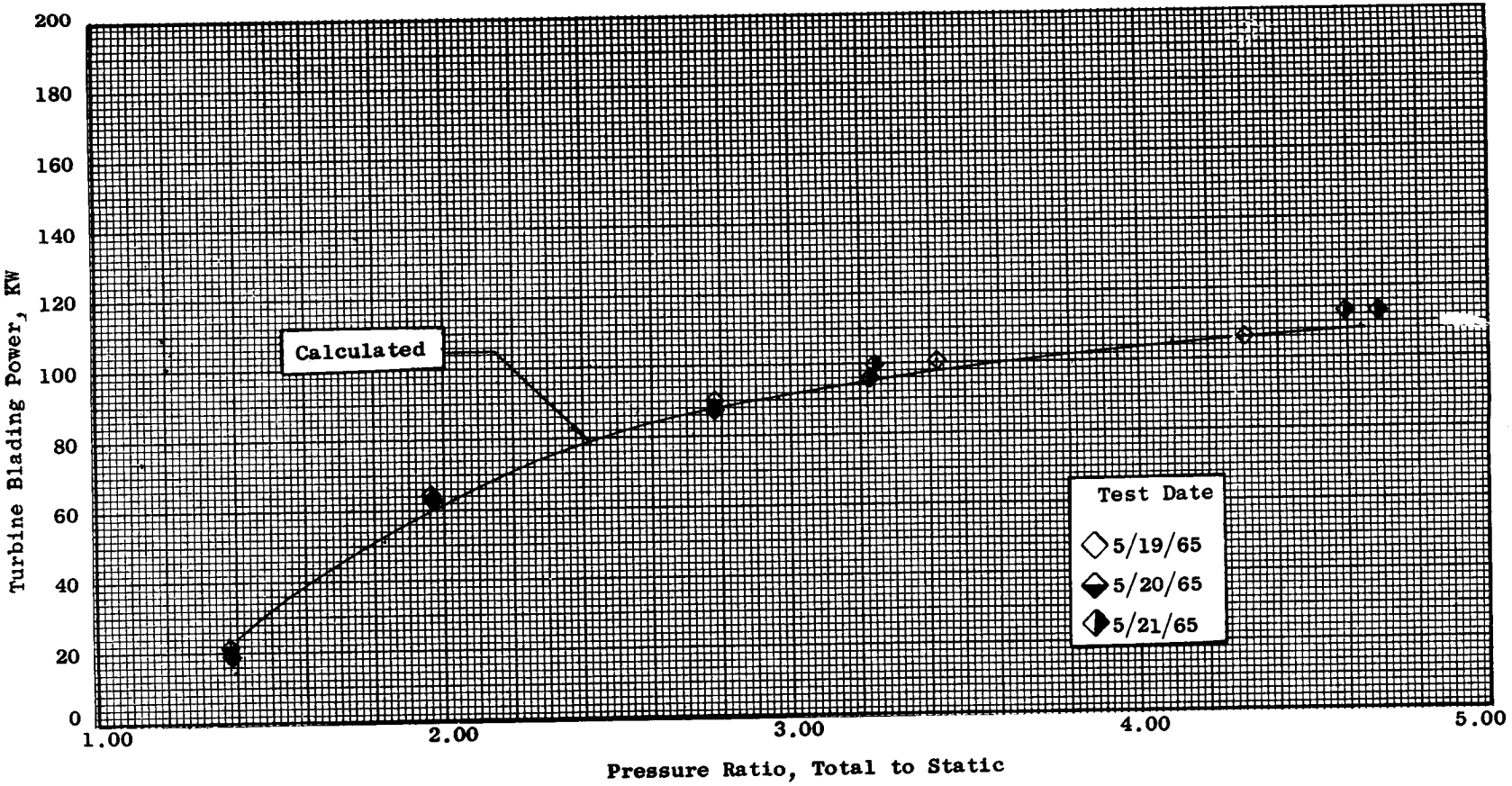

Figure 49. Comparison of Measured and Calculated Turbine Blading Power Versus Total to Static Pressure Ratio. Inlet Temperature, 1450°F, Rotative Speed, 17,300 rpm.

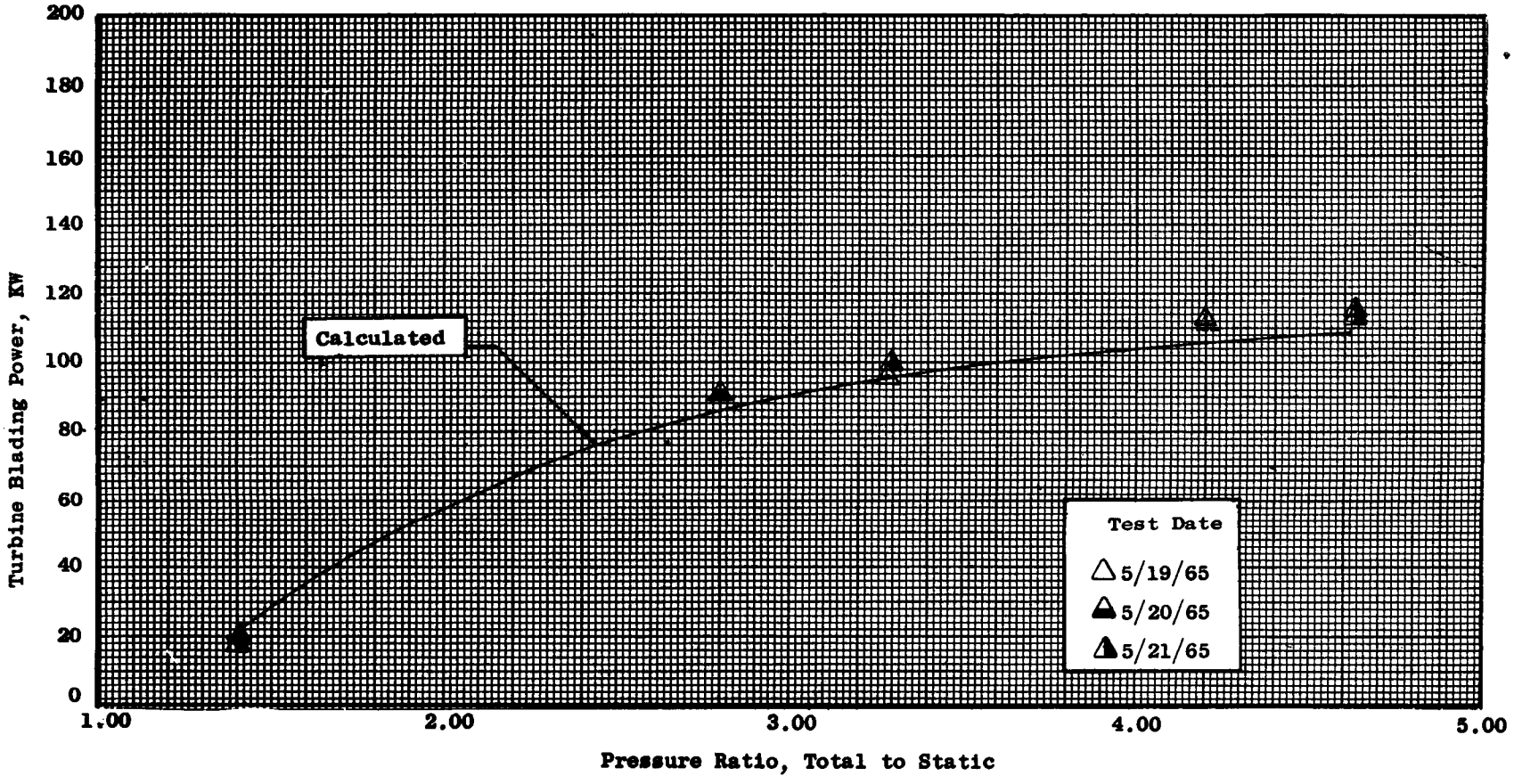

Figure 50. Comparison of Measured and Calculated Turbine Blading Power Versus Total to Static Pressure Ratio. Inlet Temperature, 1450°F, Rotative Speed, 18,300 rpm.

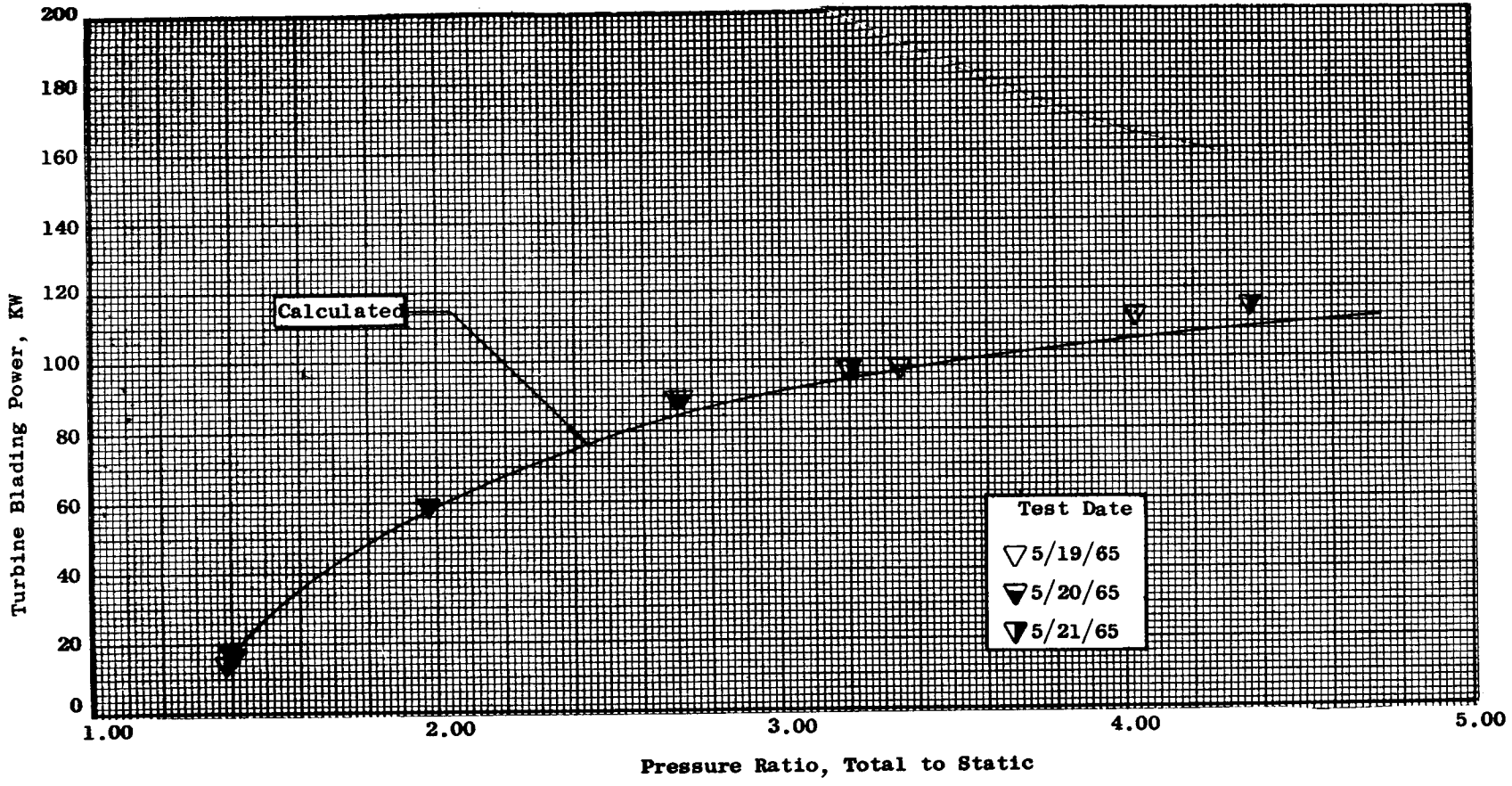

Figure 51. Comparison of Measured and Calculated Turbine Blading Power Versus Total to Static Pressure Ratio. Inlet Temperature, 1450°F, Rotative Speed, 19,300 rpm.

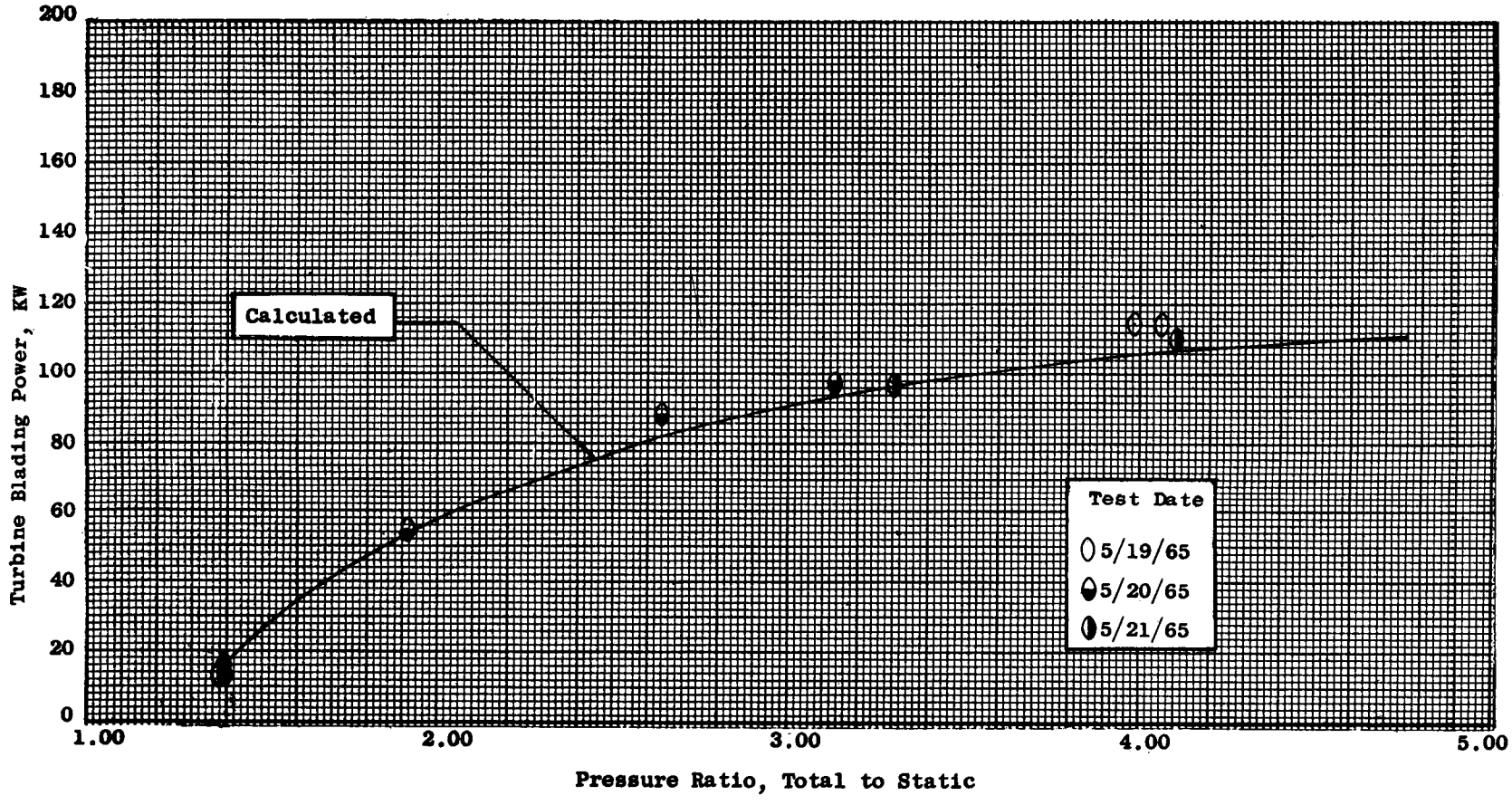

Figure 52. Comparison of Measured and Calculated Turbine Blading Power Versus Total to Static Pressure Ratio. Inlet Temperature, 1450°F, Rotative Speed, 20,000 rpm.

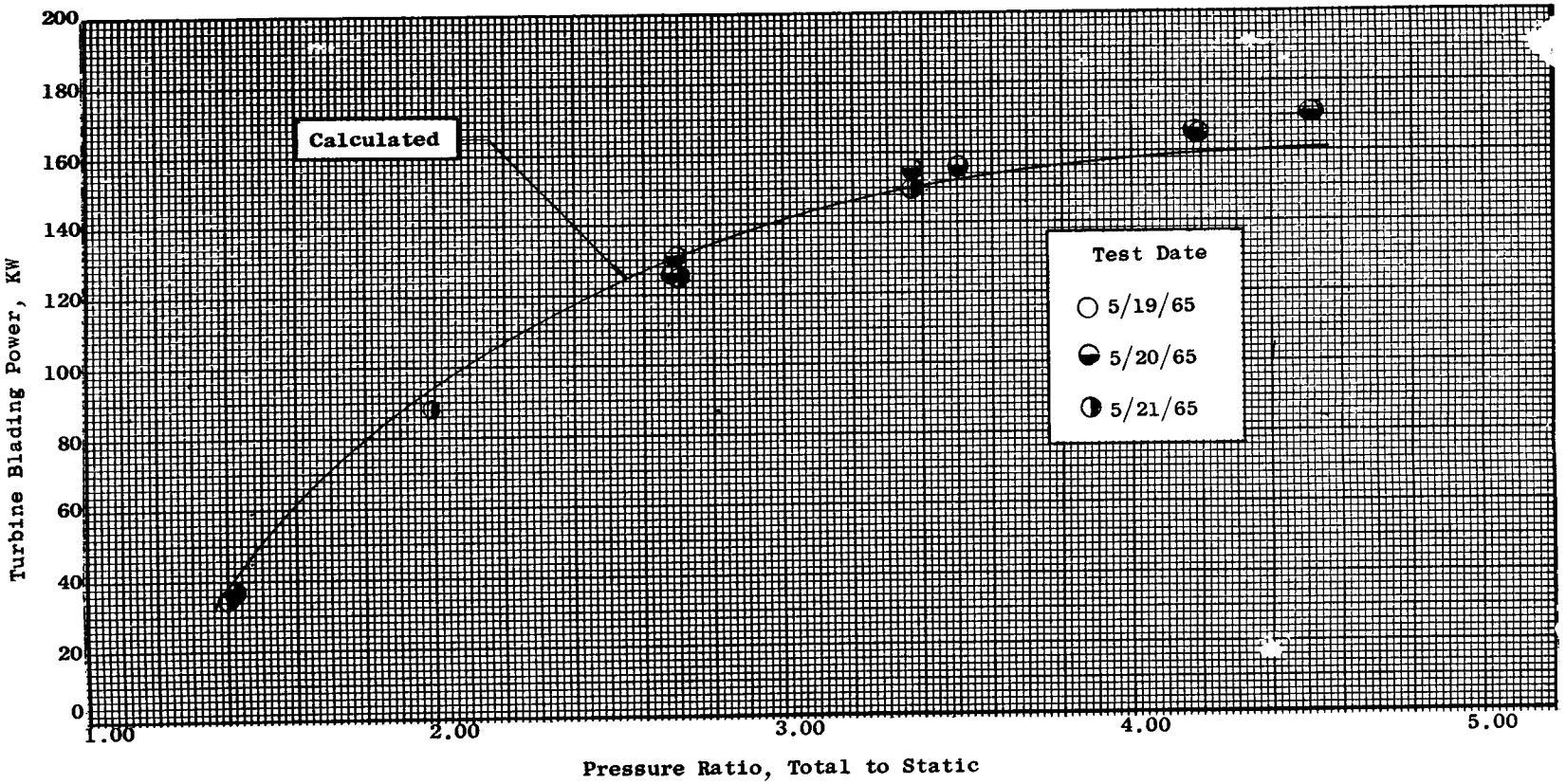

Figure 53. Comparison of Measured and Calculated Turbine Blading Power Versus Total to Static Pressure Ratio. Inlet Temperature 1550°F, Rotative Speed, 15,400 rpm.

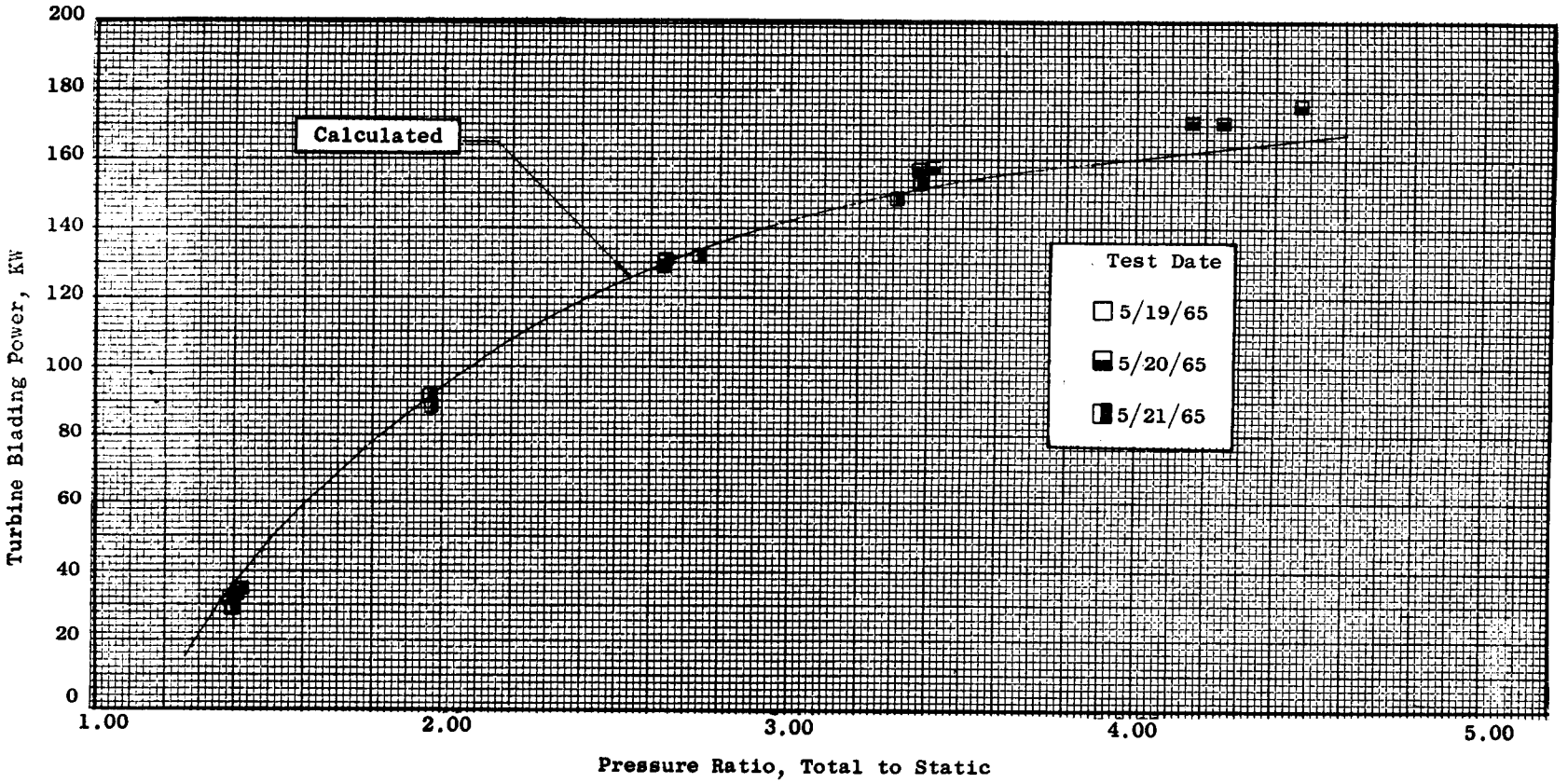

Figure 54. Comparison of Measured and Calculated Turbine Blading Power Versus Total to Static Pressure Ratio. Inlet Temperature, 1550°F, Rotative Speed, 16,400 rpm.

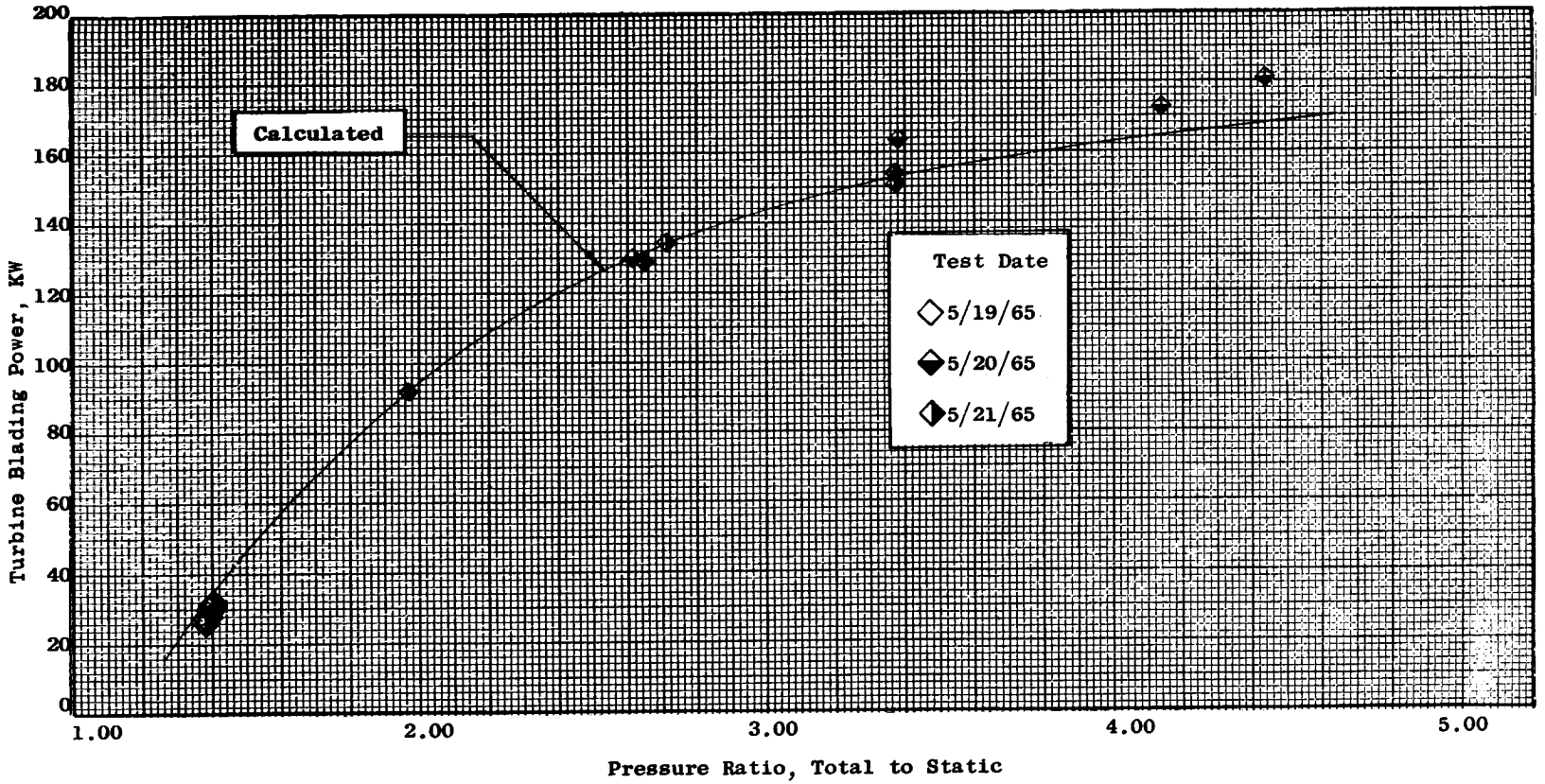

Figure 55. Comparison of Measured and Calculated Turbine Blading Power Versus Total to Static Pressure Ratio. Inlet Temperature, 1550°F, Rotative Speed, 17,300 rpm.

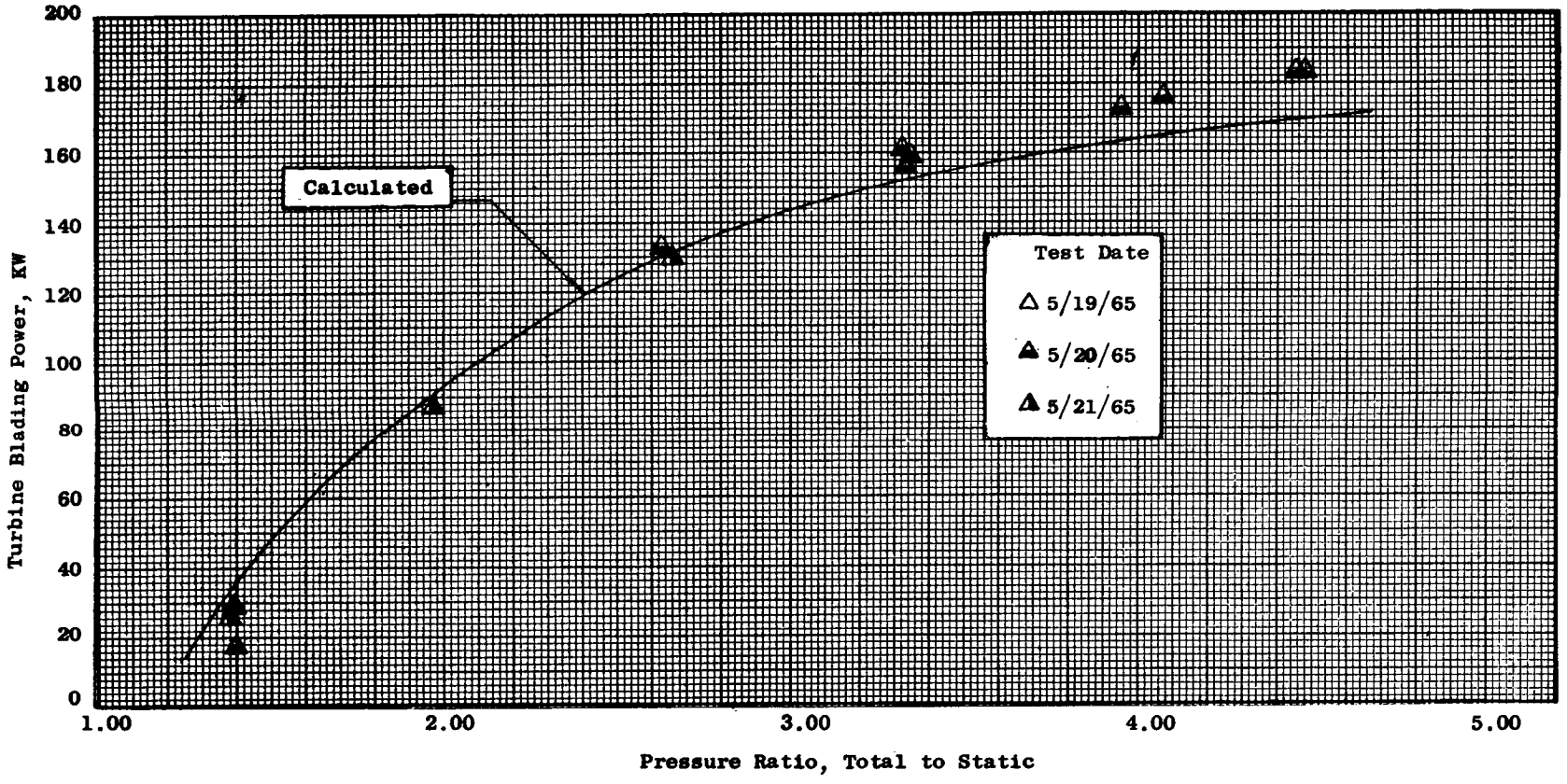

Figure 56. Comparison of Measured and Calculated Turbine Blading Power Versus Total to Static Pressure Ratio. Inlet Temperature, 1550°F, Rotative Speed, 18,300 rpm.

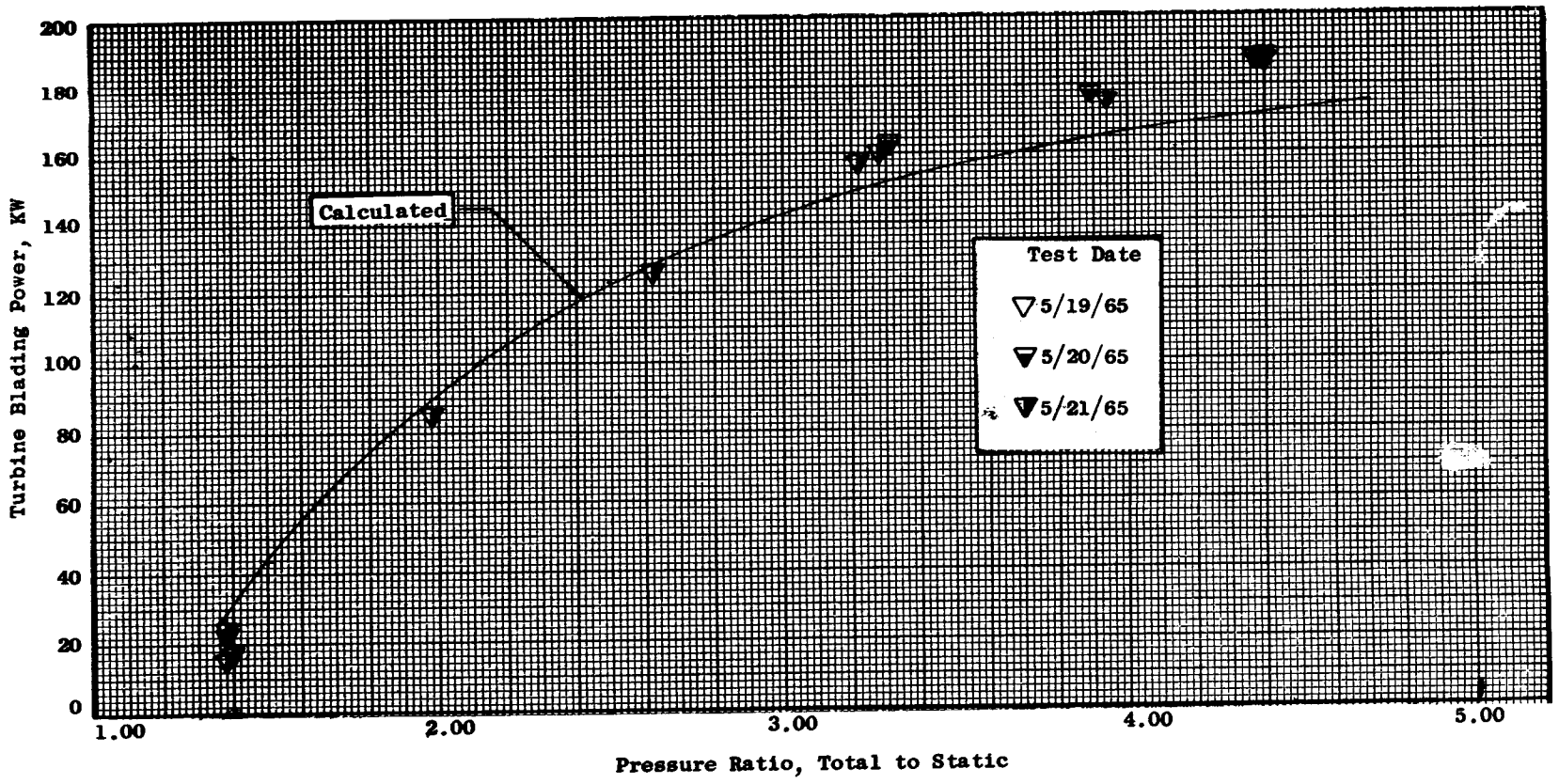

Figure 57. Comparison of Measured and Calculated Turbine Blading Power Versus Total to Static Pressure Ratio. Inlet Temperature, 1550°F, Rotative Speed, 19,300 rpm.

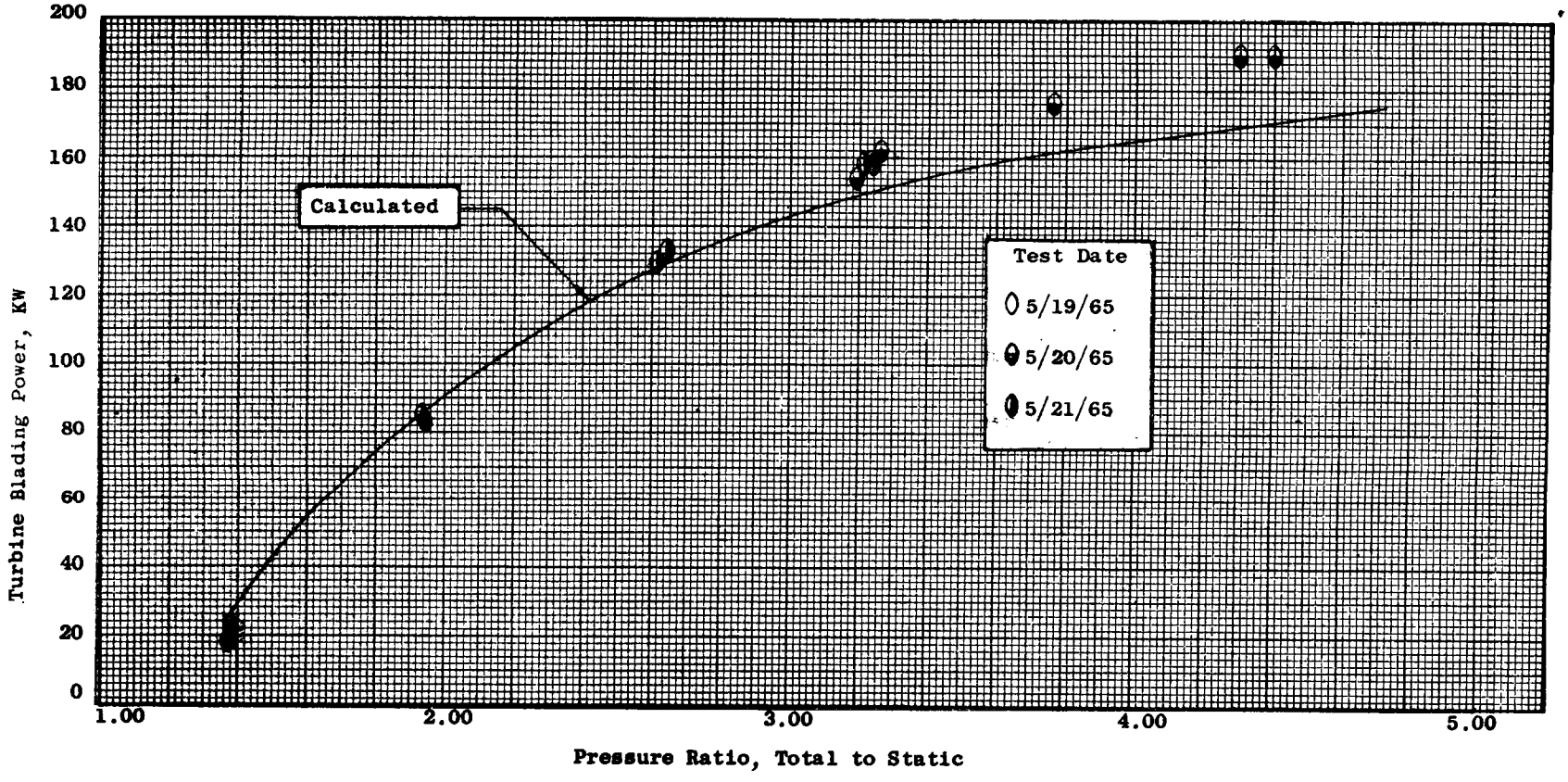

Figure 58. Comparison of Measured and Calculated Turbine Blading Power Versus Total to Static Pressure Ratio. Inlet Temperature, 1550°F, Rotative Speed, 20,000 rpm.

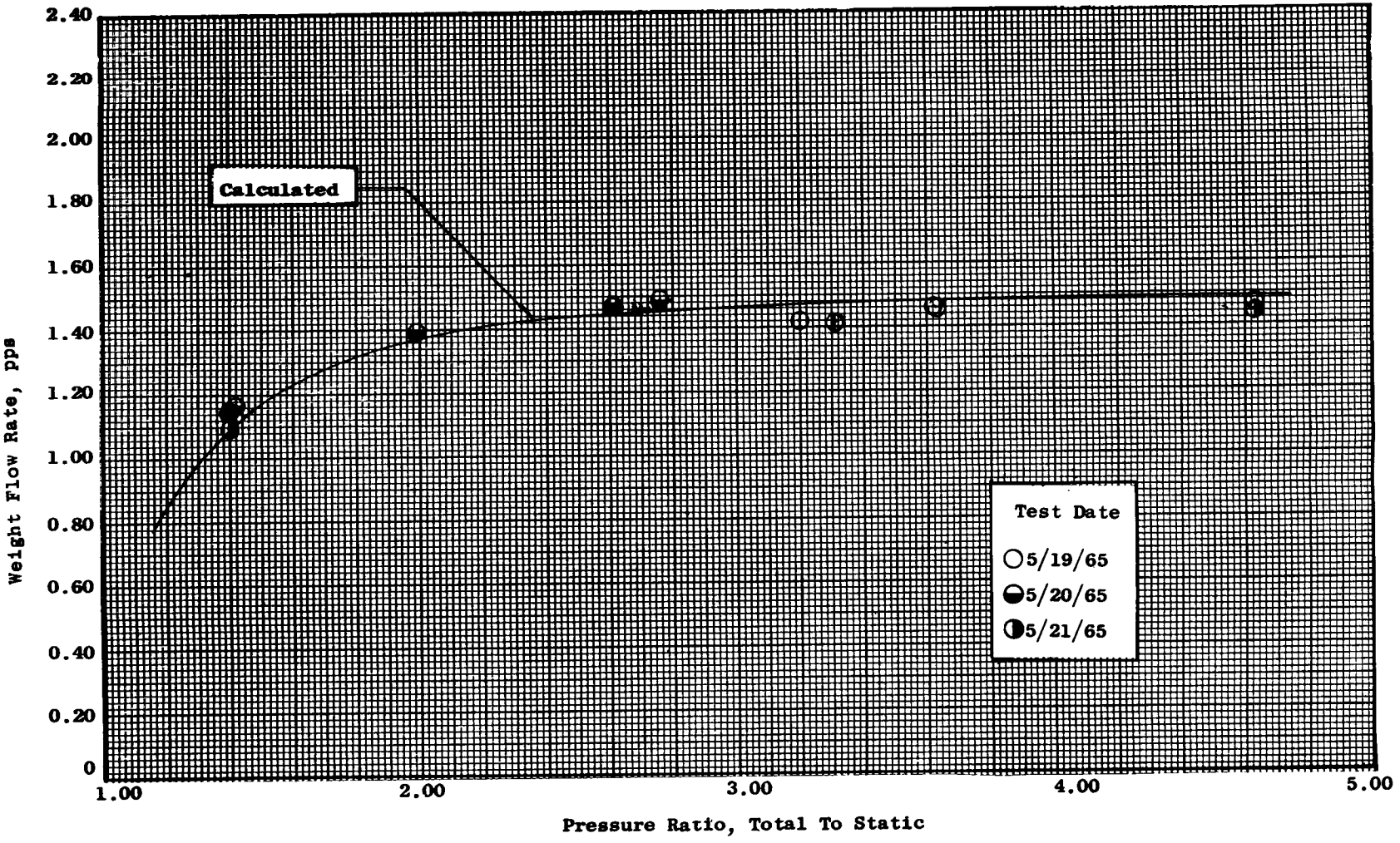

Figure 59. Comparison of Measured and Calculated Weight Flow Rate Versus Total Static Pressure Ratio. Inlet Temperature, 1450°F, Rotative Speed, 15,400 rpm.

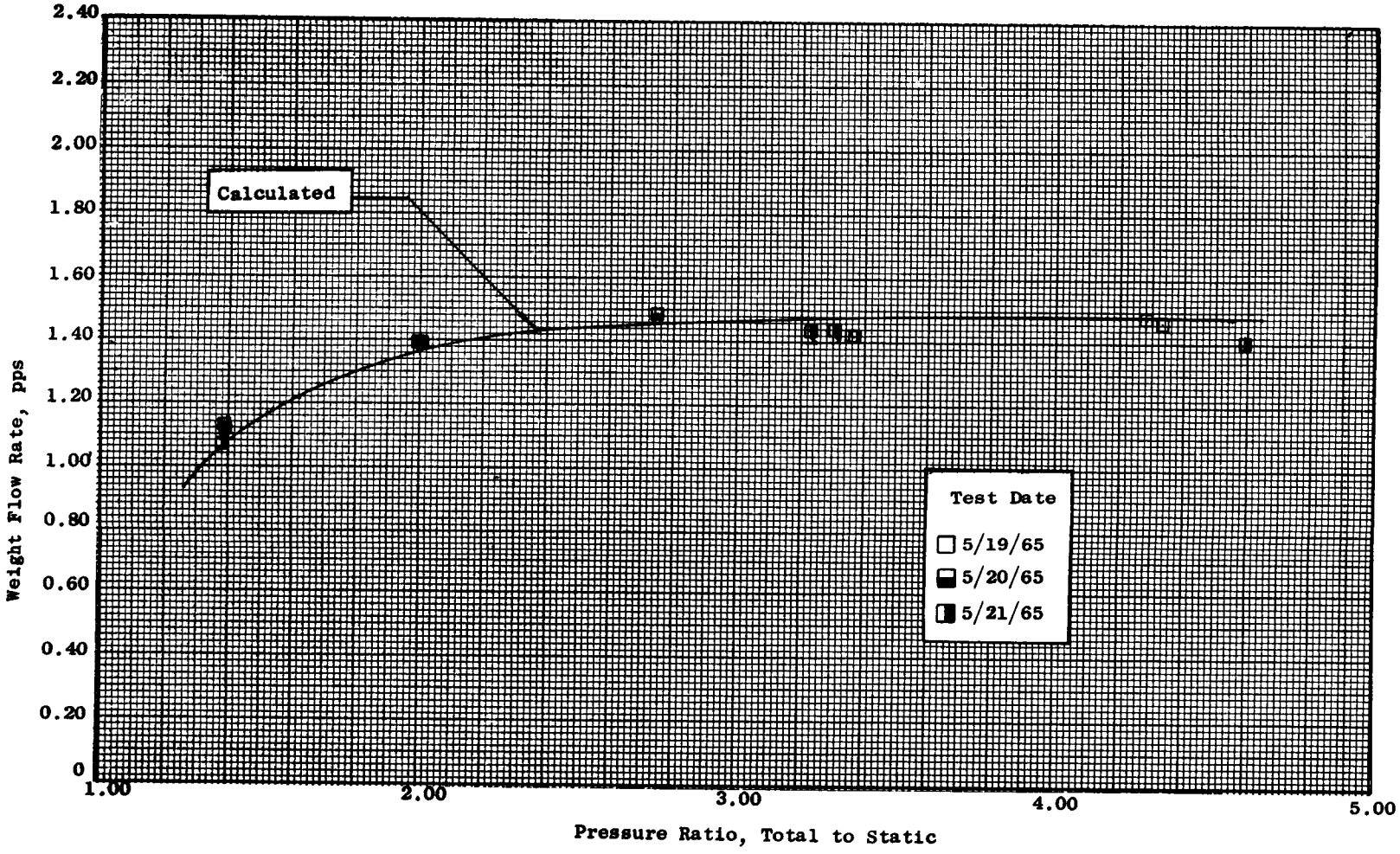

Figure 60. Comparison of Measured and Calculated Weight Flow Rate Versus Total to Static Pressure Ratio. Inlet Temperature, 1450°F, Rotative Speed, 16,400 rpm.

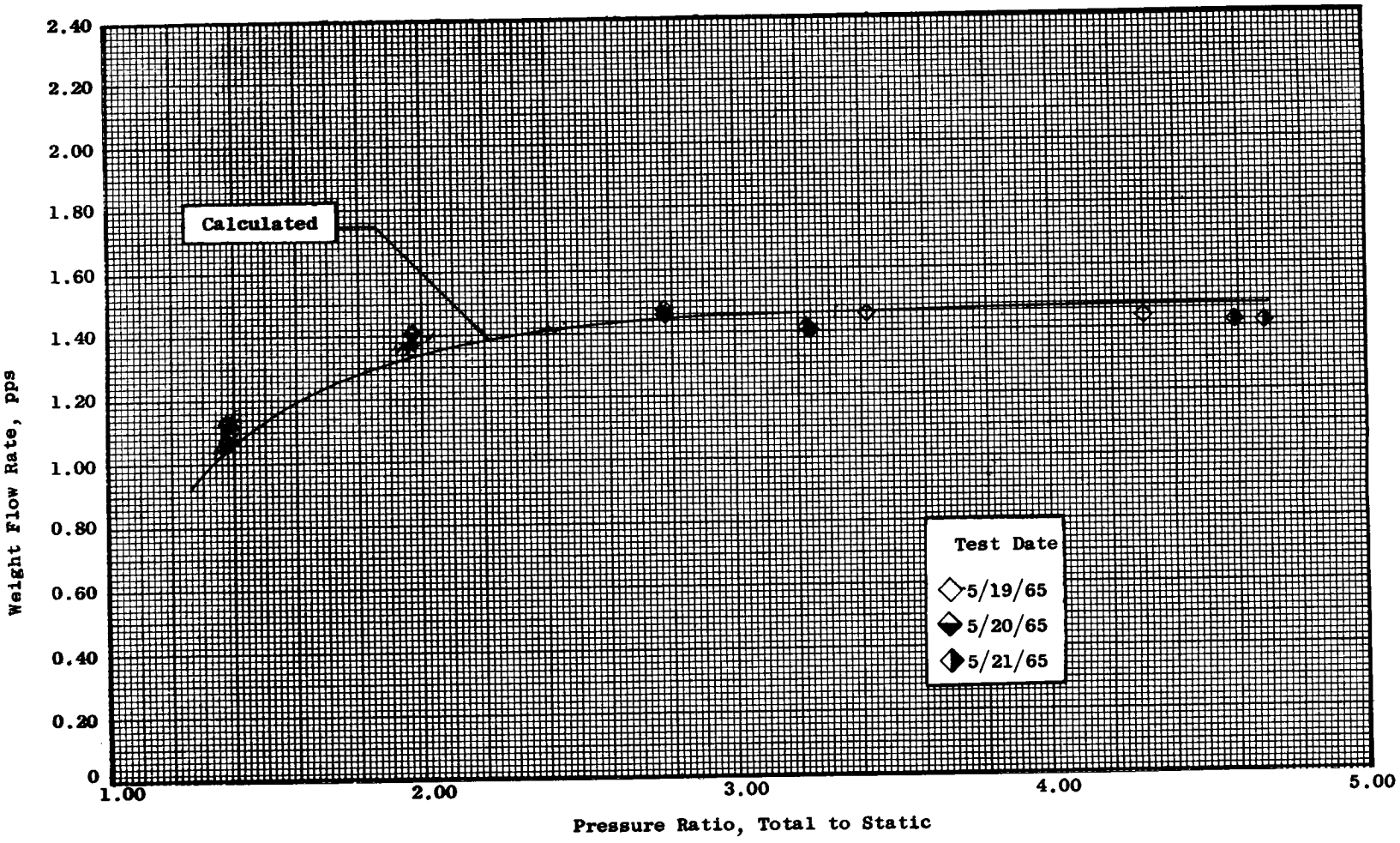

Figure 61. Comparison of Measured and Calculated Weight Flow Rate Versus Total to Static Pressure Ratio. Inlet Temperature, 1450°F, Rotative Speed, 17,300 rpm.

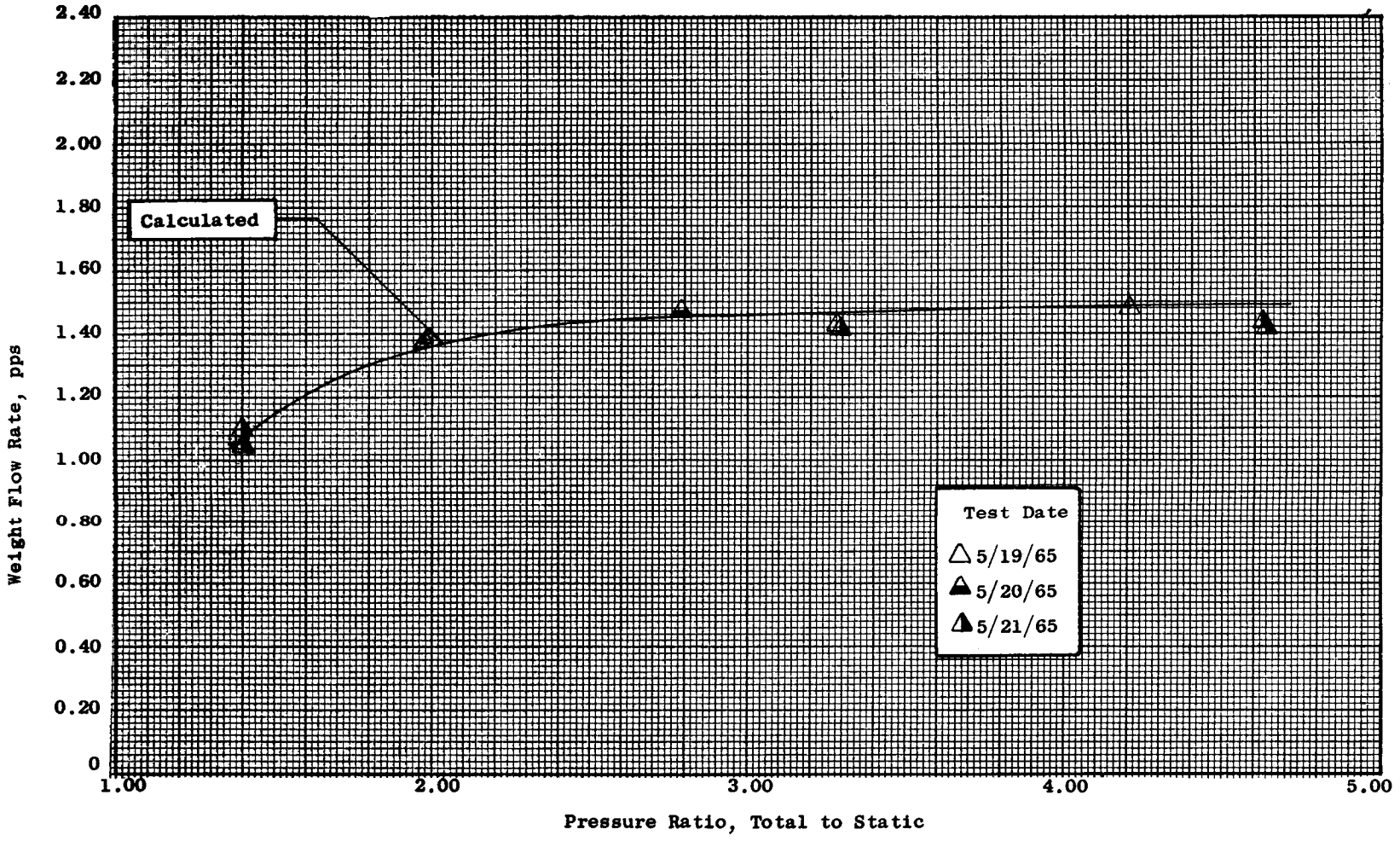

Figure 62. Comparison of Measured and Calculated Weight Flow Rate Versus Total to Static Pressure Ratio. Inlet Temperature, 1450°F, Rotative Speed, 18,300 rpm.

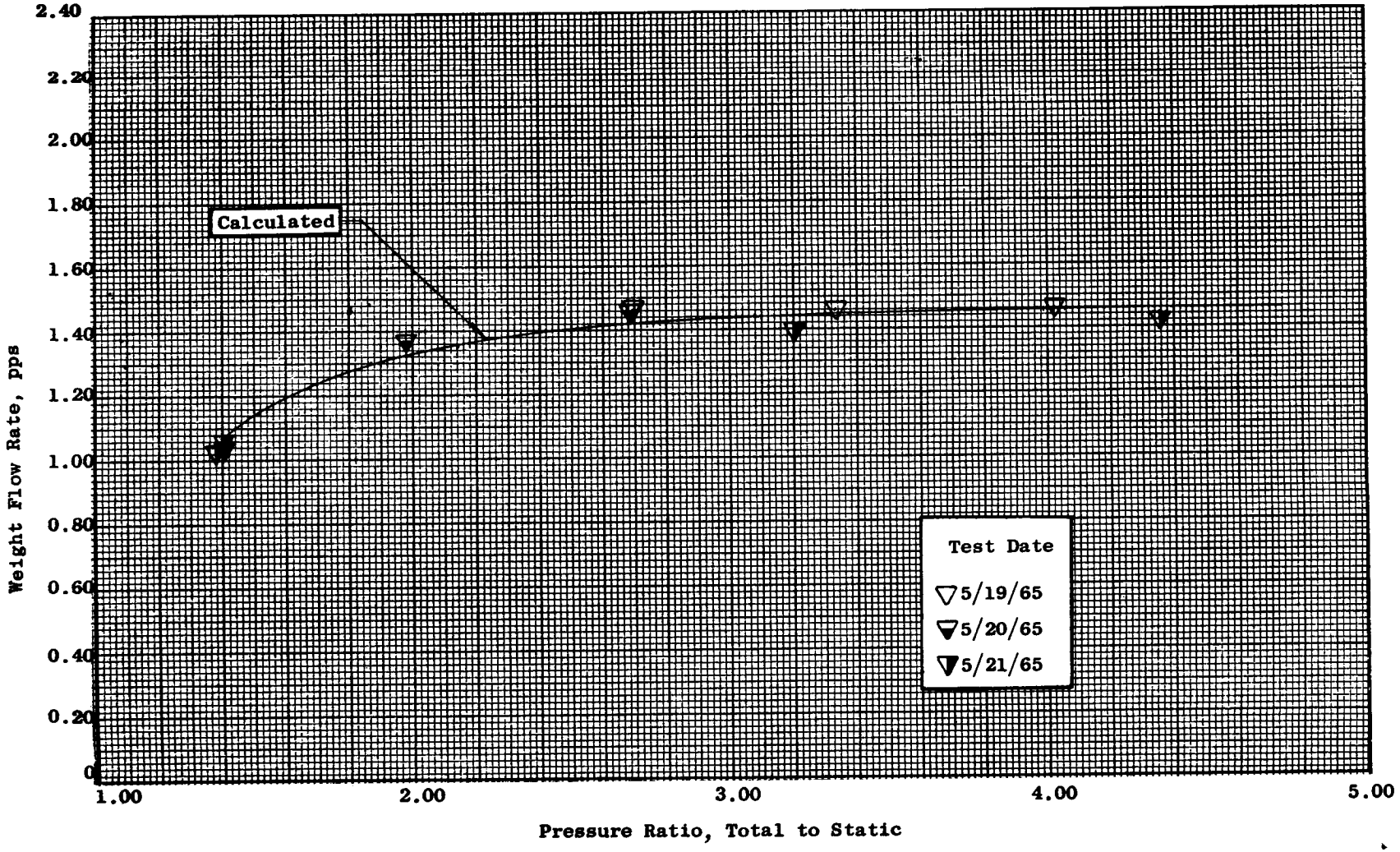

Figure 63. Comparison of Measured and Calculated Weight Flow Rate Versus Total to Static Pressure Ratio. Inlet Temperature, 1450°F, Rotative Speed, 19,300 rpm.

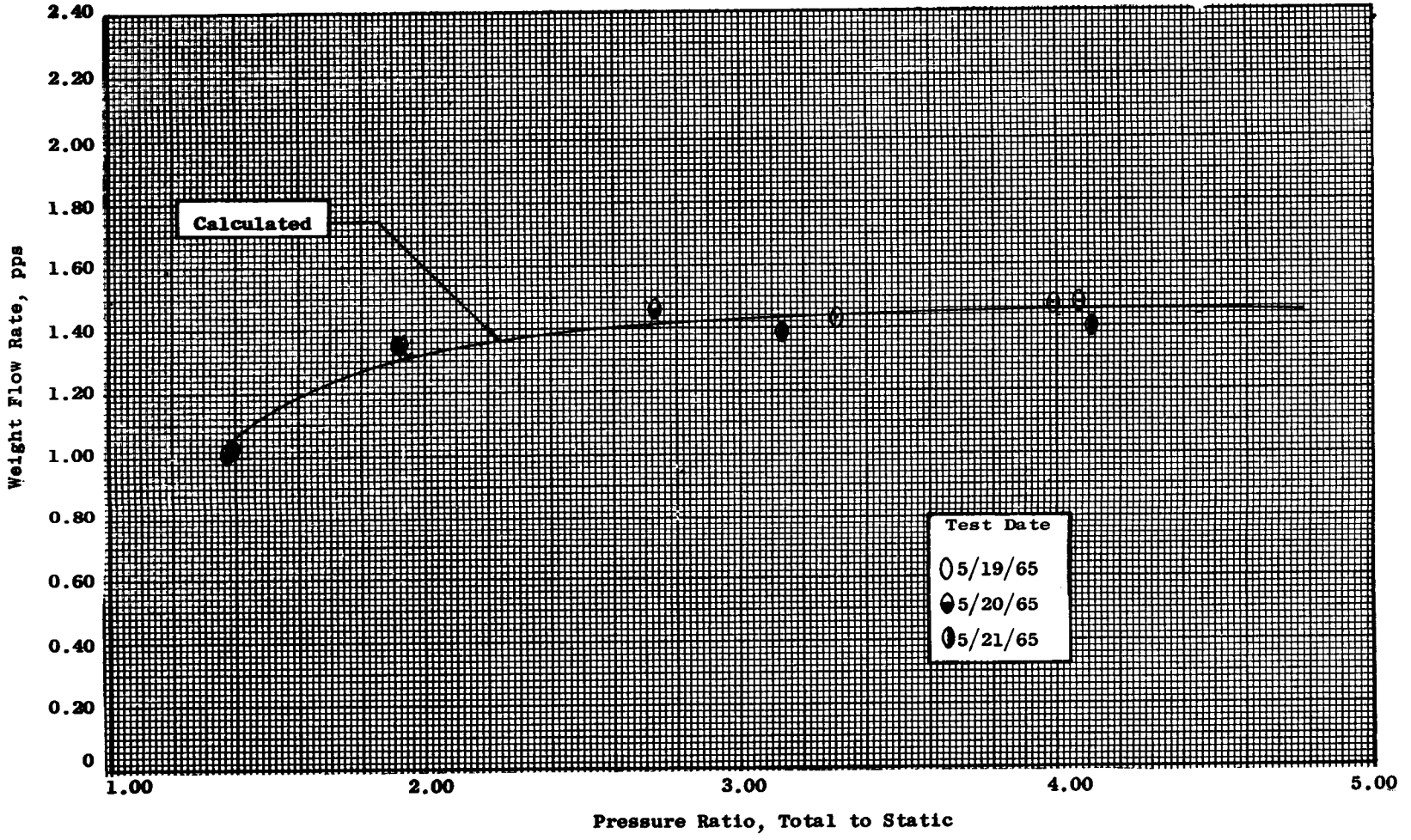

Figure 64. Comparison of Measured and Calculated Weight Flow Rate Versus Total to Static Pressure Ratio. Inlet Temperature, 1450°F, Rotative Speed, 20,000 rpm.

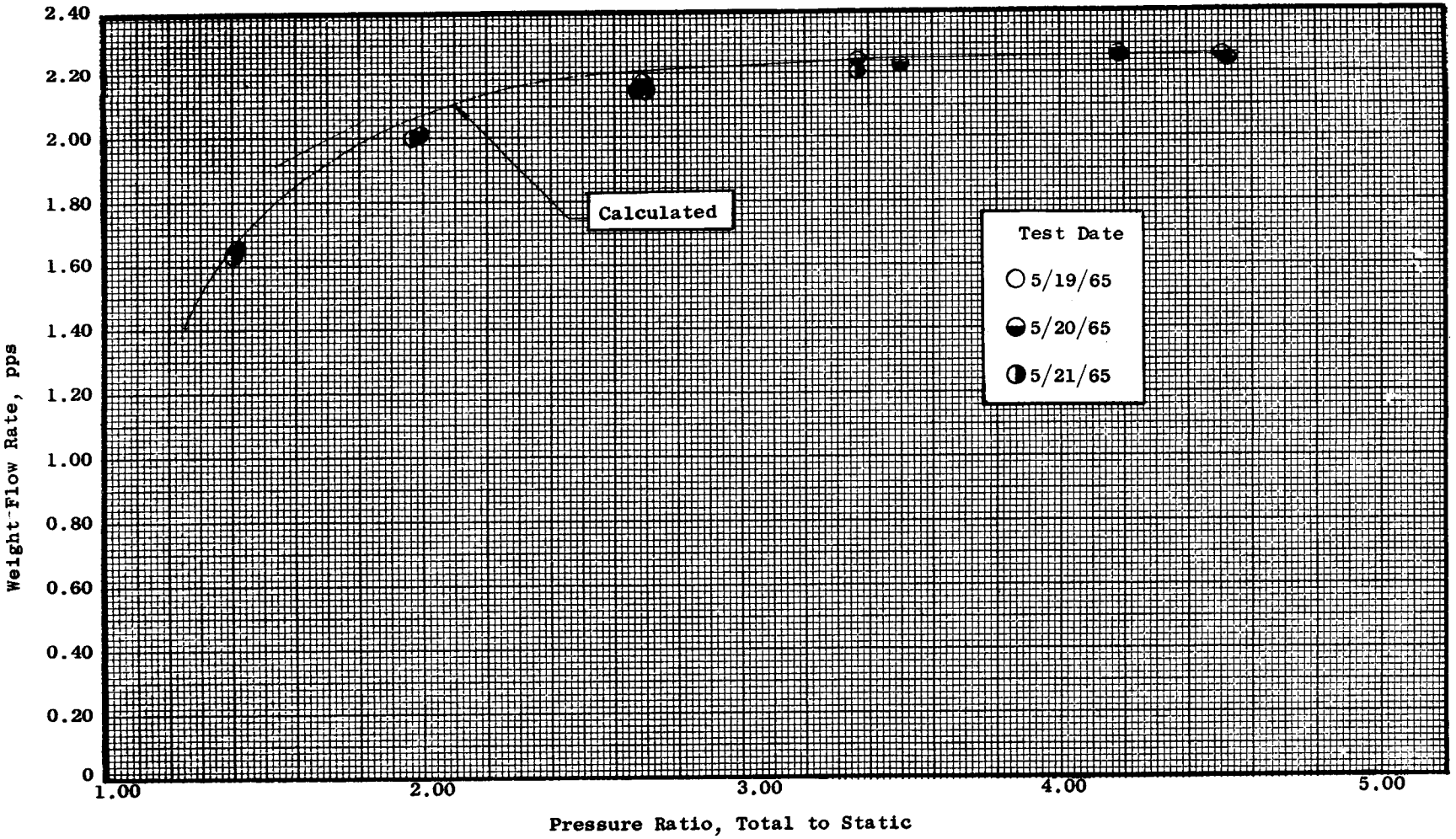

Figure 65. Comparison of Measured and Calculated Weight Flow Rate Versus Total to Static Pressure Ratio. Inlet Temperature, 1550°F, Rotative Speed, 15,400 rpm.

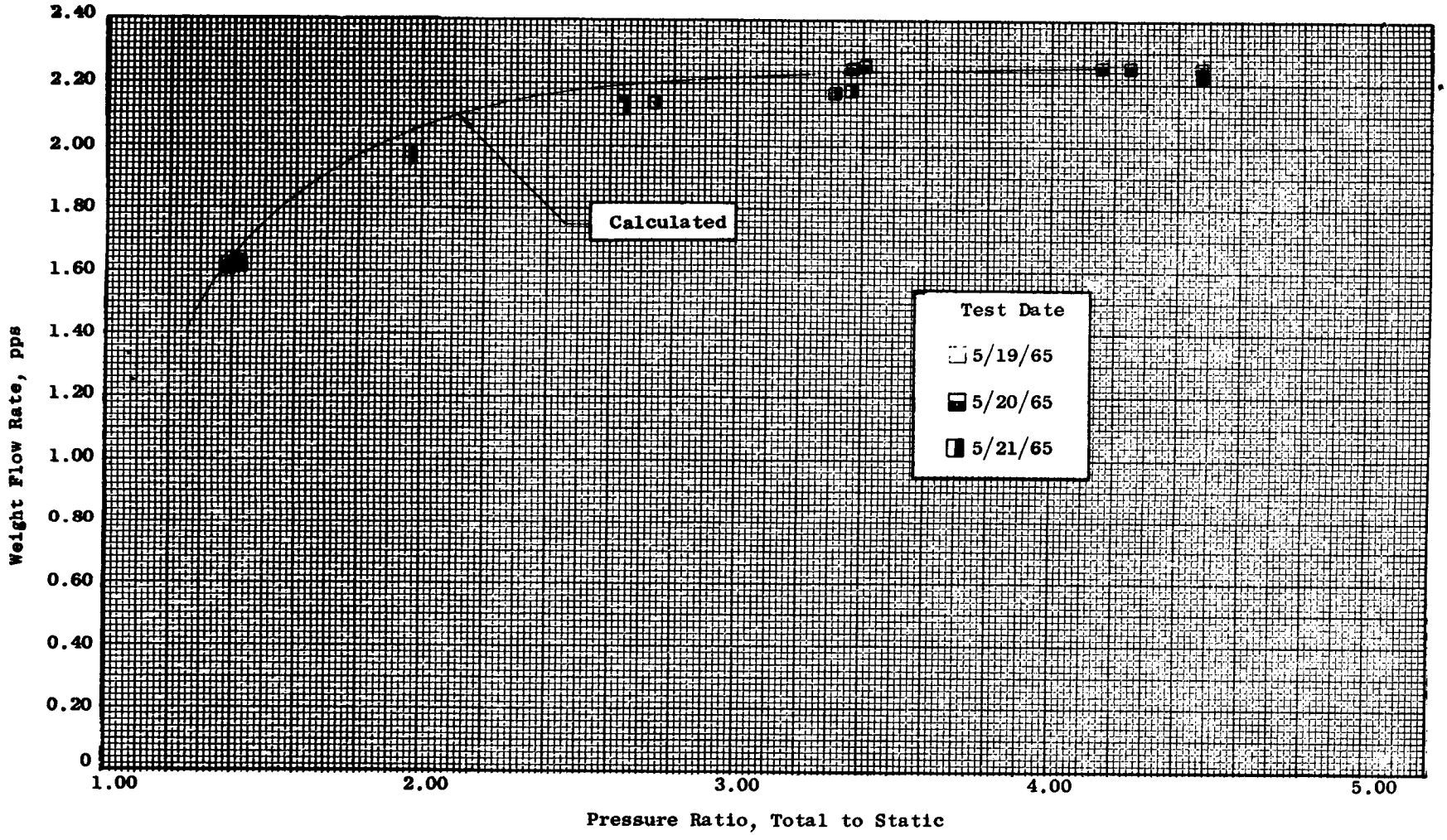

Figure 66. Comparison of Measured and Calculated Weight Flow Rate Versus Total to Static Pressure Ratio. Inlet Temperature, 1550°F, Rotative Speed, 16,400 rpm.

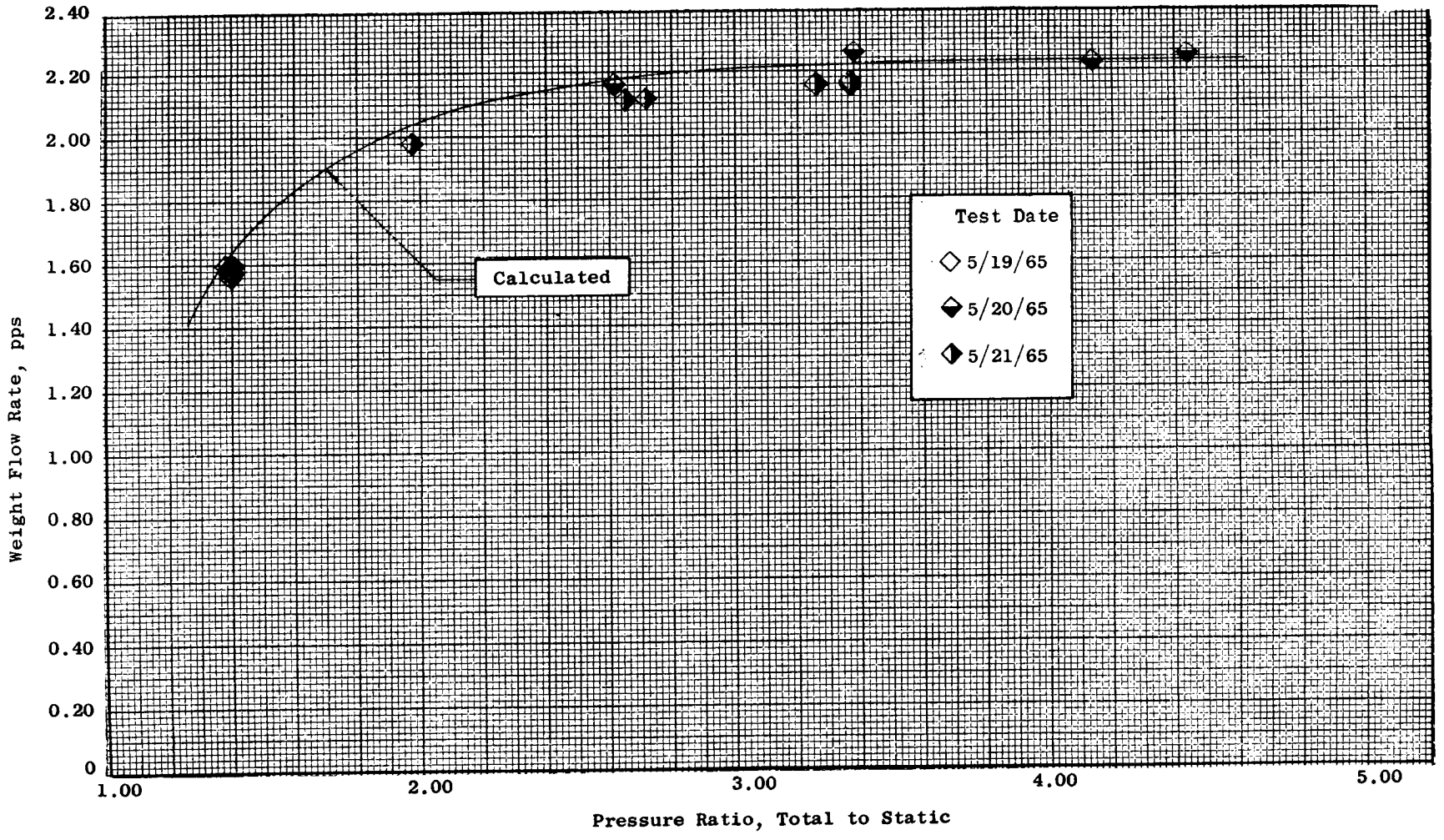

Figure 67. Comparison of Measured and Calculated Weight Flow Rate Versus Total to Static Pressure Ratio. Inlet Temperature, 1550°F, Rotative Speed, 17,300 rpm.

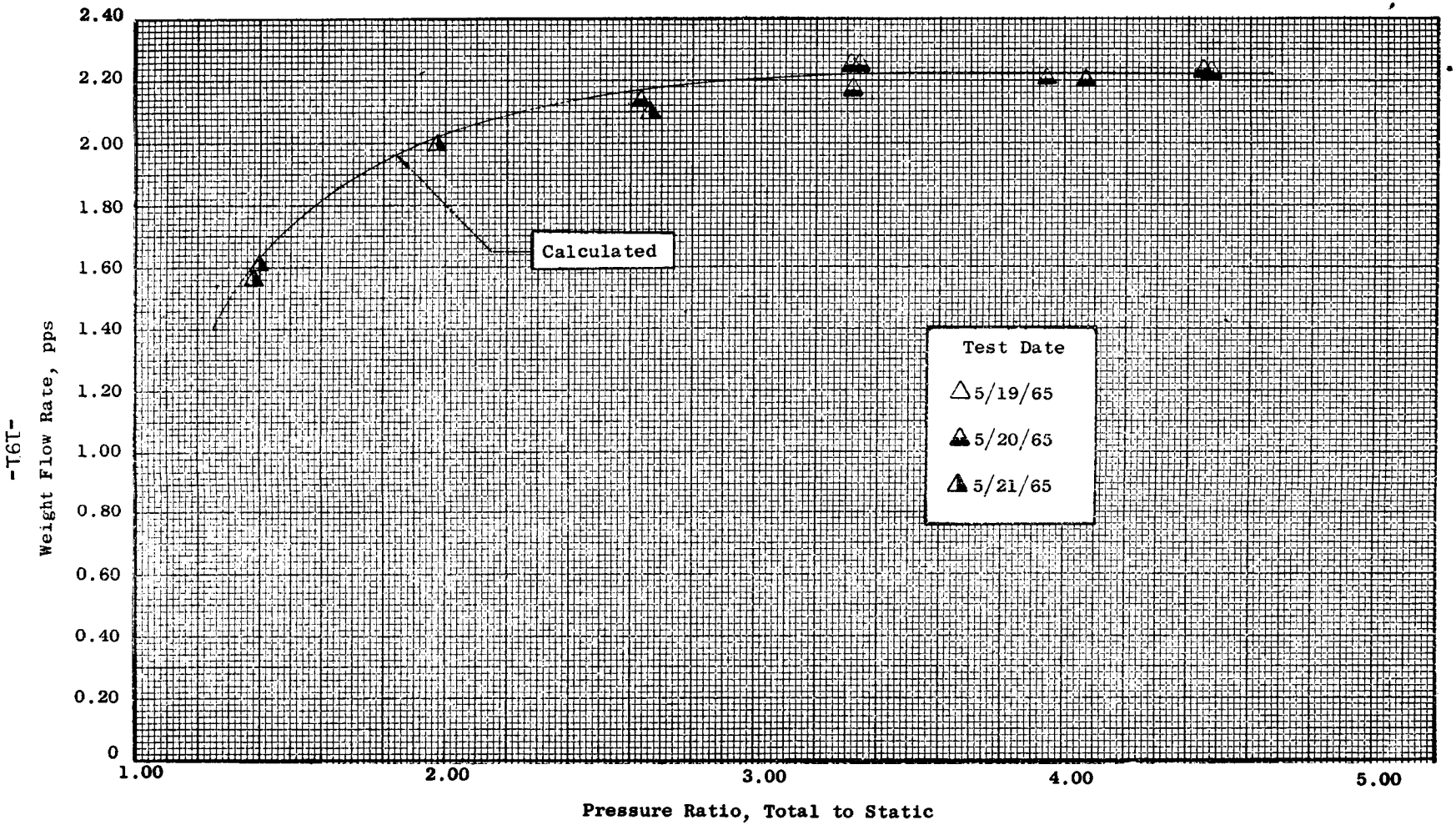

Figure 68. Comparison of Measured and Calculated Weight Flow Rate Versus Total to Static Pressure Ratio. Inlet Temperature, 1550°F, Rotative Speed, 18,300 rpm.

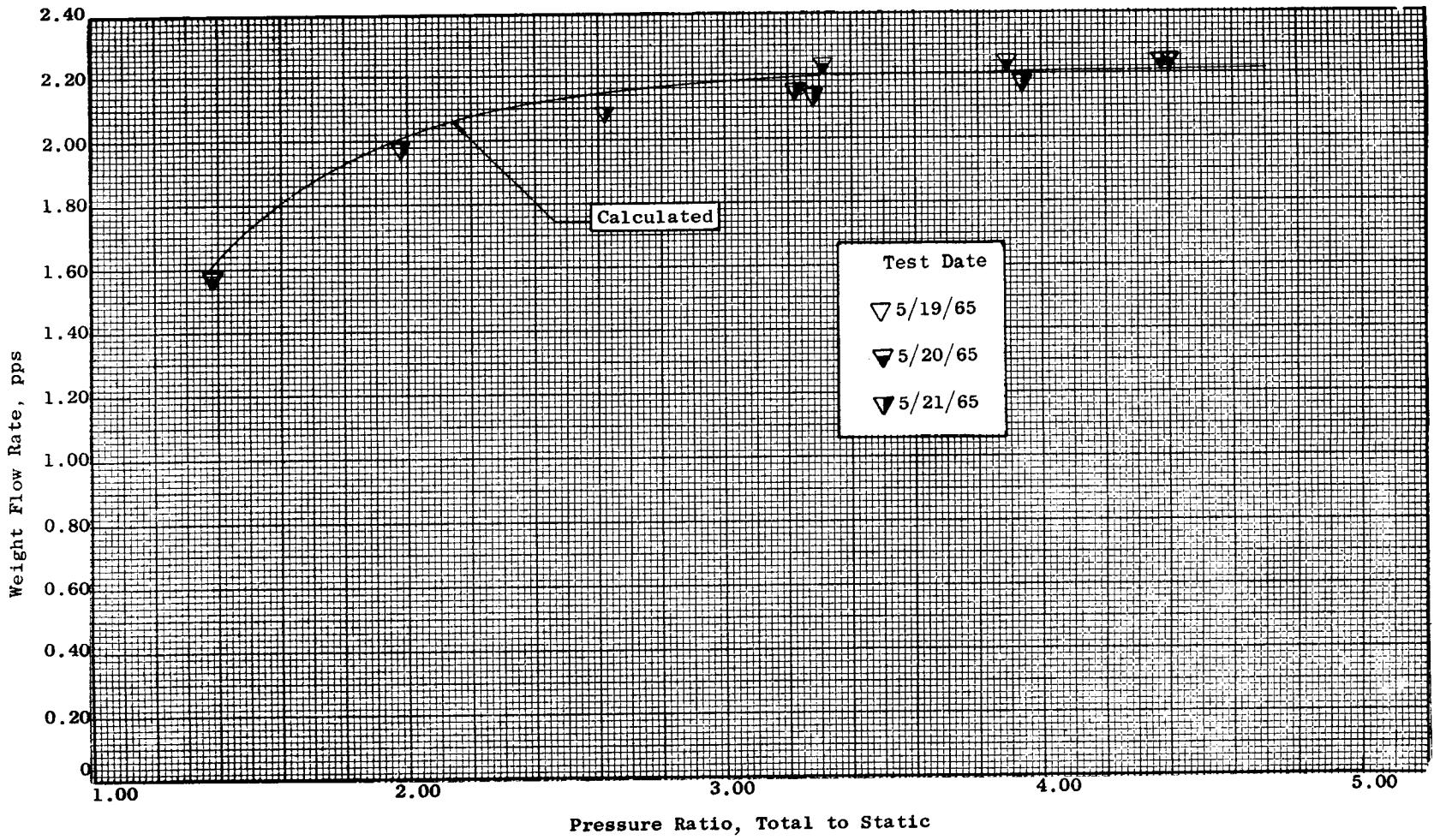

Figure 69. Comparison of Measured and Calculated Weight Flow Rate Versus Total to Static Pressure Ratio. Inlet Temperature, 1500°F, Rotative Speed, 19,300 rpm.

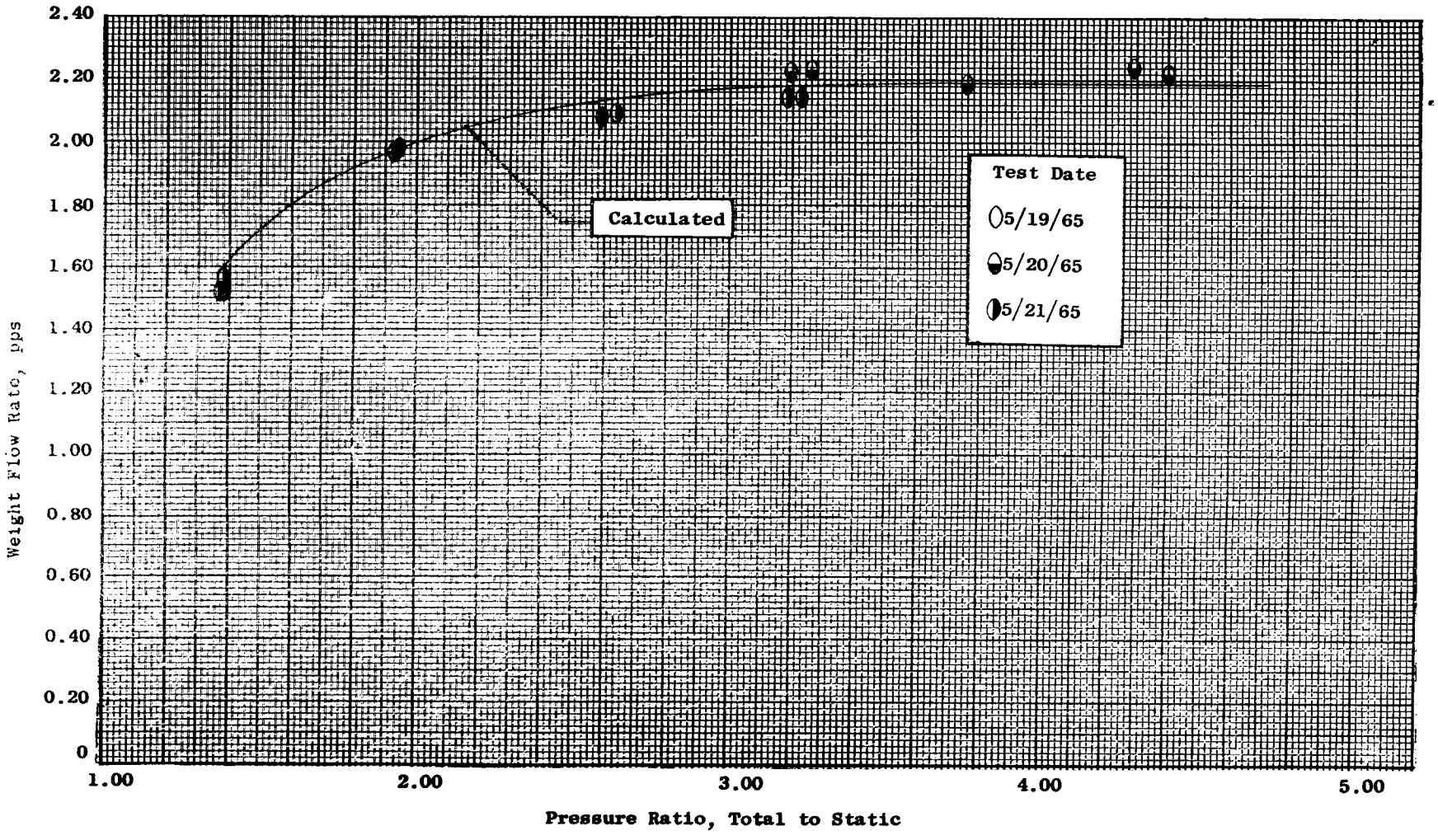

Figure 70. Comparison of Measured and Calculated Weight Flow Rate Versus Total to Static Pressure Ratio. Inlet Temperature, 1550°F, Rotative Speed, 20,000 rpm.

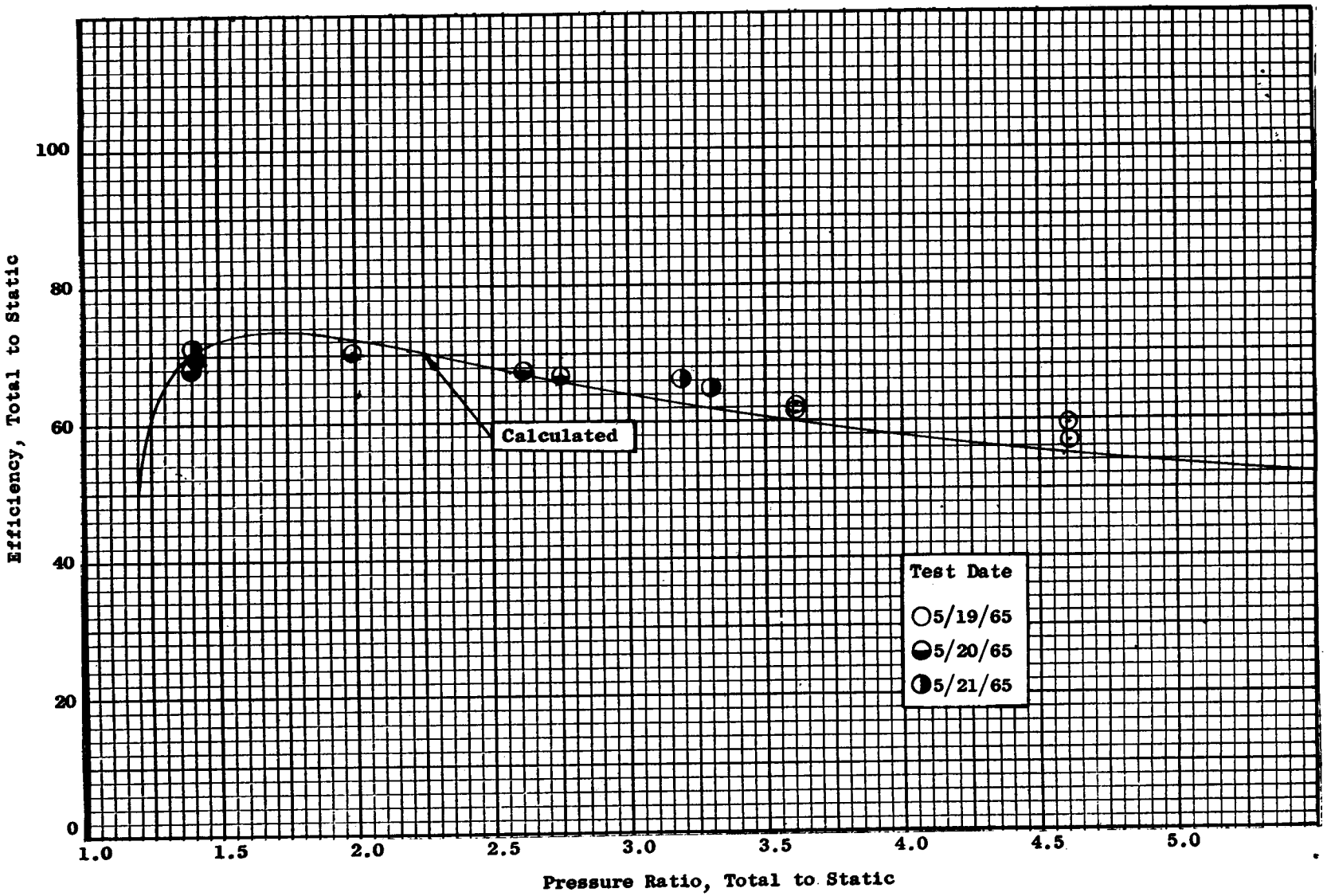

Figure 71. Comparison of Measured and Calculated Efficiency Versus Total to Static Pressure Ratio. Inlet Temperature, 1450°F, Rotative Speed, 15,400 rpm.

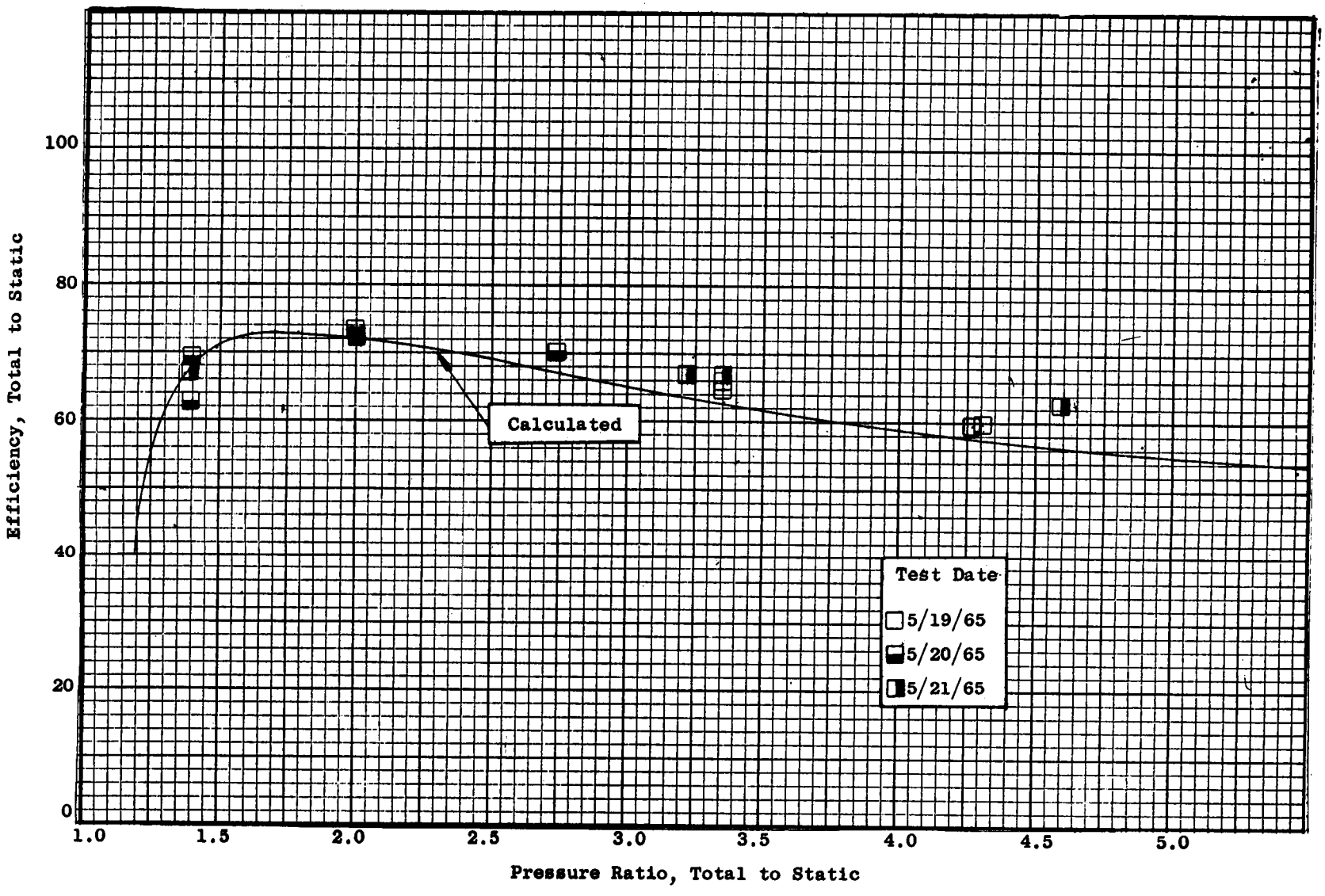

Figure 72. Comparison of Measured and Calculated Efficiency Versus Total to Static Pressure Ratio. Inlet Temperature, 1450°F, Rotative Speed, 16,400 rpm.

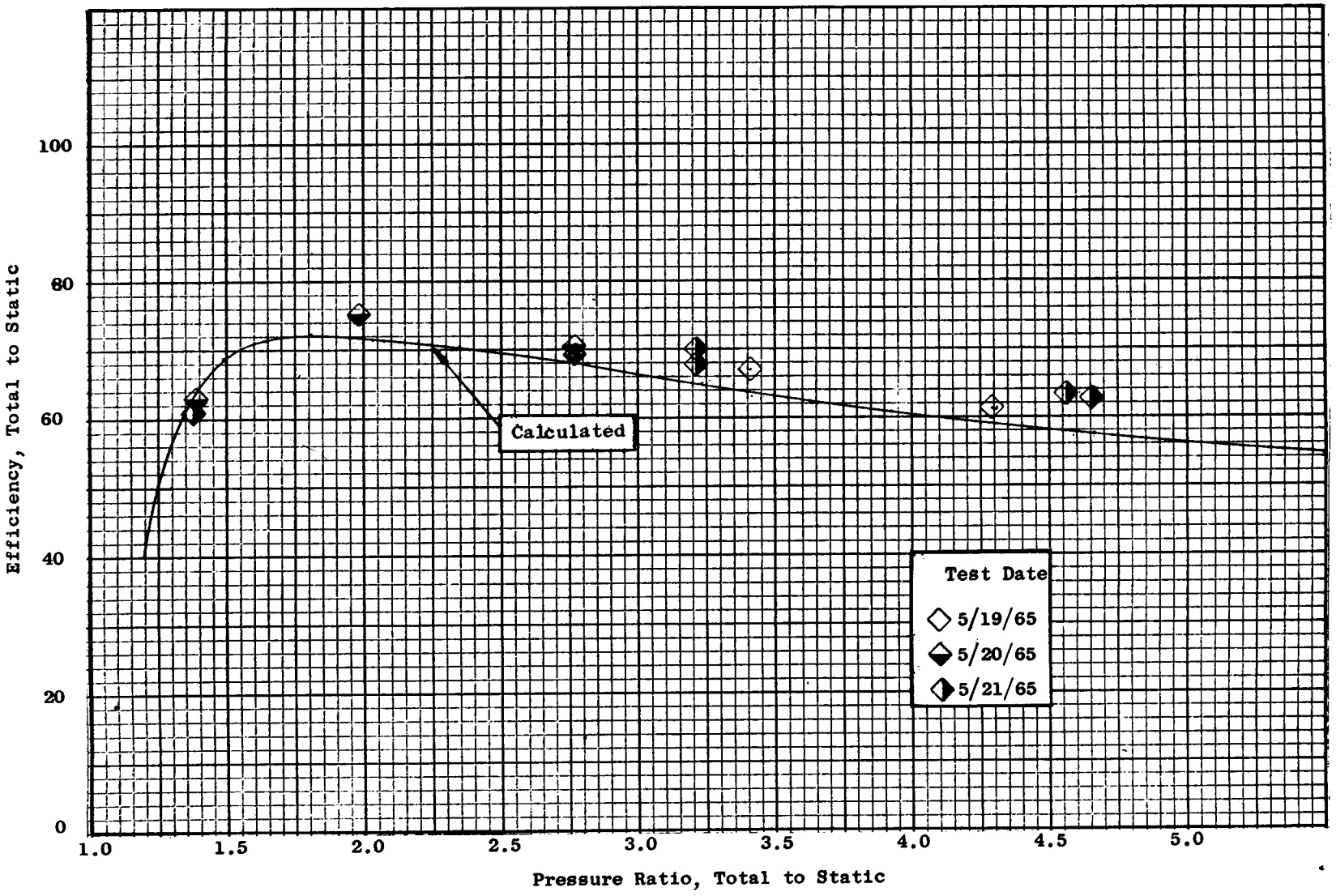

Figure 73. Comparison of Measured and Calculated Efficiency Versus Total to Static Pressure Ratio. Inlet Temperature, 1450°F, Rotative Speed, 17,300 rpm.

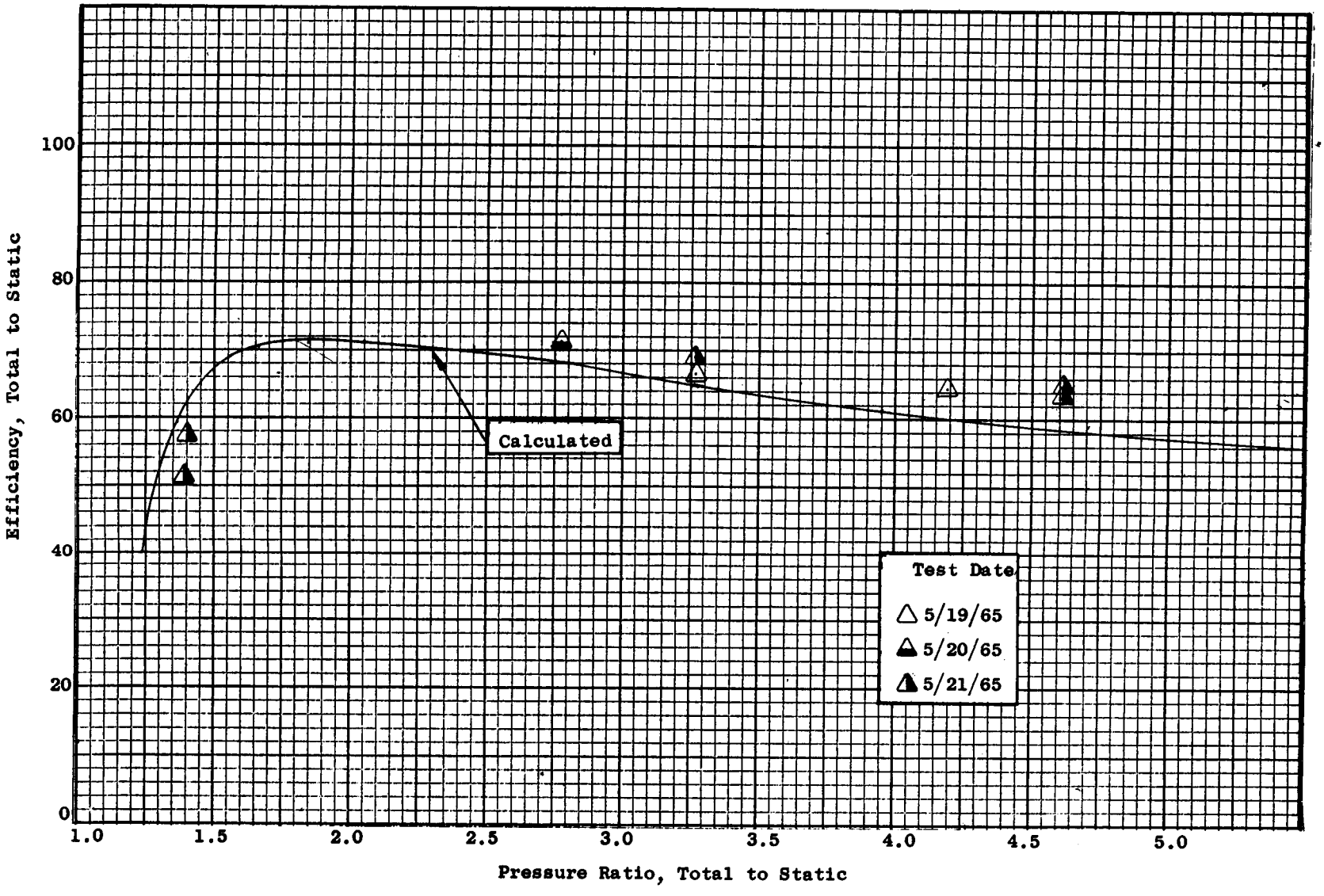

Figure 74. Comparison of Measured and Calculated Efficiency Versus Total to Static Pressure Ratio. Inlet Temperature, 1450°F, Rotative Speed, 18,300 rpm.

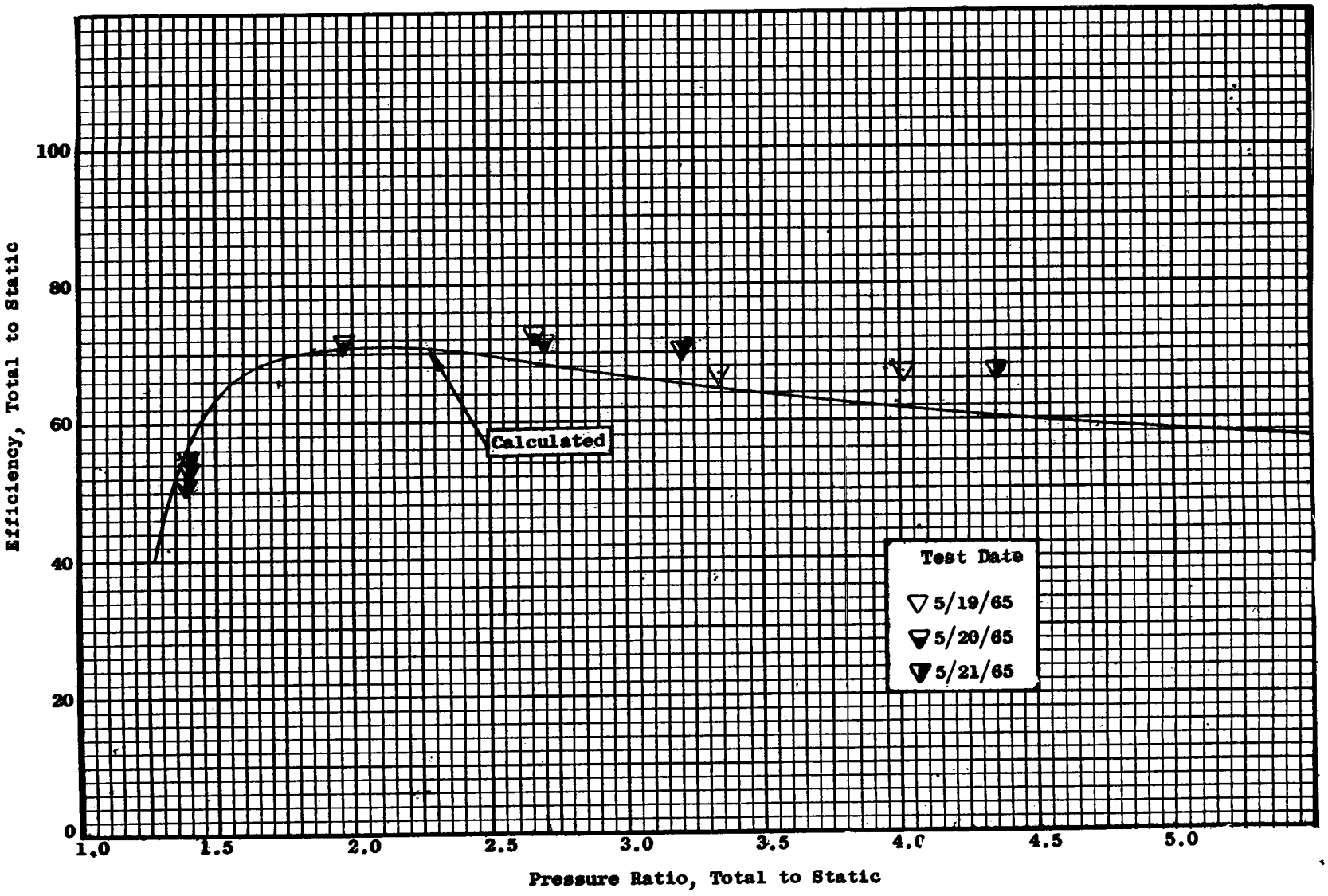

Figure 75. Comparison of Measured and Calculated Efficiency Versus Total to Static Pressure Ratio. Inlet Temperature, 1450°F, Rotative Speed, 19,300 rpm.

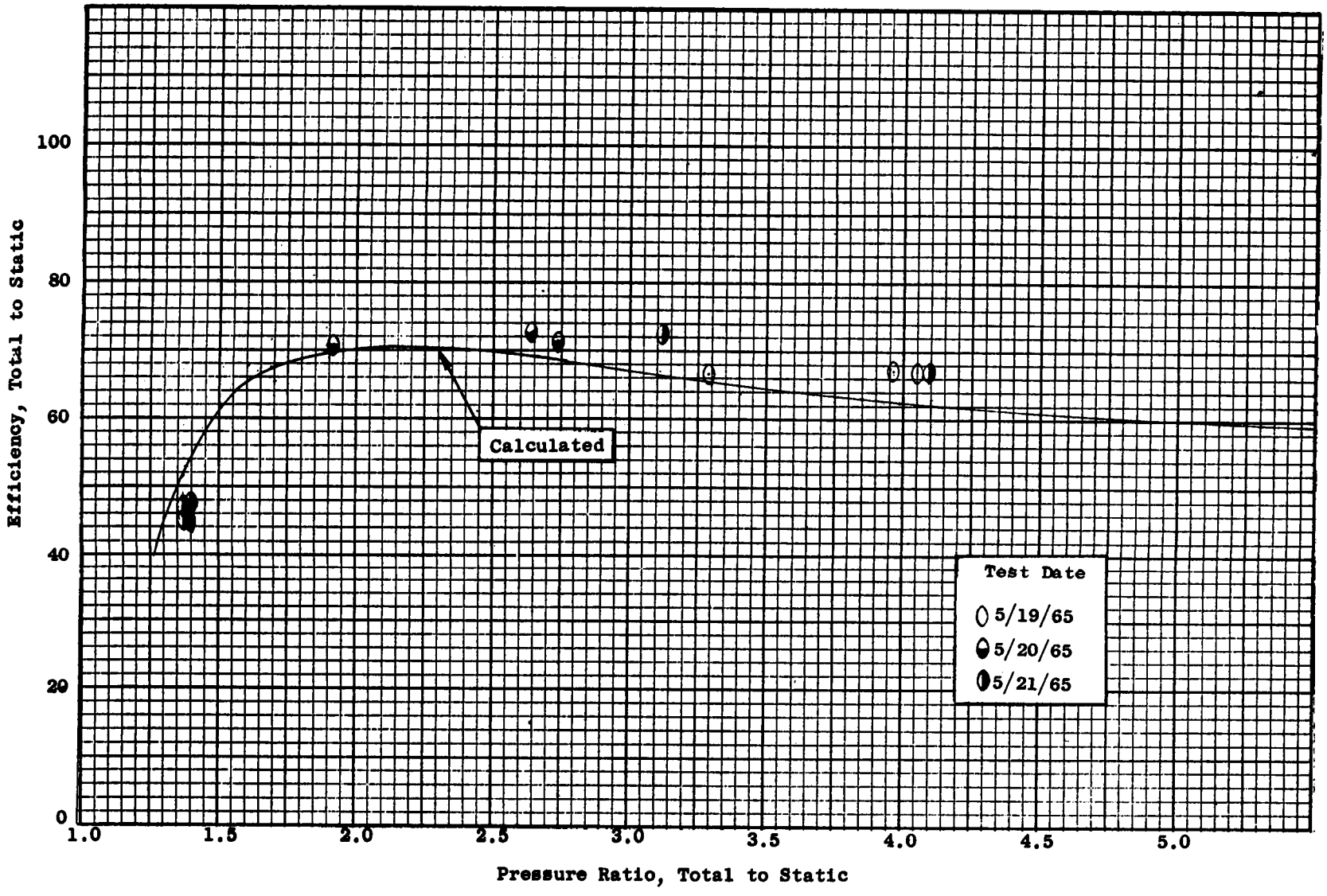

Figure 76. Comparison of Measured and Calculated Efficiency Versus Total to Static Pressure Ratio. Inlet Temperature, 1450°F, Rotative Speed, 20,000 rpm.

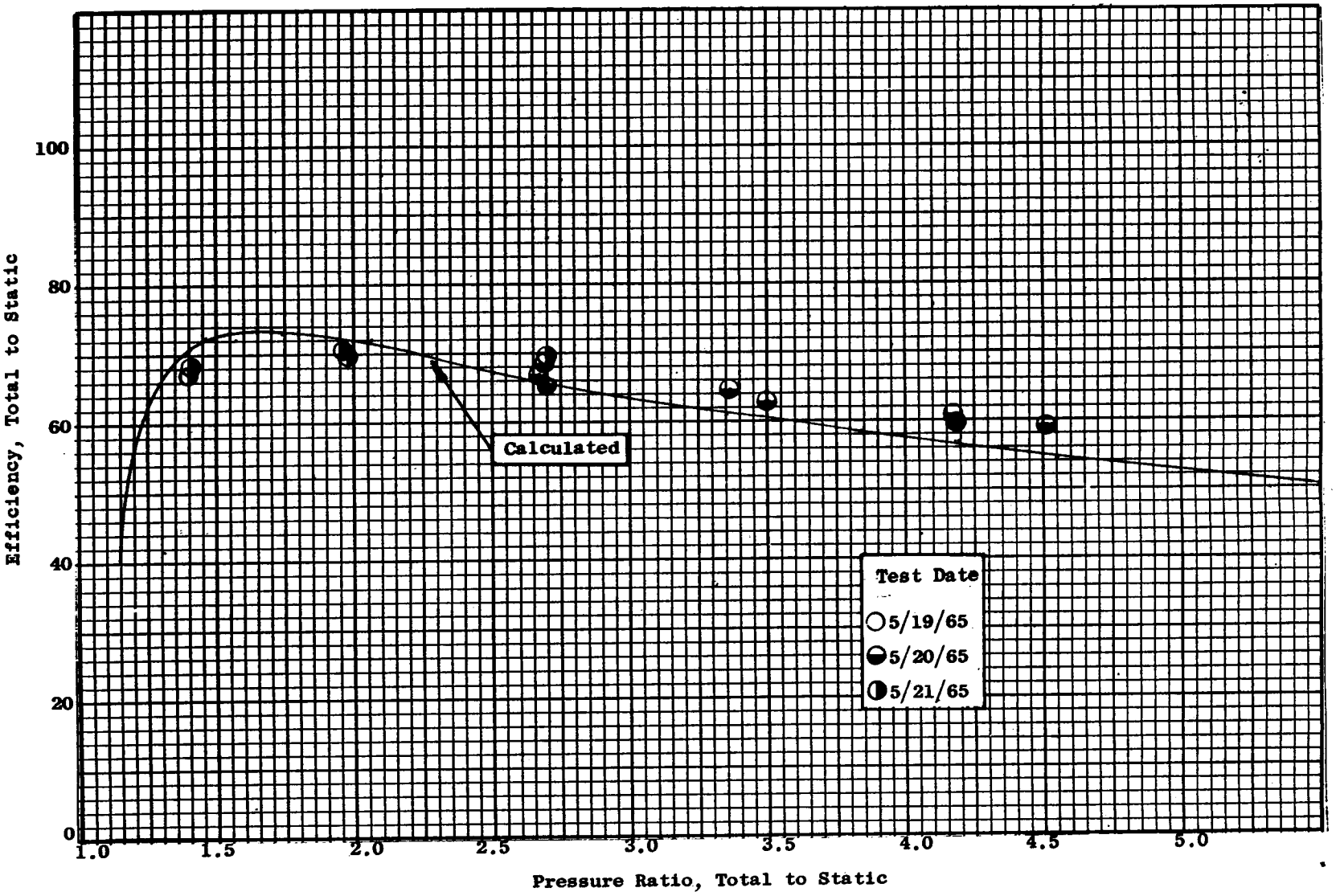

Figure 77. Comparison of Measured and Calculated Efficiency Versus Total to Static Pressure Ratio. Inlet Temperature, 1550°F, Rotative Speed, 15,400 rpm.

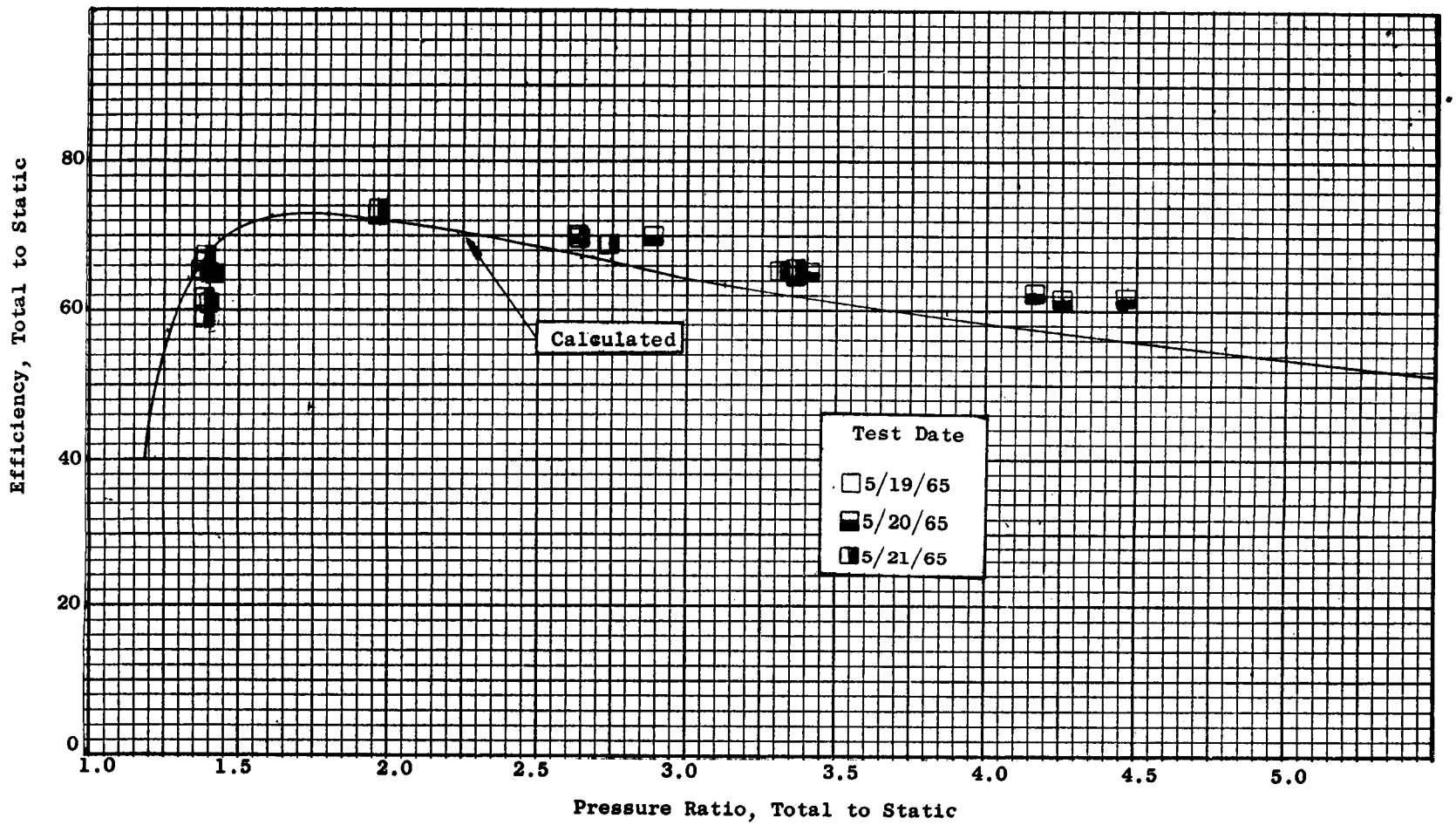

Figure 78. Comparison of Measured and Calculated Efficiency Versus Total to Static Pressure Ratio. Inlet Temperature, 1550°F, Rotative Speed, 16,400 rpm.

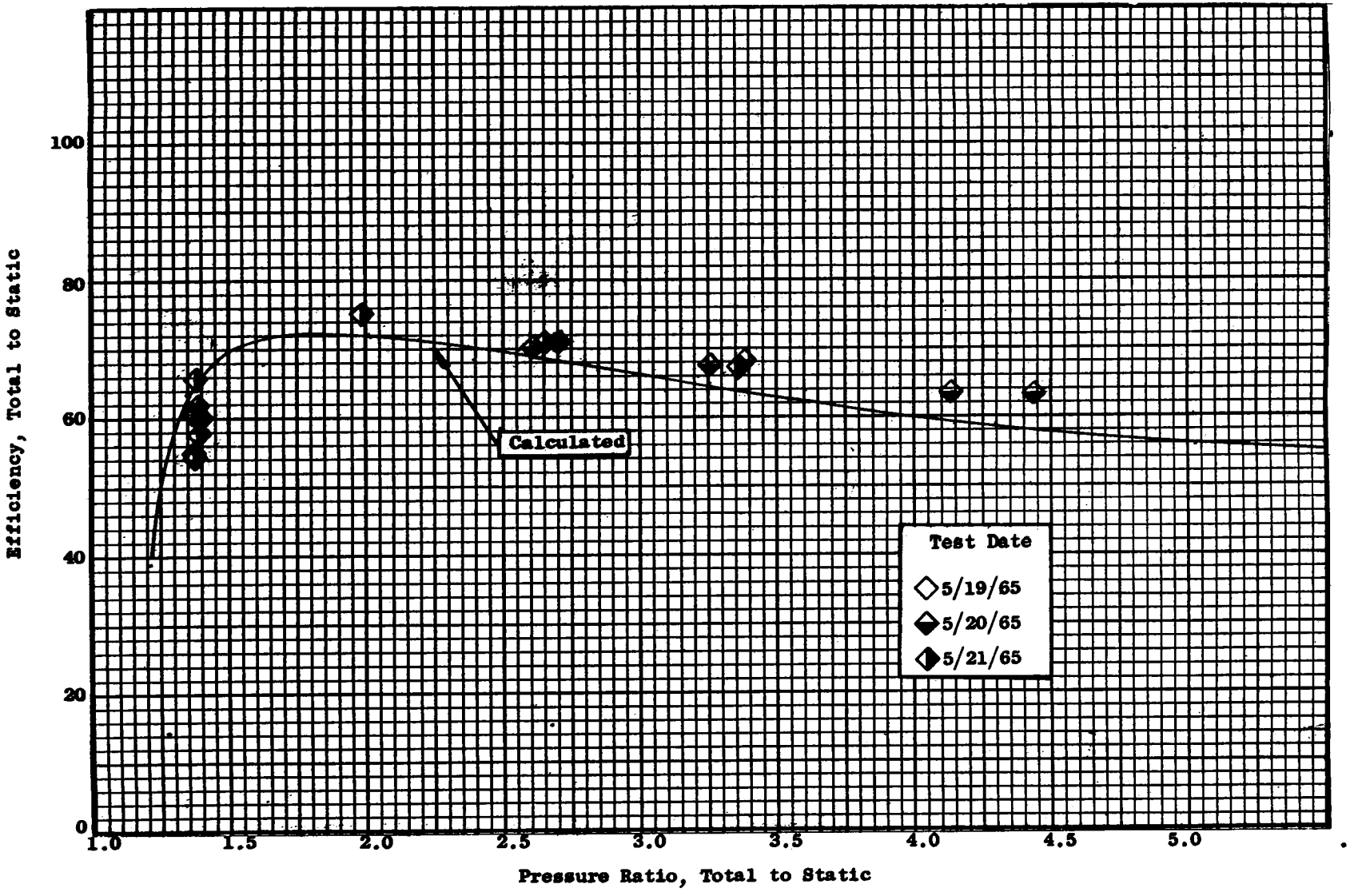

Figure 79. Comparison of Measured and Calculated Efficiency Versus Total to Static Pressure Ratio. Inlet Temperature, 1550°F, Rotative Speed, 17,300 rpm.

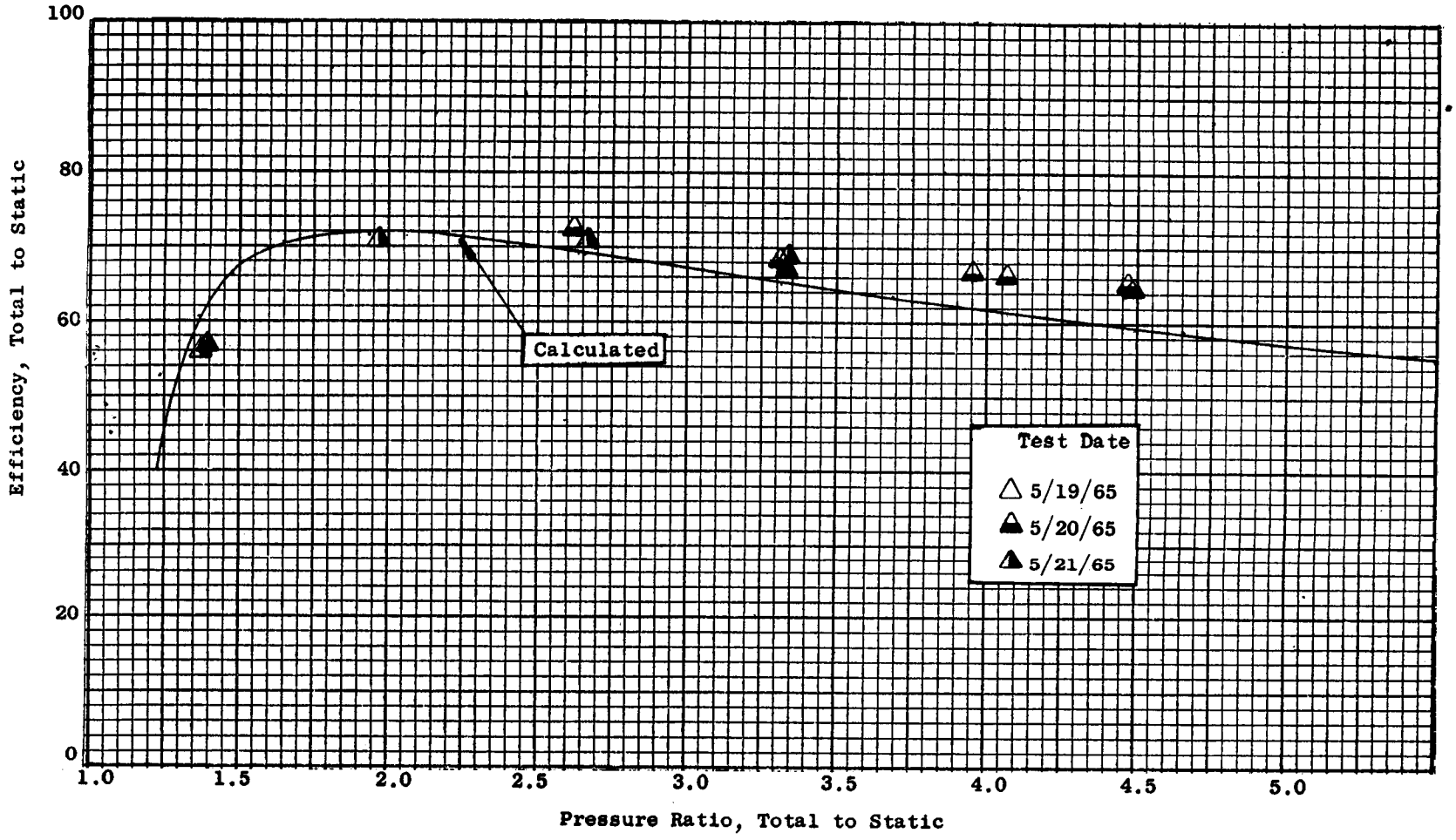

Figure 80. Comparison of Measured and Calculated Efficiency Versus Total to Static Pressure Ratio. Inlet Temperature, 1550°F, Rotative Speed, 18,300 rpm.

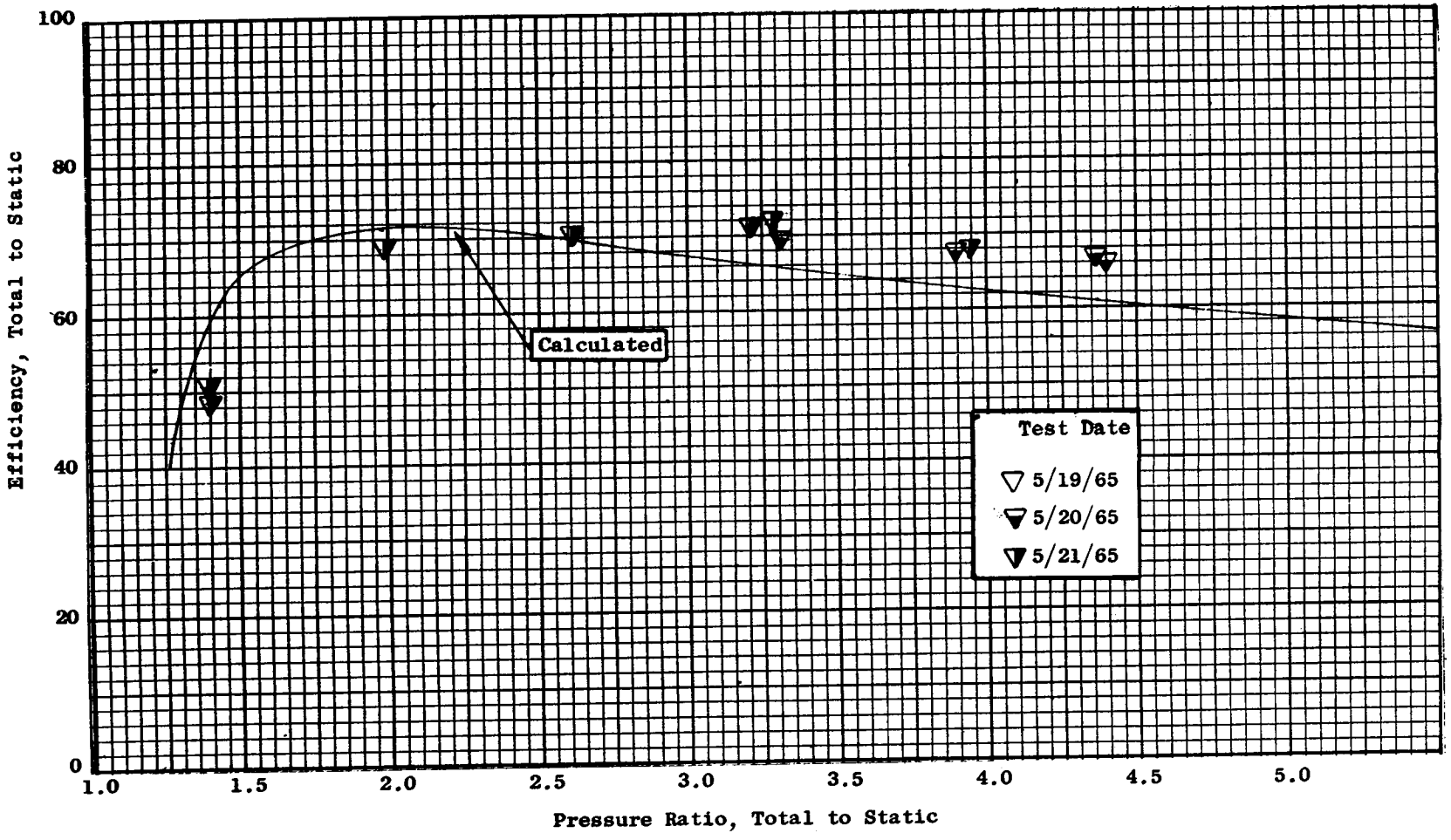

Figure 81. Comparison of Measured and Calculated Efficiency Versus Total to Static Pressure Ratio. Inlet Temperature, 1550°F, Rotative Speed, 19,300 rpm.

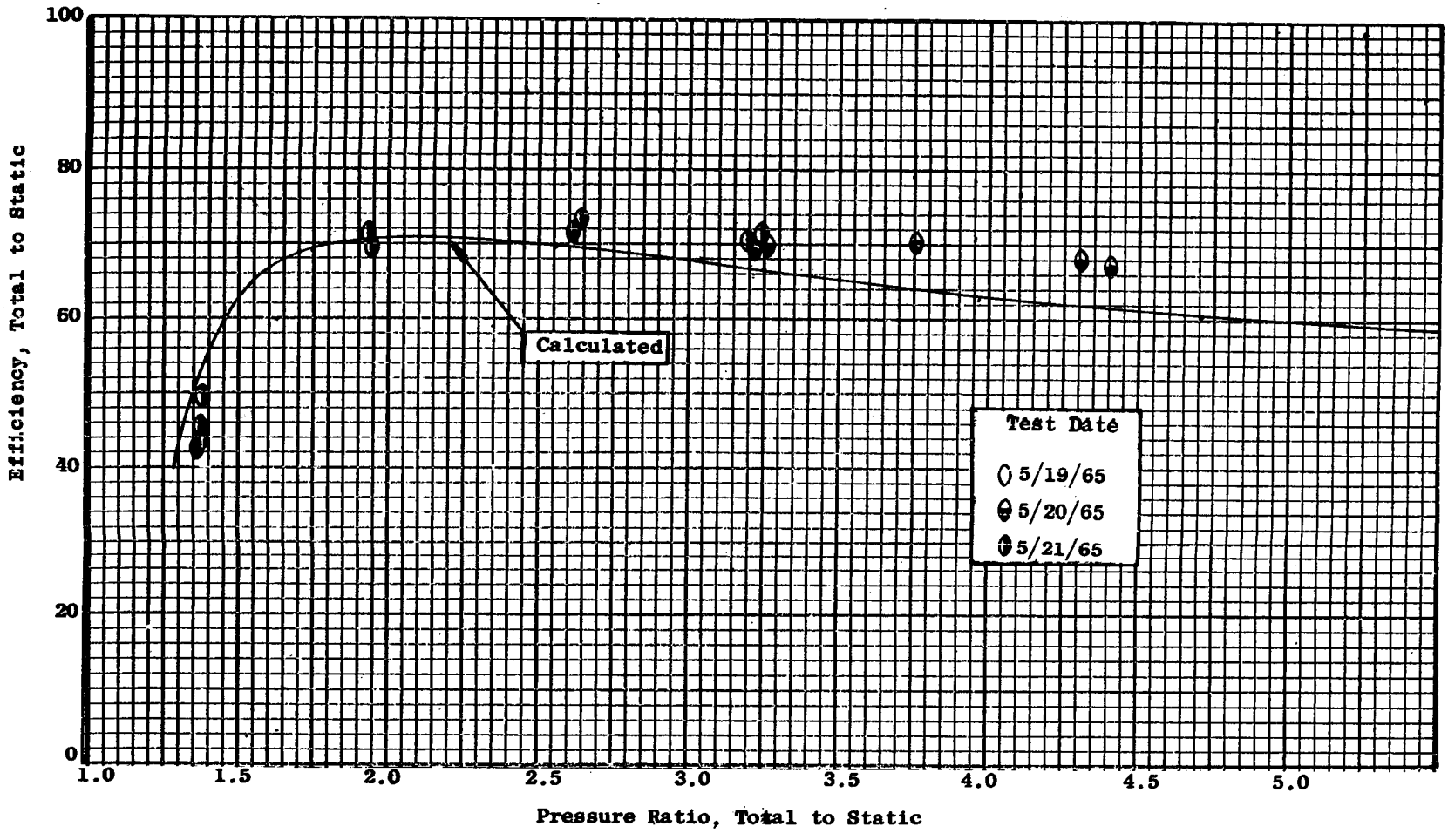

Figure 82. Comparison of Measured and Calculated Efficiency Versus Total to Static Pressure Ratio. Inlet Temperature, 1550°F, Rotative Speed, 20,000 rpm.

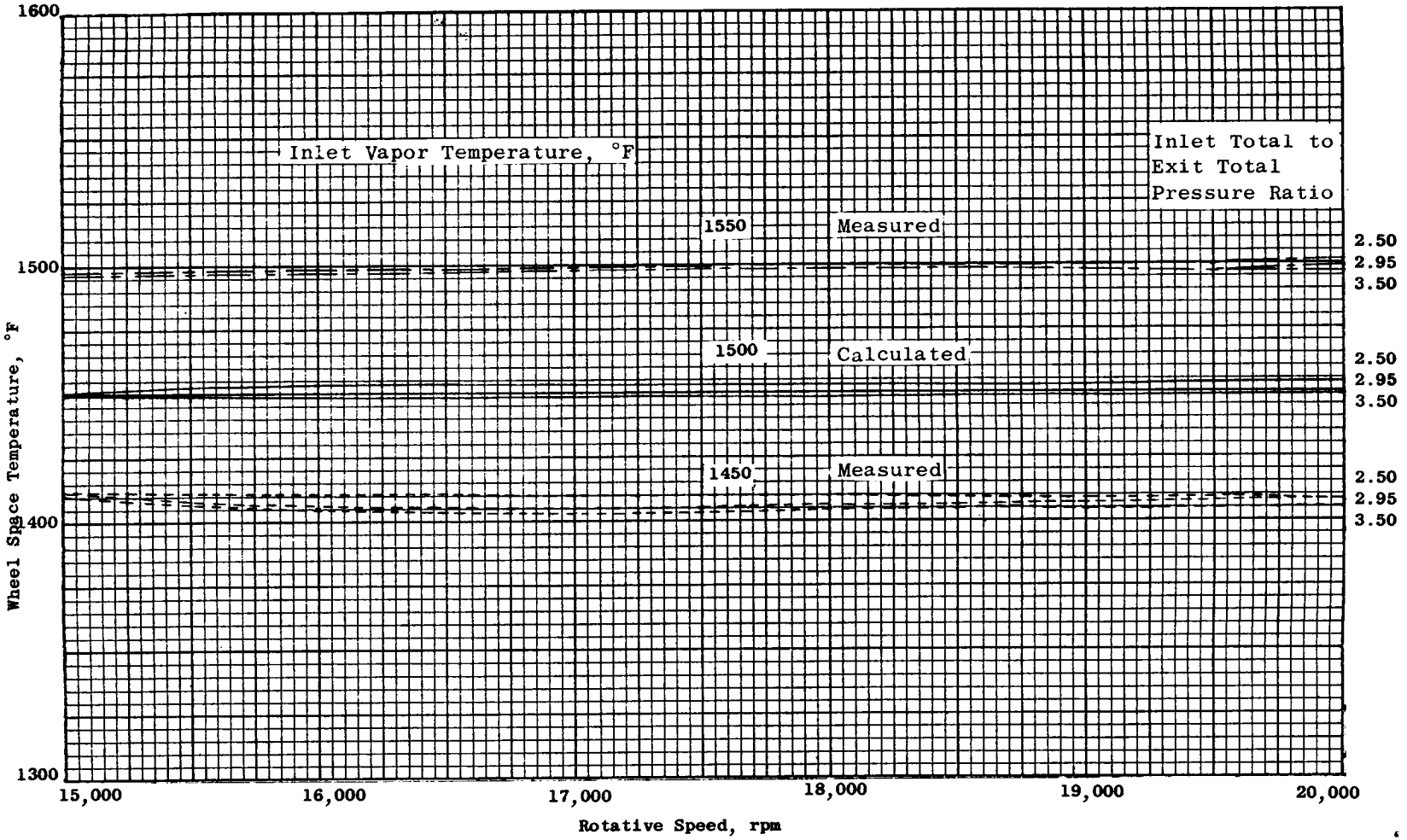

Figure 83a. Variation of Wheel-Space Temperature for Stage One With Rotative Speed and Turbine Pressure Ratio. Inlet Total To Exit Total.

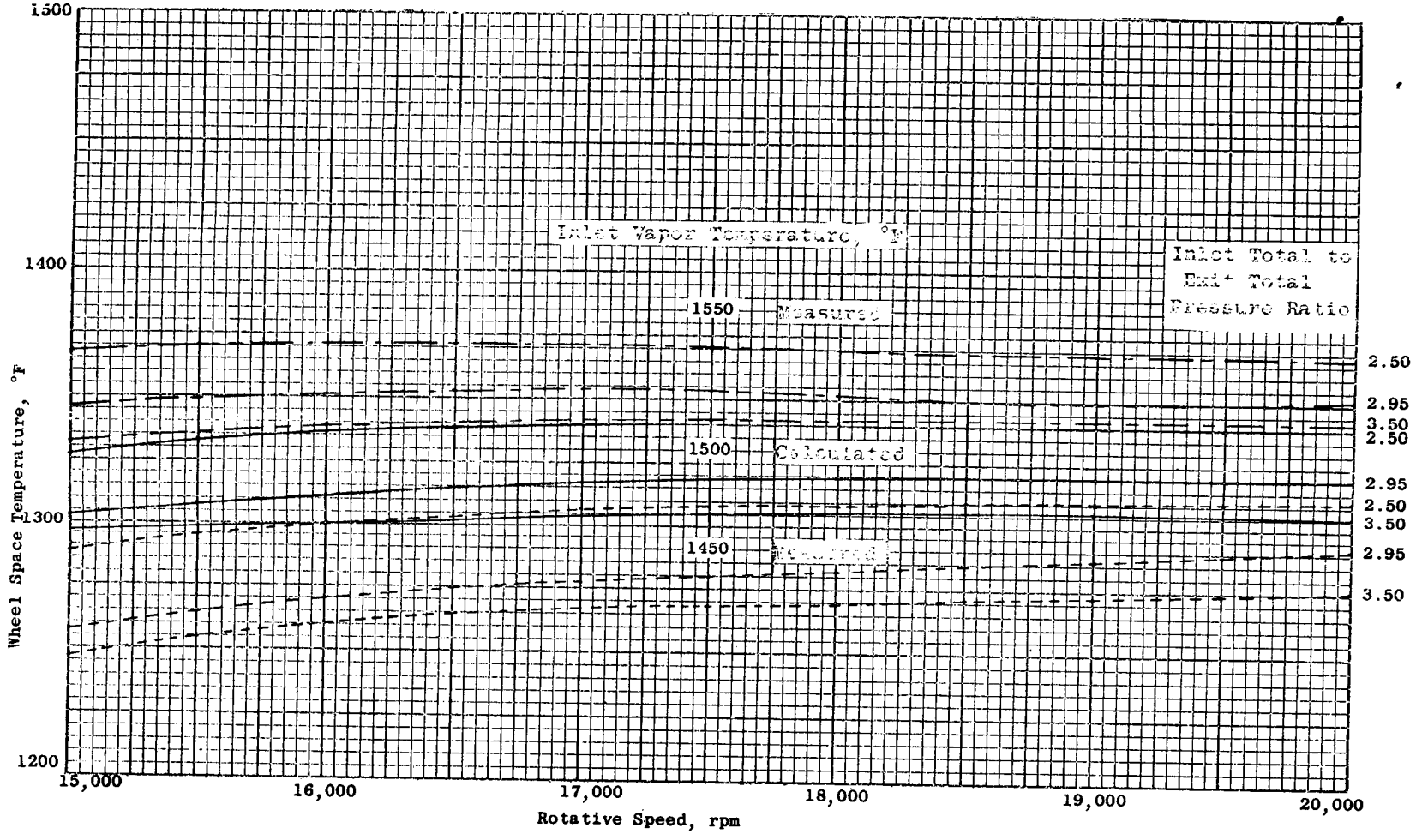

Figure 83b. Variation of Wheel-Space Temperature for Stage Two With Rotative Speed and Turbine Pressure Ratio. Inlet Total To Exit Total.

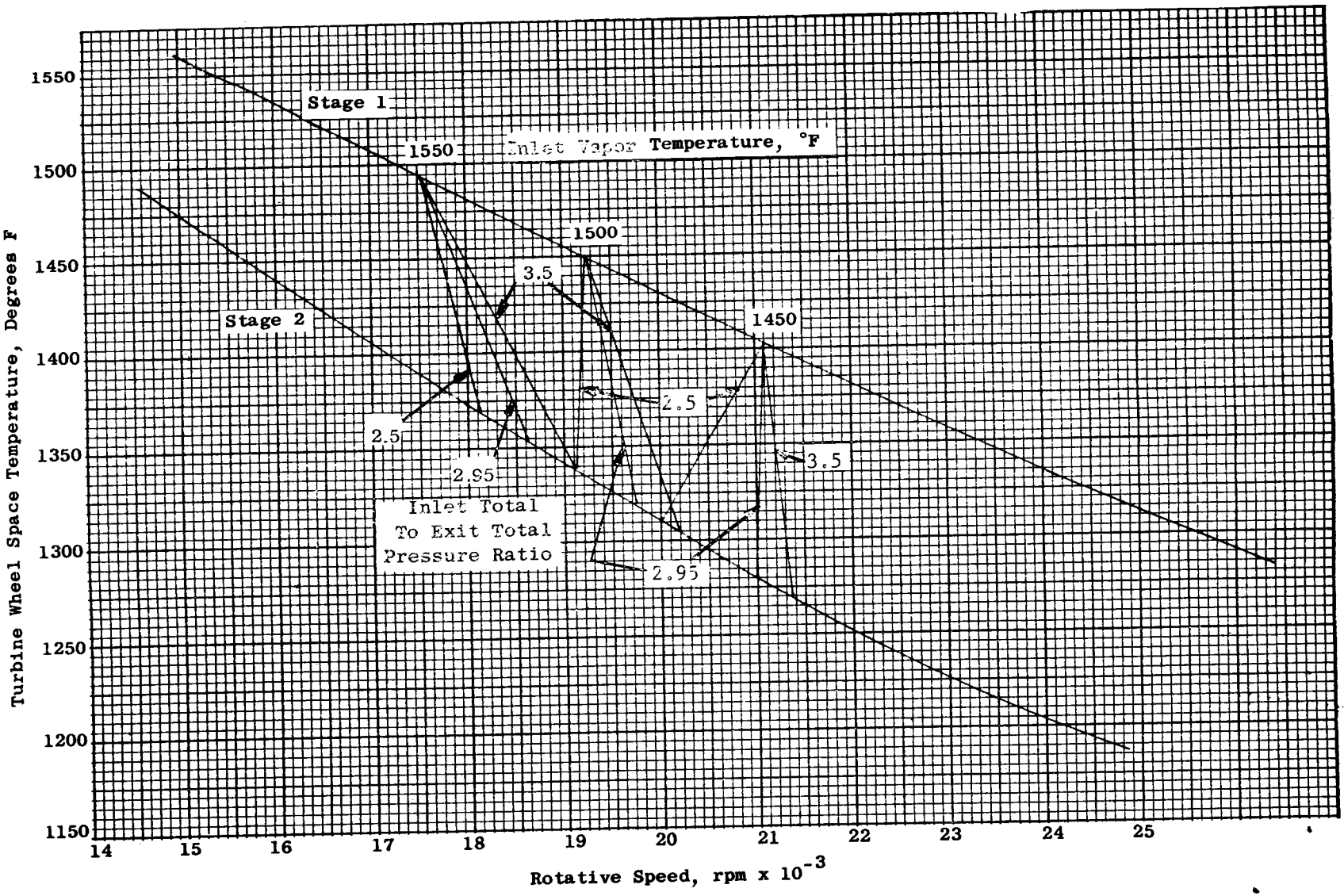

Figure 84. Allowable Turbine Operating Speeds for 2000 Hour Endurance Test.

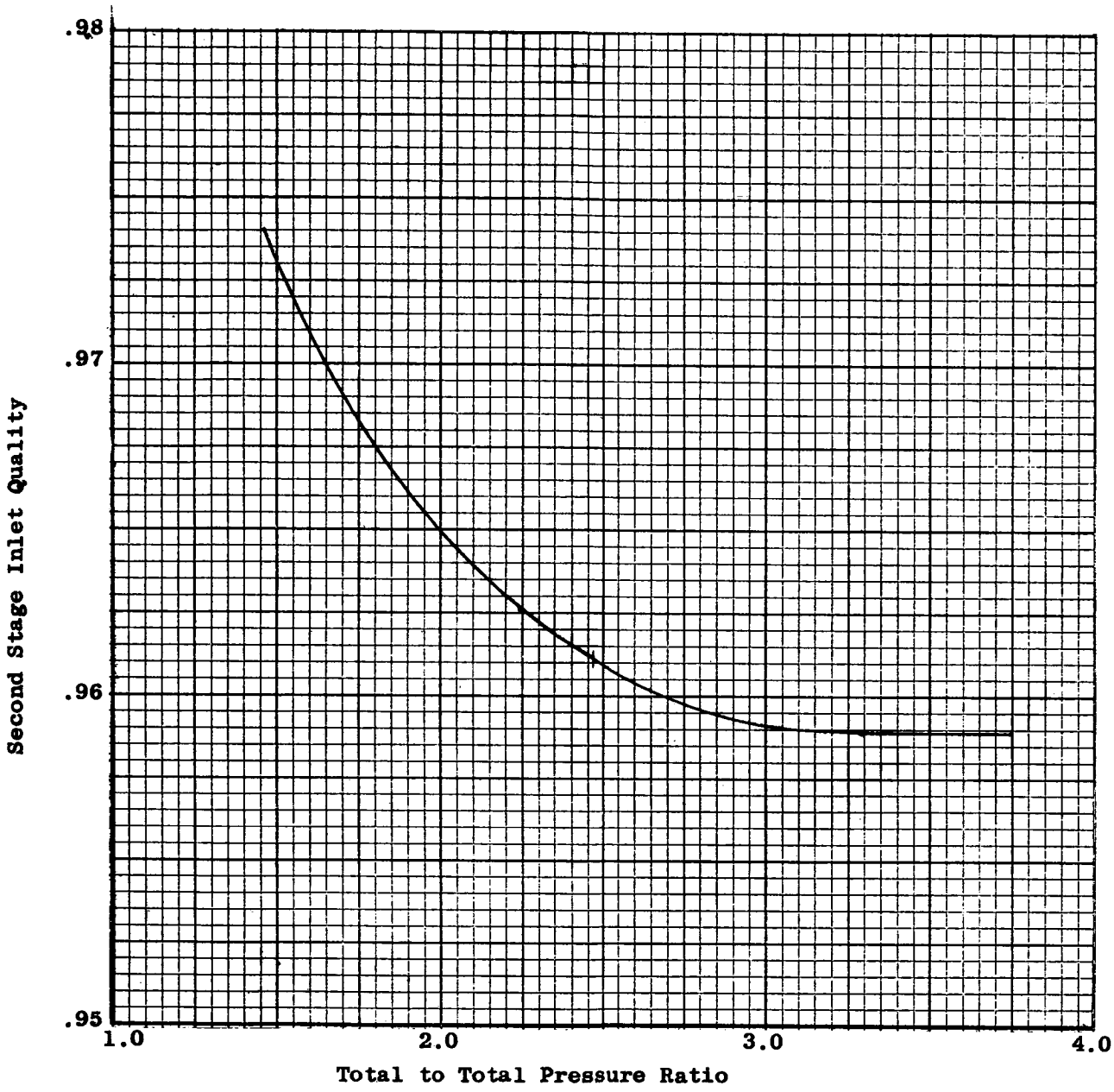

Figure 85. Variation of Second Stage Calculated Inlet Quality With Total to Total Pressure Ratio. Inlet Temperature, 1500°F; Speed, 18,250 rpm; Inlet Quality, 99 percent.

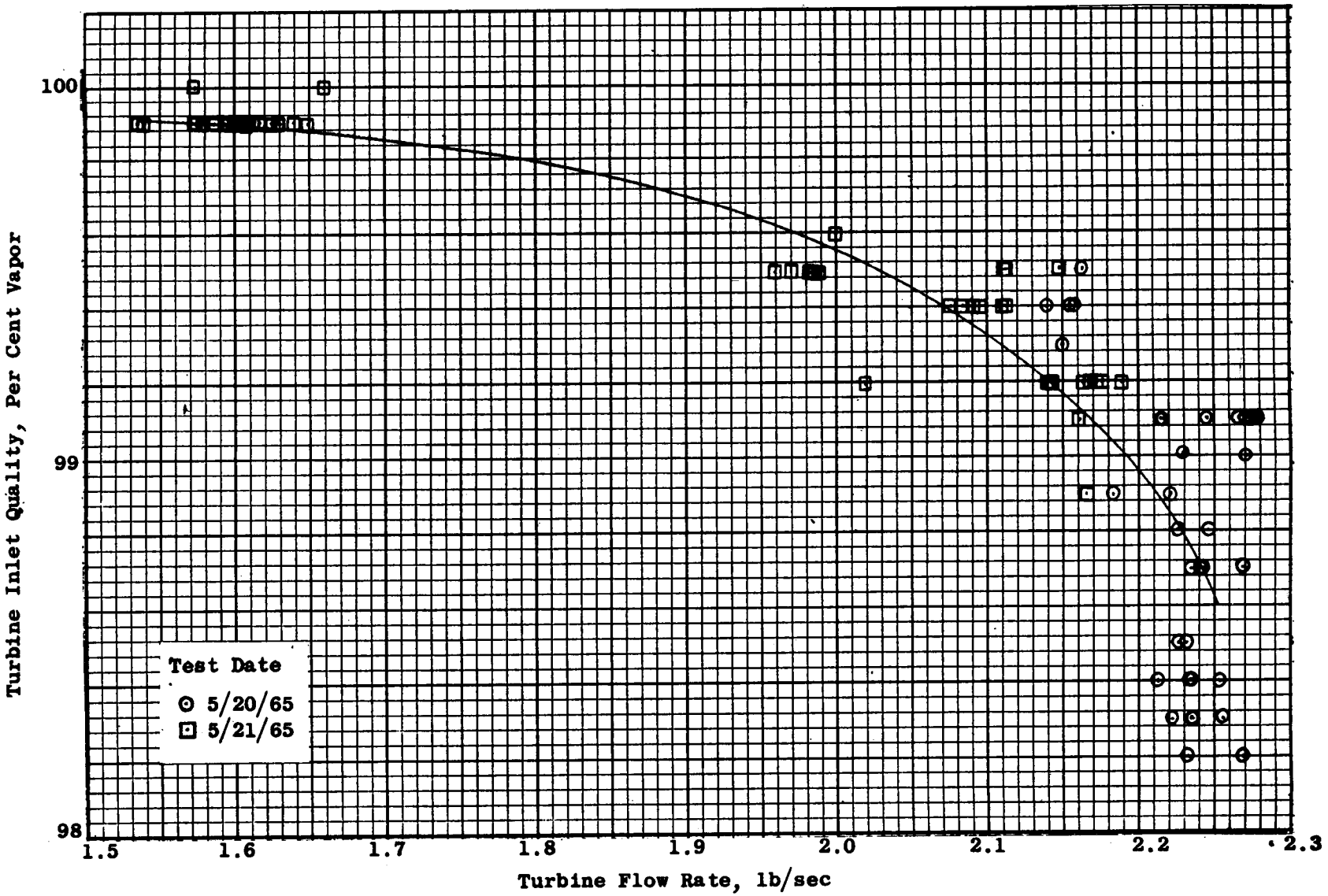

Figure 86. Variation in Turbine Inlet Quality With Flow Rate, Inlet Temperature, 1550°F.

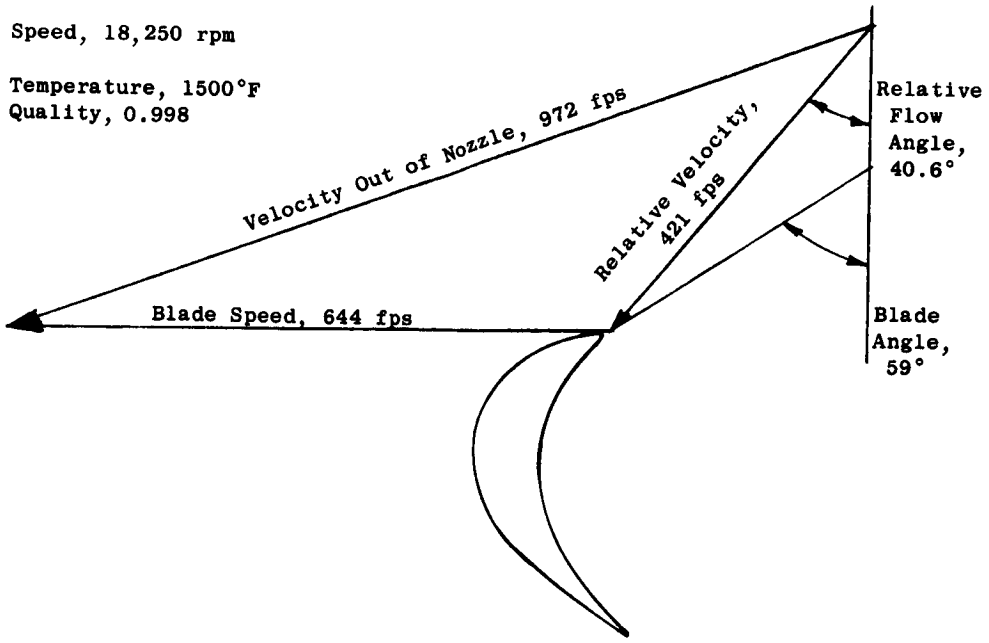

(A) First Stage

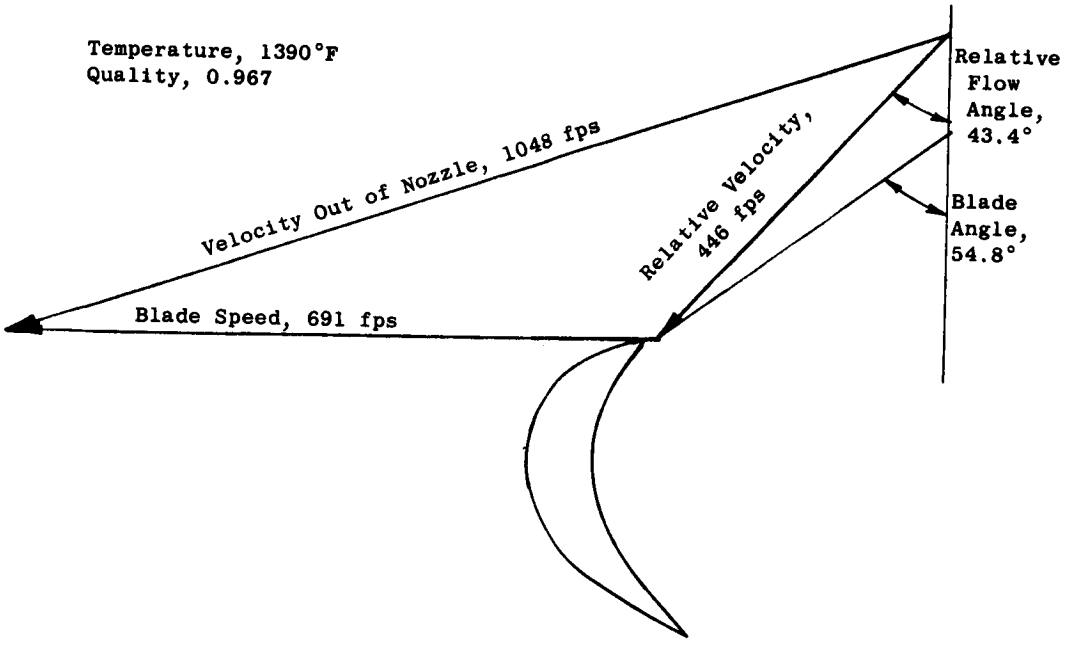

(B) Second Stage

Figure 87. Velocity Diagram for Endurance Test Condition.

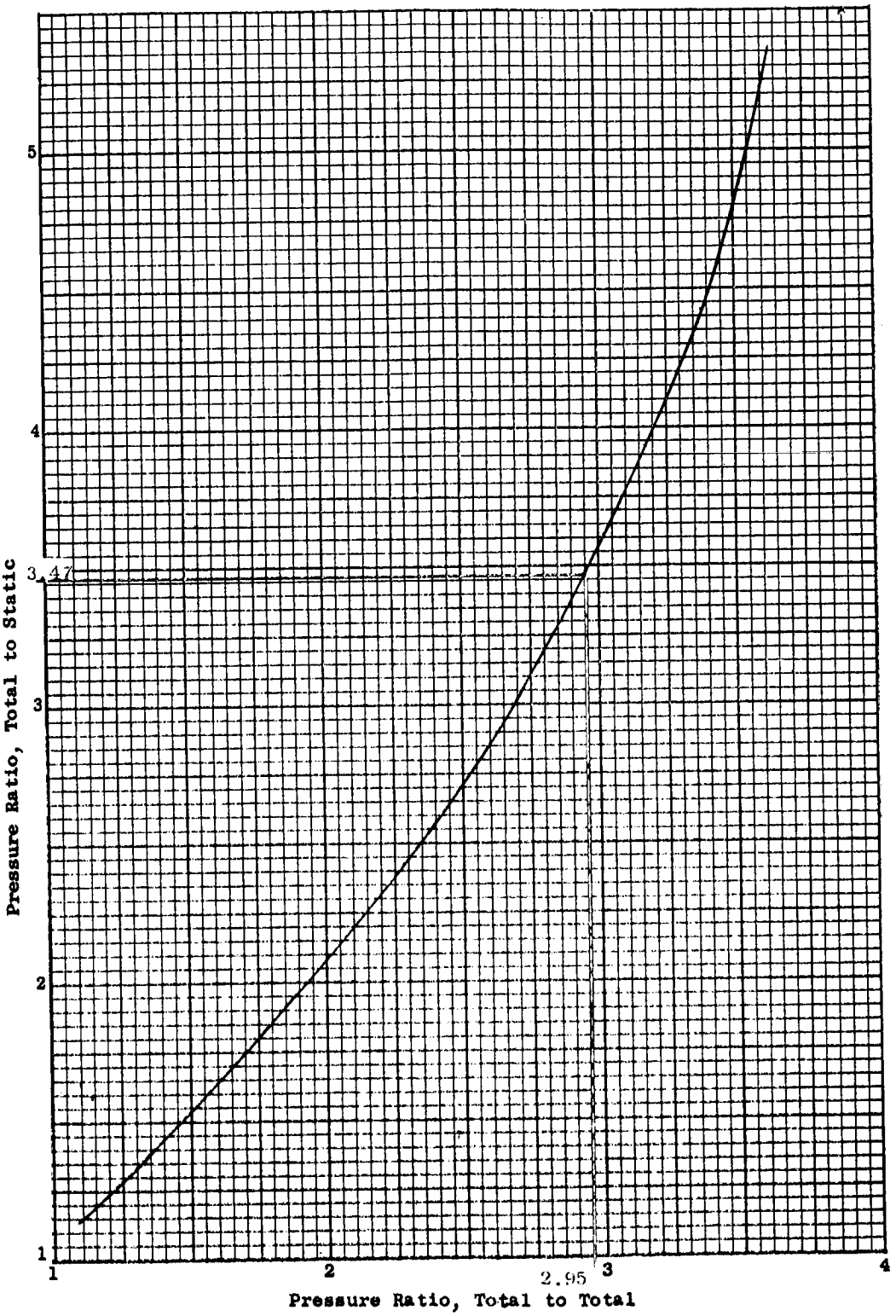

Figure 88. Calculated Variation of Total to Static Pressure Ratio Across the Turbine With Total to Total Pressure Ratio. Inlet Temperature, 1500°F.

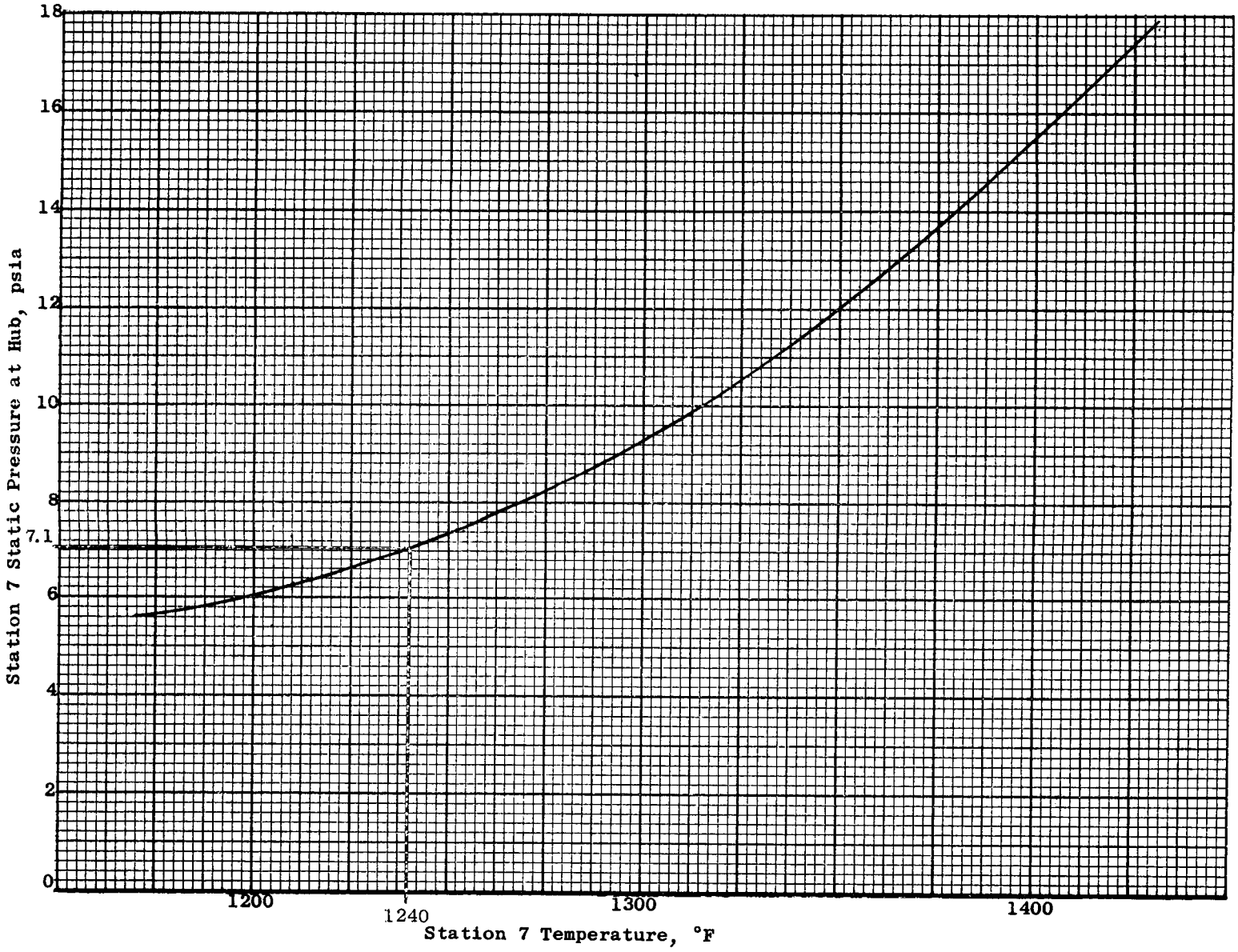

Figure 89. Correlation of Exit Temperature and Pressure For Turbine Operation at 1500°F.

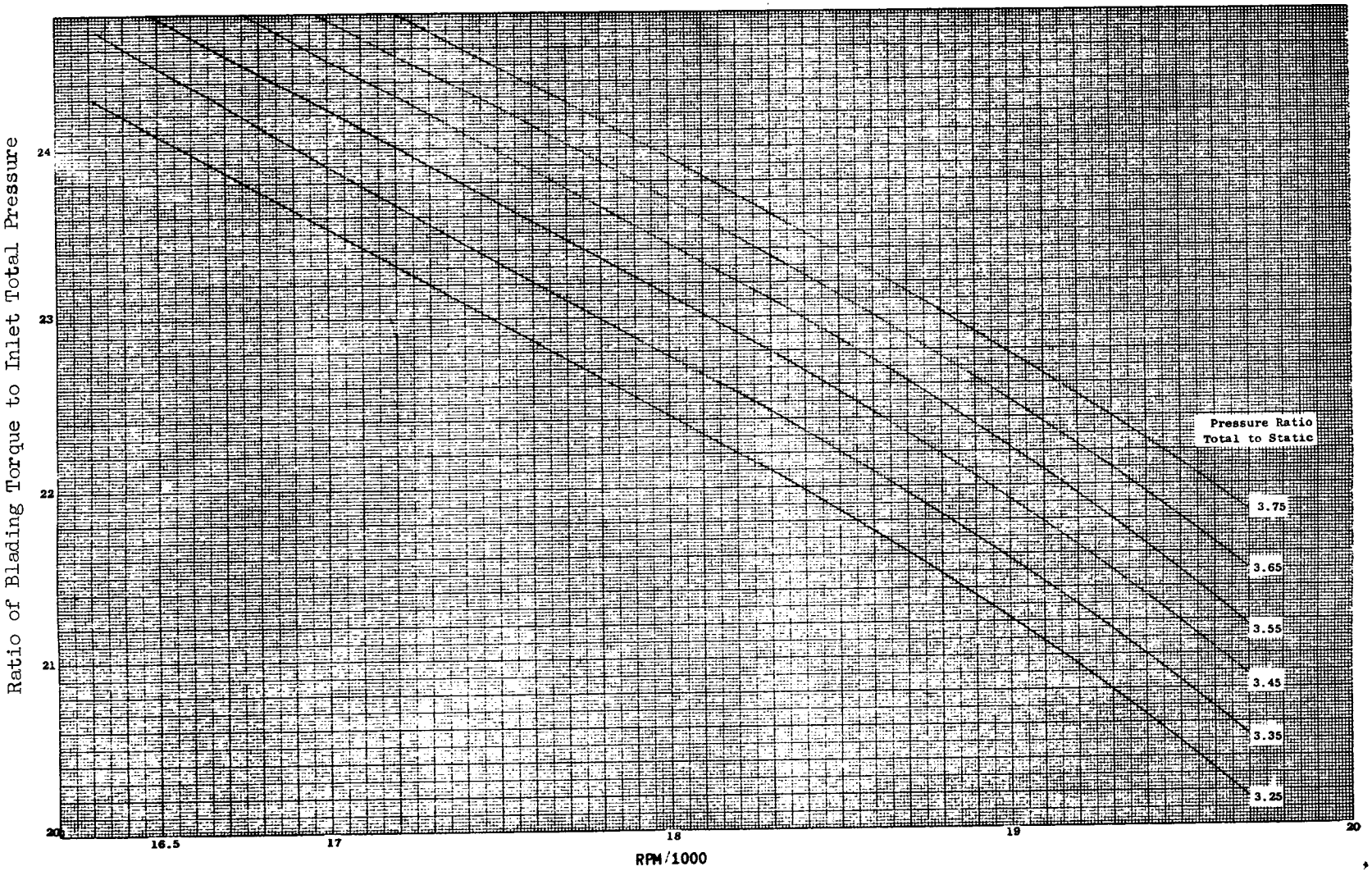

Figure 90. Calculated Variation in the Ratio of Turbine Torque to Inlet Total Pressure With Rotative Speed and Total to Static Pressure Ratio.

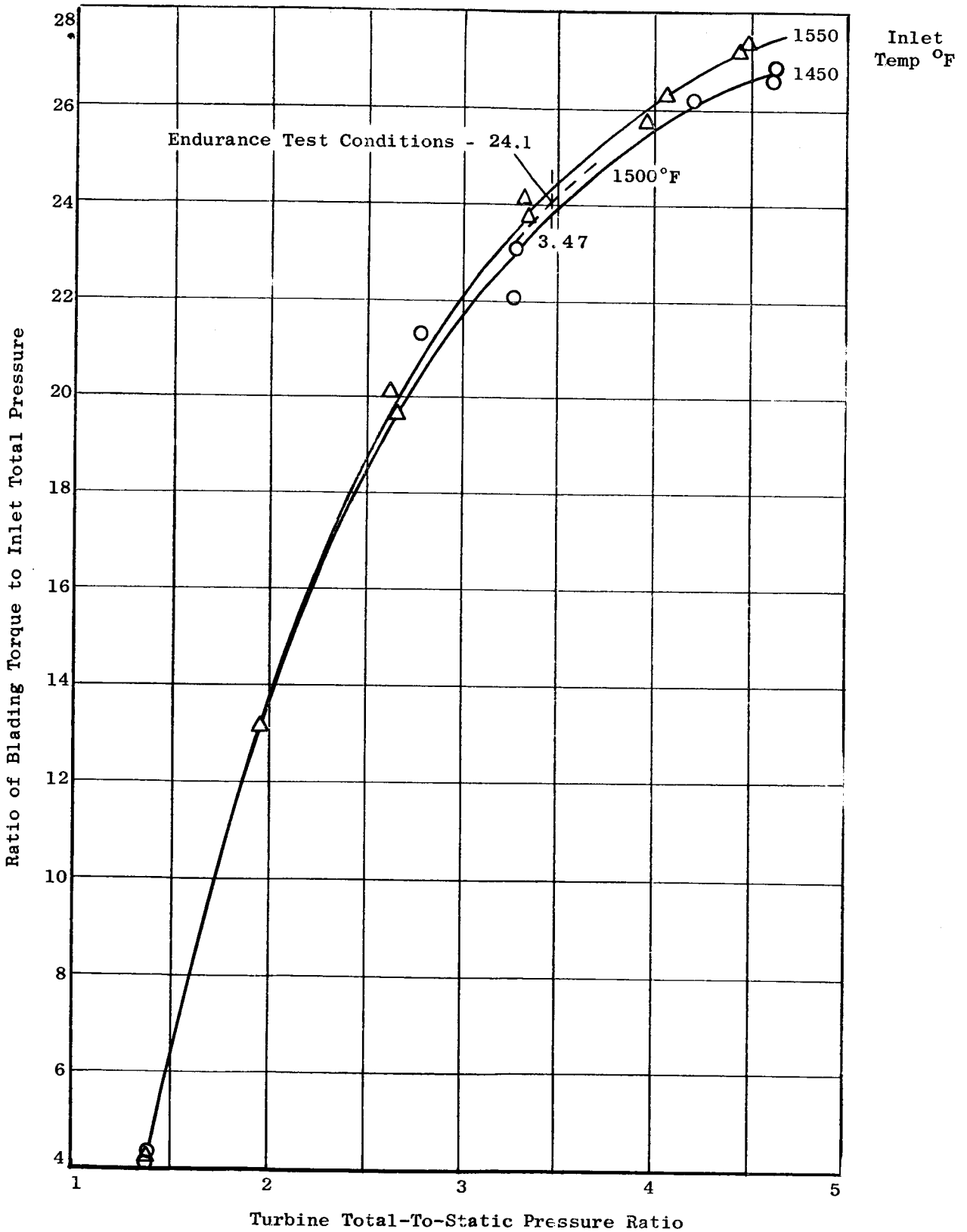

Figure 91. Variation of Turbine Torque with Pressure Ratio; 18250 rpm.

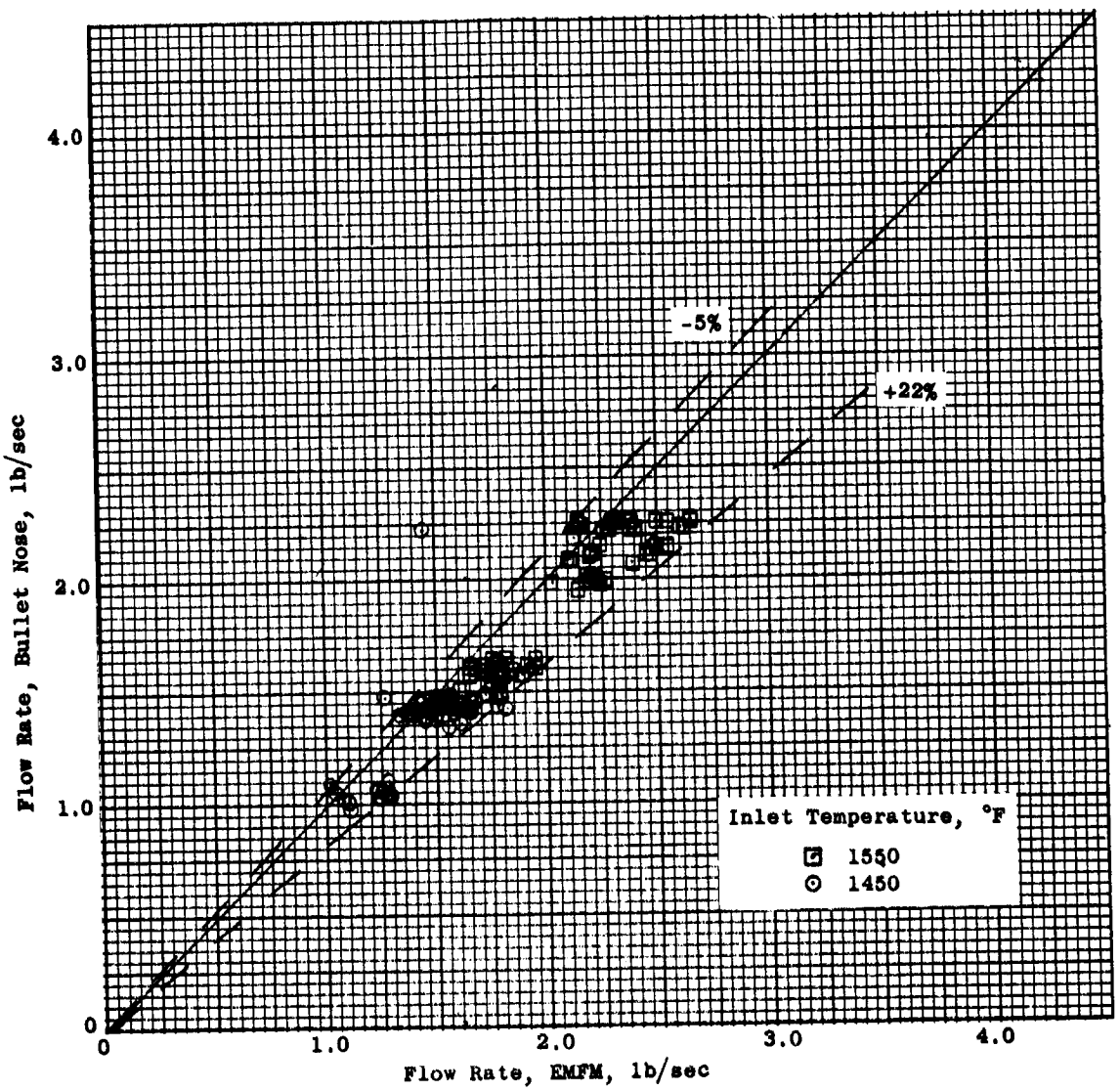

Figure 92. Comparison of Potassium Flow Rates from the EM Flow Meter and the Bullet Nose Annulus.

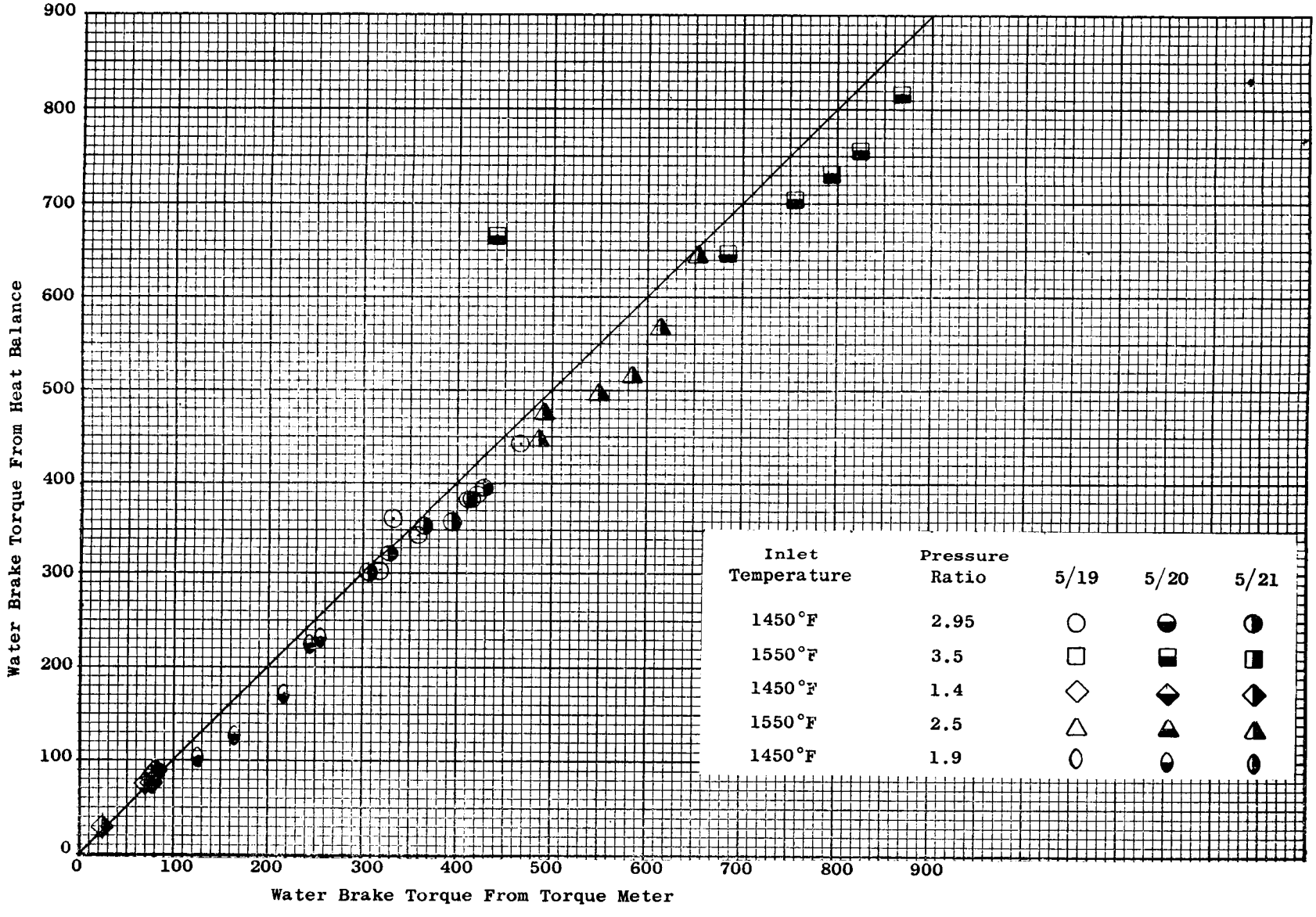

Figure 93. Comparison of Heat-Balance Torque and Torque Meter Readings.

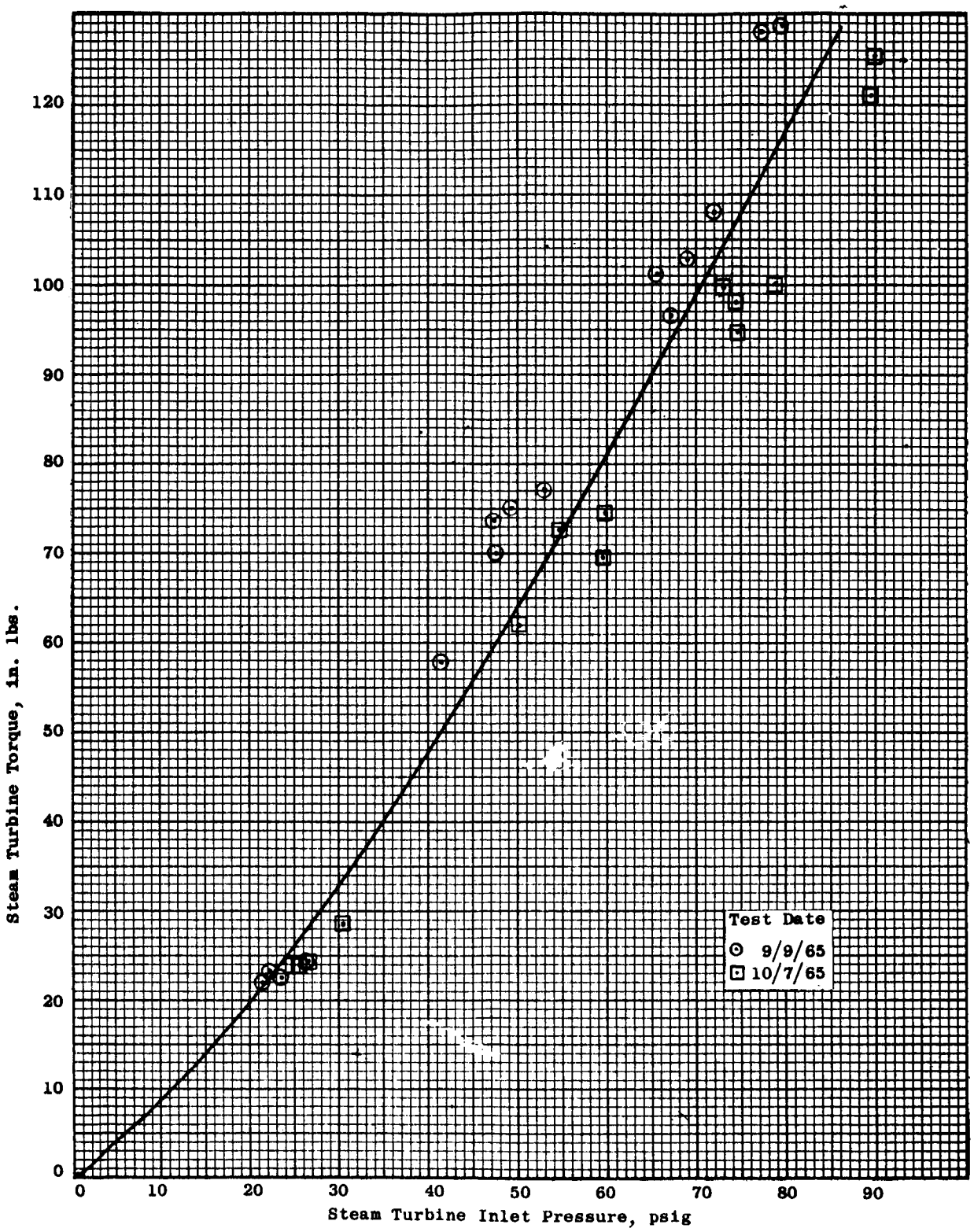

Figure 94. Variation of the Steam Turbine Torque with Steam Inlet Pressure.

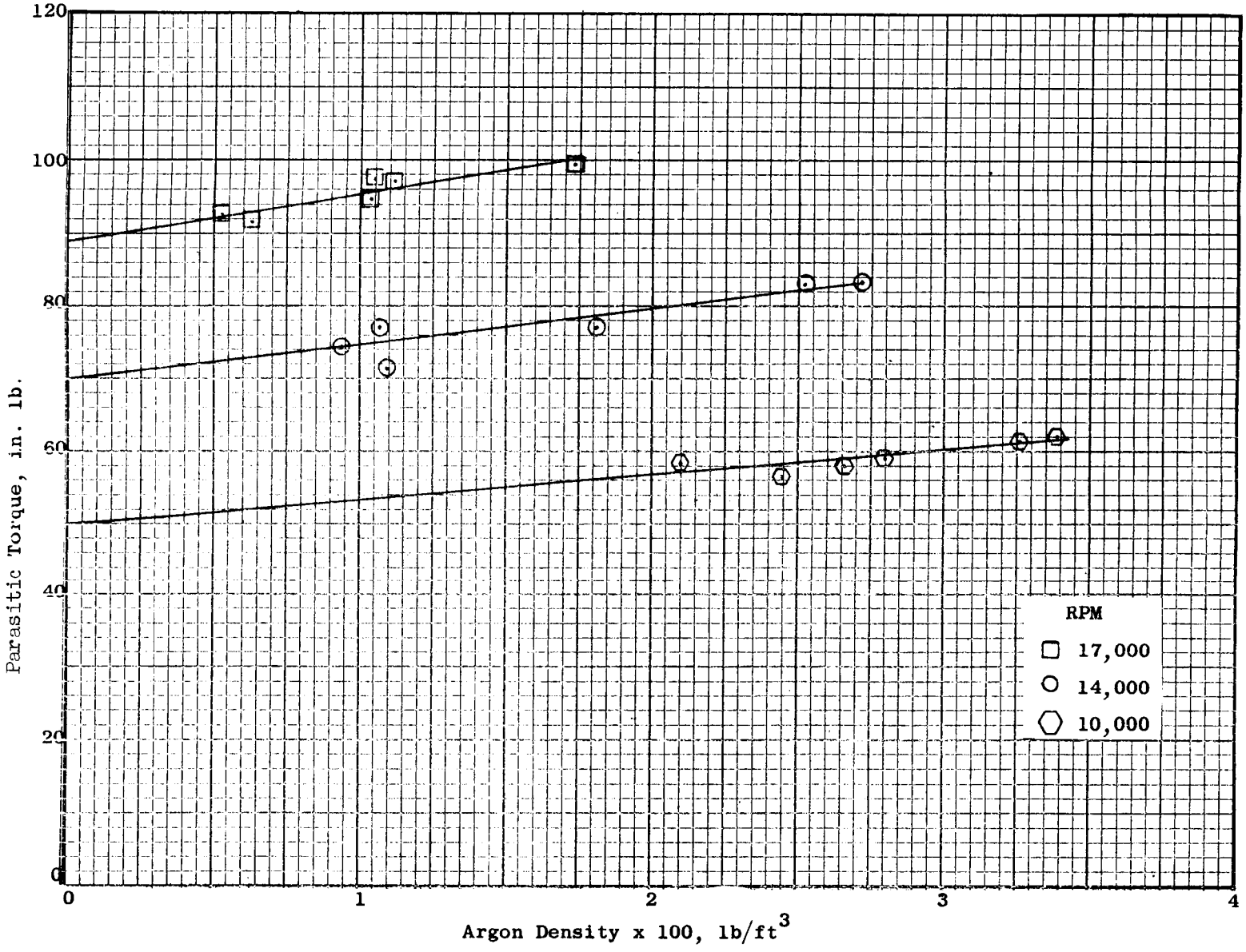

Figure 95. Parasitic Torque Variation With Rotative Speed and Density, Test Date, 9/13/65.

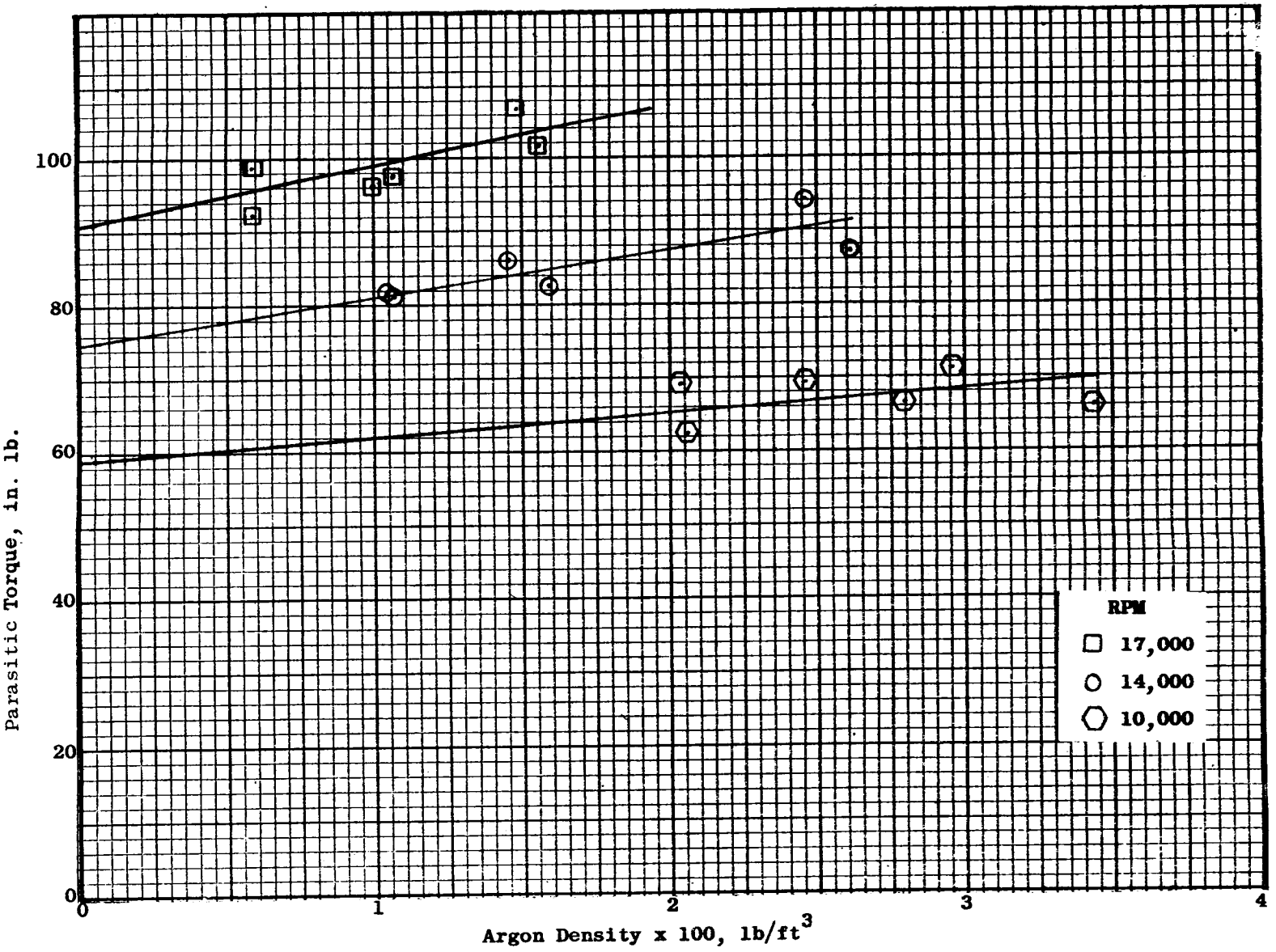

Figure 96. Parasitic Torque Variation With Rotative Speed and Density, Test date, 10/8/65.

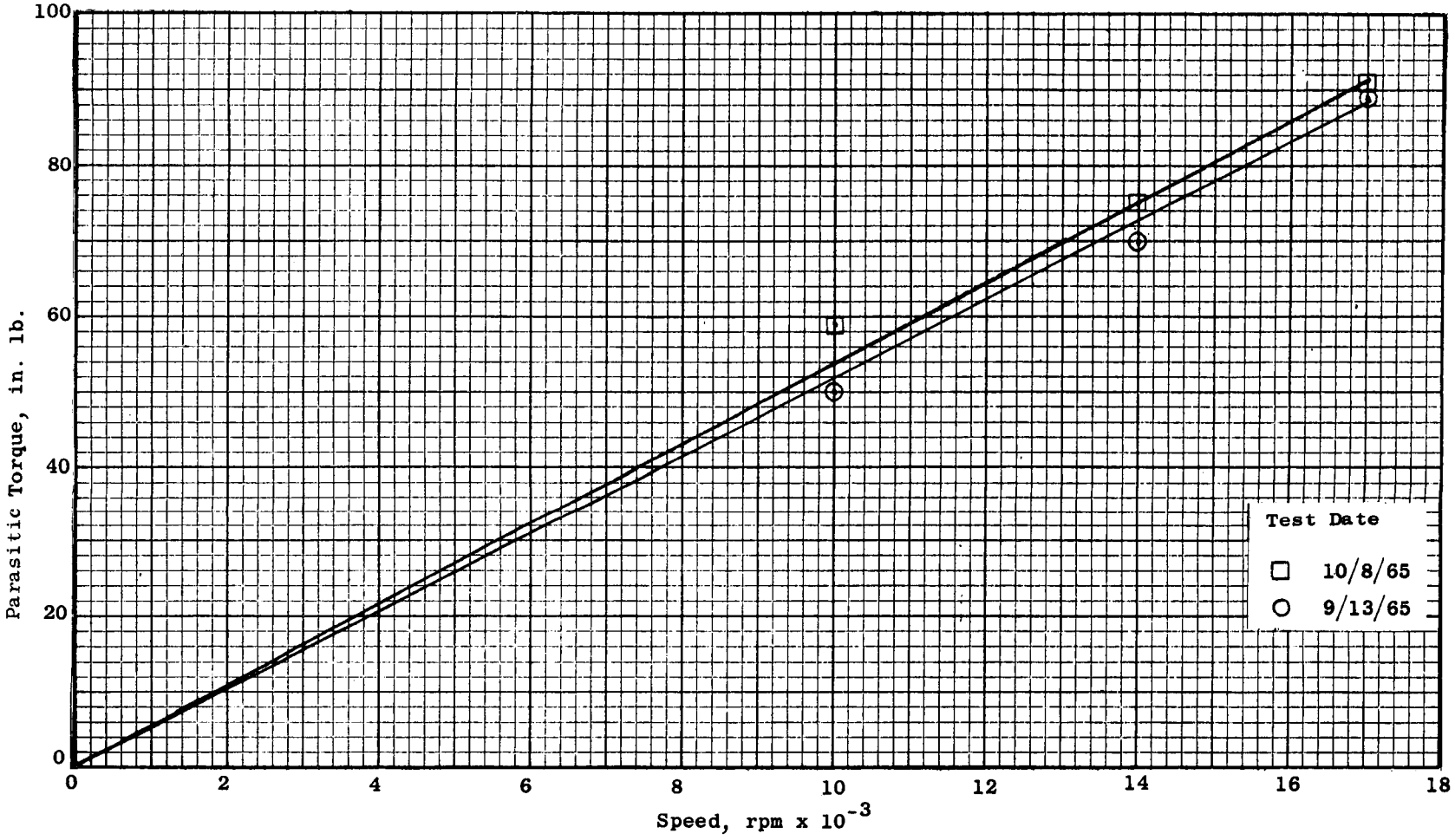

Figure 97. Parasitic Torque Variation With Rotative Speed.

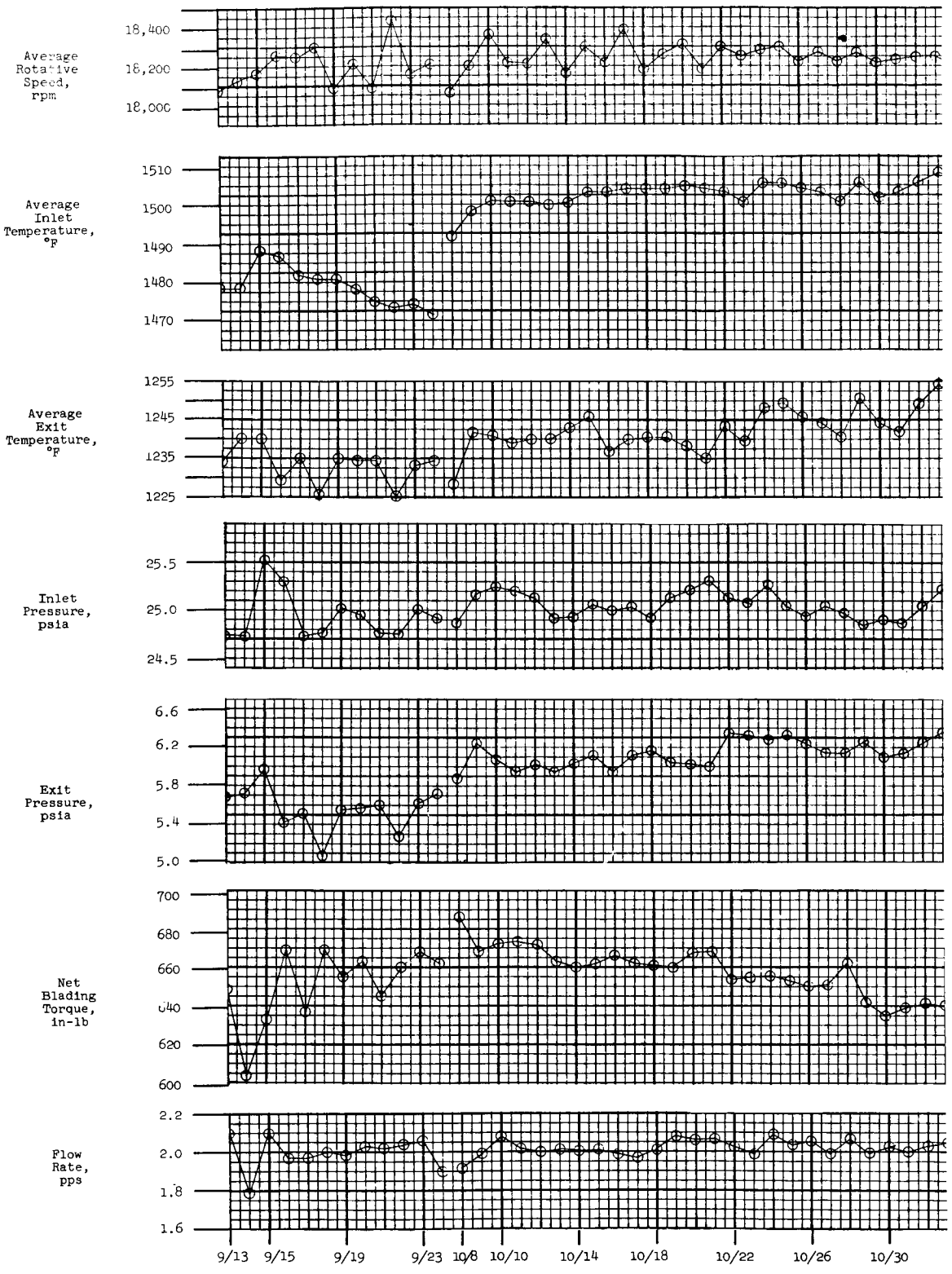

Figure 98. Variation of Turbine Parame

ters During Endurance Testing.

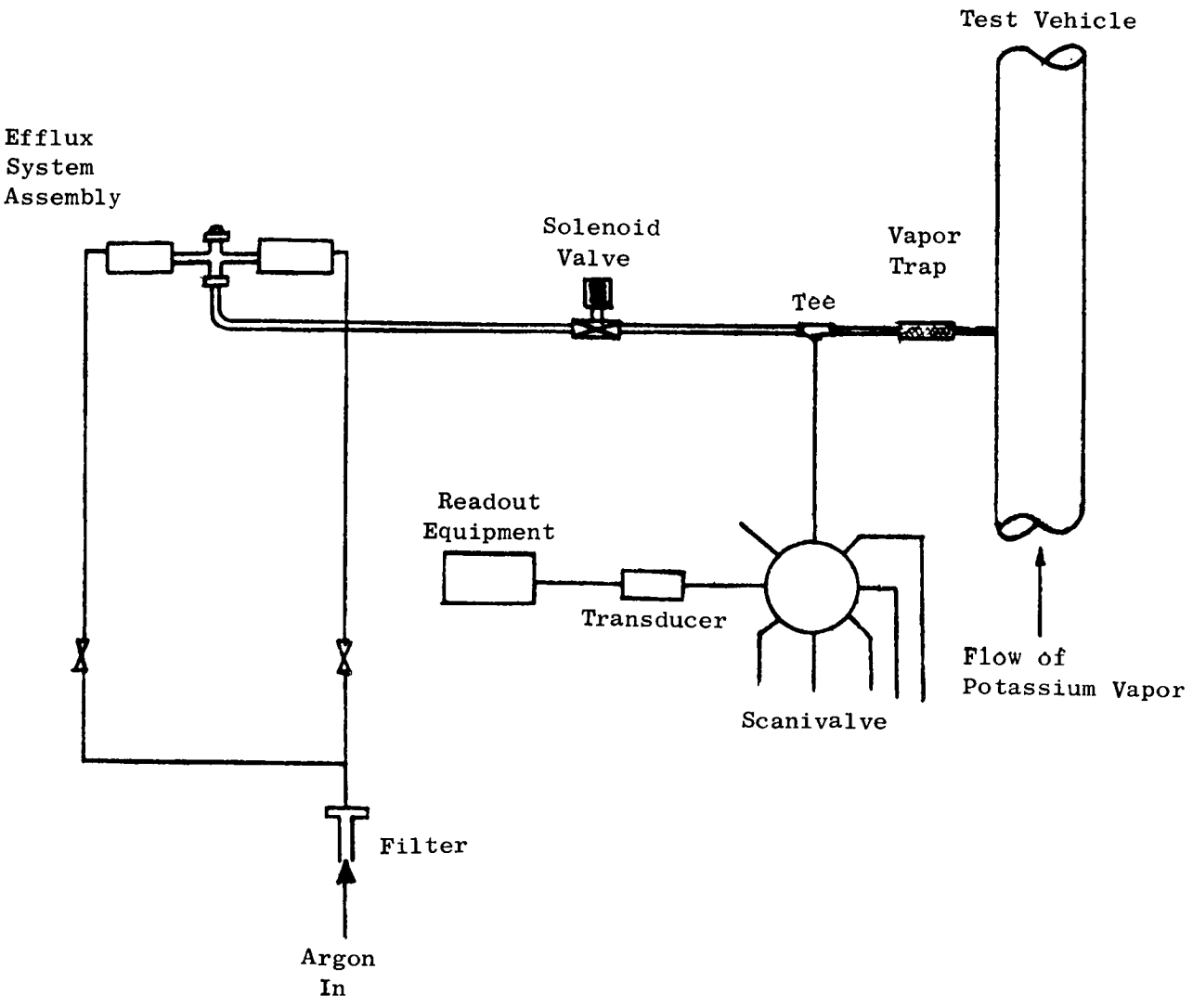

Figure A-1. Schematic Diagram of Efflux Pressure Measuring Device.

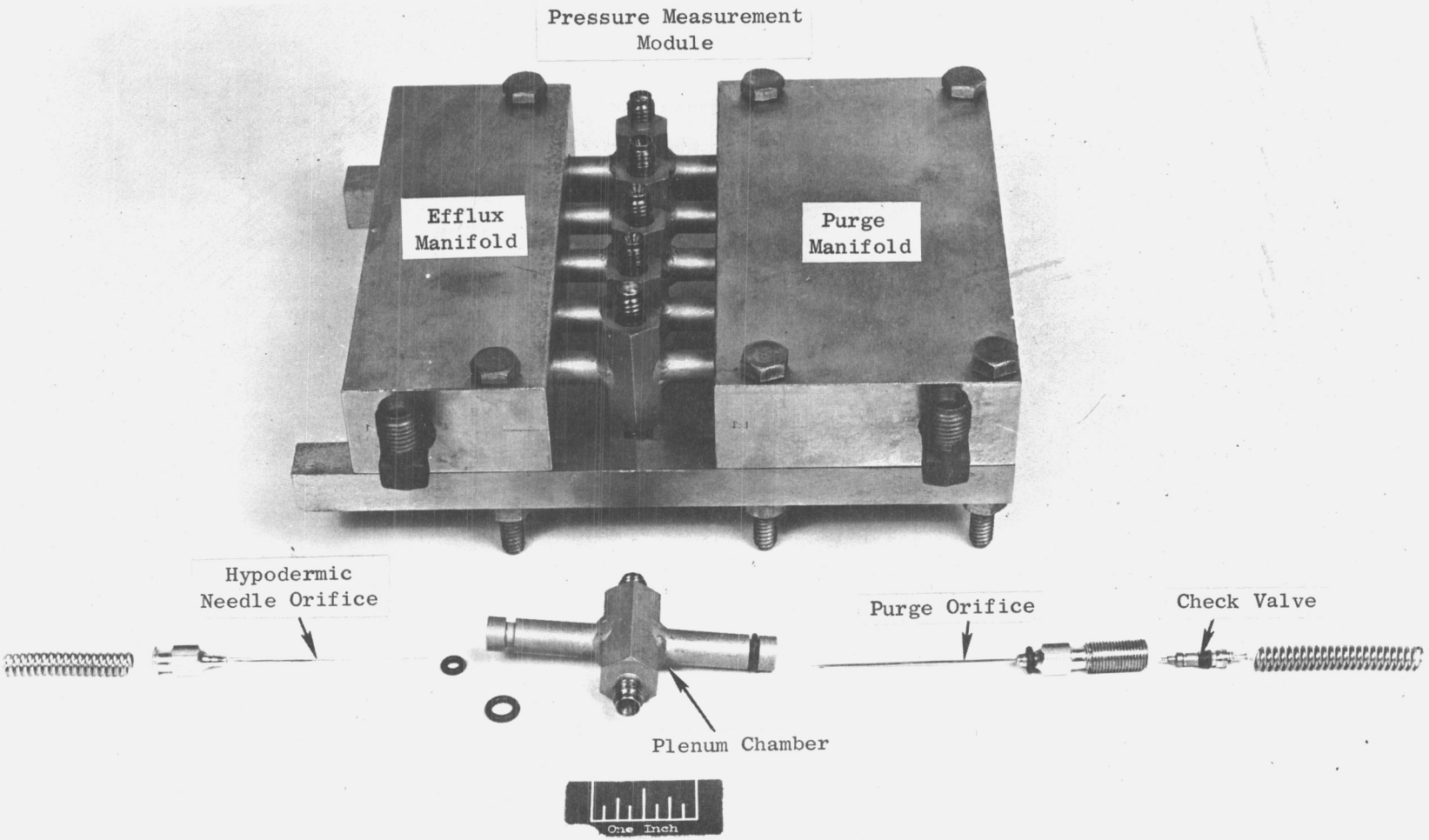

Figure A-2. Efflux System Assembly.

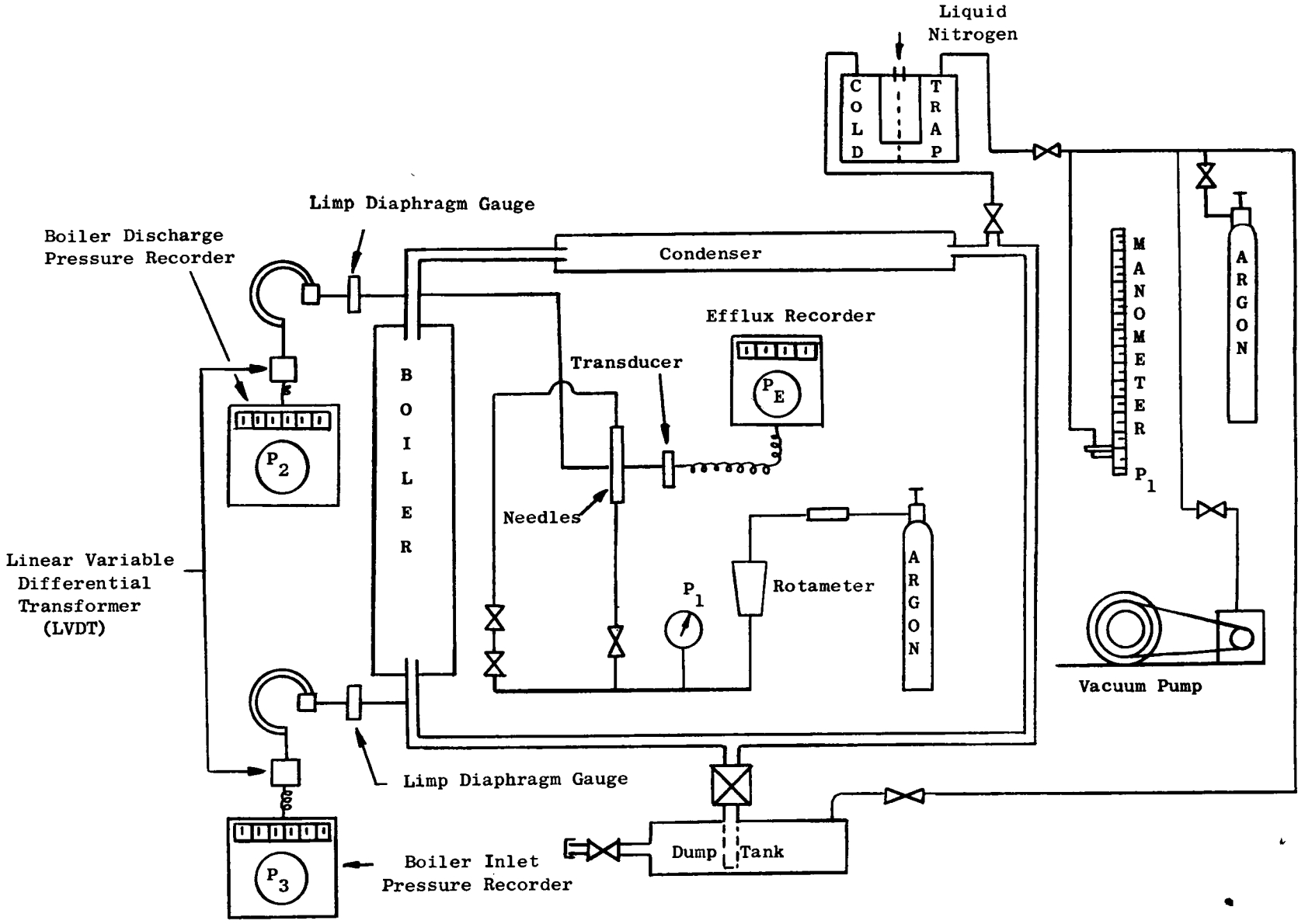

Figure A-3. Schematic of Efflux System Installed in the 50 KW Two-Phase Potassium Loop.

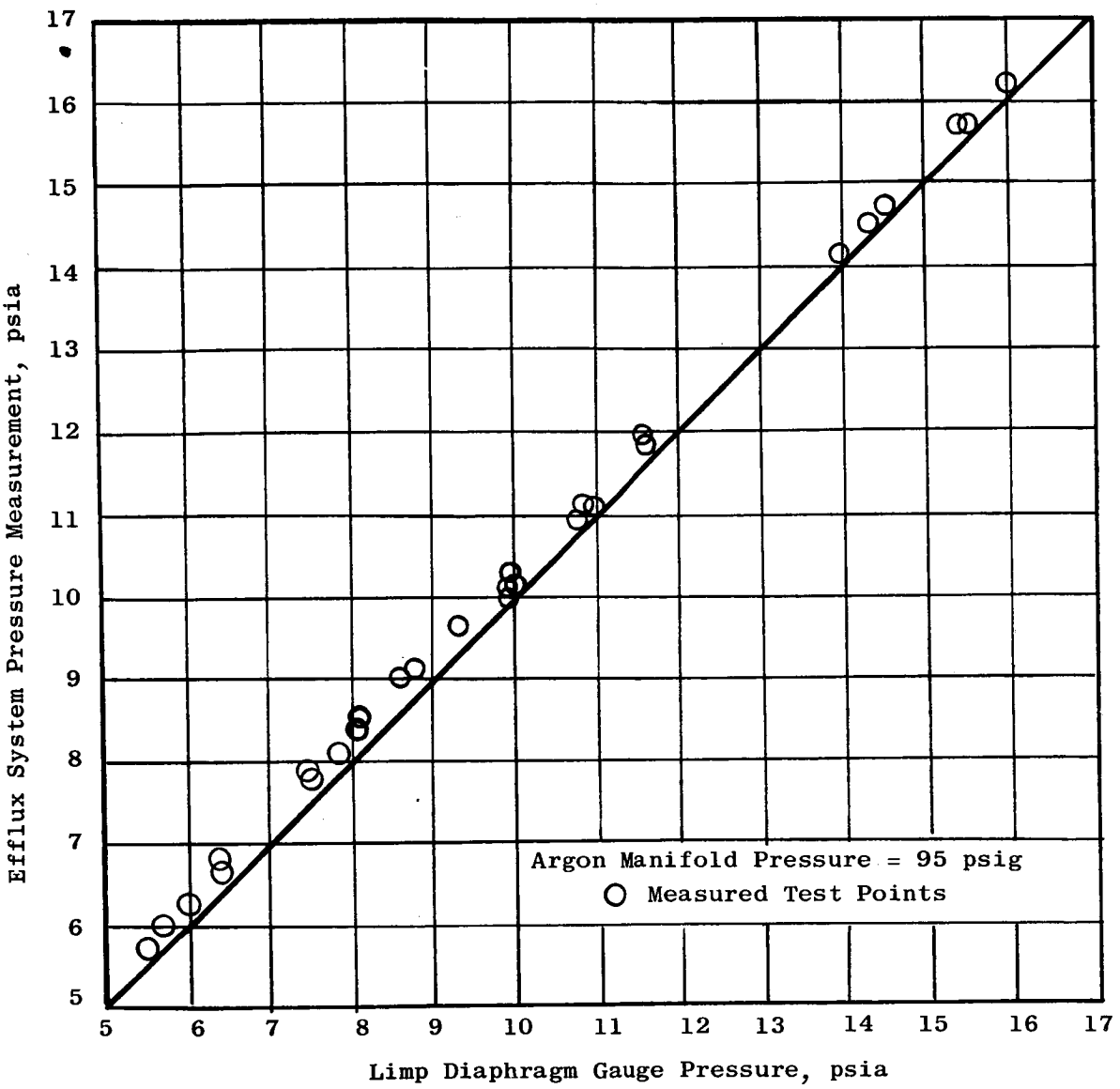

Figure A-4. Efflux Pressure Measurement Versus Limp Diaphragm Gauge.

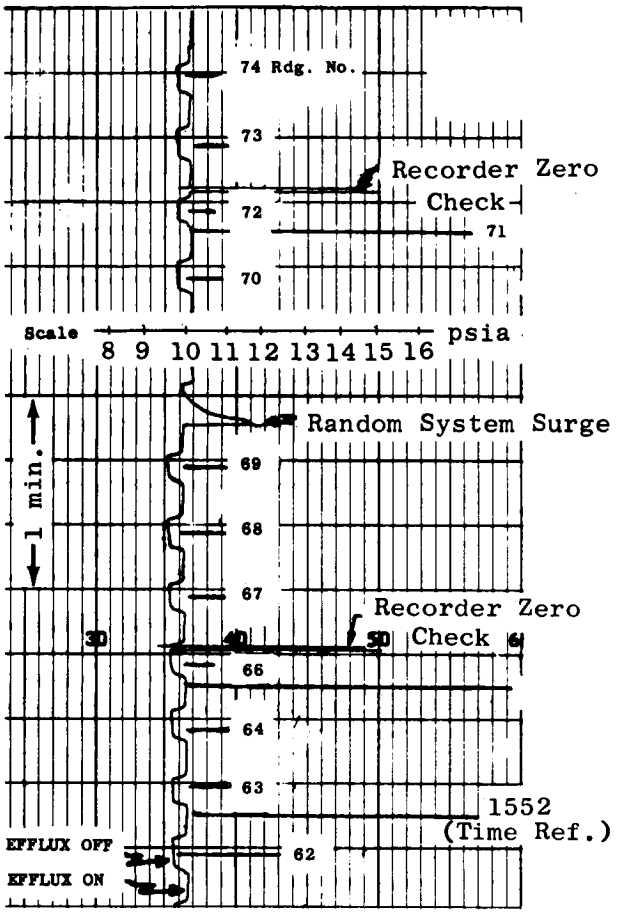

Efflux System Pressure Trace

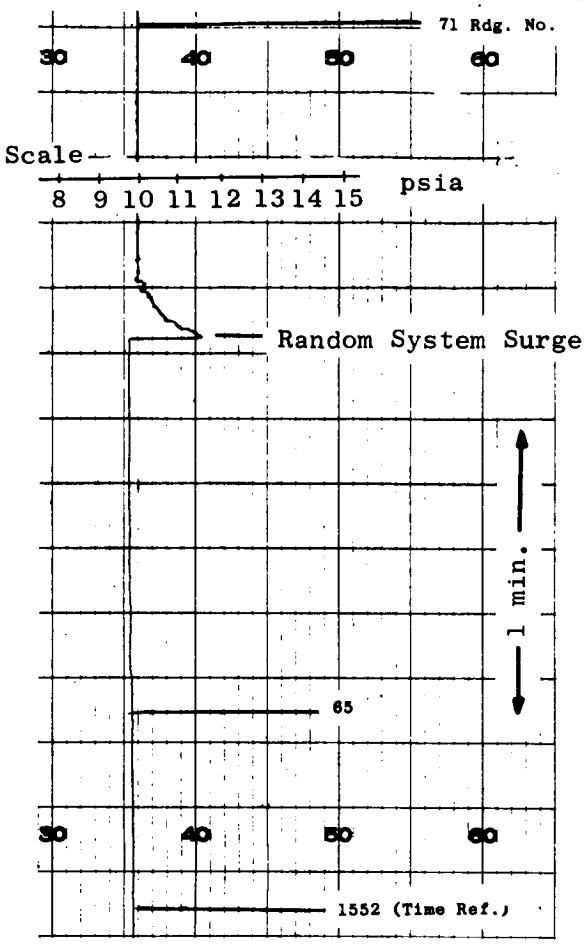

Limp Diaphragm Gauge Pressure Trace

Figure A-5. 50 KW Boiler Outlet Pressure Traces.

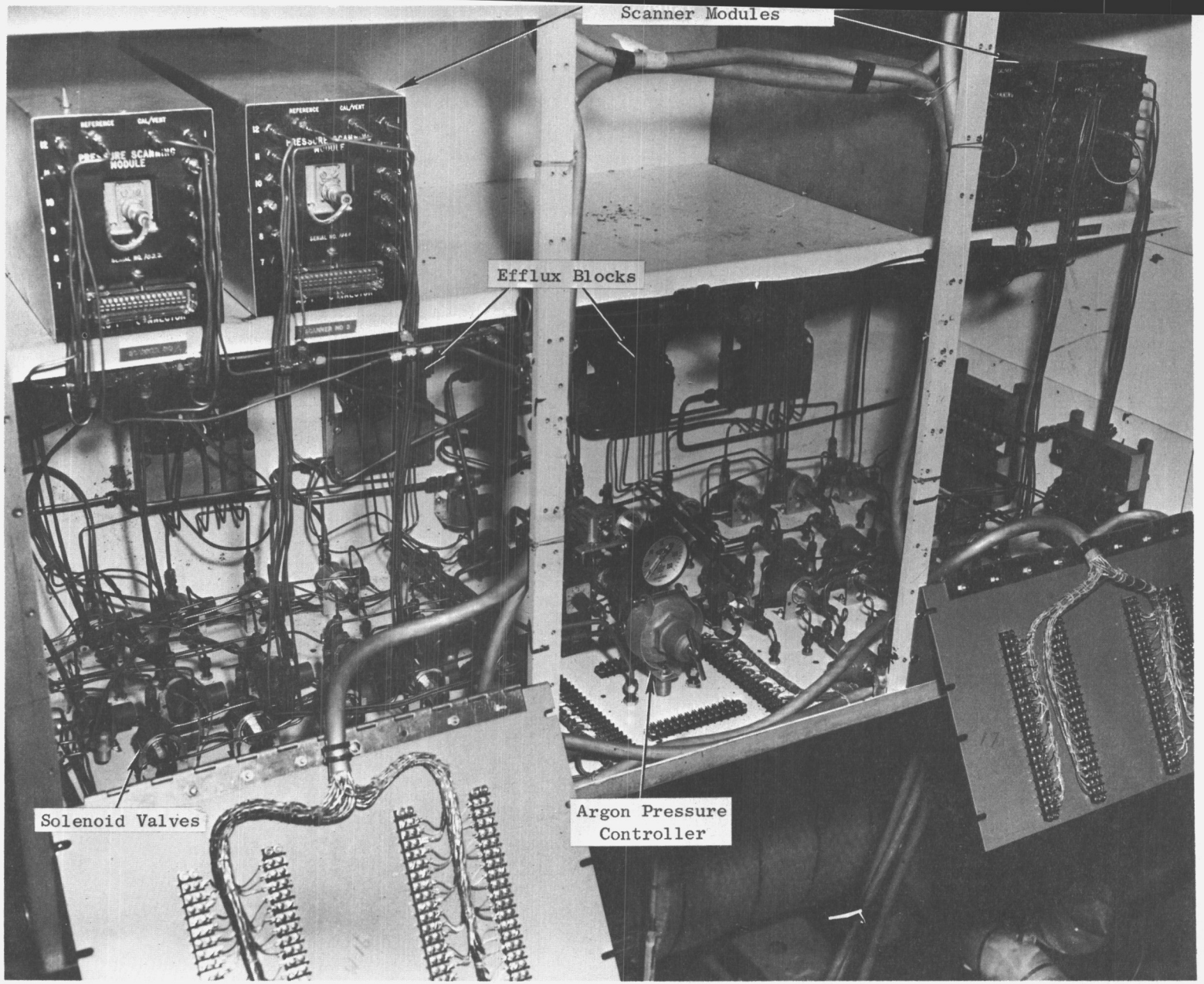

Figure A-6. Efflux System Equipment.

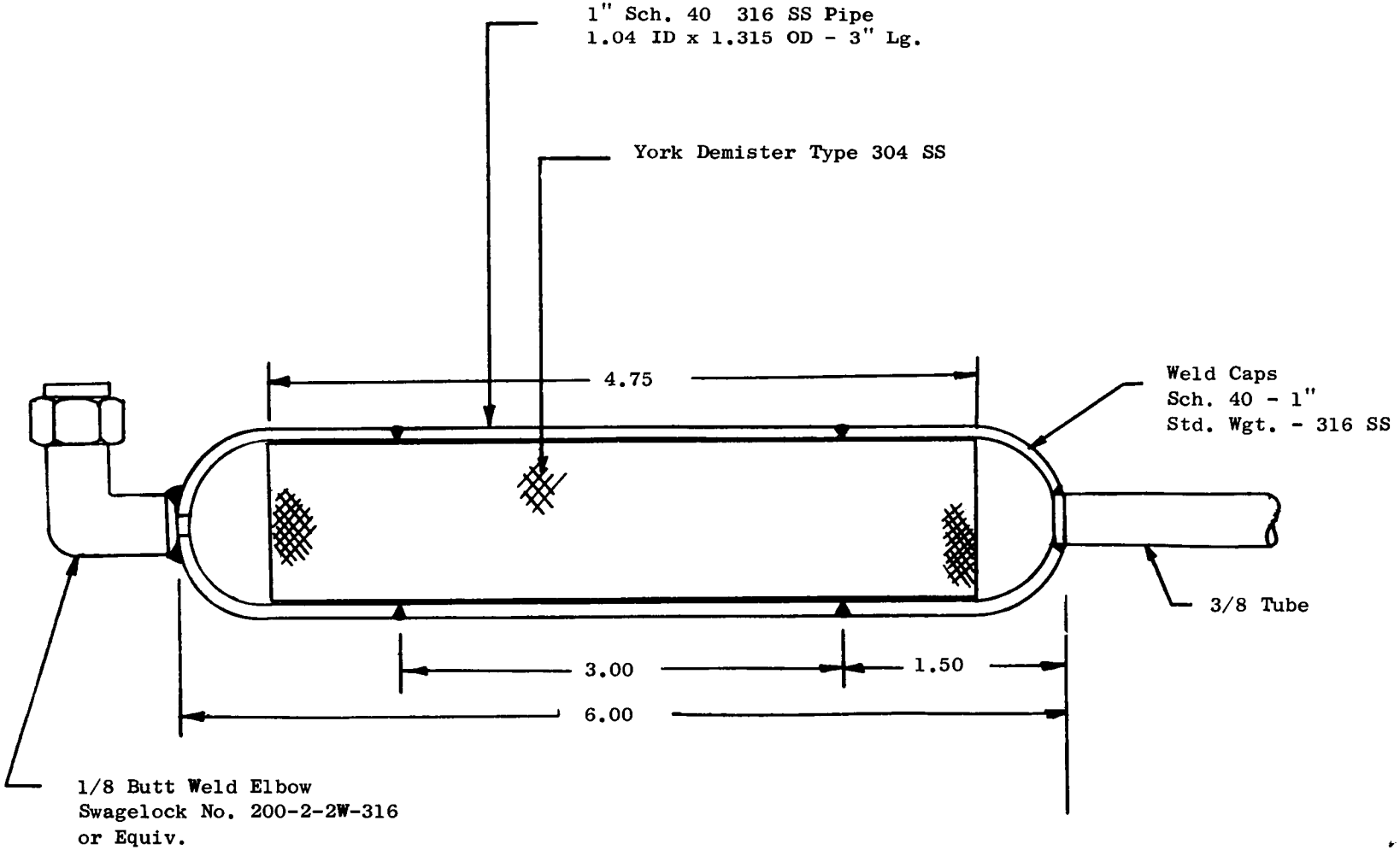

Figure A-7. Efflux Vapor Trap.

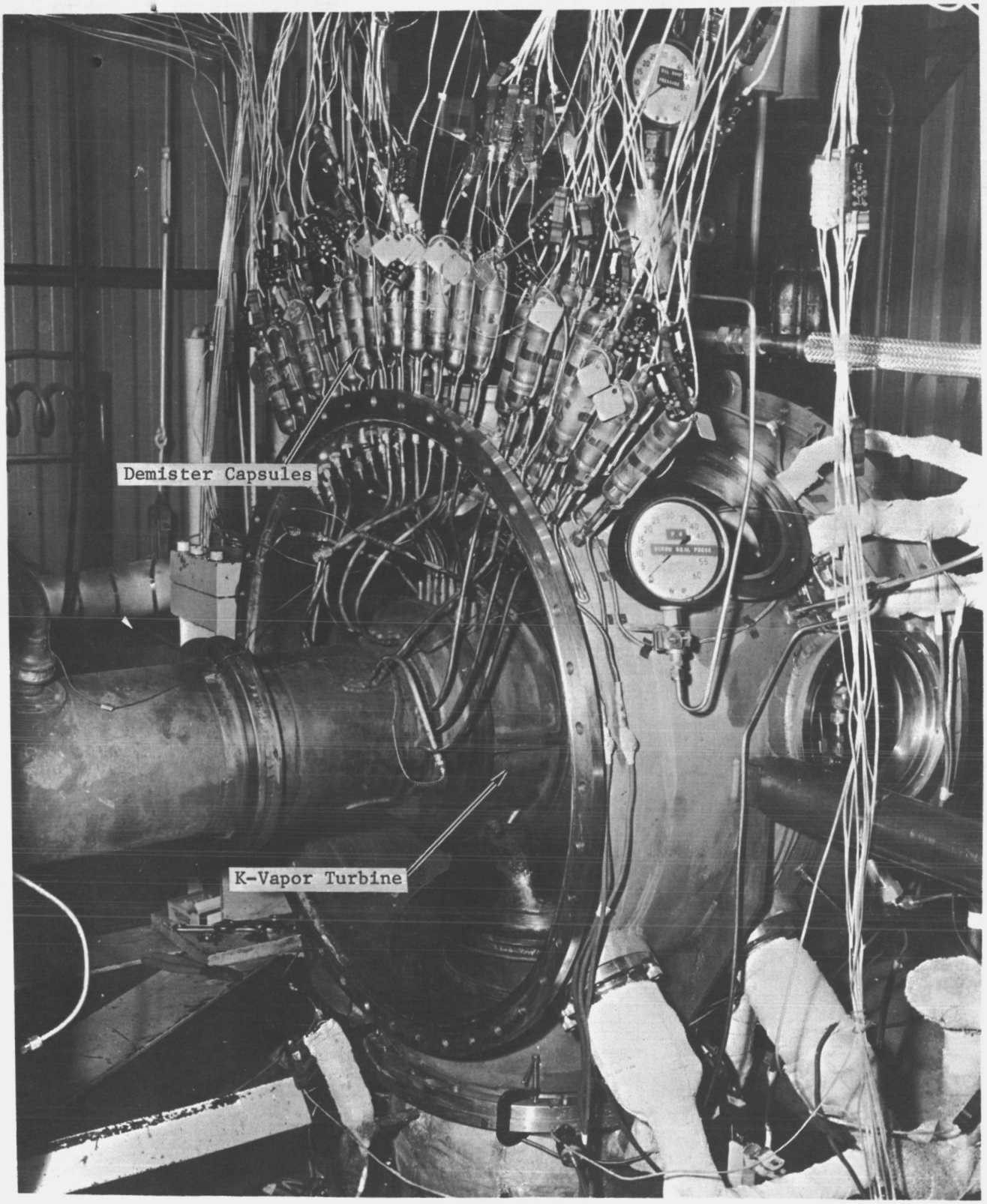

Figure A-8. Installation of the Demister Capsules on the Potassium Turbine.

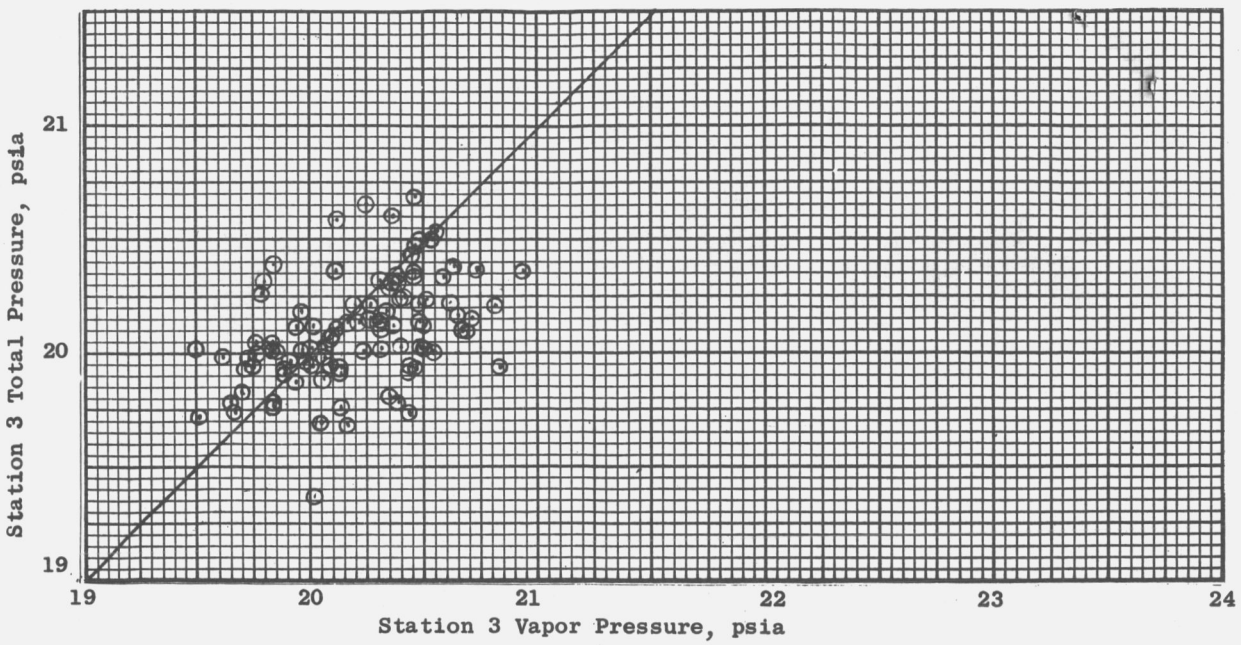

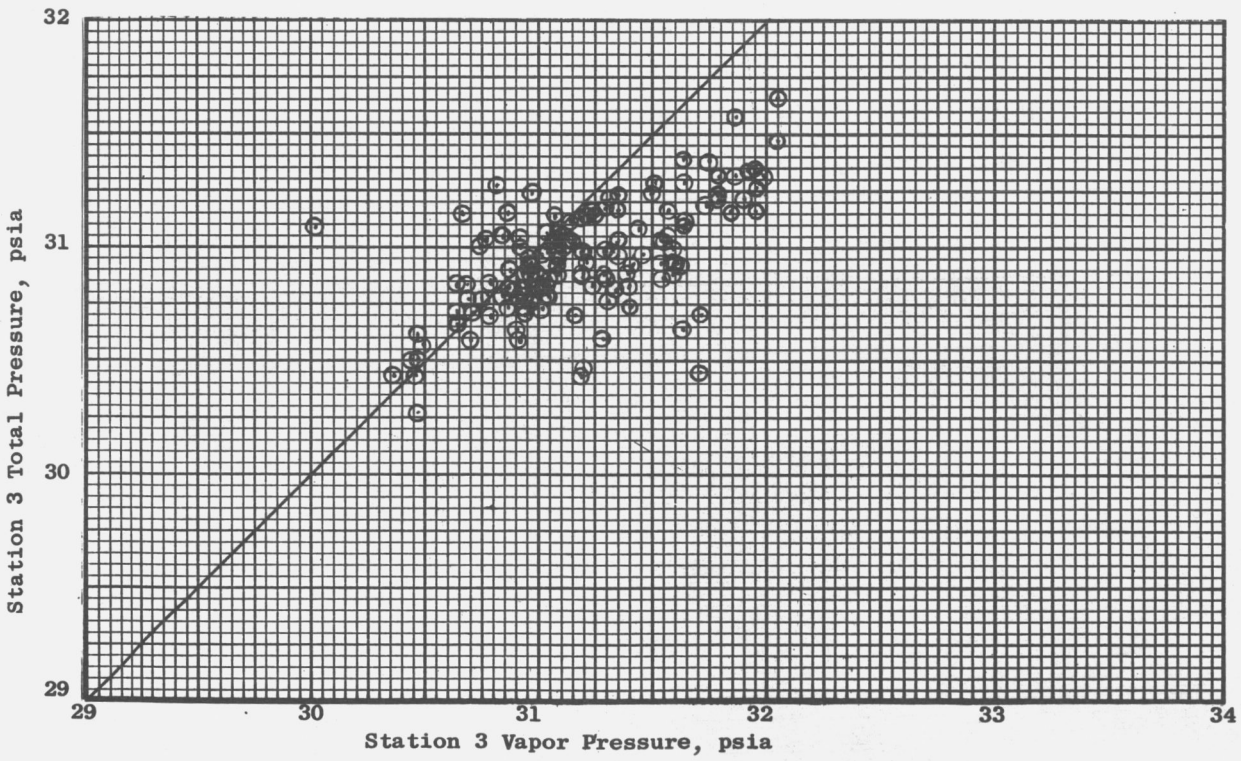

Figure A-9. Comparison of Measured Total Pressure With Vapor Pressure at Turbine Inlet.

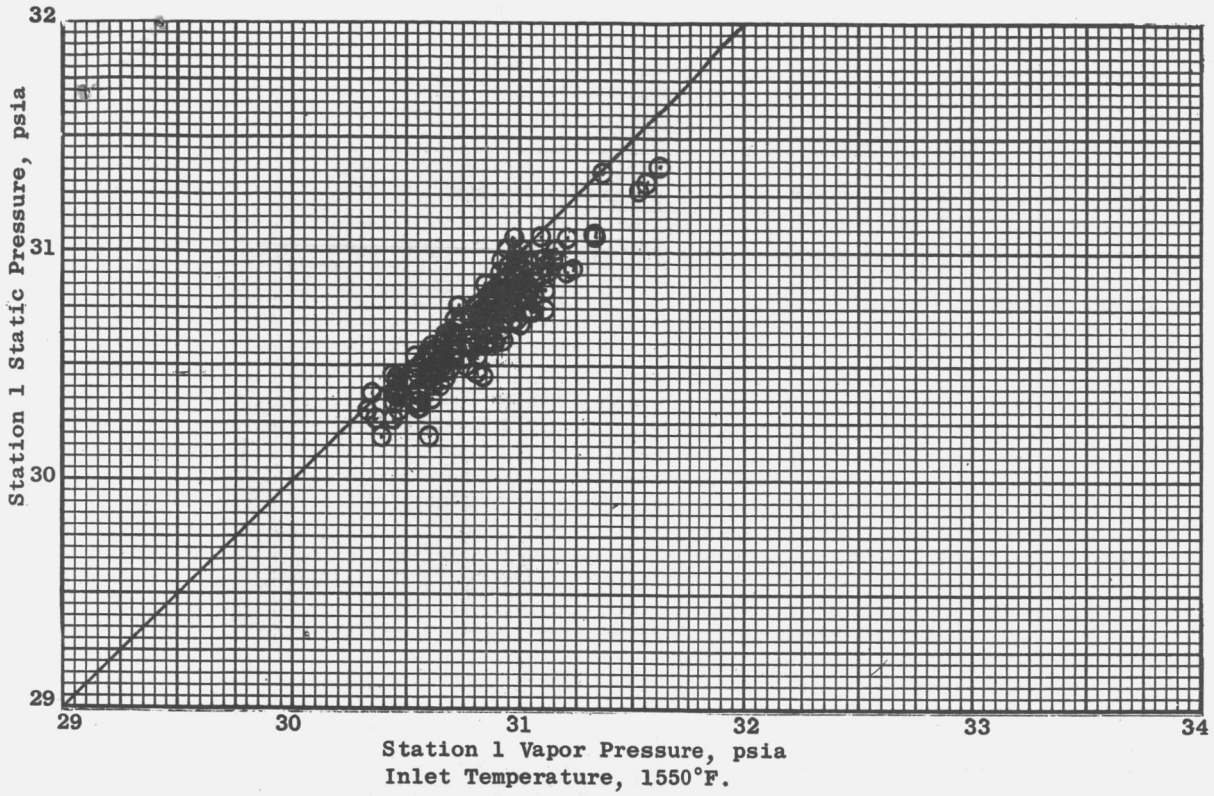

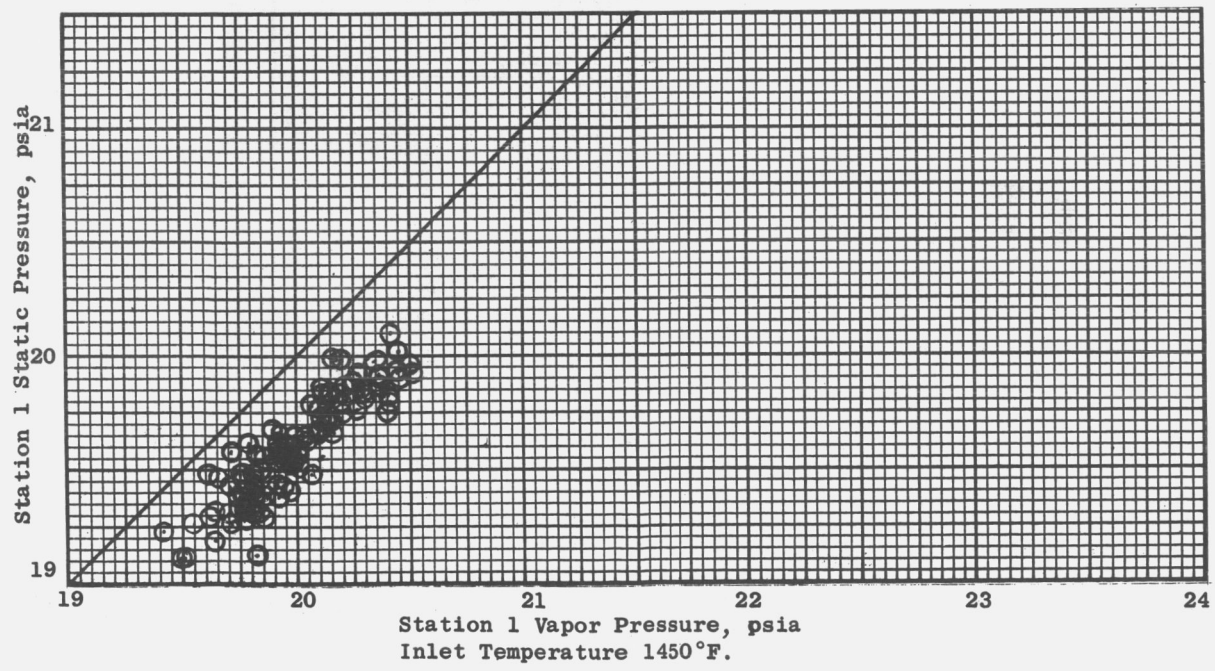

Figure A-10. Comparison of Limp Diaphragm Gauge Pressure With Vapor Pressure Upstream of Turbine.

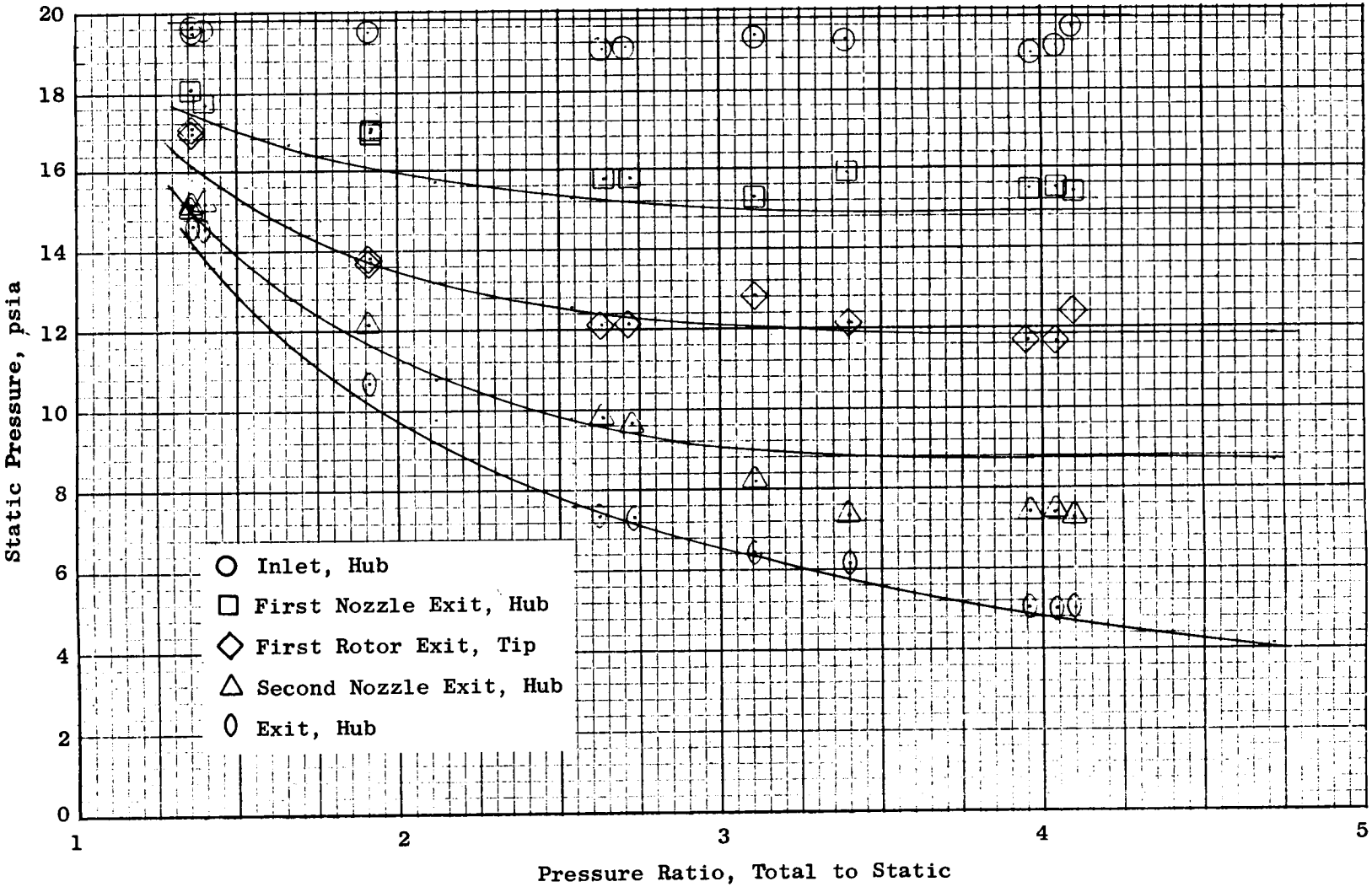

Figure A-11. Comparison of Measured and Calculated Pressure Profile. Turbine Inlet Temperature, 1450°F; Speed, 20,000 rpm.

NASA-Langley, 1967 — 3 CR-922

"The aeronautical and space activities of the United States shall be conducted so as to contribute . . . to the expansion of human knowledge of phenomena in the atmosphere and space. The Administration shall provide for the widest practicable and appropriate dissemination of information concerning its activities and the results thereof."

—NATIONAL AERONAUTICS AND SPACE ACT OF 1958

NASA SCIENTIFIC AND TECHNICAL PUBLICATIONS

TECHNICAL REPORTS: Scientific and technical information considered important, complete, and a lasting contribution to existing knowledge.

TECHNICAL NOTES: Information less broad in scope but nevertheless of importance as a contribution to existing knowledge.

TECHNICAL MEMORANDUMS: Information receiving limited distribution because of preliminary data, security classification, or other reasons.

CONTRACTOR REPORTS: Scientific and technical information generated under a NASA contract or grant and considered an important contribution to existing knowledge.

TECHNICAL TRANSLATIONS: Information published in a foreign language considered to merit NASA distribution in English.

SPECIAL PUBLICATIONS: Information derived from or of value to NASA activities. Publications include conference proceedings, monographs, data compilations, handbooks, sourcebooks, and special bibliographies.

TECHNOLOGY UTILIZATION PUBLICATIONS: Information on technology used by NASA that may be of particular interest in commercial and other non-aerospace applications. Publications include Tech Briefs, Technology Utilization Reports and Notes, and Technology Surveys.

Details on the availability of these publications may be obtained from:

SCIENTIFIC AND TECHNICAL INFORMATION DIVISION

NATIONAL AERONAUTICS AND SPACE ADMINISTRATION

Washington, D.C. 20546